Deregulation of TGF-β Family Ligands in Cancer

Robert David Bloxham

University College London

and

The Francis Crick Institute

PhD Supervisor, Caroline Hill

A thesis submitted for the degree of the Doctor of Philosophy

University College London

January 2021

Declaration

I, Robert David Bloxham, confirm that the work presented in this thesis is my own. Where information has been derived from other sources, I confirm that this has been indicated in the thesis.

Abstract

The study of signalling dynamics is important for understanding how signalling pathways operate in health and disease. Previous work within the lab investigated how cells respond to TGF-β family ligands over time, in terms of pathway activity. Cells treated with TGF-β reach maximal signal induction at one hour which rapidly attenuates to a low-level steady state despite sustained ligand exposure. Additionally, cells become unresponsive to fresh ligand. This suggests that in diseases, including cancer, where there are sustained levels of pathway activity, another ligand may be responsible for signal propagation or there is re-wiring of mechanisms underlying TGF-β signalling dynamics.

Further work in the lab demonstrated that reduced expression of components of the ESCRT machinery led to sustained pathway activity in cells exposed to TGF-β. Furthermore, it was shown that CAFs, a cell type in the tumour stroma, produce functional Activin ligand, which may also be responsible for sustained pathway activation.

The work in this thesis aimed to investigate whether these two distinct possibilities could explain the sustained TGF-β family pathway activity observed in disease states by answering two questions:

1. Does compromised ESCRT signalling lead to enhanced TGF-β-mediated output?
2. Is CAF-sourced Activin responsible for pathway signal and output, previously ascribed to TGF-β?

I have demonstrated that compromised ESCRT function leads to an enhanced TGF-β-mediated epithelial-mesenchymal transition through elevated PSMAD signalling. I have also shown that CAFs from the MMTV-PyMT mouse model of breast cancer produce Activin, that is critical for their contractility whilst affecting their proteome and transcriptome. Furthermore, I have developed in vivo experiments to determine the role of CAF-sourced Activin during tumourigenesis.

Finally, I successfully developed and validated the use of HALO technology to track TGF-β family receptors live for the first time to further our understanding of the family's signalling dynamics and inform further studies.

Impact Statement

The work described in this thesis provides many benefits to both the academic world and wider society. Academically, this work delivers insights and new understanding into a fundamental biological signalling pathway, specifically, signalling by TGF-β family ligands. This pathway is involved in the development of embryos and in many adult homeostatic processes including cell cycle arrest and immune cell regulation, becoming deregulated in many diseases including fibrosis and cancer. I provide new understanding as to how this pathway operates and elicits is function in health and disease, specifically, how family signalling output is upregulated in disease contexts such as cancer. Such understanding can help inform further investigations of this pathway and broaden our knowledge as to how it operates in downstream developmental studies and adult homeostatic processes.

Additionally, I demonstrate that TGF-β family receptors can be tracked using the HALO protein tag, removing the need for cumbersome and disruptive fluorescent tags. This work can form the foundation of a project that aims to determine how TGF-β family receptors localise throughout signalling; something that has never been done before. How, and to what extent, receptors are recycled or degraded at both basal and signalling levels has yet to be comprehensively determined. Being able to track receptors can answer critical questions as to why and how cells respond to certain signals at a pathway output and functional level. Such work would, again, greatly broaden our understanding of a fundamental signalling pathway in both health and disease.

Finally, this work is of benefit to translational studies and, potentially, of ultimate benefit for clinical use and public health. I identify Activin A/B ligands as an abundant and pro-tumourigenic signal within a mouse model of breast cancer. This work provides the foundation for targeting Activin A/B signalling clinically. Specifically, one could develop agents that bind and neutralise signalling at a ligand level, such as antibodies and ligand traps, or at the level of the receptor, with small molecule inhibitors, to ablate pro-tumourigenic signals. These agents could then be used in mouse models of cancer to further determine the effect of Activin A/B signalling on tumour growth and spread. This may provide more evidence for its targeting at a clinical level, leading to clinical trials for several cancer types. In the future, such

studies could lead to the development of anti-cancer therapies that would be of benefit to public health.

Acknowledgements

The past four years that have led to this thesis have been some of the most enjoyable and important in my academic career. I have learned a huge amount both about my project specifically but, more significantly, how to be a good scientist, critical thinker and writer. For that, I have a huge amount of people to thank, who I have had the pleasure of meeting and working with.

First, I would like to thank Caroline Hill. Caroline has been paramount to my development as a thoughtful, driven and hard-working scientist. I would like to thank her not only for giving me the opportunity to work in this lab, and on this project, but also her invaluable insights. Without which, this project would not have gone very far. I'd also like to thank her for cultivating the nicest group of people I have ever worked with.

I would also like to thank Daniel Miller for his support and insights at the initial stages of both the ESCRT and Activin projects. This thesis would not exist in its final format if not for his diligent work prior to my arrival. He also served as a good source of football chat for the first two years of my PhD. For her scientific insight, both CAF and Activin related, I'd like to thank Danielle Park, your arrival helped shape the success of my final year of experiments. Danielle is also a warm and supportive person who understood how tough a PhD can be. This leads me on to the other member of cancer club and truly fantastic PhD colleague, Louise Richardson. As well as her support experimentally, Louise was key to my survival as a PhD student. Thank you for all the distracting cat and Nintendo chat Lou-Lou! Completing the SW5 massive is Isobel Bradley, Izzy is surely one of the kindest people I will ever work with. Thank you for noticing every time things got tough for me and being there with the strawberry pencils (and also being the only person to ever notice when I had a haircut). As fellow students, it doesn't get better than Lou-Lou and Izzy!

Next, the post-docs, Andrew Economou was not only a brilliant and thoughtful scientist but a supportive friend. I hope I didn't take up too much of your spare time. Luca Guilgimi, cheers mate, keep rolling sixes. See you soon for mojitos. To Anassuya Ramachandran (Ramaham), thank you for being one of the most genuinely kind and supportive people I have ever met. You were instrumental in my development as a scientist in the early stages of my PhD. To Nisha Hirani, even though you were not in the lab, your banter and food helped me survive. To Davide

Coda, thank you for the football chat and unique/incredible sense of humour. To Merima Mehic, thank you for the Crepes and to Scott Wilcockson, the inspiring dress sense, you are marvellous! Finally, Ilaria Gori, a truly special member of the team. I would not have completed this PhD to this standard if it wasn't for you. You were always there to help with experiments and as a council during tough times. Which, by the way, you should really start charging for. This lab would suffer both scientifically and socially without you.

I'd also like to thank Claire, Thijs, Jasmine, Stephanos and Ellen for the time I got to spend working with them. Particularly Ellen who was an excellent student to supervise as part of my first authentic mentoring opportunity.

Beyond the lab, I'd like to thank pretty much every STP at the Crick, specifically, Cell Services, the BRF, EHP and bioinformatics. Thank you for dealing with my frequent emailing and questions. Your contributions to my project were paramount to its success, it honestly wouldn't exist without you! I'd like to thank Stephanie Strohbuecker for her work on the analysis of my RNA-Seq data and for increasing my knowledge of bioinformatics 1000-fold. I'd also like to thank Emma Nye, Alejandro Suarez-Bonnet and Simon Priestnall for their expert opinion and support on my histopathological data. Finally, to my thesis committee, JP Vincent, Ilaria Malanchi and Rachel Chambers. I found the prospect of meeting you all quite daunting, and then I actually met you. You were tremendously supportive and honest in every meeting. You truly helped me develop as a thinker and your invaluable insight was vital to the success of my PhD.

Beyond academia, thank you to my parents. You have supported me for the past 28 years. No one has been more important in getting me into this position, it truly could not have happened without you. Finally (really this time), to my partner Charlotte Whiting. I would surely have perished during this PhD without you. You have always been there to support me during the tough times, and to savour in the joyful times. There is absolutely no one else I would like to have had by my side during my PhD. In fact, the greatest achievement of my PhD may well have been teaching you how to identify a Western Blot. Here's to many more years of happiness! Thank you all!

Contents

List of Figures

Abbreviations

ACVR	Activin receptor
ACVRL	Activin receptor-like kinase
AMH	Anti-Müllerian hormone
BMP	Bone morphogenetic protein
BMPR	BMP receptor
BSA	Bovine serum albumin
CAF	Cancer-associated fibroblast
cDNA	Complimentary DNA
CIP	Calf intestinal phosphatase
CM	Conditioned media
CRISPR	Clustered regularly interspaced short palindromic repeats
cT	Cycle threshold
DAPI	4', 6-diamidino-2-phenylindole
DMEM	Dulbecco's Modified Eagle Medium
DNA	Deoxyribose nucleic acid
dNTP	Deoxynucleoside triphosphate
ECM	Extracellular matrix
EDTA	Ethylenediamine tetra acetic acid
EHP	Experimental histopathology
EMT	Epithelial to mesenchymal transition
ESCRT	Endosomal sorting complex required for transport
FBS	Foetal bovine serum
FGF	Fibroblast growth factor
FST	Follistatin
GDF	Growth and differentiation factor
gDNA	Genomic DNA
GFP	Green fluorescent protein
HALO	Haloalkane dehalogenase
IHC	Immunohistochemsistry
IRES	Internal ribosomal entry site

ITS	Insulin transferring selenium
Luc	Luciferase
MET	Mesenchymal to epithelial transition
MMP	Matrix metalloproteinase
MMTV	Mouse mammary tumour virus
MVB	Multi-vesicular body
NF	Normal fibroblast
OD	Optical density
PBS	Phosphate-buffered saline
PCR	Polymerase chain reaction
Prtl	Parental
PyMT	Polyoma middle T antigen
qRTPCR	quantitative real time PCR
RNA	Ribonucleic acid
RNA-Seq	RNA-Sequencing
SD	Standard deviation
SEM	Standard error of the mean
TAE	Tris-acetate EDTA
TGF-β	Transforming growth factor β
TGFBR	TGF-β receptor
WT	Wildtype

Chapter 1. Introduction

1.1 Cell Signalling

1.1.1 Cell signalling in health and disease

The study of cellular signalling is fundamental to deepen our understanding of biology in health and disease. A huge range of signalling pathways exist within biology eliciting an enormous variety of functions. Some fundamental pathways include Shh, Wnt, Notch and TGF-β family signalling. These signals provide instructions to cells from their environment, such as neighbouring cells, that cause a behavioural change. Classically, these pathways involve the binding of ligands to transmembrane receptors, which transmit the signal to intracellular mediators that typically alter transcription and, ultimately, the behaviour of the cell (Kholodenko, 2006). Many of these pathways are able to produce multiple and sometimes opposing effects in certain contexts (Purvis and Lahav, 2013). A pathway's functional output is often determined by the intensity and duration of the signal, or the signal output (Sagner and Briscoe, 2017). The signalling output is determined by a myriad of proteins, regulating signalling at a variety of levels, from the binding affinities of the ligand itself to the dynamics of receptors and internal signal mediators (Kholodenko, 2006).

Proper regulation of signalling output is critical for fundamental biological processes. For example, Wnt signalling is required for axis patterning, promoting cellular proliferation, stem cell maintenance and lineage specification in developing embryos (Petersen and Reddien, 2009). Additionally, TGF-β signalling is required for an epithelial to mesenchymal transition (EMT) in developing embryos, a process critical for cellular migration and proper tissue patterning (Wu and Hill, 2009). In adult tissues, Notch signalling is required for T cell development (Sato et al., 2012). Moreover, TGF-β family signalling is required during wound healing (Gilbert et al., 2016).

Deregulation of these pathways can lead to aberrant kinetics of signalling intensity, causing diseases such as cancer. Within tumours, there are an abundance of distinct cell types communicating with one another to enhance tumourigenesis by promoting oncogenic phenotypes. These include angiogenesis, extracellular matrix

(ECM) remodelling, immunosuppression as well as cancer cell invasion and metastasis (Hanahan and Weinberg, 2011). In fact, inappropriate redeployment of the developmental signalling processes described above are observed in cancer. For example, loss of expression of the Wnt regulator APC is observed in many cases of colorectal cancer (Anastas and Moon, 2013). The resulting elevation in Wnt signalling leads to enhanced stem cell-renewal and cellular proliferation, causing cancer (Leedham and Chetty, 2016). Additionally, TGF-β-mediated EMT is a critical process in the invasion, dissemination and metastatic spread of cancer cells (Yang et al., 2020).

Studying how cell signalling operates in a healthy state is paramount to comprehend how it becomes dysregulated in disease. This not only broadens our knowledge of fundamental biology but may inform the identification of potential therapeutic targets. One particularly important aspect in the study of signalling output and function is the signalling dynamics of a pathway, how the intensity of the signal output changes through the duration of a given signal (Purvis and Lahav, 2013).

1.1.2 Signalling dynamics

The study of signalling dynamics relates to understanding how cells respond to and interpret signal over time. Signalling pathways do not simply transmit information in a static and linear manner. Information that determines physiological output is encoded in the temporal dynamics of a given pathway (Sagner and Briscoe, 2017). These can be determined by a variety of parameters including, but not limited to: the spatial organisation and trafficking of signal mediators, such as receptors; positive and negative feedback loops to enhance or diminish activity over time; or different upstream ligands that activate the same pathway with distinct dynamics (Purvis and Lahav, 2013). Such regulation allows the same pathway to elicit distinct, and sometimes opposing, effects. A classic example of this is the MAPK pathway. Both EGF and NGF activate MAPK signalling in PC12 cells. However, stimulation with EGF induces transient pathway activation, whereas stimulation with NGF results in sustained activation. A transient response in this context promotes cell proliferation whilst sustained signalling induces differentiation (Marshall, 1995). Additionally, the IL-6 family of cytokines have been shown to have diverse and context-dependant

roles in immune modulation (Murakami et al., 2019). In some cases, family members even have contrasting pro- or anti-inflammatory outputs, despite sharing the same intracellular signalling mediator, gp130 (Murakami et al., 2019; Villarino et al., 2017). These types of regulatory mechanisms explain how a small number of signalling pathways are able to elicit the plethora of functionalities required for a functioning organism.

If appropriate signalling dynamics are not maintained, aberrant functions will arise that may lead to disease states. One such example is signalling through receptor tyrosine kinases (RTKs). RTKs mediate signalling for many ligands, including EGF and NGF. RTK signalling output is tightly regulated in a spatial and temporal fashion. Activated receptors are rapidly internalised and signal within intracellular endosomes before being degraded in the lysosome, killing the signal and preventing sustained activation (Bergeron et al., 2016). Deregulation of this spatial control is associated with tumourigenesis. If actively signalling receptors are not degraded, they continue to activate a pro-proliferative transcriptional programme that can lead to tumour development (Sangwan and Park, 2006).

The investigation of signalling dynamics is critical to our understanding of how pathways behave at a functional level in health and disease. TGF-β family signalling is no different. The theme of this thesis is how the investigation of mechanisms that regulate TGF-β signalling dynamics can inform downstream functional studies that may lead to therapeutic targets. I follow-up on 2 functional investigations established from a prior signalling dynamics study. Finally, I commence my own mechanistic study that aims to broaden our understanding of the pathway and spawn further functional investigations.

1.2 The TGF-β Signalling pathway

1.2.1 TGF-β family overview

The TGF-β family is a group of growth factors that play fundamental roles during development and adult tissue homeostasis (Wu and Hill, 2009). Deregulation of signalling is associated with a range of diseases, including cancer (Massagué, 2008). The family comprises of 33 ligands that can be categorised into subfamilies. These include the TGF-β ligands themselves, bone morphogenetic proteins (BMPs), growth

and differentiation factors (GDFs), Activins as well as Nodal and anti-Müllerian hormone (AMH). The ligands and their downstream mediators are extremely well conserved throughout evolution (Schmierer and Hill, 2007).

Despite the complexity and diversity of the cellular responses they can induce, discussed in Section 1.4, the ligands activate signalling through a relatively simple and linear pathway (Figure 1.1). Ligand dimers bind distinct sets of serine/threonine kinase receptors at the surface. These receptors are classed as either type I or type II (Shi and Massagué, 2003). Once bound, ligand dimers bring together two of each of Type I and Type II receptors to form a heterotetrameric complex (Yakymovych et al., 2018). The constitutively-active kinase domain of the type II receptor phosphorylates the type I receptor, providing a platform from which the intracellular mediators of the pathway, the receptor-regulated SMADs (R-SMADs), can bind. The R-SMADs themselves become phosphorylated by the Type I receptor and form a complex with the shared mediator, SMAD4 (Shi and Massagué, 2003). These complexes accumulate in the nucleus where they regulate transcription of a diverse array of genes in a context dependant manner (Schmierer and Hill, 2007). Different ligands activate distinct family receptors which then, generally, phosphorylate different subsets of R-SMADs. TGF-β, Activins and Nodal generally signal using SMAD2/3, whilst the BMPs and GDFs utilise SMADs 1/5/9 (Wakefield and Hill, 2013). There are exceptions to this rule that will be discussed later.

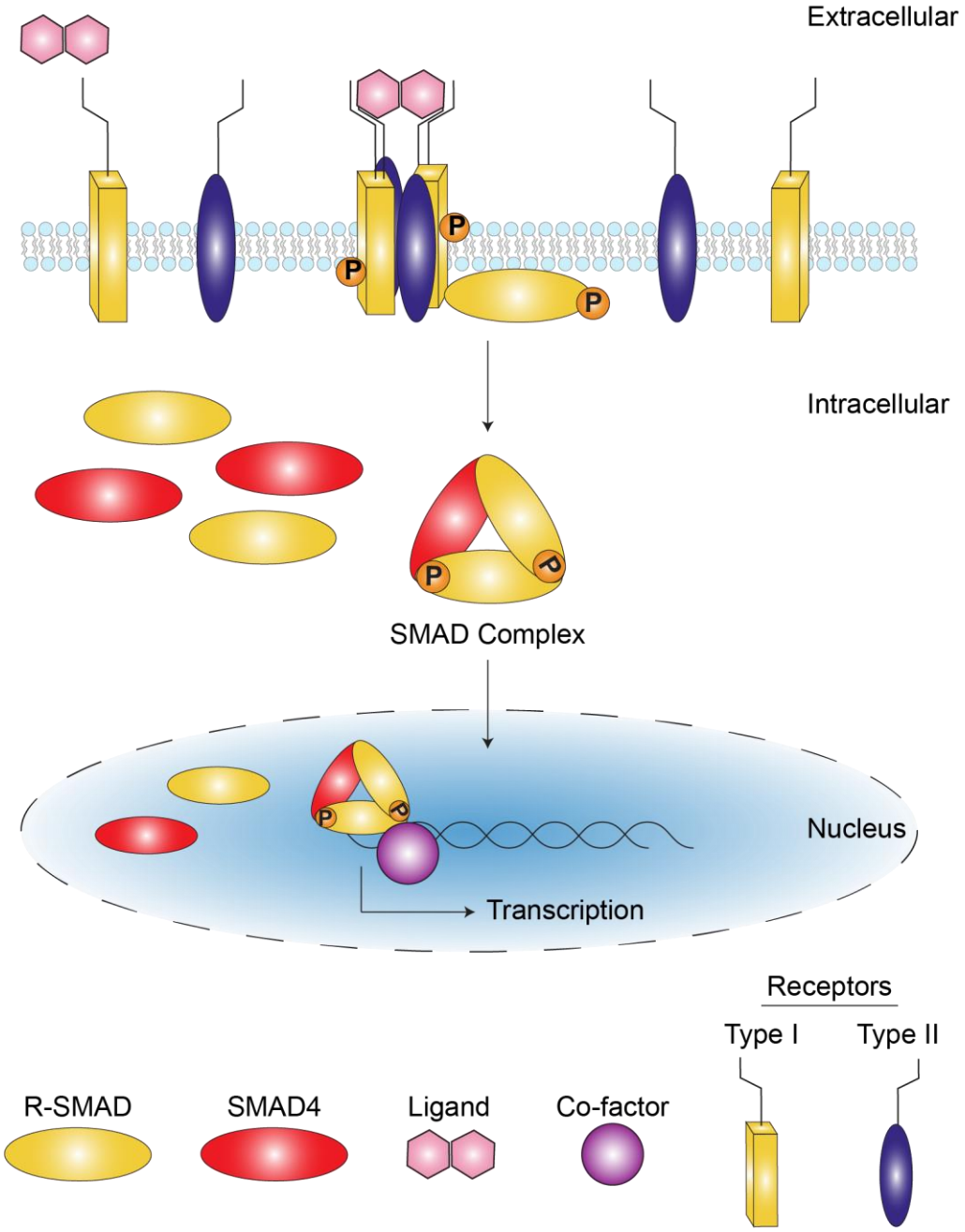

Figure 1.1. TGF-β family signalling pathway. Schematic shows canonical signalling pathway for most family ligands from receptor binding to gene transcription via the SMAD complexes. Figure inspired by Ramachandran et al., 2018.

1.2.2 TGF-β family ligands and inhibitors

As mentioned above, the TGF-β family can be divided into smaller sub-families based on sequence similarity and downstream function (Figure 1.2) (Wakefield and Hill, 2013). These include the TGF-βs themselves, Activins, Nodal, AMH, BMPs and GDFs. Ligands in these smaller families make up 30 of the family members. Antagonists of the pathway, (LEFTY1, LEFTY2 and INHA) make up the remaining 3 ligand members.

This thesis largely focusses on the TGF-β ligands themselves as well as the Activins. For the TGF-β ligands, 3 distinct isoforms exist. Specifically, TGFB1, TGFB2 and TGFB3 (Mercado-Pimentel and Runyan, 2007). In the case of Activin, 4 isoforms exist. INHBA, INHBB, INHBC and INHBE (Welt et al., 2002). These encode the proteins inhibin beta-A -B -C and -E, commonly referred to as Activin A, Activin B, Activin C and Activin E. Activins A and B are the most well studied, with little known of the role of Activins C and E (Stenvers and Findlay, 2010).

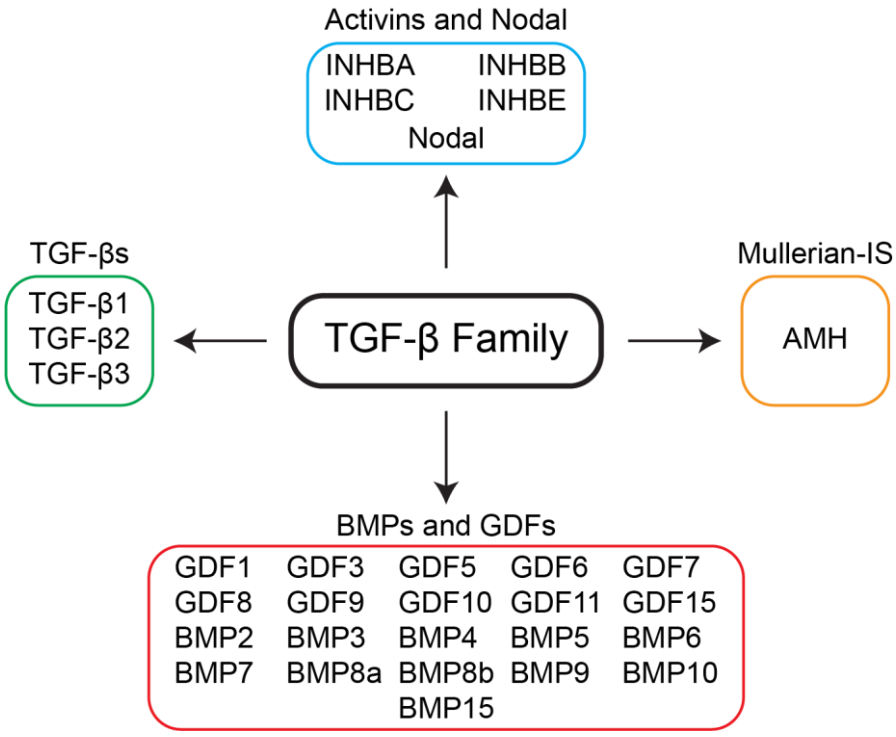

Figure 1.2. List of TGF-β family ligands. Agonists of the pathway can be grouped together into 6 distinct subfamilies detailed above. The antagonists (LEFTY1, LEFTY2 and INHA) have been omitted. Adapted from figure produced by Caroline Hill.

1.2.2.1 Ligand Structure and Activation

All family ligands are synthesised as dimeric precursor proteins with 3 regions; a large pro-domain connected to a C-terminal mature region by a Furin cleavage site (Morikawa et al., 2016). Sequence similarities between family members are shared largely within respective mature domains, with pro-domains sharing minimal homology (Derynck et al., 1988). The pro-domain is required for dimerization and processing of the proteins, whilst the mature domain is primarily responsible for receptor activation (Gray and Mason, 1990). Most ligands contain either 7 or 9 highly conserved cysteine residues within their mature regions. These form intramolecular cysteine knots as well as a single disulphide bridge between monomers, at cysteine residue 77, that serves to stabilise ligand dimers (Daopin et al., 1992; Morikawa et al., 2016; Schlunegger and Grütter, 1992). Ligands signal as homodimers in most cases, although heterodimers of some ligands have been documented (Shi et al., 2011). Notably, the Activins have been shown to signal as heterodimers. Activin A and Activin B are able to form homodimers as well as heterodimers (Antsiferova and Werner, 2012; Wang et al., 2016).

During secretion, the precursor proteins undergo cleavage by furin-like proteins at the furin site, releasing the mature region from covalent linkage to the pro domain (Dubois et al., 2001). The ligands are then secreted as pro structures, with mature ligands non-covalently associated with their pro domains. When discussing how TGF-β and Activin propagate signalling, it is important to consider these pro structures. The pro-mature structures of TGFB1 and Activin A proteins have been solved, as well as that of BMP9 (Mi et al., 2015; Shi et al., 2011; Wang et al., 2016). There is one notable difference between the pro structures of TGFB1 and Activin A. Specifically, the pro form of TGFB1 is secreted as a latent complex in which the pro domains form a closed ring ‘latency lasso’ structure around the mature ligand, preventing contact with receptors (Shi et al., 2011). Therefore, it is unable to initiate signalling in this state. This complex is also covalently linked to ECM-associated latent TGF-β-binding proteins (LTBPs) by disulphide bonds (Annes, 2003). A variety of mechanisms are able to release the mature ligand from the latent pro-mature complex, including; binding of $\alpha_v\beta_6$ integrins, proteases, thrombospondin-1 (TSP-1), low pH and reactive oxygen species (ROS) (Koli et al., 2001; Munger et al., 1997). These activators exist in areas of wound repair, angiogenesis and inflammation

(Annes, 2003). These are all instances where TGF-β plays a critical role (Massagué, 2012). This elegant system means TGF-β signalling should only be activated where it is required. Conversely, pro-Activin A has a more open structure. Activin A is able to bind receptors and activate signalling whilst the mature region is still associated with the pro-domain (Wang et al., 2016). In this instance, the pro-domain is thought to enhance solubility, allowing efficient diffusion of the ligand to its target site without unwanted aggregation (Harrington et al., 2006). Additionally, it has been shown to bind heparin-sulphates, localising it to regions where signalling is required (Wiater et al., 2006). The mature domain has a greater binding affinity for the receptor than the pro-domain. The receptor competes for the mature domain and, once bound, the pro-domain is released (Hinck et al., 2016).

1.2.2.2 Ligand inhibitors and antagonists

Naturally occurring antagonists exist for the majority of family ligands. Some antagonists operate by directly sequestering ligand, such as BMP inhibitor Noggin (Zimmerman et al., 1996), whilst others bind receptors to block signalling, including Nodal antagonists Lefty1 and Lefty2 (Hill, 2018). However, there are no known natural antagonists for any TGF-β ligand. Active signalling is largely controlled by existence of the latent form of the ligands. Conversely, Activin has two well established and potent antagonists, Follistatin and Inhibin A (INHA). A third antagonist, Follistatin-like 3, also has Activin inhibitory capacity (Schneyer et al., 2004). Follistatin operates by actively sequestering Activin ligands, preventing them from contacting the receptor and activating signalling (Ueno et al., 1987). INHA forms heterodimers with INHBA and INHBB monomers. These heterodimers are then unable to bind receptor complexes (Welt et al., 2002). Follistatin is utilised routinely throughout this thesis as an inhibitor of Activin A/B signalling.

1.2.3 TGF-β family receptors

TGF-β family receptors are comprised of 3 core regions. An evolutionary diverse and cysteine-rich extracellular domain, a single pass transmembrane domain and a highly conserved intracellular serine-threonine kinase domain (Schmierer and Hill,

2007; Shi and Massagué, 2003). Type I receptors have an additional GS domain which harbour serine/threonine residues that become phosphorylated by the Type II receptor following ligand binding (Schmierer and Hill, 2007). Type I and Type II receptors form heterotetrameric complexes upon ligand binding. Certain type I receptors activate distinct R-SMADs. Specifically, ACVR1B, ACVR1C and TGFBR1 signal through SMAD2/3 whilst ACVR1, ACVR1L, BMPR1A, BMPR1B activate SMAD1/5/9.

TGF-β ligand has been shown to bind the type I receptor TGFBR1 in combination with its type II receptor, TGFBR2 to activate signalling by SMAD2/3 (Feng and Derynck, 2005). Activin also activates SMAD2/3 signalling, but through a type I and type II combination of ACVR1B/C and ACVR2A/B (Walton et al., 2012).

1.2.3.1 Receptor activation

Generally, family ligands have a higher affinity for the type II receptors. Canonical receptor activation requires binding of ligand to the type II receptors which causes clustering of the appropriate type I receptors to form heteroterameric complexes (Huang and Chen, 2012). It had long been thought that type I and type II receptors existed as homodimers within the cell membrane prior to ligand binding (Gilboa et al., 1998). However, it has since been proven, using single molecule imaging, that in most cases receptors exist as monomers, only forming dimers once ligands bind (Zhang et al., 2009, 2010). Following complex formation, the constitutively active type II serine-threonine kinase phosphorylates the associated type I receptor within its GS domain, causing a conformational change and releasing the moderator FKBP12 and allowing downstream signalling activation (Huse et al., 1999; Shi and Massagué, 2003; Wrighton et al., 2009). Non-canonical receptor activation has also been documented, playing important roles in some physiological processes. Notably, TGF-β induced heterotetramers of TGFBR1 and TGFBR2 receptors have been shown to cluster with and phosphorylate ACVR1 through the kinase activity of TGFBR1. This, in turn, leads to TGF-β induced SMAD1/5 signalling and a transcriptional and physiological output (Ramachandran et al., 2018).

1.2.3.2 Synthesis and receptor targeting

Our understanding of TGF-β family receptor synthesis and targeting to the cell surface is largely restricted to TGF-β receptors. Little is currently known of how Activin receptors shuttle around the cell.

TGF-β receptors are synthesised in the ER before undergoing certain post-translational modifications within the golgi apparatus. These modifications serve to enhance their activity and functionality. Specifically, receptor glycosylation and fucosylation have been shown to be vital for appropriate folding complete receptor functionality (Wang et al., 2005; Zhang et al., 2020a). Types and levels of glycosylation have been shown to influence TGF-β-mediated EMT (Partridge et al., 2004; Zhang et al., 2020a). Additionally, types of glycosylation determine degrees of receptor localisation at the cell surface. Specifically, *N*-linked glycosylation is important for appropriate translocation of TGFBRII to the cell surface (Kim et al., 2012). Furthermore, Akt activation, through insulin signalling, drives translocation of intracellular pools of TGF-β receptors to the cell surface. Consequently, cells become more responsive to ligand, generating enhanced TGF-β-mediated outputs in response to ligand (Budi et al., 2015). One study aimed to determine how TGF-β receptors translocate to the surface. Investigators utilised a GFP fluorescent TGFBR2 construct to demonstrate that post-golgi vesicles containing TGFBR2 localised to microtubules, travelling towards the cell surface (Luo et al., 2014). Little is known of the synthesis and shuttling of Activin receptors.

1.2.3.3 Receptor internalisation and recycling

The receptors have been shown to internalise through multiple routes, which can determine their ultimate fate. Some studies have shown they endocytose through clathrin-coated pits whilst others have demonstrated internalisation routes by caveolin-dependant pathways (Di Guglielmo et al., 2003; Mitchell et al., 2004). Additionally, TGFBR1 has been seen to associate with caveolin-1 and clathrin double positive endosomes (He et al., 2015). The route of internalisation may be critical, as clathrin-mediated internalisation results in a more sustained level of signalling, whereas caveolin-mediated routes can be more transient (Zi and Klipp, 2007). In any

case, internalised receptors end up at early endosomes that are marked with Rab5 and EEA1, where they can continue to actively signal or become degraded.

The degradation route of TGF- β is mediated by the ESCRT machinery (endosomal sorting complex required for transport), a family of proteins responsible for various processes associated with membrane remodelling, including endosomal sorting (Miller et al., 2018; Sorkin and Von Zastrow, 2009). The machinery is composed of four subunits, ESCRT-0, -I, -II and -III (Campsteijn et al., 2016). ESCRT-0 binds the endosomes and recruits ESCRT-I and -II which induce membrane invaginations. ESCRT-II then recruits ESCRT-III monomers which form helices and constrict around the invagination, cutting the membrane and generating MVBs (Wollert and Hurley, 2010). It was shown that loss of expression of the components of the ESCRT machinery lead to loss of degradation of TGF-β family receptors and sustained signalling and pathway activation (Miller et al., 2018). The functional consequences of this phenomenon are explored in Chapter 5.ESCRT Machinery Regulates Long-term Signalling Dynamics of TGF-β

If not degraded, receptors within the endosomes can recycle back to the surface via Rab11 positive endosomes (Mitchell et al., 2004). All TGF-β family receptors undergo consistent levels of turnover at the surface, even in the absence of ligand (Doré et al., 2001; Mitchell et al., 2004). Specific Threonine residues have been shown to be critical in driving TGF-β receptor endocytosis in certain cell types (Doré et al., 2001). However, following stimulation with TGF-β, TGFBR1 and TGFBR2 receptors rapidly deplete from the surface, with TGFBR2 becoming almost entirely absent within 10 minutes of signalling (Vizán et al., 2013). Conversely, levels of Activin receptors remain steady at the surface, even when stimulated with Activin ligand (see Section 1.3 for more detail) (Miller et al., 2019). However, little is known of how this is maintained. Investigating how Activin receptors internalise, shuttle and recycle may help broaden our understanding of this phenomenon.

1.2.4 SMADs

SMADs are the intracellular mediators of the pathway, responsible for propagating signal from activated receptors to the nucleus where they work with co-factors to activate transcriptional programmes (Hill, 2016). Three subfamilies exist, the R-SMADs (SMAD1, 2, 3, 5 and 9), the common mediator SMAD (SMAD4) and the

inhibitory SMADs (I-SMADs; SMAD6 and 7). Each contain 3 key structural regions: an amino-terminal Mad Homology 1 (MH1) domain, a carboxy-terminal Mad homology (MH2) domain and a PY motif that connects the other two regions (Hill, 2016). Once activated, the type I receptors phosphorylate specific R-SMADs (SMAD2 and SMAD3 as well as SMAD1, SMAD5 and SMAD9) at two serine sites within their extreme c-terminus (Chacko et al., 2001). The specificity of R-SMADs to their cognate receptors is determined by the interaction of an L3 loop in the SMAD's MH2 domain with an L45 loop in the corresponding type I receptor (Chacko et al., 2001). Activated R-SMADs form complexes with the shared mediator, SMAD4. These complexes accumulate in the nucleus where they directly bind DNA in combination with various co-factors that work to activate or repress a transcriptional programme depending on the cellular context (Massagué, 2012). SMADs directly bind to specific SMAD binding elements (SBE) which are palindromic repeats of the 'GTCTAGAC' sequence (Hill, 2016; Zawel et al., 1998). Additionally, *in* vivo, GC rich sites, such as GGCGCC, are able to bind SMAD1/5 (Hill, 2016). As part of this thesis, I utilise cells that express a luciferase reporter under the control of these elements as a readout of pathway activity. Even in the absence of signal, SMADs constantly shuttle between the nucleus and cytoplasm, allowing them to constantly monitor signal intensity and duration (Schmierer et al., 2008). Monomeric R-SMADs are predominantly seen in the cytoplasm. Once activated and in a complex with SMAD4, their nuclear export rates are dramatically reduced which is why SMADs accumulate in the nucleus during pathway activation (Schmierer and Hill, 2007; Schmierer et al., 2008).

Levels of phosphorylated R-SMADs, as well as their nuclear accumulation, are frequently used as readouts of family pathway activity in mechanistic and functional studies (Massagué, 2008; Schmierer and Hill, 2007). Additionally, specific transcriptional programmes and expression of SMAD target genes are used as readouts of pathway activity (Kim et al., 2011; Levy et al., 2007; Mullen et al., 2011). However, these readouts are not exclusive to any one family ligand, or the family itself. For example, as discussed, TGF-β and Activin are able to induce phosphorylation of SMAD2 and SMAD3 leading to shared transcriptional and functional outputs. Specifically, SMAD2 and SMAD3 have been shown to activate transcription of collagens, integrins and MMPs that contribute to wound repair and fibrosis (Margadant and Sonnenberg, 2010; Verrecchia et al., 2001; Walton et al.,

2017; Yuan and Varga, 2001). Despite the shared transcriptional and functional outputs that can contribute to disease pathogenesis, the bulk of research conducted largely focusses on TGF-β ligand. This has resulted in, arguably, a disproportionate focus on targeting TGF-β ligands therapeutically. This is discussed further in 1.4.3.4.

1.3 TGF-β Family Signalling Dynamics

1.3.1 TGF-β ligand signalling dynamics

As discussed, the signalling dynamics of a given pathway are critical in determining functional output. The same is true for TGF-β ligand signalling (Miller et al., 2018; Vizán et al., 2013). Upon treatment, cells reach maximal signal induction, as read-out by levels of PSMAD2, within one hour of signalling. Levels of pathway activity then decline to a low level steady state (Vizán et al., 2013). Additionally, cells enter into a refractory state, whereby they do not respond to active ligand at the surface (Figure 1.3) (Vizán et al., 2013).

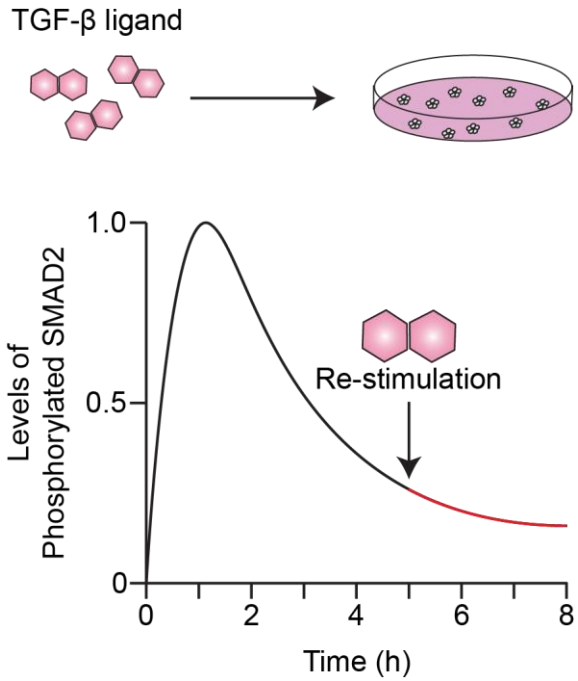

Figure 1.3. Profile of TGF-β pathway activation over time. Graph depicts relative levels of PSMAD2 over time in cells treated with TGF-β ligand. Red line denotes profile of PSMAD2 over a period in which cells are stimulated with fresh ligand.

It was shown that levels of surface receptor are critical determinants of this profile. Following treatment, TGFBR1 and TGFBR2 receptors rapidly deplete from

the surface, TGFBR2 within 10 minutes, and do not reaccumulate for up to 48 hours (Vizán et al., 2013). This results in cells being unable to detect and respond to TGF-β ligand at the surface. Cells only become responsive to signal once ligand has depleted, allowing receptors to reaccumulate at the surface.

Once internalised, activated receptors are preferentially shuttled to the lysosome for degradation. However, some are able to actively signal within the cell. In fact, signalling persists in internalised compartments for 1-2 hours following induction (Miller et al., 2018). The ESCRT machinery are then responsible for the transport of activated receptors from early endosomes to the lysosome for degradation (Miller et al., 2018).

1.3.2 Other TGF-β family member signalling dynamics

The signalling dynamics of Activin and BMP have also been investigated. For the purposes of this introduction, I will focus on comparing TGF-β and Activin A. Following Activin treatment, cells reach maximal induction of pathway activity within one hour, in a similar fashion to TGF-β. This phenomenon is irrespective of cell type. Conversely, the attenuation pattern for Activin A is much more moderate than that of TGF-β in cell lines that actively produce Activin/Nodal. Additionally, Activin A-treated cells do not enter into a refractory state, meaning treatment with fresh ligand is able to induce a further response (Miller et al., 2019). Similarly to TGF-β ligands, these dynamics are largely dictated by levels of surface receptor (Miller et al., 2019). Levels of ACVR1B and ACVR2A remain at a steady level at the cell surface. This allows cells to continuously monitor signal at the cell surface. This explains why they are able to respond to fresh ligand and activate further signalling (Figure 1.4). Again, it is worth highlighting that little is known of shuttling and recycling of actively signalling Activin receptors.

Duration of TGF-β family signalling is critical for the functional output of this pathway. These outputs are fundamental throughout biology, from development to adult tissue homeostasis. Functional loss of the mechanisms that regulate these established dynamics would lead to aberrant signalling and disease. Indeed, loss of regulation of family signalling at multiple levels is strongly associated with many disease states including cancer.

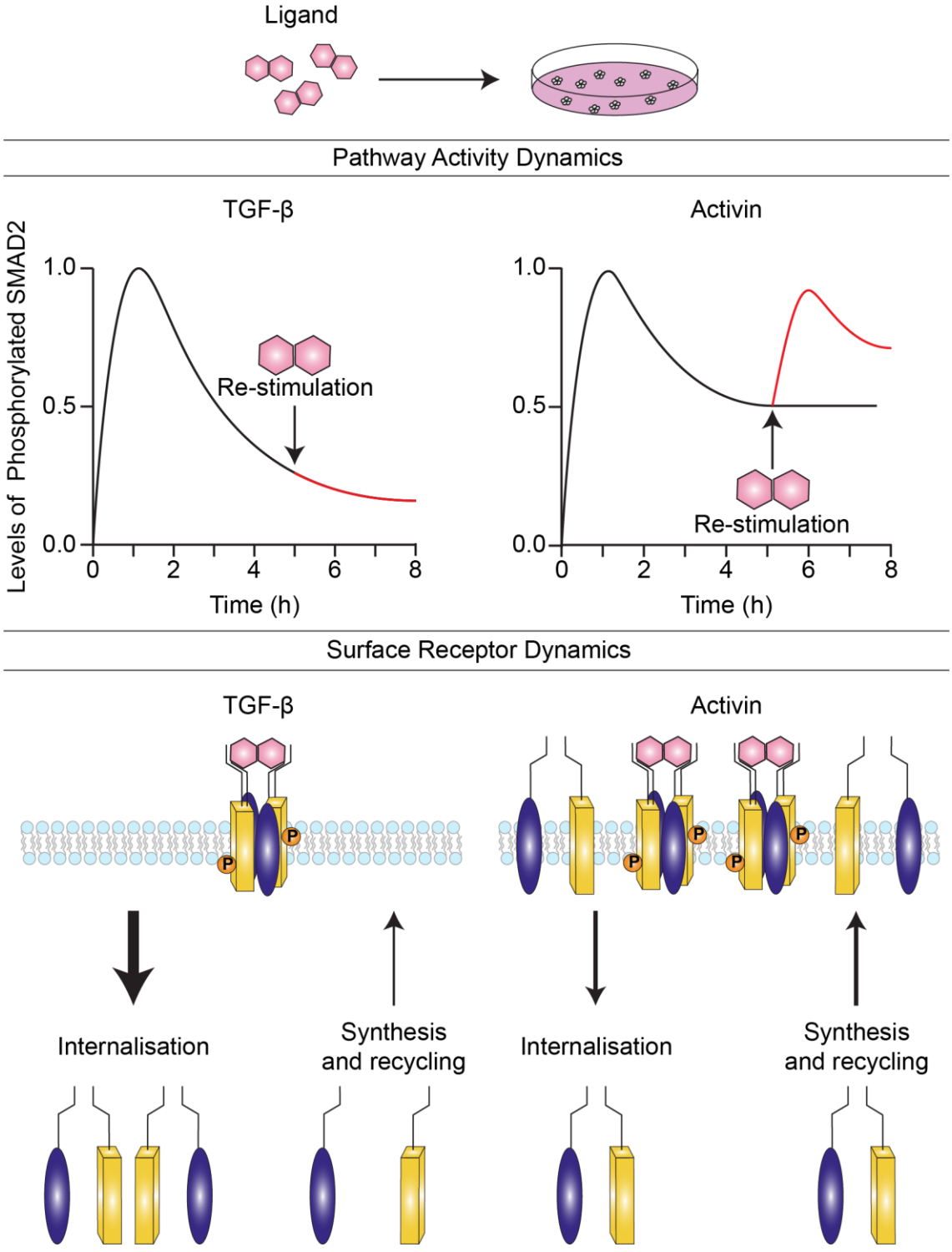

Figure 1.4. Comparing the pathway activity and receptor dynamics of TGF-β and Activin ligands. Top – Graphs show pathway activity, as read out by levels of PSMAD2, in cells treated with TGF-β or Activin ligands. Red line denotes profile of PSMAD2 over a period in which cells are stimulated with fresh ligand. Bottom – cartoon depicting

distribution of shuttling routes for corresponding surface receptors following stimulation with TGF-β or Activin. Figure inspired by Miller et al., 2019.

1.4 TGF-β and Activin Signalling Function

1.4.1 Signalling during embryonic development

The TGF-β family ligands have critical roles during development. They act as morphogens, diffusing across fields of cells during embryonic development. Cells proximal to the source receive stronger signal than those that are more distal. This causes induction of distinct cell fates in a concentration and time dependant manner (Hill, 2018). Of the family members, Nodal and the BMPs are significant players during development. They are responsible for germ layer specification and patterning; and downstream tissue patterning in developing embryos (Wu and Hill, 2009). Additionally, TGF-β and Activin have documented roles during development and in the culture of stem cells.

TGF-β's primary role during development is the migration of cells through initiating EMT (Wu and Hill, 2009). Such a process is vital for correct patterning of developing embryos (Nieto et al., 2016). Specifically, TGF-β is responsible for inducing EMT within the endocardial cells during heart development, a process crucial for proper heart valve formation (Moskowitz et al., 2011). Moreover, loss of TGFB1 or TGFBR2 disrupts formation of blood vessels within the yolk sac (Goumans and Mummery, 2000). Additionally, TGF-β2 and TGF-β3 are required for a complete programmed cell death in the interdigital space in developing mouse embryos. Incomplete signalling results in limb malformation (Dünker et al., 2002).

Activin's most well-documented role in developmental biology is in the culture of embryonic stem cells (ESCs) where it acts as a surrogate for NODAL signalling (Toivonen et al., 2013). Activin A treatment is required to maintain pluripotency in human ESCs through induction of the pluripotency transcription factor Nanog (Xu et al., 2008). However, sustained Activin A exposure induces definitive endoderm differentiation in mouse ESCs (Rothová et al., 2016; Toivonen et al., 2013). *In vivo*, injections of Activin mRNA in *Xenopus* embryos established the ligand as a potent morphogen capable of inducing mesoderm and endodermal populations in a dose dependant manner (Green and Smith, 1990; Nastos et al., 1998). However,

ambiguity was cast over Activin's role in these processes by studies that showed Follistatin treatment of Xenopus embryos had no effect on development (Marchant et al., 1998). It is now thought that conclusions drawn from the earlier studies may be due to Nodal signalling, with Activin acting as surrogate, as in ESCs (Kiecker et al., 2016).

Deregulation of signalling through these ligands can lead to abnormal development (Wu and Hill, 2009). Additionally, re-deployment of these functional outputs in adult tissues can be observed in many disease pathologies (Massagué, 2008, 2012). This is discussed in Section 1.4.3.

1.4.2 Signalling during adult tissue homeostasis

As well as development, many family ligands play vital roles in adult tissues. These include, but are not limited to, cell cycle arrest, apoptosis, migration, induction of specific cytokine programmes in inflammatory cells and ECM production (Heldin et al., 2009; Li and Flavell, 2008; Massagué, 2012; Roberts et al., 2006). Once again, I will specifically discuss the roles of TGF-β and Activin in differentiated adult cells.

1.4.2.1 TGF-β

One of the most well-documented roles of TGF-β ligand in adult cells is its ability to cause growth arrest of epithelial and endothelial cells (Siegel and Massagué, 2003). TGF-β halts the cell cycle at G1 through induction of the cyclin-dependant kinase inhibitors CDKN2B and CDKN1A as well as suppression of growth stimulating factors such as the ID proteins and c-MYC (Kang et al., 2003). As well as its cytostatic properties, TGF-β limits cell growth in a variety of epithelial cells by acting as a pro-apoptotic factor (Siegel and Massagué, 2003). It does so by upregulating pro-apoptotic transcription factors such as TGF-β-inducible early-response gene (TIEG) and death-associated protein kinase (DAPK) (Jang et al., 2002; Tachibana et al., 1997).

TGF-β signalling is also tightly associated with immune cell regulation, particularly of lymphocyte populations. It largely works to prevent hyperactivity and the onset of autoimmune disorders (Li and Flavell, 2008). TGF-β is responsible for the maintenance of peripheral regulatory T cells (Treg) and CD4+ lymphocytes (Li et

al., 2006; Marie et al., 2005). Treg cells modulate active immune responses by inhibiting the activity of effector T cells (Bettelli et al., 2006). Additionally, TGF-β silences expression of transcription factors TBET and STAT4, which are required for differentiation of CD4+ cells to a Th1 phenotype (Lin et al., 2005b). The Th1 phenotype promotes a more active cytotoxic immune response (Mailliard et al., 2002). Furthermore, TGF-β inhibits cytotoxicity of CD8+ by silencing expression of granzyme B and IFN-gamma which are integral for their lytic function (Thomas and Massagué, 2005). Additionally, TGF-β promotes an anti-inflammatory phenotype in macrophages. Specifically, it upregulates SMAD7 expression which binds TAK1, a mediator of pro-inflammatory NF-kB and c-jun, preventing it from activating downstream signalling (Hong et al., 2007). Finally, although less extensively studied, TGF-β acts to suppress the activity of neutrophils by reducing their secretion of lactoferrin following stimulation with lipopolysaccharide (LPS) (Shen et al., 2007).

In addition to these functions, early studies identified TGF-β as a factor that is able to remodel the extracellular matrix by enhancing collagen deposition (Roberts et al., 1986). TGF-β generally promotes collagen deposition through activation of myofibroblasts, which then actively produce ECM components (Verrecchia and Mauviel, 2007). Additionally, TGF-β is responsible for the maintenance of the vasculature. Aberrant signalling is associated with a variety of vascular pathologies (Ten Dijke and Arthur, 2007). Collagen deposition and vasculature management are required for wound healing, a process in which TGF-β is pivotal (Nall et al., 1996). Aberrant or absent TGF-β signalling is observed in chronic wounds that fail to heal completely (Pastar et al., 2010).

1.4.2.2 Activin

Activin's roles in differentiated tissues are less studied than those of TGF-β. The most well-documented role of Activin is in the homeostasis of reproductive systems. The balance of Activin levels with its natural antagonist inhibin are essential for successful maintenance, proliferation and differentiation of somatic cell lineages, namely the granulosa cells of the ovary and Sertoli cells of the testis (Bilezikjian et al., 2006; Stenvers and Findlay, 2010). Additionally, in females, Activin signalling is vital for healthy decidualization through induction of MMP9 expression (Jones et al.,

2006). These roles in the reproductive system demonstrate the pro-proliferative and ECM remodelling capabilities of Activin signalling. However, Activin has also been documented to suppress growth of certain cell types. It is known to potently moderate muscle growth in combination with myostatin (Latres et al., 2017; Lee et al., 2005). Inhibition of Activin A and myostatin signalling increased muscle mass in mice, likely through upregulation of the ERBB2 pathway, which plays a role in skeletal muscle mass synthesis and metabolism (Hellyer et al., 2006; Latres et al., 2017).

Furthermore, Activin has potent wound healing properties (Antsiferova and Werner, 2012). Increased expression of Activin is observed in mice, humans and zebrafish models (Hübner et al., 1996; Jaźwińska et al., 2007). Activin acts directly on fibroblasts within wounds to enhance their migration by upregulating filopodia formation (Cangkrama et al., 2020a). Additionally, Activin alters the transcriptome of fibroblasts within wounds, ultimately altering the matrisome. Specifically, it promotes collagen type I expression (Wietecha et al., 2020). These altered fibroblast behaviours increase wound healing, but also lead to scar formation (Cangkrama et al., 2020b). Moreover, mouse keratinocytes expressing mutant ACVR1B showed significant delay and re-epithelisation during wound healing (Bamberger et al., 2005). Accelerated granulation tissue formation and ECM deposition was observed in mice overexpressing Activin, specifically in Keratinocytes (Munz et al., 1999). It is thought this effect is due to Activins' effect on immune cells, specifically by increasing mast cells, altering the phenotype of regulatory T cells and decreasing numbers of Langerhans cells within the wounds (Antsiferova et al., 2013; Haertel et al., 2018; Stoitzner et al., 2005).

Activin has further documented roles in the modulation of the immune system, akin to TGF-β. Activin has profound and pleiotropic effects on activated macrophages. LPS-activated macrophages show reduced phagocytotic capacity and an anti-inflammatory phenotype following Activin treatment (Morianos et al., 2019; Wang et al., 2008). Conversely, Activin can promote a pro-inflammatory M1 polarised phenotype in granulocyte-macrophage colony-stimulating factor (GM-CSF) treated macrophages (Sierra-Filardi et al., 2011). Activin also elicits complex and contrasting roles on lymphocyte populations. It is a potent differentiation factor of the T_{FH} cell population (Locci et al., 2016). This population is generally pro-inflammatory, causing B cells maturation to target foreign antigens (Fazilleau et al., 2009). Conversely, it induces expression of FoxP3 in lymphocytes, promoting expansion

and survival of peripheral anti-inflammatory Treg cells (Huber et al., 2009; Ni et al., 2018).

TGF-β and Activin clearly share functional outputs in a tissue- and context-dependant manner. If control of these signalling molecules is lost, the functional programmes detailed above could lead to a variety of disease states.

1.4.3 Signalling in cancer

1.4.3.1 Overview

Deregulation of TGF-β family signalling is observed in an abundance of diseases. These can be associated with germline or somatic mutations of the pathway and its regulators (Wakefield and Hill, 2013; Wu and Hill, 2009). This highlights the need for a comprehensive understanding of the pathway as it may lead to therapeutic targets. For the purposes of this thesis, I will primarily focus on the role of Activin and TGF-β signalling in cancer.

For tumours to successfully develop, they must meet ten criteria as outlined by Hanahan and Weinberg, 2011. These include, but are not limited to, sustained proliferation whilst avoiding growth suppressive signals, restraint and evasion of the immune system, inducing angiogenesis and activating invasion and spread of cancer cells (Hanahan and Weinberg, 2011). As previously discussed, TGF-β and Activin are associated with many of these roles in normal adult cells as well as in developing embryos (see 1.4.1 and 1.4.2). Therefore, it is no surprise that aberrant signalling from these ligands allows tumours to develop. Deregulation of their roles in immune cell regulation, angiogenesis, cell growth and EMT can provide a perfect storm for cancer cells to develop and thrive.

1.4.3.2 TGF-β

TGF-β is a prominent player in tumourigenesis, however, its role is complicated. In the early stages of tumour development, TGF-β acts as a tumour suppressor, its growth suppressive signals prevent the sustained proliferation required for tumour development (Siegel and Massagué, 2003). However, as tumours progress, cancer cells can lose response to its anti-proliferative signals through malfunction of the

downstream cytostatic programme or loss of key TGF-β pathway mediators such as SMAD4 (Massagué, 2008). TGF-β continues to maintain its other functions such as immune suppression and EMT to promote tumourigenesis.

EMT is a critical process during tumour spread and metastasis, one that is tightly associated with TGF-β (Ye and Weinberg, 2015). TGF-β upregulates expression of transcription factors SNAIL, TWIST and ZEB (Nieto et al., 2016). The downstream transcriptional programme causes loss of epithelial junction proteins such as CDH1 and TJP1, whilst promoting expression of mesenchymal markers, such as vimentin, and remodelling actin alignment to generate stress fibres (Hao et al., 2019; Tsai and Yang, 2013). It is important to mention that EMT is not a binary process and cells are able to return to a more epithelial state. Such a process is also integral for tumourigenesis, allowing cells to embed in distal sites (Yang et al., 2020).

Immune suppression is another tumour promoting role of TGF-β. Suppression of effector T cells is a key driver of tumour development (Hanahan and Weinberg, 2011). As discussed, TGF-β works to diminish Th1 cells as well as promote survival and expansion of Treg lymphocytes. TGF-β strongly suppress an immunogenic response against cancers (Batlle and Massagué, 2019). Additionally, elevated levels of TGF-β correlate with immune cell exclusion in colorectal tumours, and such a phenotype strongly correlates with poor prognosis (Tauriello et al., 2018).

Finally, another role of TGF-β within the tumour microenvironment (TME), is the activation of cancer-associated fibroblasts (CAFs) (Calon et al., 2014). This population of cells has a variety of tumour promoting functional outputs, many of which are associated with TGF-β family pathway activity and transcriptional outputs (Calon et al., 2012). TGF-β family signalling and CAFs are a significant focus of this thesis, and CAFs are discussed in greater depth in Section 1.5.

1.4.3.3 Activin

Activin's roles in tumour development are less well-documented. However, many studies identify Activin A as a prognostic factor, and its activity is often associated with poor outcome. For example high circulating levels are associated with lower survival in colorectal and prostate cancer patients (Staudacher et al., 2017b, 2017a). Additionally, amplification of the gene harbouring the Activin subunits is observed in

certain cohorts of breast cancer patients (Seachrist and Keri, 2019; Sjöblom et al., 2006). Furthermore, levels of phosphorylated SMAD2 at the leading edge of tumours has been seen to correlate with levels of the Activin receptor ACVR1B (Landis et al., 2005).

One of the most well-established outputs of Activin A in cancer patients is the muscle wasting disorder cachexia (Toledo et al., 2016). Up to 50% of cancer patients can suffer from this disorder, depending on the type of cancer and its phenotype (Tisdale, 2009). The extent of weight loss and muscle wasting correlates with a poor prognosis (Tisdale, 2009). Activin plays a key role in this process. This makes sense due to its muscle growth modulatory roles in adult tissue homeostasis (discussed in Section 1.4.2.2). Blockade of its signalling through pharmaceutical inhibition of ACVR2B halts and even reverses muscle wasting in mouse models of lung and colon cancer (Toledo et al., 2016; Zhou et al., 2010).

A large proportion of evidence for Activin's oncogenic roles come from models of skin cancer. Work on these models shows that elevated levels of Activin A and its downstream signalling correlate with a pro-tumourigenic immune environment (Antsiferova and Werner, 2012). Specifically, Activin A caused an increase in Langerhans and Treg cells as well as a depletion of γδ T cells. Consequently, this promoted the formation and spread of tumours (Antsiferova et al., 2011). Additionally, work in a similar model showed a correlation between Activin A and tumour infiltrating macrophages. These macrophages exhibited gene expression patterns seen in tumour-associated macrophages (TAMs) that work to promote ECM degradation and angiogenesis, enhancing tumourigenesis (Antsiferova et al., 2017). Moreover, loss and gain of function studies revealed Activin to have a pro-metastatic effect in both human and mouse melanoma models. Melanoma cells overexpressing Activin A increased tumour growth and lung metastasis when injected into mice. This effect was not observed in immune-compromised mice, suggesting the oncogenic effect of mice may be through inhibition of anti-tumour immunity (Donovan et al., 2017).

Despite the evidence correlating Activin A with tumour progression, studying its role in tumourigenesis using genetic knockout models has proved difficult. Activin type I and type II receptor mutants cause embryonic lethality due to their essential role in early tissue patterning through the shared ligand NODAL (Gu et al., 1998; Song et al., 1999). Additionally, knockout of the ligand monomers *Inhba* and *Inhbb*

in mice result in death shortly after birth (Matzuk et al., 1995). Identifying the source of signalling or tissue-specific timed knockouts may be the best approach.

Finally, Activin, like TGF-β, has also been documented to activate CAFs within the tumour stroma in pancreatic cancer models. These CAFs then go on to promote tumourigenesis. (Cangkrama et al., 2020a). The roles of Activin and TGF-β family signalling in the function of CAFs is discussed more broadly in Section 1.5.

1.4.3.4 Therapeutic targeting of the pathway

These observations largely correlate TGF-β and Activin levels with more aggressive tumour progression. Therefore, it may be beneficial to target these ligands therapeutically. Indeed, there are a variety of therapeutic agents currently in development at a variety of stages. They largely target, with varying degrees of success, signalling by TGF-β ligand, specifically the ligand itself or its type I receptor TGFBR1 (Batlle and Massagué, 2019). The most notable of which is Galunisertib (Eli Lilly), a small molecule inhibitor of TGFBR1 kinase activity, as well as ACVR1B and ACVR1C. Use of this agent has shown modest therapeutic benefits in phase II clinical trials of prostate cancer patients and hepatocellular carcinomas (Faivre et al., 2014; Melisi et al., 2018; Tauriello et al., 2018). Various agents that target TGF-β ligand themselves are also in development. For example, 1D11 has demonstrated therapeutic success in pre-clinical mouse models (Rodríguez-Ruiz et al., 2019). Its humanised counterpart, Fresolimumab, has been shown to increase immune infiltrate in metastatic breast cancers (Formenti et al., 2018). Many other ligand and receptor targeted therapies are in development in pre-clinical as well as phase I/II clinical trials. These are more extensively reviewed in Batlle and Massagué, 2019.

However, development of these agents has been difficult. Small molecule inhibition of TGFBR1 resulted in cardiac toxicity in preclinical models (Anderton et al., 2011). Additionally, targeting of TGF-β ligands with monoclonal antibodies has shown similar cardiac toxicity (Mitra et al., 2020). Moreover, blockade of signalling may inhibit TGF-β's tumour suppressive effects in certain cancer contexts. Much of the research that justifies development of TGF-β targeted therapies are based on 'TGF-β' gene signatures and elevated SMAD signalling that could equally be caused by other family ligands. For example, expression of a manually curated TGF-β gene signature set in fibroblast populations correlated with lower immune cell infiltrate,

unresponsiveness to immunotherapy and poor patient survival in urothelial cancer patients (Mariathasan et al., 2018). Further work then went on to target TGF-β ligand in mouse models.

Whilst targeting TGF-β has had clear therapeutic benefits in a variety of models and clinical trials, it seems odd that less work has been done to investigate the therapeutic targeting of Activin signalling. Ligand traps for Activin A have been developed for treatment of solid tumours and cachexia, such as STM-434. However, this soluble ligand trap showed off-target inhibition of BMP9 and minimal effect on tumour growth in a cohort of 32 patients with solid tumours (Tao et al., 2019). More specific targeting of Activin ligands may work to supplement or surpass the benefits seen in TGF-β therapies. In any case, targeting the source of each of these ligands in tumours may also be a prudent approach. One cell population that is both abundant within the tumour stroma and has strong associations with TGF-β and Activin signalling is the CAF cell type (Calon et al., 2014; Cangkrama et al., 2020a).

1.5 Cancer-associated Fibroblasts

1.5.1 CAF overview

CAFs are a highly heterogeneous population of non-transformed cells with a plethora of different functions. They are often the most populous cell type within the tumour stroma (Cohen et al., 2017). Certain CAF subtypes are responsible for tumour-promoting functions, including: remodelling the extracellular matrix (ECM), promoting angiogenesis, modulating the immune system and promoting cancer cell invasion (Östman and Augsten, 2009) (see Section 1.5.4). Many of these functions are dependent on CAFs' ability to mechanically manipulate their environment (Park et al., 2020a). CAFs can also elicit these functions through the secretion of a battery of cytokines that act in autocrine and paracrine manners to influence their own behaviour and that of other stromal cell populations (Cirri and Chiarugi, 2012).

Due to their heterogeneity, accurately defining and identifying CAFs is not straightforward. There is no universal or unique marker that distinguishes CAFs from other cell types (Östman and Augsten, 2009). Classically, a CAF is any morphologically elongated cell within a tumour that possesses mesenchymal properties combined with a complete lack of epithelial, endothelial and leukocyte

markers. Additionally, they do not harbour any of the genetic mutations seen in cancer cells (Sahai et al., 2020). One mesenchymal marker routinely used in the identification of CAFs is αSMA (Öhlund et al., 2017). Additional markers include, but are not limited to, NG2, fibroblast activation protein (FAP), PDGFRβ and fibroblast specific protein (FSP1) (Calon et al., 2014). However, it is becoming increasingly apparent that these specific markers identify distinct sub-populations with unique functions (Sahai et al., 2020). Because of the lack of a 'true' CAF marker, they are frequently identified through their functional properties. Specifically, their propensity for aggressively degrading and remodelling the extracellular matrix (Park et al., 2020a).

1.5.2 CAF origin

Determining the true origin of CAFs is difficult. This is because no unique marker exists for CAFs and have multiple proposed cells of origin. This makes accurate lineage tracing studies problematic. Despite this, CAFs have been shown to arise from various cell types. These include resident fibroblasts, pericytes and mesenchymal stem cells (MSCs) (Karnoub et al., 2007; Puram et al., 2017; Sahai et al., 2020). All of these cell types are morphologically similar and express some of the same markers including PDGFRβ, αSMA and FAP (Augsten, 2014). Generally, however, it is accepted that the large proportion of CAFs originate from tissue-resident fibroblasts. Microarrays have been employed to identify a CAF gene expression profile. These show that, as cancers progress, resident fibroblasts adopt an increasingly 'activated fibroblast' expression profile (Paulsson and Micke, 2014). In addition to the cell types mentioned above, CAFs have also been documented to arise from adipose and endothelial cells (Alt et al., 2010; Zeisberg et al., 2007). No matter the cell of origin, specific signals and mechanisms have been identified that work to activate cells towards a more CAF-like phenotype.

1.5.3 CAF activation

A huge range of signals can activate resident fibroblasts to become CAFs; specifically, Notch signalling through contact between fibroblasts and cancer cells

(Strell et al., 2019). Additionally, NF-κB and JAK-STAT activation via IL-1 and IL-6 respectively work to promote a CAF phenotype (Erez et al., 2010; Sanz-Moreno et al., 2011). Furthermore, environmental changes and stresses work to generate CAF formation. Specifically, an increase in tissue stiffness and tension, frequently seen in cancers, induces SRF and YAP-TEAD-mediated transcriptional profiles indicative of CAFs (Calvo et al., 2015).

One particularly prominent signal that activates CAFs is TGF-β family signalling, as with myofibroblasts during fibrosis. Active SMAD2/3 signalling has been shown to be critical for the activation of fibroblasts to an activated αSMA positive CAF phenotype (Evans et al., 2003). Blockade of TGF-β signalling through overexpression of BAMBI, a TGF-β family receptor with no kinase activity, in MSCs blocked their capacity to differentiate to CAFs via TGF-β induction (Shangguan et al., 2012). As discussed, Activin is also able to activate SMAD2/3 signalling. It therefore follows that if Activin is available within stromal compartments that it too may be able to induce activation of fibroblasts to CAFs. Indeed, this has been documented. In a mouse model of skin cancer, Activin expression correlated with an increase in CAF activation through elevated mDia2 protein transcription via SMAD2. mDia2 is a member of the diaphanous-related formin family which are responsible for actin-nucleation. This signalling also resulted in an elevation of a pro-tumourigenic matrisome and CAF secretome (Cangkrama et al., 2020a).

Irrespective of the responsible signal, once activated, CAFs undergo dramatic cytoskeletal changes including increased focal adhesions and stress fibre formation, contributing to their contractility (Calvo et al., 2013; Öhlund et al., 2014). This is, in part, orchestrated by an elevation in CDC42EP3 activity, resulting in co-ordination and alignment of an Actin-Septin network within CAFs that works to increase their tension and contractile properties (Calvo et al., 2015). Additionally, they synthesise many ECM components, such as fibronectin and collagen (Attieh et al., 2017; Nguyen et al., 2019). Additionally, production of lysyl oxidase-like enzymes by CAFs has been shown to cross-link ECM components, specifically collagens (Emon et al., 2018; Nguyen et al., 2019). A combination of these factors serves to further increase tumour stiffness. This elevation in stiffness sustains CDC42 signalling and nuclear YAP activation, maintaining CAFs in a self-sustaining activated state (Calvo et al., 2015). This activation process is similar to that of myofibroblasts. Myofibroblasts are activated from tissue-resident fibroblasts, through many of the same signals

described above, during wound healing (Kalluri and Zeisberg, 2006). Once activated, they too lay down ECM components to heal the insult. However, once the wound has been repaired, numbers of myofibroblasts diminish dramatically through programmed cell death (Hinz, 2016). CAFs elicit this same function, specifically in the context of a tumour (Sahai et al., 2020). Cancer itself has long been described as 'the wound that never heals' (Flier et al., 1986). And so, due to the sustained stiffness of tissue, numbers of activated CAFs remain high throughout tumourigenesis, where they perpetually elicit their tumour promoting functions.

1.5.4 Functions of CAFs within the tumour stroma

As mentioned, certain CAF subtypes are responsible for many tumour promoting functionalities. These include, but are not limited to, ECM remodelling, promoting cancer cell invasion, enhancing angiogenesis and modulating the immune system (Figure 1.5) (Park et al., 2020a). It is important to note that different CAF subtypes will elicit each of these functions to varying degrees. Certain populations may be more immune suppressive and others can more aggressively remodel the ECM (Bartoschek et al., 2018).

1.5.4.1 ECM remodelling

As discussed, one of the main functions of CAFs is their ability to remodel the ECM. They do so by secreting various degradative factors, such as matrix metalloproteinases (MMPs), including MMP9, and laying down more ECM components including collagens (Paulsson and Micke, 2014; Stuelten et al., 2005). This remodelling increases the stiffness of tumours dramatically. In doing so, this creates a less permissive environment for therapeutics and immune populations to penetrate the tumour, resulting in poorer prognosis (Mohammadi and Sahai, 2018). Furthermore, CAFs are responsible for enhancing tumour stiffness by cross-linking components of the ECM. This is orchestrated by secretion of lysyl oxidase enzymes that directly crosslink these proteins (Pickup et al., 2013). Additionally, as mentioned above, this increased stiffness promotes YAP/TAZ transcriptional outputs in CAFs and cancer cells. Such a transcriptional programme enhances EMT and metastasis in cancer cells (Dupont et al., 2011). The ECM remodelling capacity of CAFs is tightly

associated with Rho/ROCK signalling; greater levels of phosphorylated myosin light chain (PMLC), a readout of pathway activity, correlate with greater degrees of matrix remodelling and cancer cell invasion (Calvo et al., 2015). Specific subpopulations of CAFs, such as those with high αSMA expression, are particularly responsible for eliciting these functions (Öhlund et al., 2017).

1.5.4.2 Cancer cell invasion

CAFs are also responsible for promoting cancer cell invasion. The ECM remodelling described above creates tracks in which cancer cells can invade and metastasise (Gaggioli et al., 2007). Furthermore, the degree of alignment of collagen that CAFs lay down correlates with enhanced cancer cell invasion, by creating permissive 'superhighways' that direct cancer cell migration (Park et al., 2020b). Additionally, contact signalling between CAFs and cancer cells through Eph-Ephrin signalling has been shown to promote invasion (Astin et al., 2010). In a similar fashion, contact between CAF-expressed N-cadherin and cancer cell-expressed E-cadherin allows CAFs to mechanically pull cancer cells behind them (Labernadie et al., 2017). Moreover, cytokines produced by CAFs can promote invasion. Specifically, HGF has been shown to enhance invasion of cancer cells through Rho/Rac signalling (De Wever et al., 2004). CAFs also permit cancer cells to embed themselves at metastatic sites. Specifically, they produce the ECM component tenascin C, expression of which correlates with enhanced metastatic potential of cancer cells (Oskarsson et al., 2011).

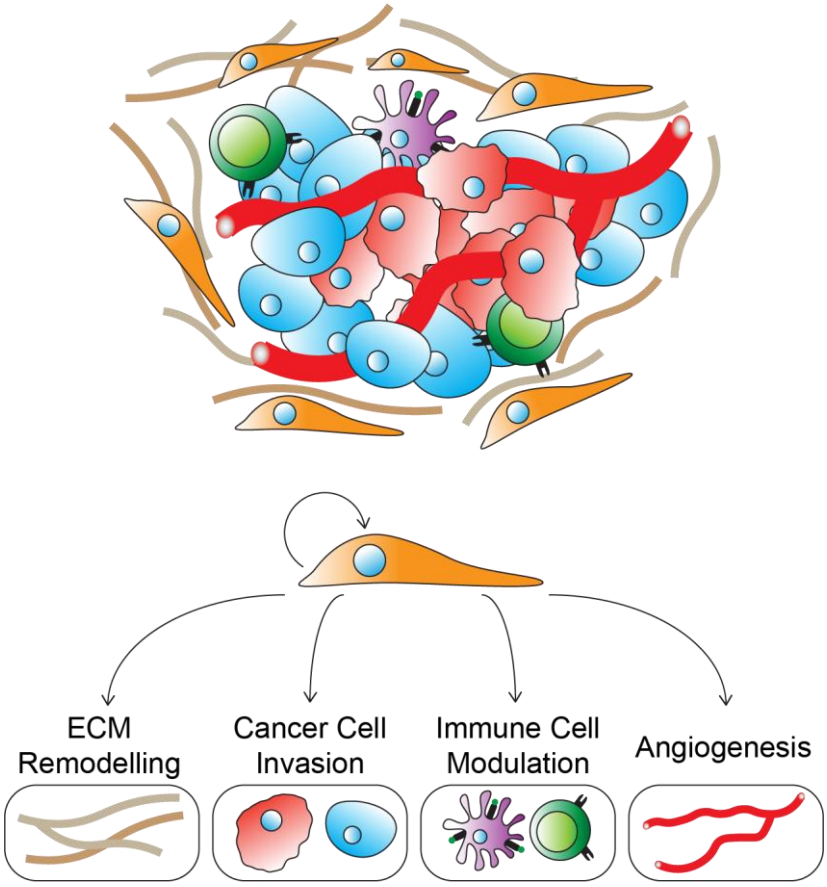

Figure 1.5. CAF functionality within the tumour stroma. CAFs exist within the tumour stroma alongside cancer cells, blood vessels, immune populations and components of the ECM. They elicit the annotated functions via secretion of a range of cytokines.

1.5.4.3 Immune cell modulation

CAFs also promote tumourigenesis through modulation of the immune system. Specifically, they prevent the infiltration of immune populations and, generally, create an immune suppressive phenotype (An et al., 2020). This is achieved both mechanically, physically blocking infiltration, or chemically through soluble factors. For example, ECM deposited by CAFs can generate a barrier around the tumour. Such a barrier creates a less permissive environment in which immune populations can infiltrate, this is compounded by increased tissue stiffness (Hartmann et al., 2014). This obstructive ECM composition is associated with FAK activity, inhibition of which has been shown to increase T cell infiltration (Jiang et al., 2016). Additionally, CAFs are able to influence the phenotype of the local immune cells. Primarily, they generate an immune suppressive environment and inhibit the cytotoxicity of T cells (Monteran and Erez, 2019). For example, CAFs have been

shown to generate an immune suppressive and tumour promoting macrophage phenotype through expression of SDF-1 in pancreatic and breast cancer development (Zhang et al., 2015). In both cases, this phenotype correlated with poorer prognosis (Gok Yavuz et al., 2019; Zhang et al., 2017). Additionally, CAFs influence T cells within the tumour stroma, promoting a more suppressive phenotype. Specifically, CAFs promote Treg and Th2 phenotypes through secretion of CXCL12 and thymic stromal lymphopoietin (TSLP) respectively (Costa et al., 2018; De Monte et al., 2011). Treg and Th2 phenotypes correlate with poor prognosis in cancer (Dushyanthen et al., 2015). Certain CAF sub-populations are more proficient at modulating the immune system. For example, CAFs that secrete CXCL12 promote Treg differentiation and survival (Costa et al., 2018).

1.5.4.4 Angiogenesis

Finally, CAFs have been shown to promote tumourigenesis by enhancing angiogenesis. Stromal cells, including CAFs, secrete a variety of pro-angiogenic cytokines. These include vascular endothelial growth factors (VEGFs) primarily VEGFA (Fukumura et al., 1998). VEGFA works to promote angiogenesis through the survival and migration of endothelial cells. Additionally, it promotes microvascular permeability, allowing cancer cells to more easily extravasate into the bloodstream where they can metastasise to distal sites (Shibuya and Claesson-Welsh, 2006). Another pro-angiogenic cytokine secreted by CAFs is IL-6. IL-6 production by CAFs correlated with enhanced angiogenesis during colon cancer. Blockade of IL-6, using an anti IL6R antibody, suppressed angiogenesis, resulting in better prognosis in a model of colon cancer (Nagasaki et al., 2014). Furthermore, CAFs can promote angiogenesis through their ECM remodelling capacity. Secretion of MMPs and the ECM protein fibronectin by CAFs creates tracks in which endothelial cells can penetrate tumours (Kalluri and Zeisberg, 2006).

1.5.4.5 CAF plasticity

As outlined above, a variety of CAF subtypes exist that can elicit a range of oncogenic functions within the tumour stroma. This raises the question of whether CAFs are plastic, allowing them to switch between these distinct functional subtypes, recent research suggests this may be a possibility. For example, stellate cells

isolated from PDAC mouse models can be differentiated into distinct CAF subtypes including myofibroblastic CAFs (with strong ECM remodelling capabilities) or inflammatory CAFs (Biffi et al., 2019). JAK signalling inhibition in pancreatic tumour bearing mice shifted these inflammatory CAFs to a more myofibroblastic subtype, suggesting that CAF populations are indeed plastic (Biffi et al., 2019; Pereira et al., 2019). Additionally, CAFs can differentiate into different subtypes depending on the type of ECM they are exposed to; for example, high tissue stiffness generates CAFs with high αSMA and low FAP expression, whilst the inverse is true when they are exposed to a less stiff environment (Avery et al., 2018; Sahai et al., 2020). Gene expression profiling and functional assays indicated that high αSMA CAFs are more contractile, whilst low αSMA exhibited greater gelatinase activity (Avery et al., 2018). Further work showed that changing a CAFs environment from high to low stiffness causes them to switch between these subtypes, highlighting the plasticity of CAFs (Avery et al., 2018). Given their plasticity, one prudent approach may be to therapeutically target CAFs to a less tumourigenic subtype.

1.5.5 Therapeutically targeting CAFs

Intuitively, given the pro-tumourigenic functions of CAFs, it follows that removing them from the stroma would result in a better prognosis. However, two studies have shown that their depletion results in enhanced tumour aggressiveness and poorer prognosis. One study demonstrated that stromal CAF depletion resulted in enhanced levels of angiogenesis, increased proliferation, and poorly differentiated tumours in a mouse model of pancreatic cancer (Rhim et al., 2014). This suggests that CAFs can also restrain tumour growth. Addition of an anti VEGF receptor (VEGFR) antibody partially reversed this phenomenon (Rhim et al., 2014). A separate study also showed that induced αSMA-positive cell depletion resulted in more aggressive and less differentiated tumours. Both at precursor and late stages (Özdemir et al., 2014). In this case, depletion resulted in an increase in FoxP3 positive regulatory T cells and an immune suppressive environment. This same study also correlated fewer numbers of myofibroblasts with lower survival in PDAC patients (Özdemir et al., 2014).

This paradoxical finding further indicates that great heterogeneity exists amongst CAFs. Specific subpopulations may have tumour-promoting or suppressive roles. Therefore, it may be a more prudent approach to target certain signals to shift CAFs towards the tumour suppressive phenotype or inactivate them to their normal state. One particularly pro-tumourigenic signal associated with CAFs is TGF-β family signalling.

1.5.6 TGF-β family signalling and CAFs

As mentioned in Section 1.5.3, TGF-β signalling is responsible for activating resident cells to CAFs within the tumour stroma. Such activation keeps CAFs in a self-sustained state of activation, perpetually propagating their pro-tumourigenic outputs (Sahai et al., 2020). It is important to highlight that these outputs, in certain contexts, could be caused by Activin signalling, since they can activate the same intracellular mediators despite engaging different receptors (see Section 1.4.3.4). CAFs themselves have been shown to secrete Activin A in colorectal cancer. Secretion of Activin A was associated with an elevation in EMT and cancer cell invasion (Bauer et al., 2020). Additionally, as discussed, one of CAFs primary tumour promoting roles is modulating the immune system. It is unsurprising that one secreted cytokine associated with this output is TGF-β, given its own potent immune cell modulating capacity. CAF-sourced TGF-β has recently been implicated in immune cell exclusion. Specifically, high expression of a TGF-β transcriptional profile was associated with absence of cytotoxic T cells in colon and prostate cancer, resulting in poorer survival (Mariathasan et al., 2018; Tauriello et al., 2018). In the colorectal cancer study, administration of Galunisertib, a small molecule inhibitor of TGFBR1, partially reversed this phenotype when combined with checkpoint inhibitor therapy (Tauriello et al., 2018).

As discussed in Section 1.4.3.4, targeting TGF-β family signalling may have therapeutic benefits in cancer treatment. Such targeting may lead to reprogramming of CAFs, reducing their oncogenic influence over tumours. Since the removal of CAFs correlates with more aggressive tumours, this may be a more nuanced and successful approach. Therefore, further study of the nature of TGF-β family signalling is of great interest.

1.6 Work Leading to my Project

1.6.1 Comparative study of TGF-β family signalling dynamics

In the work described in this thesis, I wanted to determine how TGF-β family ligands cause the pathway activation and functional outputs observed in disease contexts based on their signalling dynamics. I was also interested in understanding the underlying mechanisms regulating these dynamics. As discussed in Section 1.3, cells become unresponsive to TGF-β ligand, in terms of PSMAD induction, during sustained exposure to ligand (Vizán et al., 2013). Conversely, other family ligands, namely Activin and BMP4, generate high levels of PSMAD induction over sustained periods (Miller et al., 2019). This finding presents us with a paradox when certain diseases exhibit high levels of TGF-β coupled with prolonged pathway activity and associated functional outputs (Landis et al., 2005; del Pozo Martin et al., 2015; Walton et al., 2017). How do cells maintain sustained levels of PSMAD activity if they become unresponsive to circulating TGF-β ligand? I hypothesised that there were two possible explanations:

1. Another family ligand is responsible for perpetuating the active signal.
2. There is re-wiring of the mechanisms responsible for maintaining the established cellular response to TGF-β ligand.

Each of these ideas are discussed in this thesis. I also explored how one may be able to track TGF-β family receptors over time. This was of interest as receptor localisation was shown to be responsible for the signalling dynamic profiles for each family ligand (Section 1.3.2). My projects grew out of work by a previous graduate student in the lab, Daniel Miller. Using a candidate approach, he discovered that CAF populations from a mouse model of breast cancer secrete Activin A/B and not TGF-β, suggesting that Activin may be propagating TGF-β family signalling and functionality during tumourigenesis. In addition, using a genome-wide siRNA screen, he discovered that the ESCRT family of proteins were responsible for regulating the proper signalling output of cells in response to TGF-β (Miller et al., 2018).

1.6.2 Aims

The overall aim of this thesis is to determine, based on the known signalling dynamics of the TGF-β family ligands, why and how family signalling output and downstream functionality is observed in disease contexts. The specific aims of my PhD were as follows:

1. Knockout expression of Activin A and B to determine their role in CAF functionality.
2. Determine whether the ‘re-wiring’ of the TGF-β pathway by depletion of the ESCRT machinery affects the functional output of the pathway.
3. Develop a method of tracking TGF-β family receptors to determine the molecular basis for the distinct signalling dynamic profiles for different TGF-β family members.

Chapter 2. Materials and Methods

2.1 Molecular Biology

The following solutions were provided by Cell Services at the Francis Crick Institute: 20% SDS, 1 M Tris HCl (pH 7.5 and 8.0), 0.5 M EDTA (pH 6.0), 1 M and 5 M NaCl, Luria broth (LB), antibiotic-containing LB agar plates, foetal bovine serum (FBS) and 1 M KCl.

2.1.1 Overview of construct generation

PCR was used to amplify a genomic region of interest from source DNA. PCRs were designed to insert flanking restriction digest sites. These fragments were digested alongside a plasmid backbone before a ligation reaction was conducted. Resulting reactions were transformed into competent bacteria and expanded. DNA was extracted from bacterial cultures and sequenced to verify the plasmid sequence. Glycerol stocks of constructs were subsequently made. For sgRNA plasmids, 5' and 3' sgRNA oligos were ordered from Thermo Fisher Scientific (Thermo) and annealed before ligation into pSpCas9(BB)-2A-GFP (PX458) backbones. This process is described in detail in Section 2.2.2. The following plasmids were used for stable and transient transfections, as template DNA or as backbones for downstream ligation of PCR fragments:

Construct	**Source**
pcDNA3.1-Hygro(+)	Thermo
pcDNA3.1-ACVR1B-KPN1	Constructed
pcDNA3.1-ACVR1B-HALO (C-terminal)	Constructed
pcDNA3.1-ACVR1B-HALO (N-terminal)	Constructed
pcDNA3.1-FST-IRES-mCherry	Daniel Miller, Caroline Hill Lab
pHTC HaloTag CMV-neo Vector	Promega
pPB transposase	Louise Richardson, Caroline Hill Lab
pPB mCherry CAAX	Sanger
px458	Addgene
px458-Acvr1b sgRNA	Constructed
px458-Inhba sgRNA	Constructed

px458-Inhbb sgRNA	Constructed

2.1.2 DNA Extraction

2.1.2.1 QuickExtract DNA Extraction

Cells from a confluent 6-well plate were trypsinised and pelleted in Eppendorf tubes. QuickExtract DNA Extraction Solution 1.0 (Lucigen) (100 µl) was added to cell pellets and vortexed for 10 seconds. The samples were then incubated at 65 °C for 1 min before a further vortex for 15 seconds. The samples were then incubated at 98 °C for 2 min before a final vortex for 30 sec.

2.1.2.2 Salting out DNA for extraction

This method was carried out as described in Miller et al., 1988. Cells from a confluent 6-well plate were trypsinised, pelleted and re-suspended in 3 ml of nuclei lysis buffer (NLB).

NLB (pH 8.2)

Tris-HCl	10 mM
NaCl	500 mM
Na_2EDTA	2 mM

Cell suspensions were then shaken overnight, with 0.1 ml of 20% SDS and 0.5 ml of protease K solution, at 37 °C to digest the cells.

Protease K solution (10 ml)

Protease K	1 mg
SDS	1%
EDTA	2 mM

The following day, 1 ml of 6 M NaCl was added to the suspension which was then shaken vigorously for 15 sec. Suspensions were then spun in a swinging bucket centrifuge (Beckman Coulter) at 2500 rpm for 15 min. The supernatant was transferred to a fresh tube before adding 6 ml of absolute ethanol. Tubes were then

inverted until DNA precipitated. DNA was picked out using a pipette tip and placed in an Eppendorf with 200 µl of TE buffer.

TE buffer (pH 7.5)

Tris-HCl	10 mM
Na_2EDTA	0.2 mM

DNA was dissolved whilst shaking in a Thermomixer (Eppendorf) at 37 °C for 2 h. DNA concentration was determined by measuring optical density (OD) using a NanoDrop Spectrophotometer (NanoDrop).

2.1.3 Polymerase Chain Reaction

A QIAGEN Taq Polymerase kit was used for PCR reactions. These were conducted in a Veriti 96-well Thermal Cycler (Applied Biosystems).

QIAGEN Taq Mix

PCR buffer	1X
dNTPs (Invitrogen)	0.2 mM
Forward primer	0.4 µM
Reverse primer	0.4 µM
Taq polymerase	0.625 U
DNA template	10 ng
Distilled water	Up to 25 µl

PCR conditions:

Cycle 1.	94 °C for 2 min
Cycles 2 to 36.	94 °C for 30 sec, 55 °C for 30 sec, 72 °C for 1 min.
Cycle 37.	72 °C for 5 min
Cycle 38.	4 °C indefinitely

PCR primers used for purposes of subcloning are detailed below:

Construct	Primers	Backbone	Restriction site
ACVR1B-KPN1	1st cycle: Fwd: TCGCCGGCAGCGGCGGGTCCG GTACCGGGCCCCGGGGGATCCAGG Rev: CCTGGATCCCCCGGGGCCCGG TACCGGACCCGCCGCTGCCGGCGA 2nd cycle: Fwd: GGCCAAGCTTATGGCGGAGTCGG CCGGA Rev: GGCCCTCGAGTTAAATCTTCACAT CTTC	pcDNA3.1-Hygro	HindIII/ Xho1
ACVR1B-HALO (C-terminal)	Fwd: GGCCGAATTCATGGCGGAGTC GGCCGGA Rev: GGCCCTCGAGAATCTTCACATC TTC	pHTC HaloTag CMV-neo Vector	EcoR1/ Xho1
ACVR1B-HALO (N-terminal)	Fwd: GGCCGGTACCGGATCCGAAAT CGGTACT Rev: GGCCGGTACCACTTCCACCGCC TCCAGAACCTCCTCCACCACCGGA AATCTCCAGAGT	pcDNA3.1-ACVR1B-WT	Kpn1

2.1.4 Agarose gel electrophoresis

Following PCR, products were run on an agarose gel (1% w/v). Gels were prepared by dissolving agarose (Invitrogen) in 1X TAE buffer and heating in an 800W microwave. The liquid was briefly cooled and 0.5 µg/ml of ethidium bromide was

added. The liquid was poured into a sealed gel tray with a comb and left to solidify. 1X TAE was poured into the gel tank, before individual wells were loaded with PCR products or plasmid DNA alongside a DNA ladder (New England Biosciences, NEB). Gels were run at 100 V for 15–45 minutes. Gels were then imaged under ultraviolet illumination using a UVP 2UV Transilluminator. If the PCR product was to be used for subsequent ligation reactions, bands were excised, whilst under a low power UV lamp, and the DNA was extracted using a QIAquick Gel Extraction Kit (QIAGEN) according to the manufacturers' instructions.

2.1.5 Restriction digest and ligation reactions

Digestion of plasmid DNA and PCR products was conducted with restriction endonucleases from NEB. Reactions were 40 µl mixes of recommended 1X NEB buffer (depending on endonuclease used), restriction endonucleases at a final concentration of 1 U/µg of DNA as well as the template DNA or PCR product. These mixes were incubated in a Thermomixer at 37 °C for 1 h. Afterwards, a further 1 U/µg of DNA of restriction endonucleases was added to the reaction mixture. Reactions were incubated at 37 °C for a further hour. For restriction digests containing plasmid backbones, 1 U/µg of DNA of Calf Intestinal Alkaline Phosphatase (CIP, NEB) was also added for the second hour of incubation at 37 °C. This removed 5' phosphate residues to prevent re-ligation of the plasmid DNA. Digested plasmids and PCR products (insert DNA) were mixed at a molar ration of 1:3 (plasmid:insert DNA) with 1 µl of T4 DNA Ligase (NEB) and 1X Ligase Buffer (NEB). This mixture was incubated at 16 °C overnight.

2.1.6 Transformation and bacterial expansion

Plasmid DNA and ligation reactions were transformed into competent TG1 cells to amplify the DNA for downstream mammalian cell transformation or sequencing reactions. Briefly, 50 µl of TG1 cells were thawed on ice and mixed with 50 ng of plasmid DNA or 5 µl of ligation reactions. This was incubated on ice for 20 minutes. Cells were then heat-shocked at 42 °C for 45 seconds and placed on ice for 2 min. LB (450 µl) was added and placed in a shaking thermomixer at 37 °C for 1 h. Suspensions were centrifuged at 8,000 rpm using a benchtop centrifuge (Eppendorf). Four-hundred and fifty microlitres of supernatant was removed and the

pellet was re-suspended in the remaining 50 µl. The suspension was then plated out on LB agar plates containing appropriate antibiotic overnight at 37 °C. Individual colonies were then picked with a pipette tip and placed in 10 ml of LB (Miniprep) or 250 ml of LB (Maxiprep). Cultures were shaken overnight at 37 °C. For Minipreps, DNA was extracted from cultures using a QIAprep Spin Miniprep Kit (QIAGEN). For Maxipreps, DNA was extracted using a GenElute HD Plasmid Maxiprep Kit (Sigma Aldrich, Sigma). Each was performed according to the manufacturers' instructions. In both cases, DNA was re-suspended in distilled water and quantified by measuring the OD at an absorbance wavelength of 260 nm using a NanoDrop Spectrophotometer (NanoDrop) and using an extinction coefficient of 0.020 $(\mu g/ml)^{-1}$ cm^{-1}.

2.1.7 Sequencing

To verify plasmid or cellular DNA sequences, Sanger sequencing reactions were conducted.

Sequencing mix

DNA template	500 ng
BigDye Terminator (BDT) Applied Biosystems)	8 µl
Sequencing primer	20 ng
Distilled water	Up to 20 µl

Sequencing mixtures were made in PCR tube strips of eight and run in a Veriti 96-well thermal cycler under the following conditions:

Cycle 1-30. 96 °C for 10 sec, 50 °C for 5 sec and 60 °C for 4 min
Cycle 31. 60 °C for 1 min
Cycle 32. 4 °C indefinitely

Unincorporated dye terminators were removed using a DyeEx 2.0 Spin Kit (QIAGEN) according to manufacturers' instructions. The resulting pellet was dried at 42 °C in a SpeedVac centrifuge (Thermo) for 20 min. Sanger sequencing was then conducted

by the Equipment Park at the Francis Crick Institute. Returned sequences were analysed using 4Peaks software.

2.1.8 RNA work

2.1.8.1 RNA extraction

One millilitre of Trizol was added to cells seeded on single wells of a 6-well plate. This was left for 3 min until cells were lysed. The mixture was transferred to a fresh Eppendorf before addition of 200 µl of water-saturated chloroform. The mixture was vortexed to mix thoroughly. The tube was centrifuged at 4°C at 17,000 x g for 15 minutes in a benchtop centrifuge. The aqueous solution was then taken (approximately 500 µl) and added to a fresh Eppendorf with an equal amount of isopropanol. This mixture was then precipitated on ice for 10 min. The suspension was spun as before. The supernatant was discarded and the pellet was washed in 1 ml of 70% ethanol. The suspension was centrifuged for a third time in the same way. The supernatant was discarded and the pellet was left to dry at room temperature. Samples were then re-suspended in 50 µl of distilled water and warmed at 55°C in a heating block (Eppendorf) to aid complete resuspension. Concentrations of all samples were quantified by measuring the OD at 260 nm using a NanoDrop Spectrophotometer and using an extinction coefficient of 0.025 $(\mu g/ml)^{-1}$ cm^{-1}.

2.1.8.2 cDNA Synthesis

cDNA was synthesised from 2 µg of RNA template using the AffinityScript cDNA Synthesis Kit (Agilent). The following mix was made up for each synthesis reaction in a strip of 8 PCR tubes:

10x AffinityScript RT Buffer	2 µl
100mM DTT	2 µl
100 ng/µl Random 9-mer primers	3 µl
25mM dNTPs	0.8 µl
AffinityScript Reverse Transcriptase enzyme	1 µl
RNAsein enzyme	0.5 µl
Distilled water	Up to 20 µl

RNA template	2 µg

PCR tubes were then placed in a Veriti 96-well thermal cycler under the following conditions:

Cycle 1. 25 °C for 5 minutes
Cycle 2. 42 °C for 15 minutes
Cycle 3. 55 °C for 15 minutes
Cycle 4. 95 °C for 15 minutes
Cycle 5. 4 °C indefinitely

One hundred and eighty microlitres of distilled water was then added to each reaction prior to assaying via quantitative real-time PCR (qRT-PCR).

2.1.8.3 qRT-PCR

qRT-PCR reactions were made for separate genes and samples in distinct wells of a 96-well MicroAmp Fast Optical plate (Applied Biosystems). Reactions (10 µl) were made up as follows:

Syber Green (Invitrogen)	5 µl
3 µM forward primer	1 µl
3 µM reverse primer	1 µl
cDNA	2 µl
Distilled water	1 µl

Wells were made up in triplicate per target gene and the plate was sealed with MicroAmp Optical Adhesive Film (Applied Biosystems). Plates were then briefly centrifuged using a benchtop plate centrifuge. Plates were then loaded into a QuantStudio 7 Flex qRT-PCR machine (Applied Biosystems). During each round of a 40-cycle PCR, Sybr Green from the reaction mix is incorporated into the PCR product, generating fluorescence. Levels of fluorescence are measured for each gene and sample and the cycle was calculated at which each well reached a fluorescence threshold (Ct value). Every sample had a Ct measure for *GAPDH* which

was used as a reference value. Relative levels of mRNA for the target genes were then calculated as follows:

Relative mRNA expression = $2^{(GAPDH\ Ct) - (target\ gene\ Ct)}$

mRNA levels for the target genes across all samples were then normalised to a control sample. This generates a value for relative fold change expression for each gene between samples.

Primers were designed using PrimerBlast software with gene inputs from NCBI. A table containing all primers used for qRT-PCR throughout this thesis is below:

Target	**Forward**	**Reverse**
Acvr1b-HALO	TGGAAGTGGTACCGGGCC	GGGGACCCTGAGGTCAAT
Col4a3	GAAAGGGCAACCAGGTCGAA	CAGTGGTTCCAGGATAGCCC
Cxcl5	GCCCCTTCCTCAGTCATAGC	AGCTTTCTTTTTGTCACTGCCC
Gapdh	TCTTGTGCAGTCCAGCCT	CAATATGGCCAAATCCGTTCA
Fst	TGCAACTCCATCTCGGAAGA ACGG	GCCCAAAGGCTATGTCAACAC TGA
Hgf	TAGGGATCAGTCTGCTCGAA	GAAGGCCTTGCAAGTGAACG
Inhba	GGGACCCGAAAGAGAATTTGC	TCCTCTCAGCCAAAGCAAGG
Inhbb	CTTTGCAGAGACAGATGGCCT	GCCTGCACCACGAATAGGTT
Mapk13	CGGTGTGCTCGGCCAT	GGTGCATGTGCTTCAAGAGC
Mmp3	TTGTTCTTTGATGCAGTCAGC	GATTTGCGCCAAAAGTGC
Nptx2	AGACAGAGAGCACGCTGAAC	TTGAATGCACTGTTGCCTCG
Pcolce2	TGCAGATACGACTACGTGGC	CTCAGACACGATCGGCACAG
Plxnc1	AGTACCTGCGAGAGGGATGT	TATGTTTTGCCCACCGCTGA
Ptx3	CGTGCATCCTGTGAGACCAA	TAGGGGTTCCACTTTGTGCC
Spp1	AATCTCCTTGCGCCACAGAA	GGACATCGACTGTAGGGACG
Stard8	GTTGACAACGGCTAAGCAGC	CCAGGGGGAATACACCTTCTTC
Vegfa	GGCCTCCGAAACCATGAACT	CTGGGACCACTTGGCATGG
Vps28	CTACTCCTGGTGTTGGAGCC	GTCATACTTCTCCCGCTCCC

2.1.8.4 RNAScope coupled to Immunofluorescence

RNAScope was conducted on sections from FFPE tumours. Unless otherwise stated, all buffers used as part of this protocol were provided in the RNAScope kit. Slides were baked at 60°C for 1 h. Sections were then deparaffinised by bathing them in xylene for two sets of 5-min washes. Fresh xylene was used for each wash. Sections were then rehydrated by incubating slides in 100% ethanol for 2 sets of 5-min washes before a 70% ethanol wash. Finally, slides were washed for at least 5 min in distilled water. Subsequent steps were conducted using RNAScope reagents (Advanced Cell Diagnostics, ACD). A hydrophobic barrier was drawn around sections. RNAScope hydrogen peroxide was added to deparaffinised sections for 10 min. Slides were then washed twice in distilled water, using fresh water each time. Heat-mediated antigen retrieval (HMAR) was then conducted. Two containers were placed in a steamer (Russel Hobbs), one containing 200 ml of distilled water and the other 200 ml of 1X Target Retrieval Reagent. The steamer was turned on to allow the contents of each container to reach boiling point. Slides were then added to distilled water for 10 sec to acclimatise them before placing them in the Target Retrieval Reagent for 15 minutes. Following HMAR, the container was left under a barely running tap to slowly cool and end the reaction. Slides were transferred to absolute ethanol for 3 min and then left to air dry. RNAScope Protease Plus was added to sections and slides were placed in a rack in a HybeZ oven at 40 °C for 24 min. Slides were then washed in distilled water. Subsequently, probe hybridisation was conducted. Probes were added to sections and slides were placed in a rack in the HybeZ oven at 40°C for 2 h.

RNAScope probes used

Target	Cat no.
Inhba	455871
Inhbb	475271
Ubc (positive control)	310779
Dapb (Negative control)	310043

Slides were then washed twice in 1X wash buffer for 2 min per wash. Fresh wash buffer was used each time. Amplification probes were subsequently added over various rounds to enhance the downstream signal detection. Between each amplification step, slides were washed twice in 1X wash buffer as previously described.

RNAScope amplification cycles

Probe	Temperature	Time
AMP1	40 °C	30 min
AMP2	40 °C	15 min
AMP3	40 °C	30 min
AMP4	40 °C	15 min
AMP5	Room temperature	30 minutes
AMP6	Room temperature	15 minutes

RED working solution was made by mixing RED-A and RED-B at a ratio of 60:1 which was then added to sections and incubated for 10 minutes at room temperature. Slides were then washed in distilled water.

Following signal development, immunofluorescence (IF) was conducted to co-stain with αSMA. Blocking solution (10% FBS and 1% bovine serum albumin (BSA, Sigma) in PBS (Thermo)) was added to sections for 1 h at room temperature. Primary antibody was incubated for 48 h at 4 °C. Primary antibodies used are shown in Section 2.4.4. Slides were then washed twice in PBS for 5 min and once in PBS-Tween (PBS-T) (0.01% Tween (Sigma) in PBS) for 5 min. Secondary antibody was added to slides at 1:400 in 1%BSA/PBS for 1 h before a repeat of the washes described above. Slides were stained with DAPI (Roche) at 0.2 µg/ml in PBS for 10 min before a final wash in PBS for 5 min. Slides were mounted with coverslips using non-fluorescent mounting medium (DAKO). Coverslips were then sealed using nail varnish. Slides were subsequently imaged using a Zeiss LSM Upright 710 Confocal microscope running ZEN software. Images were processed using Fiji software.

2.2 CRISPR/Cas9 Knockouts

2.2.1 Parental clone selection

Prior to transfection with CRISPR guides, parental clones were selected. These clones had to be accurate representations of the polyclonal pool to avoid any possibility that downstream results may be due to a clonal artefact. Clones were selected based on qRT-PCR analysis of gene expression for specific genes of interest.

2.2.2 sgRNA design and transfection

sgRNAs were designed to interfere with nucleotide sequences encoding a functionally relevant protein domain of the target of interest. Sequences were submitted to Zhang CRISPR guide design software (https://zlab.bio/guide-design-resources). Guides were then selected based on sequence homology and lack of estimated off-target effects. Respective guide sequences were then ordered from Thermo. Top and bottom strand oligos were ordered with specific overhangs (highlighted in red; BbsI restriction sites) to allow for downstream ligation into the Px458 vector (Addgene). This vector contains a scaffold for the sgRNA as well as regions encoding Cas9 and GFP proteins. A CMV enhancer drives expression of the Cas9 and GFP transcripts which are separated by a 2A sequence. A U6 promoter drives gRNA expression.

sgRNA oligos

Target gene	5’	3’
ACVR1B	CACCGATTATTGGCAAGGGTCGGTT	AAACAACCGACCCTTGCCAATAATC
Inhba	CACCGGGCTTGGAGTGCGACGGCA	AAACTGCCGTCGCACTCCAAGCCCC
Inhbb	CACCGAGACATCGCATCCGCAAACG	AAACCGTTTGCGGATGCGATGTCTC

Oligos were then phosphorylated and annealed in the following reaction mixture:

Top Oligo (100 µM)	1 µl

Bottom Oligo (100 µM)	1 µl
10X T4 Ligation Buffer (NEB)	1 µl
Distilled water	6.5 µl
T4 Polynucleotide Kinase (PNK) (NEB)	0.5 µl

Reaction mixtures were then put in a Veriti 96-well thermal cycler under the cycle conditions:

Cycle 1. 37 °C for 30 min

Cycle 2. 95 °C for 5 min and then decrease to 25 °C by 5 °C/min

Annealed oligos were subsequently diluted 1:200 and ligated into Bbsl-digested Px458 vectors. Px458 digests and ligations were conducted as described in Section 2.1.5. Ligation reactions were then transformed and sequenced as described in Sections 2.1.6 and 2.1.7.

Plasmids were transiently transfected into cells of interest (see Section 2.3.4). Forty-eight hours after transfection, cells were harvested for flow cytometry. Single GFP-positive cells were sorted into individual wells of a 96-well plate in 200 µl of 20% DMEM (see Section 2.3.8).

2.2.3 Clonal expansion and screening

Cells were expanded and split into 6-well plates. Once confluent, they were split into T25 flasks and seeded for screening analysis. T25s were subsequently frozen for later use. Screening of clones involved the following methods: extracting DNA for sequencing target regions (see Section 2.2.4) as well as generating protein lysates and probing for expression of target genes (see Section 2.4.1).

2.2.4 Sequencing clones

Two separate methods of sequencing were used to determine any genomic mutations introduced following CRISPR guide transfection.

2.2.4.1 pGemT cloning and sequencing

DNA was extracted from CRISPR knockout clones of interest using the QuickExtract DNA Extraction method described in Section 2.1.2.1. Extracted DNA (5 µl) was used

in a PCR reaction with primers that flank the CRISPR target region under conditions described in Section 2.1.2. PCR reactions were then ligated into PGemT easy vectors (Promega) using conditions outlined in Section 2.1.5. Sequencing reactions were then conducted using the plasmid as a template and flanking T7 and U6 primers. T7 and U6 sites flank the multiple cloning site (MCS) of the PGemT easy vector. Returned sequences were then analysed using 4Peaks software.

Primers used for PCR of genomic region of interest

Target gene	Forward primer	Reverse primer
ACVR1B	CTGTTTGTGTTCACTCTTTC	TTTCTTTCTACGGGTTACAA
Inhba	ATTGCTTGTGAGCAGTGCCA	GGGGCTGTGACCCCTCATGC
Inhbb	GAAGGTGGACCTGAAACGTA	GGTACTGGTTCACCACGGCT

2.2.4.2 MiSeq sequencing

DNA was extracted using the method described in Section 2.1.2.2. Following extraction, DNA was prepared for sequencing on the Illmina MiSeq System as per manufacturers' instructions. I conducted an initial PCR reaction in a Veriti 96-well thermal cycler. The same oligos used to amplify the genomic region of interest prior to PGemT sequencing (Section 2.2.4.1) were utilised in this initial amplicon PCR. However, they had a barcoding sequence appended to either end, highlighted in red below, so that the amplicons could be identified in the final sequencing reaction.

Amplicon PCR mix

DNA (5 ng/µl)	2.5 µl
Forward primer (1 µM)	5 µl
Reverse primer (1 µM)	5 µl
2X KAPA HiFi HotStart ReadyMix (Roche)	12.5 µl

Amplicon PCR reaction

Cycle 1. 95 °C for 3 min

Cycles 2-26. 95 °C for 30 sec, 55 °C for 30 sec and 72 °C for 30 sec

Cycle 27. 72 °C for 5 min

Cycle 28. 4 °C indefinitely

Amplicon PCR oligos

Target gene	Forward primer (red lettering denotes barcode)	Reverse primer (red lettering denotes barcode)
Inhba	TCGTCGGCAGCGTCAGATGTGTATAAGAGACAGATTGCTTGTGAGCAGTGCCA	GTCTCGTGGGCTCGGAGATGTGTATAAGAGACAGGGGGCTGTGACCCCTCATGC
Inhbb	TCGTCGGCAGCGTCAGATGTGTATAAGAGACAGGAAGGTGGACCTGAAACGTA	GTCTCGTGGGCTCGGAGATGTGTATAAGAGACAGGGTACTGGTTCACCACGGCT

Subsequently, PCR products were submitted to the Advanced Sequencing Facility (ASF) at the Francis Crick Institute for a clean-up reaction, a secondary indexing PCR, and a further PCR clean-up before PCR libraries were quantified and denatured prior to MiSeq sample loading on the Illumina MiSeq system. This was performed as per the manufacturers' instructions (Ilumina). Initial amplicons could be identified by their unique barcodes and separate products (alleles) identified by their unique index. Relative distribution of allele sequences was then determined by the enrichment of specific index sequences.

2.3 Cell Culture

2.3.1 Cell lines used

The following cell lines have been used as part of this thesis:

Cell line	**Source**
CAF1	Erik Sahai, Francis Crick Institute
HaCaT	Cell Services, Francis Crick Institute
HEK293T	Cell Services, Francis Crick Institute
HEK293T-CAGA-Luc-TK Renilla	Daniel Miller, Francis Crick Institute
NF1	Erik Sahai, Francis Crick Institute

NMuMG	ATCC
PyMT cancer cells	Isolated from primary tumours of MMTV-PyMT mice
PyMT-GFP	Ilaria Malanchi, Francis Crick Institute

Additionally, I generated and used the following knockout cell line from those detailed above using CRISPR/Cas9 technology (see Section 2.2):

Cell Line	**Mutation**
Activin A-null CAF (1 and 2)	*Inhba*$^{-/-}$
Activin B-null CAF (1 and 2)	*Inhbb*$^{-/-}$
Activin A/B-null CAF (1 and 2)	*Inhba*$^{-/-}$/ *Inhbb*$^{-/-}$
ACVR1B-null HEK293T	*ACVR1B*$^{-/-}$

2.3.2 Culture conditions

2.3.2.1 General

The majority of cell lines had a base medium of Dulbecco's Modified Essential Medium (DMEM) (Thermo) supplemented with 10% FBS and 1X Penicillin/Streptomycin (Pen/Strep) solution (Thermo). HaCaTs and HEK293T cells and their variants were cultured in this base medium alone. CAF1 and NF1 cells were cultured in this base medium supplemented with 1X Insulin-Transferin-Selenium (ITS) solution (Thermo). NMuMGs were cultured in base medium supplemented with 10 µg/ml of human Insulin solution (Sigma). All these cell lines were cultured at 10% CO_2 and 37°C.

All cells were routinely grown in respective medium conditions and trypsinised every 2-3 days. Cells were washed in PBS before addition of 0.25% Trypsin solution (Sigma). Once cells were detached, trypsin was neutralised in serum containing medium, specifically over double the amount of Trypsin. Cells were then diluted at an appropriate level and added to fresh medium in a new flask.

2.3.2.2 PyMT cancer cells

Prior to seeding these cells, 15-cm dishes were coated in Collagen solution, comprised of the following:

Hanks' Balanced Salt Solution (HBSS) (Sigma)	500 ml
Bovine Serum Albumin (100 mg/ml)	500 µl
HEPES 1M (Thermo)	10 ml
Type I Rat Tail Collagen (3 mg/ml) (Corning)	5 ml

Plates were then incubated at 37°C for 30 min before aspirating the solution. Cells were then seeded in base medium with the following components:

DMEM/F12 (Thermo)	500 ml
Glutamax (100x) (Thermo)	5 ml
Heat-Inactivated FBS (Thermo)	10 ml
Pen/Strep	5 ml
Human Insulin solution	500 µl
Epidermal Growth Factor (Peprotech) (20 µg/ml)	500 µl

These cells were cultured at 37°C and 5% CO_2 in an incubator exclusively used for primary cells. Since they were primary, cells were never used beyond P1. Before use in experiments, they were trypsinised as detailed above.

2.3.3 Ligand and drug treatments

For various experiments, ligands and drugs were utilised. Standard ligand and drug concentrations were as follows unless otherwise indicated in the text.

Drug/Ligand	**Source**	**Concentration**	**Solvent**
Activin A	PeproTech	20 ng/ml	4.4 mM HCl, 0.1% BSA
BMP4	PeproTech	20 ng/ml	4.4 mM HCl, 0.1% BSA
Follistatin	R&D	500 ng/ml	PBS
LY2424087	Eli Lilly	1 µg/ml	PBS
Noggin	PeproTech	500 ng/ml	Water
SB-431542	Tocris	10 µM	DMSO
SB-505124	Tocris	10 µM	DMSO
TGF-β1	PeproTech	2 ng/ml	4.4 mM HCl, 0.1% BSA

2.3.4 Plasmid transfection

For transfections in 6-well plates, the following solution was made and incubated at room temperature for 20 minutes before thoroughly mixing:

Optimem (Thermo)	200 µl
Plasmid DNA	5 µg
FuGENE HD (Promega)	5 µl

For transient transfections, this solution was added to 60% confluent cells the day after plating. Downstream experiments were performed 48 h post-transfection. This was scaled up 5-fold for the transfections in T75 flasks as part of CRISPR guide transfection.

Transfections were also conducted to obtain stable cell lines. Cells were plated on a 10-cm dish. The following day, the solution detailed above was scaled up 6-fold and added to cells. A parallel mock transfection without DNA was conducted as a control. Forty-eight hours post-transfection, media containing the appropriate antibiotic was added to cells, the concentration of which was determined by a kill curve. Once all control cells had died, surviving cells in experimental wells were considered transfected. These were then expanded and used in downstream experiments. I generated the following cell lines for use in this way:

Cell Line	**Antibiotic**
Parental CAF/FST	Hygromycin (500 µg/ml)
Activin A/B-null CAF 1/FST	Hygromycin (500 µg/ml)
Activin A/B-null CAF 2/FST	Hygromycin (500 µg/ml)
HEK293T ACVR1B-HALO	Hygromycin

Other stable cell lines were generated through transfection of PiggyBac constructs. Parental CAF/FST and Activin A/B-null CAF 1/FST were transfected as previously described with pPB transposase and pPB mCherry CAAX constructs. This generates membrane-specific mCherry expression in transfected cells. Forty-eight hours post-transfection, mCherry-positive cells were sorted (as described in Section 2.3.8). These populations were then expanded and used in downstream experiments.

2.3.5 siRNA transfection

All siRNA experiments in this thesis were conducted in NMuMG cells. Cells were plated to be 50% confluent the following day. Twenty-four hours after plating, a solution of appropriate siRNA (20 nM) (GE Healthcare) was added to 200 µl of Optimem. This solution was incubated at room temperature for 5 min. INTERFERin (Polyplus) (8 µl) was added to the suspension and incubated for a further 15 min. The solution was added to cells in fresh media. Downstream experiments were performed 72 h post-transfection.

2.3.6 Contraction assay

CAF populations and NF1 cells were seeded in collagen suspensions on a 24-well glass bottom plate (Mattek). Collagen-cell suspensions were made on ice.

Collagen-cell suspensions

Fibroblasts ($6x10^6$/ml)	10 µl (60,000 cells per gel)
Type I rat tail collagen	5 mg/ml
5X collagen Buffer	5X volume of Type I Rat Tail Collagen
FBS	10 µl
DMEM	Up to 100 µl

5X collagen buffer

Alpha MEM powder (Thermo)	2.5 g
HEPES 1M	5 ml
$NaHCO_3$	1 g
Water	Up to 50 ml

Solutions were scaled up depending on the number of wells to seed. Additionally, excess of 1.5X the desired solution was made to compensate for loss of solution in the pipette. Some gel mixes were supplemented with 10 µM of SB-505124. Once seeded, gels were left to set for 45 minutes at 37°C. Media was added to gels with or without 10 µM SB-505124. Gels were imaged immediately and at every

subsequent 24-h time point for 72 h with a Leica MZFLIII light microscope. Gel areas were quantified using FIJI software. Lines were manually drawn around the gel before calculating the area. Percentage contraction was then calculated for untreated and SB-505124 treated control wells using the following equation:

Percentage gel contraction = 100 – (1 / (initial gel area / final gel area)) * 100

In all cases, final gel contraction was the value of untreated wells relative to SB-505124-treated wells.

2.3.7 Spheroid invasion assays

Spheroid suspensions

Methylcellulose	360 µl
mCherry CAFs	20,000 cells/ml
GFP PyMT cancer cells	20,000 cells/ml
Type I rat tail collagen	5 µg/ml
5% FBS-containing media	Up to 2 ml

To make the methylcellulose solution, 6 g of methylcellulose powder (Sigma) was autoclaved in a 100 ml bottle with a magnetic stirrer. DMEM (50 ml) was added to the bottle and incubated at 60°C for 15 minutes. The bottle was shaken vigorously and stirred with a magnetic stirrer for 20 min. DMEM (40 ml) was then added and stirred for 4 h on a magnetic stirrer. The bottle was stored overnight at 4°C and 1 ml of 100X Pen/Strep was added the next day. The bottle was mixed vigorously, and the solution was transferred into two 50 ml falcons before centrifugation at 4000 rpm for 20 min at 4 °C. Supernatants were then transferred to fresh falcons.

Twenty-five microlitres of spheroid droplets were added to the underside of a lid from a 10-cm dish. The dish was filled with PBS and the lid was placed on top. Dishes were then incubated for 72 h at 37°C and 5% CO_2. Following this period, lids were inverted, placed inside a 15 cm dish and inspected under a light microscope. Spheroids that were not uniform and spherical in structure were discarded. The remaining spheroids were harvested in media and transferred to a falcon where they

were left for 10 min to settle. Media was then aspirated, and spheroids were washed with PBS. Spheroids were left to settle once more, and PBS was aspirated. Finally, they were re-suspended in PBS and poured into a well of a 6-well plate.

Collagen solution was then made as in Section 2.3.6. However, extra media was added in lieu of fibroblasts. Collagen solution (100 µl) was added to individual wells of Black 96-well Clear Flat Bottom TC-treated Imaging Plates (Corning) whilst on ice. Individual spheroids were then pipetted in 4 µl of PBS and added directly to the centre of the collagen. At least ten spheroids were seeded per condition to increase the chance that sufficient spheroids did not sink to the bottom. This would result in cells growing as a monolayer rather than a spheroid. Once all spheroids had been seeded, the plate was stored at 37°C for a series of 1-min incubation periods. At the end of each minute, the plate was inverted to help ensure spheroids did not sink to the bottom. Once set, the plate was left bottom side down for 30 min, and 100 µl media was then added to each well. Plates were incubated at 37°C and 10% CO_2.

After 72 h, spheroids were washed in PBS four times and fixed in 4% paraformaldehyde solution (Sigma) for 30 min before four more PBS washes. Gels were then permeabilised using 0.2% Triton (Sigma) in PBS before four more PBS washes. DAPI stain in PBS (0.2 µg/ml) was added to spheroids for 30 min. Spheroids were washed in PBS four more times and left at 4°C overnight in PBS. Spheroids were examined on a Zeiss Invert780 Confocal Microscope running ZEN software. Wells harbouring spheroids that were not at the bottom and within focal range were imaged and z-stacks made. Images were than analysed using Fiji software. Specifically, channels were segmented and areas and perimeters were calculated based on fluorescence. The following equations were then used to calculate factor shape and percentage fragmentation.

$$\text{Factor shape} = \text{Perimeter}^2 / (4\pi * \text{area})$$

$$\text{Percentage fragmentation} = (\text{Area of released cancer cells} / \text{total cancer cell area}) * 100$$

2.3.8 Flow cytometry

Fluorescent cells were trypsinised, pelleted and washed in PBS. Cells were then pelleted once more before washing in Optimem. Cells were pelleted one final time before re-suspension in 3 ml of Optimem. Suspensions were transferred to a polyethene FACs tube. Cells were sorted based on the fluorophore of interest using a FACS Aria Fusion machine (BD Biosciences). Positive cells were sorted either as single cells into a well of a 96-well plate, or as a pool for subsequent expansion.

2.3.9 Conditioned media

2.3.9.1 PSMAD2 induction in HaCaTs

Fibroblasts were seeded in 10 ml of media to be 80% confluent 24 h later. They were then cultured for 72 h to allow for abundant cytokine production. Media was then harvested and concentrated in a swinging bucket centrifuge at 3000 g in a 10,000MW Centriprep centrifugal filter unit (Millipore) until only 2 ml remained. Waste media was disposed of. The conditioned media (CM) was then added to naïve HaCaTs for 1 h in combination with various ligand antagonists.

2.3.9.2 Cytokine array

CM was harvested and processed as detailed above. However, in this case, CM was added directly to activated membranes of the Proteome Profiler Mouse XL Cytokine Array kit (R&D). The experiment then proceeded as per manufacturers' instructions. Briefly, CM was washed away in PBS. Membranes were subsequently incubated with the Detection Antibody Cocktail. Membranes were then incubated with Streptavidin-HRP before developing with Chemi Reagents 1 and 2. Membranes were finally exposed to autoradiography film (GE Healthcare). The resultant dots, corresponding to specific cytokine expression, were then quantified relative to reference points using Fiji.

2.3.10 CAGA-Luc Assay

HEK293T-$CAGA_{12}$-Luc cells, expressing TK Renilla as an internal control, were seeded in triplicate in individual wells of a 96-well plate to be 60% confluent the following day. Two days after seeding, each well was treated with respective ligand

in complete media or CM for 1 h. Media was then removed and cells were washed in PBS. Luciferase was then detected in cells using the Dual-Luciferase Reporter Assay System (Promega) according to manufacturers' instructions. Briefly, 100 µl of 1X Passive Lysis Buffer was added to each well and plates were shaken vigorously for 30 minutes. Using a multichannel, 30 µl of the lysate was transferred to individual wells of a white polystyrene 96-well plate. To each well, 30 µl of Luciferase Assay Reagent II was added and luciferase fluorescence in each well was detected using an EnVision Multilabel Plate Reader (PerkinElmer). Subsequently 30 µl of 1X Stop and Glo Buffer was added to each well and Renilla fluorescence was detected in the same way. Luciferase measurements were made relative to respective Renilla readings in downstream quantifications.

2.4 Protein work

2.4.1 Western Blot

2.4.1.1 Cell lysis

Lysates were harvested from cells seeded on individual wells of a 6-well plate. Cells were washed twice in PBS and scraped in 150 µl of D0.4 buffer.

D0.4 buffer

EDTA (pH 7.5)	5 mM
EGTA (pH 7.5)	10 mM
Glycerol	10% (v/v)
HEPES pH 7.5	20 mM
KCl	0.4 M
Triton X-100	0.4% (v/v)
Sodium β-Glycerophosphate	25 mM, added prior to lysis
NaF	25 mM, added prior to lysis
Protease inhibitor (Roche)	1x, added prior to lysis

Lysates were transferred to Eppendorfs and sonicated for 10 sec in an ice bath sonicator (VWR). Samples were centrifuged at 17,000 g for 10 min at 4°C. Supernatants were then transferred to fresh Eppendorfs. To determine protein

concentration, 1 µl of lysate was pipetted into individual wells of a 96-well plate alongside known concentrations of BSA (NEB) and 198 µl of Bradford assay reagent (Biorad) diluted 1:5 in PBS was added. The OD of each well was measured at 595 nm using a SpectraMax Plus spectrophotometer (Molecular Devices). Protein concentration was then calculated using a standard curve generated by the OD of known concentrations of BSA.

2.4.1.2 Lysate Processing

In some cases, samples were treated with peptide N-glycosidase (PNGase, NEB) to de-glycosylate proteins. To do this, 500 U/µg was added to lysates for 1 h in a benchtop thermomixer at 37°C for 1 h. In all cases, 4X sample buffer was added at one-third of the volume of lysate to be run on SDS-PAGE.

4X Sample buffer (10.5 ml)

20% SDS	4 ml
1M Tris-HCl pH 6.8	2 ml
100% glycerol	4 ml
β-mercaptoethanol (Sigma)	0.4 ml
Bromophenol blue	0.025% (w/v)

Samples were then boiled for 10 minutes.

2.4.1.3 SDS-PAGE

Proteins were separated based on size using SDS-PAGE. Varying percentages of acrylamide gels were made to resolve proteins. Resolving gel mix (50 ml) was poured into pre-constructed glass plates. Specifically, two glass plates (10 cm x 20 cm) were lined by silicon tubing and 0.8 mm plastic spacers at either end to form a seal. Glass plates were then clamped using four foldback clips. Water was then added to the top of the gel to level it. Once the gel had polymerised, the water was poured away and replaced with 5 ml of stacking gel. A 24-well comb was then placed within the stacking gel.

Gel mixes

	Resolving gel (%)		**Stacking gel**
	15	20	
40% (w/v) acylamide	5.625 ml	7.5 ml	0.625 ml
2% (w/v) bisacrylamide	0.645 ml	0.49 ml	0.333 ml
1.5 M Tris-HCl (pH 8.8)	3.75 ml	3.75 ml	-
1.0 M Tris-HCl (pH6.8)	-	-	0.625 ml
20% (w/v) APS	40 µl	40 µl	15 µl
TEMED (Sigma)	30 µl	30 µl	10 µl

Once stacking gels had polymerised, gels were held within electrophoresis tanks (Cambridge Electrophoresis Ltd). The comb was then removed and 750 ml of 1X SDS running buffer was poured into the tank. Wells were flushed and aligned. Prepared lysate was loaded into each well alongside pre-stained markers (NEB). Gels were then run at 230 volts and 65 mA for 1.5 h.

1X SDS running buffer

Glycine	384 mM
Tris base	50 mM
SDS	0.1% (w/v)

2.4.1.4 Western blotting

Immobilon-P PVDF transfer membranes (Millipore), cut to the same as SDS-PAGE gels, were activated in methanol before three washes in distilled water. Membranes were then transferred to 1X transfer buffer with six pieces of Whatman paper cut to the same size as the gel. The gel, having run for 1.5 h, was removed from the glass case and placed in the 1X transfer buffer. Transfer 'sandwiches' were then constructed in a Semi-Dry Blotter Units (Scie-Plas). Specifically, 3 Wattman cards were placed down first, followed by the membrane, the gel and, finally, 3 more Wattman cards. Units were then sealed and transfers conducted for 1 hr at 100 volts and 165 mA per gel.

1X Transfer buffer

Glycine	1.5 M
Tris Base	200mM
SDS	0.1% (w/v)
Methanol	20% (v/v)

Membranes were then stained with Ponceau Red (Sigma) to visualise proteins. Membranes were washed three times in distilled water to remove the stain before addition of blocking solution for 1 h at room temperature. Blocking solution was 5% milk powder (Marvel) in 0.1% PBS-T or 5% BSA powder in PBS-T for phosphorylated protein detection. After blocking, primary antibodies were added in the same block solution overnight on a rocker at 4°C. The following day, membranes were washed in three 5-min washes in PBS-T. After the final wash, HRP-conjugated secondary antibodies were added for 1 h at room temperature. Three more 5-min washes in PBS-T were conducted. Luminata Classico or Luminata Crescendo HRP substrate (Millipore) was then added to blots for 3 minutes to detect bound HRP. Crescendo was utilised over Classico if the signal was expected to be weak. Membranes were finally exposed to autoradiography film (GE Healthcare) to detect luminescence. If the signal was expected to be strong, detection was conducted in an ImageQuant LAS 4000 mini (GE Healthcare). Resulting films and images were analysed and quantified using Fiji. Protein densitometry measurements were made relative to that of loading controls.

2.4.2 Immunofluorescence

2.4.2.1 Cells

Cells were seeded on glass coverslips in individual wells of a 6-well plate. Experimental procedures were then conducted on respective cells. Once experiments were complete, cells were fixed in either 4% PFA for 10 min at room temperature, for phalloidin (Sigma) staining, or methanol acetate (1:1) for 20 min at -20°C, for CDH1 and TJP staining. Cells were subsequently washed three times in PBS. Blocking solution was then added for 1 h at room temperature.

Blocking solution (in PBS)

BSA	0.3%
FBS	10%
Na Azide	0.08%
Triton-X 100	0.3%

Antibodies were then added in blocking solution overnight at 4°C. Coverslips were then washed three times in PBS before adding appropriate fluorophore-conjugated secondary antibody in blocking solution at 1:1000 for 1 h at room temperature. Coverslips were then washed three times in PBS for 5 min each. The second of which contained 0.2 µg/ml of DAPI stain. Alternatively, in lieu of primary and secondary antibody stains, phalloidin stain was added for 1 h at room temperature before subsequent washing and DAPI staining as detailed above. Coverslips were then mounted on slides in Mowiol mounting media (Sigma) and sealed with nail varnish. Slides were stored at 4°C until they were imaged on a Zeiss LSM Upright 710 Confocal microscope running ZEN software. Images were processed using Fiji software.

2.4.2.2 Paraffinised Sections

The following protocol was used for PSMAD2 and αSMA co-staining. Slides were deparaffinised as described in Section 2.1.8.4. For HMAR, 400 ml of citrate buffer was poured into a container within a steamer (Russel Hobbs). A separate container of distilled water was placed beside it. The steamer was turned on to allow liquids within each container to reach boiling point. Once they had done so, slides were added to boiling water for 10 sec to acclimatise them before transferring them to the citrate buffer. Slides were left in citrate buffer for 40 min. Following HMAR, citrate buffer and slide containers were left under a barely running tap to slowly cool and end the reaction.

Citrate buffer (pH 6)

Tri-sodium citrate	2.94 g
HCl (0.2 M)	18 ml
Distilled water	Up to 1 L

Following HMAR, slides were washed in 1X Tris-buffered saline (TBS) with 0.01% Tween-20 (TBS-T) and subsequently incubated in 3% H_2O_2 (Sigma) in methanol for 30 min. Slides were washed again in TBS-T. A hydrophobic barrier was drawn around sections and 200 µl of blocking solution (3% BSA in TBS-T) was added for 1 h.

10X TBS solution (pH 7.5)

Tris base	121.14 g
NaCl	87.66 g
HCl	(To pH to 7.5)
Distilled water	Up to 1 L

Primary antibodies were added to slides in blocking solution overnight at 4°C. The following day, slides were washed three times in TBS-T before adding secondary antibodies in blocking solution at 1:400 for 1 h. Secondary antibodies were fluorophore-conjugated (αSMA) or biotin-conjugated (PSMAD2) for downstream signal amplification. A further three washes in TBS-T were then conducted. Slides were incubated for 30 minutes with streptavidin-HRP (Perkin Elmer) diluted 1:100 in blocking solution. Three more TBS-T washes were conducted before incubating the slides for 8 min with biotinylated tyramide (Perkin Elmer) diluted 1:50 in accompanying amplification diluent (Perkin Elmer). Slides were incubated for 30 min with an alexa-flourophore 488-conjugated streptavidin diluted 1:100 in blocking solution. Slides were washed three more times in TBS-T before incubation with 0.2 µg/ml of DAPI in TBS-T. Slides were washed once more in TBS-T before bathing them in 0.1% sudan black solution (Sigma) for 15 minutes to remove background signal. Three final TBS-T washes were conducted for 10 minutes each. Slides were mounted with coverslips and non-fluorescent mounting solution (DAKO). Slides were imaged using a Zeiss LSM Upright 710 Confocal microscope running ZEN software. Images were then processed using Fiji.

2.4.3 Immunohistochemistry

2.4.3.1 CD4, CD8 and FoxP3 stains

Deparaffinisation, HMAR and H_2O_2 incubation was conducted as described in Section 2.4.2.2. A hydrophobic barrier was subsequently drawn around sections and 200 µl of blocking solution (1% BSA in PBS) was added to slides in a humidified chamber overnight at 4 °C. Primary antibodies were then added in blocking solution for 1 h at room temperature. Slides were washed twice in PBS for 5 min before a final wash in PBS-T for 5 min. Secondary antibodies were added to sections in blocking solution for 45 min. Avidin Biotin Complex (ABC) solution (Vector Laboratories) was then made, according to manufacturers' instructions, and left to stand for at least 30 minutes. Slides were washed as before. The ABC solution was then added to slides and incubated for 30 min. A further wash cycle was conducted as above. DAB chromogen (Vector Laboratories) solution was then made according to manufacturers' instructions and added to sections for up to 10 min. Slides were monitored microscopically to check if the reaction was not becoming saturated. After 10 min, or if the signal had reached saturation, slides were washed in distilled water to terminate the reaction. Finally, a haemotoxylin counterstain was conducted to stain nuclei. This stain and subsequent mounting of coverslips was performed by the Experimental Histopathology (EHP) facility at the Francis Crick Institute using TissueTek Prisma automated slide staining machine (Sakura).

2.4.3.2 S100a9 and F4/80 stains

Samples to be stained for these targets were submitted to the Francis Crick Institute EHP facility for automated staining using a Ventana Discovery Ultra (Roche). Antibodies against these targets use a trypsin antigen retrieval protocol.

2.4.4 Antibodies used

Primary antibodies

Target	Supplier	Cat. No	Species	Application	Dilution
ACVR1B	Abcam	ab133478	Rabbit	WB	1:1000
αSMA	Sigma	A2547	Mouse	WB	1:1000

αSMA	Dako	M0851	Mouse	IF	1:750
CD4	Abcam	ab183685	Rabbit	IHC	1:500
CD8	Invitrogen	14-0808-82	Mouse	IHC	1:100
CDH1	Invitrogen	610181	Mouse	IF	1:300
F4/80	Thermo	14-4801	Rat	IHC	
FoxP3	CST	12653	Rabbit	IHC	1:100
INHBA	Santa-Cruz	sc-166503	Mouse	WB	1:1000
INHBB	Santa-Cruz	sc-376971	Mouse	WB	1:1000
MLC	CST	3672	Rabbit	WB	1:1000
PMLC	CST	3674	Rabbit	WB	1:500
PSMAD1	CST	13820	Rabbit	WB	1:1000
PSMAD2	CST	3108	Rabbit	WB/IF	1:500/ 1:250
PSMAD3	Abcam	ab52903	Rabbit	IHC	1:1000
s100a9	Cell Services at the Francis Crick Institute	n/a	Mouse	IHC	
SMAD1	Invitrogen	38-5400	Rabbit	WB	1:1000
SMAD2/3	BD Biosciences	610842	Mouse	WB	1:1000
TJP1	Invitrogen	61-7300	Rabbit	IF	1:300
Tubulin	Abcam	ab6160	Rat	WB	1:5000

Secondary antibodies

Target	**Supplier**	**Cat. No**	**Conjugate**	**Species**
Mouse IgG	Dako	P0447	HRP	Goat
Mouse IgG	Invitrogen	A21203	Alexa-Fluor 594	Donkey
Rabbit IgG	Dako	P0448	HRP	Goat
Rabbit IgG	Invitrogen	A21206	Alexa-Fluor 488	Donkey
Rabbit IgG	Jackson Immune	711-065-152	Biotin	Donkey
Rat IgG	Jackson Immune	712-035-153	HRP	Donkey
Rabbit IgG	Vector labs	BA-1000	Biotin	Goat
Rat IgG	Vector labs	BA-4001	Biotin	Rabbit

2.4.5 HALO staining

2.4.5.1 HALO ligands

Fluorescent HALO ligands were obtained from Luke Lavis at Janelia Research Campus, USA. Ligands were re-suspended to a stock of 1 mM in DMSO and 5 µl aliquots were made (Grimm et al., 2017). For all experiments in this thesis, working concentrations of 100 nM were used. Only JF-HALO 646i (impermeable) and JF-HALO 564 (permeable) were used in experiments detailed here.

2.4.5.2 Fixed cells staining, imaging and quantification

Cells expressing HALO constructs were seeded on glass coverslips, to be 60% confluent the following day, in individual wells of a 6-well plate. The following day, timepoint 0 h wells were fixed in 4% PFA supplemented with JF-HALO 646i for 30 min on ice. These wells were washed quickly three times in PBS before addition of JF-HALO 564 in PBS for a further 30 min. The wells were then washed three more times before addition of 0.2 µg/ml of DAPI stain in PBS for 5 min and a final three PBS washes. In parallel, the same routine of HALO ligands was added to other experimental wells in base medium to be harvested at later timepoints. Following addition of HALO ligand to these latter wells, cells were treated with Activin A ligand for varying periods of time and immediately returned to the incubator at 37°C and 10% CO_2. At the end of these respective Activin A treatment periods, cells were fixed in 4% PFA for 30 minutes at room temperature and washed three times in PBS before adding DAPI stain as previously described. Cells were washed three more times in PBS. Glass coverslips were then removed and mounted on individual slides using Mowiol mounting medium. Coverslips were sealed using nail varnish and stored at 4°C. Slides were then imaged using a Zeiss LSM Upright 710 Confocal microscope running ZEN software. Images were then processed using Fiji.

2.4.5.3 Live cells

Cells expressing HALO constructs were seeded on 6cm-glass bottom dishes (Mattek) to be 60% confluent the next day. The following day, media was replaced with JF-HALO 646i-containing media for 30 min on ice. Cells were washed three times in PBS before media containing JF-HALO 564 was added for a further 30 min.

Cells were washed three more times in PBS and complete media was added to cells. Dishes were quickly set-up for imaging on a Nikon CSU-W1 Spinning Disk Microscope using Nikon imaging software. Images were taken every 5 min over a 6-hour timecourse. 'Movies' were subsequently made out of the sequence of images taken.

2.5 RNA-Seq

Bioinformatics analysis was performed by Stephanie Strohbuecker from the Bioinformatics and Biostatistics Service (BABS) at the Francis Crick Institute.

2.5.1 RNA extraction and library preparation

RNA was extracted as previously described (Section 2.1.8.1). The RNA extracted was then purified using the RNeasy kit (QIAGEN) as per manufacturers' instructions. RNA samples were submitted in biological triplicates to the Advanced Sequencing Facility (ASF) at the Francis Crick Institute for quality control and library preparation. RNA quality was assessed using a Bioanalyzer (Agilent, California, USA). Libraries were prepared using polyA KAPA mRNA Hyper Prep kit (KAPA Biosystems) for sequencing using the Illumina HiSeq 2500 platform.

2.5.2 RNA-Seq data analysis

Raw reads were quality and adapter trimmed using cutadapt-1.9.1 (Martin, 2011) prior to alignment. Reads were then aligned and quantified using RSEM-1.3.0/STAR-2.5.2 (Dobin et al., 2013; Li and Dewey, 2011) against the mouse genome GRCm38 and annotation release 89, both from Ensembl. Transcripts Per Kilobase Million (TPM) values were also generated using RSEM/STAR. Differential gene expression analysis was performed in R-3.6.1 (R Core Team, 2019) using the DESeq2 (Love et al., 2014) package (version 1.24.0) with two different contrasts:

1. Pairwise comparison between each Activin-A/B null condition to the parental control
2. Comparison between the combined Activin-A/B null and the parental conditions.

Differential genes were selected using a 0.05 false-discovery rate (FDR) threshold. Normalisation and regularized-log transformation (rlog) was applied on raw counts before performing principal component analysis and euclidean distance-based clustering.

Gene ontology (GO) enrichment analysis was performed in R3.6.1 using the clusterProfiler (Yu et al., 2012) package (version 3.12.0) with a p- and q-value cutoff of 0.05.

Reactome pathway enrichment analysis was performed in R3.6.1 using the ReactomePA (Yu and He, 2016) package (version 1.28.0) with default parameters. Heatmaps were generated in R-3.6.1 using the ComplexHeatmap (Gu et al., 2016) package (version 2.0.0). For highlighting general changes between Activin-A/B null and parental changes average regularized-log transformed counts for each Activin-A/B null condition and the parental CAFs were calculated. Subsequently the data was scaled by subtracting the average regularized-log transformed counts of the parental condition from all conditions. Only those genes were visualised that are significantly differentially expressed between the combined Activin-A/B null and the parental condition. For highlighting genes from specific Reactome pathways and gene ontology terms log2 fold changes between each Activin-A/B null cell line with the parental cell line are shown for those genes that show significantly differential expression between the combined Activin-A/B null and the parental condition.

2.6 Mouse work and tumour processing

All experimental mice were fed and checked daily for any signs of health deterioration by the BRF staff at the Francis Crick Institute. Female BRAM-FVB/NJ mice were used for all injection experiments. Additionally, BRF staff conducted unique ear clippings to mice in the same cage as identifiers. All animal work was performed under Home Office Licence PPL6038402.

2.6.1 Pre-injection cell processing

Cells required for injection were trypsinised, re-suspended in complete media and counted using Cellometer Disposable Counting Chambers and a Cellometer Auto T4 Bright Field Cell Counter (Nexlecom) as per manufacturers' instructions. The required number of cells were then taken and pelleted. Supernatant was discarded

and cell pellets were washed in calcium- and magnesium-free PBS (CMF-PBS, Sigma). This washing process was repeated once more. Cells were then re-suspended in CMF-PBS (30 µl per injection), transferred to 2 ml cryovials (Falcon) and placed on ice. Prior to injection, varying amounts of Vitrogel (Tebu-Bio) or growth factor reduced matirgel (GFR-matrigel, Corning) were added to suspensions.

2.6.1.1 Co-injection

For all co-injection experiments, $4x10^6$ CAFs were mixed with $0.5x10^6$ PyMT cancer cells per injection. Prior to injection, 70 µl of Vitrogel per injection was added to cell suspensions. Suspensions were then mixed thoroughly and 100 µl was drawn from the tube in 1 ml syringes and left on ice.

2.6.1.2 CAF only injection

For CAF only injections, $2x10^6$ CAFs were used per injection. Prior to injection, 70 µl of Vitrogel or 270 µl of GFR-matrigel was added to suspensions. Suspensions were mixed thoroughly. Either 100 or 300 µl of suspension was drawn up as previously described for Vitrogel and GFR-matrigel injections respectively.

2.6.2 Injection and programme of work

Individually, mice were anaesthetised using 5% isoflourane in an induction box at a flow rate of 2 litres per minute (LPM). Mouse responsiveness was checked by conducting a toe pinch. Once mice were unresponsive, airflow was changed to the facemask valve and isofluorane reduced to 2.5%. The mouse's nose was placed in the facemask. A small amount of 70% ethanol was rubbed onto the mammary fat pad of mice. Suspensions were then injected into the mammary fat pad of mice. Isofluorane was reduced to 0% to allow mice to recover on oxygen. Mice were then weighed and returned to their cage where they recovered. Anaesthetic induction was carried out using a vaporiser, oxygen supply generator, induction chamber and facemask supplied by AW Anaesthesia Services. For co-injection experiments, height and diameter of tumours was measured twice weekly by BRF staff using callipers. Tumour volume was calculated using the following equation:

$$\text{Tumour volume} = ((d^2) * D) / 2$$

In this equation, ‘d’ and ‘D’ are the smaller and larger measurements respectively.

Mice were culled at pre-designated timepoints or when tumours reached 1.2 cm in diameter, the limit of the permitted severity threshold. Tumours were subsequently harvested and fixed before downstream analysis. For CAF only injections, mice were culled 5 to 8 days after injection and injected plugs were harvested for fixation and downstream analysis.

2.6.3 Sample processing

2.6.3.1 Sample excision and fixation

Once culled by cervical dislocation, mice were dissected and the entire mammary fat pad flank bearing tumours or Vitrogel/GFR-matrigel plugs was excised using autoclaved dissection tools supplied by the BRF. Samples were then sealed in pre-labelled Histosette cassettes before placing in 10% formalin for at least 72 h to allow for complete fixation. After fixation, formalin was disposed of and replaced with 70% ethanol. Samples were placed at 4 °C for long-term storage or room temperature for 48 h prior to processing.

2.6.3.2 Processing and embedding

Samples were submitted to the Francis Crick Institute EHP facility for processing and embedding. Tissue samples were processed to wax using a Tissue-Tek VIP 6 AI. Samples were subsequently embedded in wax. Briefly, samples were trimmed and resected and placed in a metal mould with a layer of hot wax to cover the bottom face of tissues. Moulds are then placed on a cold plate to allow wax to solidify. A Histosette is then placed on top of the mould and hot wax is then poured in to cover the tissue. Moulds are left on the cold plate. Once the wax is set, moulds are removed and blocks are ready for sectioning.

2.6.3.3 Sectioning and staining

Sections were cut from blocks at 5 µm thickness using a Leica RM2255 microtome. Sections were floated out on a water bath at 40 °C to remove any creases. Sections were then mounted on glass slides. IHC, IF and RNAScope stains were conducted as previously described. Haemotoxylin and eossin (H&E) as well as Massons’ trichome stains were conducted by the EHP facility.

2.6.3.4 PyMT cancer cell isolation

PyMT cancer cells were isolated from tumour bearing FVB/MMTV-PyMT mice. The entire protocol was conducted in sterile conditions. Mice were culled and dissected as previously described. Tumours were excised and placed in PBS on ice. Tumours were brought up to our tissue culture hoods and poured with the PBS into 10 cm dishes. Using the dissection scissors, tumours were minced until they reached a jam like consistency. Tumours were then put in 5 ml of digestion media in a falcon and shaken at 37°C for 2 h.

Digestion media

CMF-HBSS (Thermo)	4.823 ml
Liberase TH (5 mg/ml)	76 µl
Liberase TM (5 mg/ml)	76 µl
DNase (5 mg/ml)	25 µl

Digestion reactions were terminated by adding 20 ml of complete PyMT cancer cell medium. Mixtures were re-suspended thoroughly before passing them through a 100 µm cell strainer (Falcon). Suspensions were pelleted in a swinging bucket centrifuge and washed with 10 ml of complete media. Cells were filtered and washed once more. One millilitre of cell suspension was added to collagen coated plates and cultured as described in Section 2.3.2.2. The following day, cells were incubated at 37°C for 10 minutes with 3 ml of 1mM EDTA in PBS. This removes weakly adhering cells. Media is then gently removed and 3 ml of trypsin is added to cells at 37°C for 10 minutes. Cells were re-suspended in 7 ml of PyMT complete media and pelleted. Pellets were re-suspended in freezing media and aliquoted into Cryovials (Falcon) before placing them in a Mr. Frosty cryovial vessel filled with isopropanol. The vessel was then stored at -80°C for 48 h. Cryovials were then transferred to liquid nitrogen storage for later use.

Freezing media

DMSO	1 ml
FBS	4 ml
DMEM/F12	5 ml

Chapter 3. Activin Signalling in Cancer-associated Fibroblasts

3.1 Introduction

As discussed in the introduction, work within the lab has shown that cells enter a refractory state when exposed to TGF-β ligand for prolonged periods. During which time, they do not respond to the ligand (Vizán et al., 2013). However, many tumours present with prolonged TGF-β pathway activation, specifically PSMAD activity and a TGF-β transcriptional output (Landis et al., 2005; del Pozo Martin et al., 2015). This chapter explores one of the possibilities as to why we observe continual pathway activation. Specifically, that another family ligand is perpetuating this signal.

This hypothesis led to a candidate approach conducted by former PhD student Daniel Miller that aimed to determine family ligand production in CAFs isolated from the MMTV-PyMT mouse model of breast cancer. CAFs were selected for this approach as they are often the most abundant stromal population and have a strong association with cytokine production as well as TGF-β family signalling (Calon et al., 2014; Cohen et al., 2017). This approach, discussed in more detail as part of this chapter, showed that Activin was produced by these CAFs and not TGF-β. This added evidence to the hypotheses that, in some cases, Activin production may be responsible for active TGF-β family signalling within the tumour stroma. Additionally, Daniel showed that blockade of the kinase activity of type I receptors resulted in a loss of contractility in CAFs. Contractility is a core functionality of CAFs that is associated with enhanced ECM remodelling and tumourigenesis (Calvo et al., 2015). Since Daniel had shown that these CAFs exclusively secrete Activin, it was thought that blockade of the type I receptor kinase activity worked exclusively to ablate autocrine Activin signalling. It was therefore posited that Activin signalling may be responsible for the contractile capacity of CAFs. Consequently, it became of interest to comprehensively interrogate the nature of Activin signalling in CAFs.

In this chapter, I will outline the initial work conducted by Daniel that identified Activin as the TGF-β family ligand produced by these CAFs. Then, I will detail experiments I conducted that aimed to determine the role of Activin signalling on CAF functionality. Briefly, I conducted CRISPR/Cas9 knockouts of Activins A and B

individually and in combination. I then characterised knockout clones at a transcriptional and secretome level to determine Activin's role on CAF signalling and functionality.

For this work, as mentioned, the CAFs were isolated from the MMTV-PyMT mouse model of breast cancer. This model expresses the polyoma middle T (PyMT) oncoprotein under the control of the mouse mammary tumour virus (MMTV) promoter. This restricts PyMT oncogene expression to the mammary epithelium, causing spontaneous breast tumours to arise at puberty (Lin et al., 2003). CAFs from this model were favoured as the tumours histologically represent human breast cancer progression. They have four histologically identifiable stages, progressing from pre-malignant to invasive and metastatic tumours, akin to human cancers. Additionally, they express many of the same biomarkers as late stages human cancers. Specifically, there is loss of estrogen and progesterone receptors as well as sustained expression of cyclinD1 (Lin et al., 2003). Furthermore, and importantly, cancer cells from this model have been shown to have active TGF-β family signalling. Cells within these tumours show positive PSMAD3 staining (del Pozo Martin et al., 2015).

3.2 Results

3.2.1 CAFs Produce Functional Activin

Before conducting a candidate approach to determine CAF ligand production, Daniel first aimed to determine the nature of TGF-β family pathway activity in the MMTV-PyMT tumours taken from mice. Tumours taken from mice were sectioned and stained for levels of PSMAD3 (Figure 3.1). Strong positive staining of PSMAD3 is observed both within the tumour bulk and at the periphery. Cells at the periphery morphologically resemble CAFs. This suggests that both CAFs and the PyMT cancer cells themselves are positive for PSMAD3 and, therefore, TGF-β family signalling. Thus, the MMTV-PyMT model is appropriate for investigating which TGF-β family ligands are present in the tumour stroma.

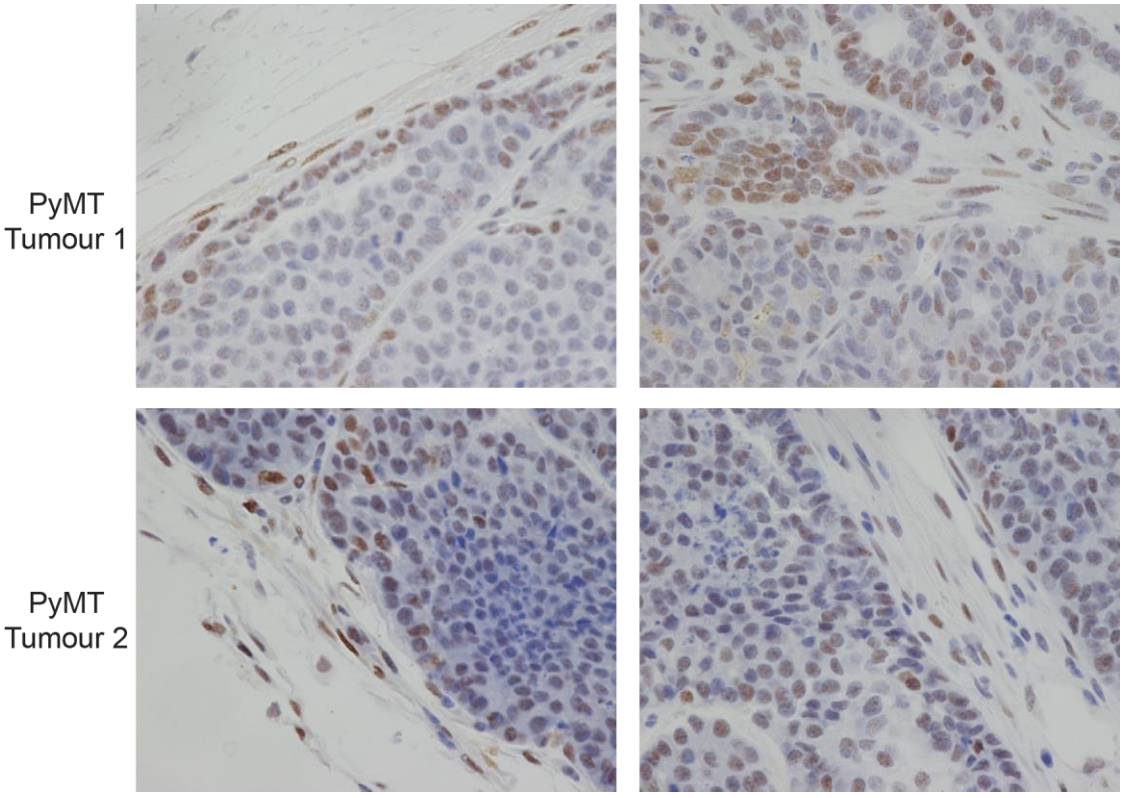

Figure 3.1. PSMAD3 IHC on MMTV-PyMT tumours. Two representative fields of view of PSMAD3 staining (brown) and nuclei (blue) for MMTV-PyMT tumours from two separate mice. Figure is adapted from data produced by Daniel Miller.

Following this result, Daniel wanted to determine if the CAFs within this model were producing any TGF-β family ligands that may be inducing this signal. CAFs were selected due to their abundance within the tumour stroma and their association with cytokine production (Cirri and Chiarugi, 2012). As mentioned, such an experiment was intriguing as work within the lab suggested family ligands beyond TGF-β may be propagating these signals in tumour contexts. To do so, Daniel added various family ligand inhibitors in conjunction with CAF CM to naïve HaCaTs (Figure 3.2). HaCaTs treated with recombinant Activin exhibit a strong induction of PSMAD2 over the untreated condition, as expected. CM from normal fibroblasts (NFs) fails to elevate PSMAD2 above untreated levels, suggesting they do not produce any active family ligands. Conversely, CM from the CAFs induces PSMAD2 to levels seen in recombinant Activin treated cells. This induction is completely ablated when CAF CM is added in conjunction with the Activin antagonist Follistatin. Conversely, when CAF CM is added in conjunction with TGF-β blocking antibody LY, levels of induction remain the same as CAF CM. This indicated that the CAF cell line from the MMTV-PyMT model produces Activin rather than TGF-β.

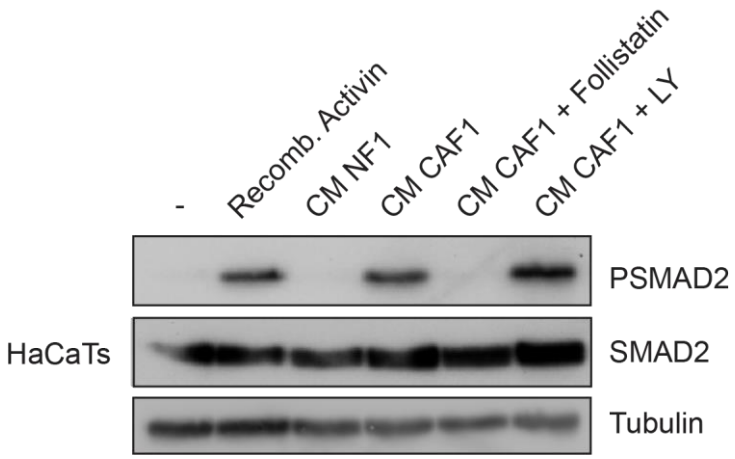

Figure 3.2. PSMAD2 induction in HaCaTs treated with CAF1 CM in combination with ligand inhibitors. Media was taken from normal fibroblasts (NF) and CAFs 72 hours after plating. The media was concentrated 4-fold and added to HaCaTs for 1 hour in combination with a TGF-β blocking antibody (LY) or Activin antagonist Follistatin (500ng/ml). Recombinant Activin treated (20ng/ml) and untreated (-) HaCaTs were used as positive and negative controls respectively. Blot is representative of 4 biological replicates. Figure adapted from data produced by Daniel Miller.

After showing that CAFs produce Activin, Daniel wanted to determine if Activin expression is a prognostic factor. In some tumour types, he found that *INHBA* and *INHBB* expression correlated with poorer patient survival. He produced Kaplin-Meier plots for the cancer types that exhibited a significant correlation (Figure 3.3). *INHBA* expression correlates with poorer survival in invasive breast carcinoma (p=0.0204) and head and neck squamous cell carcinoma (HNSCC) (p=0.00197). For *INHBB,* expression correlates with poorer survival in HNSCC (p=0.0059) and colorectal adenocarcinoma patients (p=0.000402). This suggests that, in certain cancers, Activin levels may be a prognostic factor.

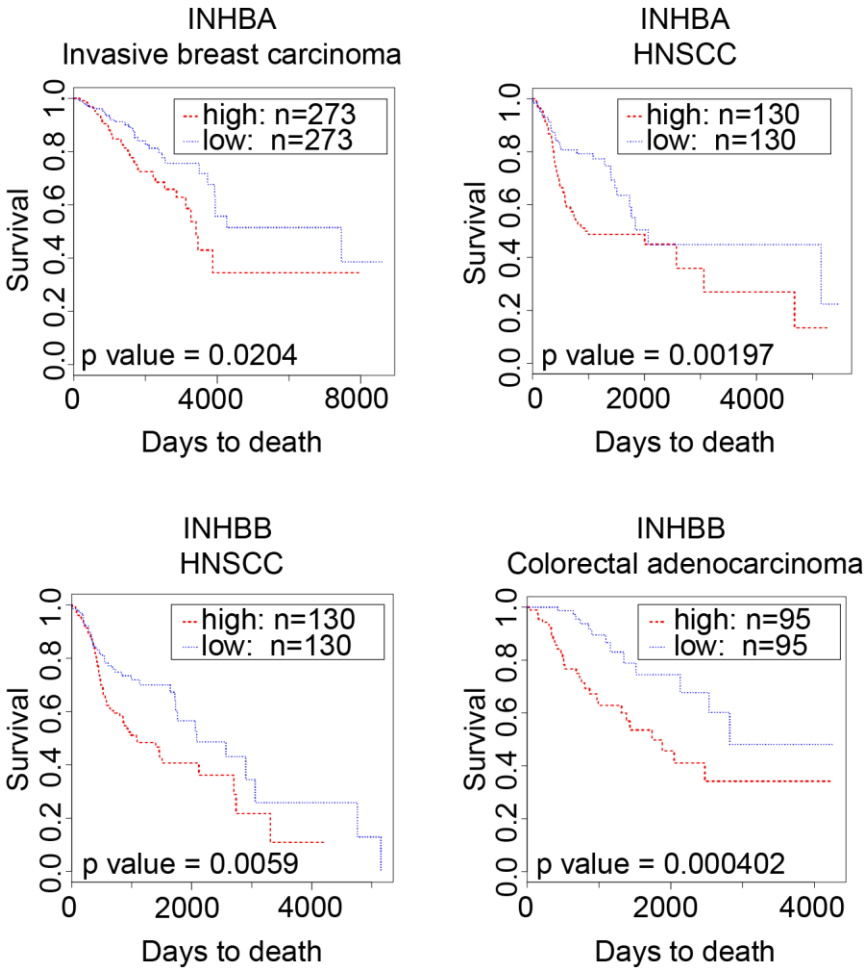

Figure 3.3. Kaplin-Meier plots showing correlation between survival and levels of Activin expression. mRNA expression of human *INHBA* and *INHBB* transcripts was submitted for TCGA analysis. Cancers with significant correlation between high levels of each transcript and respective cancer types are displayed above. Red and blue lines denote high and low levels of Activin expression respectively. This analysis was conducted by Daniel Miller.

Next, Daniel directly compared levels of Activin expression in matched cancerous and normal tissue (Figure 3.4). Across various cancer types, there are elevated levels of *INHBA* and *INHBB* expression in tumour vs normal tissues. Invasive breast carcinoma, colorectal adenocarcinoma, HNSCC and stomach adenocarcinoma all exhibit significantly elevated levels of *INHBA* expression in tumour tissue against normal tissue. Colorectal and stomach adenocarcinoma also express higher levels of *INHBB* in tumours (Figure 3.4). This suggests that, in various cancer types, Activin expression correlates with a tumourigenic phenotype.

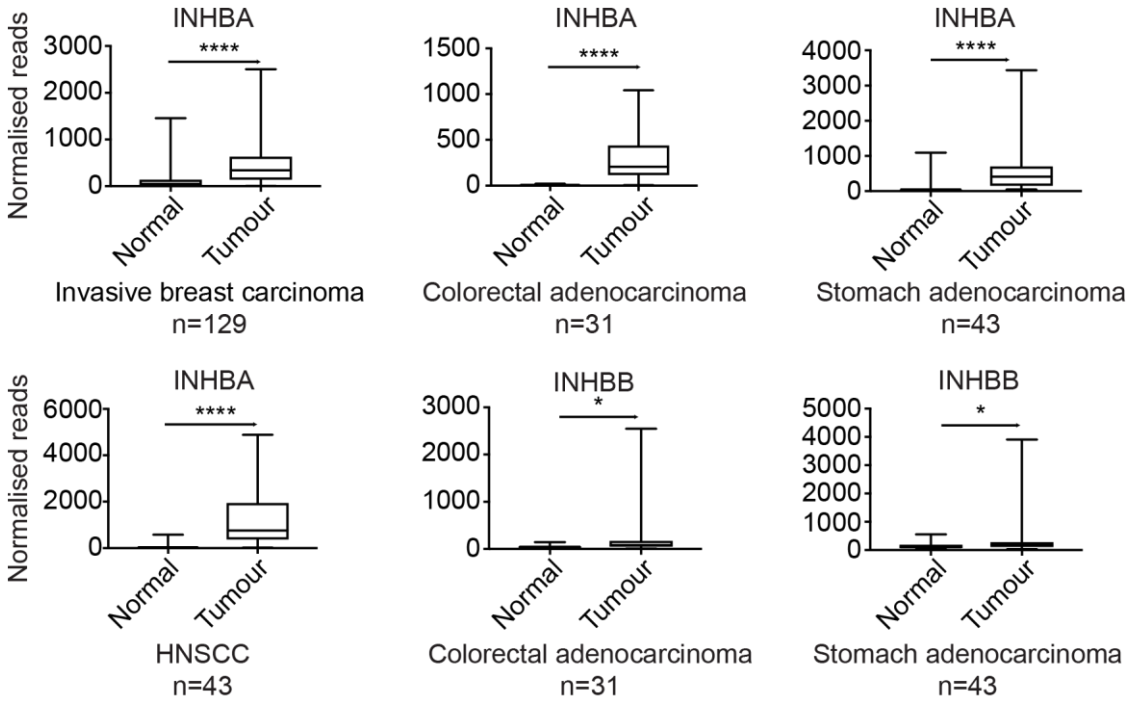

Figure 3.4. Boxplots showing expression of *INHBA* and *INHBB* in matched tumour and normal tissues. TCGA analysis of levels of transcript expression in matched tumour and normal tissues. Only those with significant differential levels of expression are shown. Boxes represent quartiles and lines represent limits of minimal and maximal data points. Number of patients included in the analysis is represented by 'n'. This analysis was conducted by Daniel Miller.

Daniel then went on to show that inhibition of type I receptor kinase activity in CAFs, through SB-43152 (SB) treatment (Inman et al., 2002), resulted in the loss of CAF contractile activity (data not shown). Since he had previously shown that CAFs secrete Activin, and not TGF-β, it was thought that treatment with SB exclusively blocked Activin signalling. Therefore, Activin signalling in CAFs may be integral to their contractile properties. Subsequently, determining the complete role of Activin signalling in CAFs became of great interest.

I joined the lab following the work described above. I wanted to build on the preliminary data Daniel had conducted to further characterise Activin signalling in these CAFs. Subsequently, I aimed to determine what role it plays on CAF functionality, if any. First, I wanted to show that CAFs specifically were positive for PSMAD. Daniel had shown PSMAD signalling was active but had not conducted any co-stains with CAF markers (Figure 3.1). I conducted a PSMAD2 and αSMA IF co-stain on sections from MMTV-PyMT tumours (Figure 3.5).

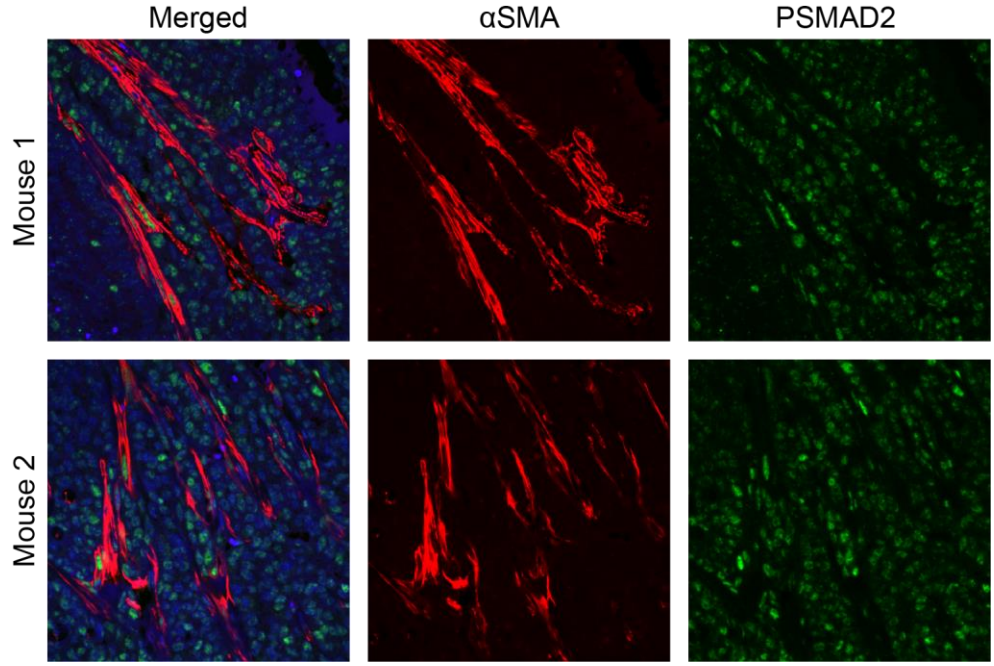

Figure 3.5. PSMAD2 and αSMA immunofluorescence on MMTV-PyMT mouse tumours. PyMT tumours were taken from 4 tumour-bearing mice. Sections were taken and stained for αSMA and PSMAD2. Slides were imaged in 5 distinct regions positive for αSMA staining. Images shown are the best representation of all samples. Merged images have DAPI stain.

Similar to the IHC shown in Figure 3.1, positive PSMAD2 staining can be observed in the PyMT tumours. In multiple instances, PSMAD2 positive staining can be observed in the nuclei of αSMA positive cells, a marker of CAFs (Östman and Augsten, 2009). This indicates that CAFs from MMTV-PyMT tumours have active TGF-β family signalling. However, not all αSMA positive cells exhibit PSMAD2 staining. Additionally, the surrounding cells in the tumour stroma, likely to be cancer cells, are also PSMAD2 positive.

Next, I wanted to confirm that these CAFs were also producing Activin within the tumour, not just *in vitro*. Therefore, I conducted *Inhba* and *Inhbb* RNAScope with an αSMA IF co-stain (Figure 3.6). Transcripts of *Inhba and Inhbb* show direct co-localisation with many αSMA-positive cells. This indicates that CAFs express both *Inhba* and *Inhbb*, the transcripts encoding Activin A and B respectively. Additionally, staining for each of *Inhba* and *Inhbb* is observed beyond αSMA-positive cells. Interestingly, it appears the majority of *Inhba* within these tumours is produced by αSMA-positive cells. Conversely, *Inhbb* transcripts co-localise with αSMA-negative and αSMA-positive cells equally. This suggests that Activin A is mainly produced by CAFs whereas Activin B is produced equally by both CAFs and cancer cells.

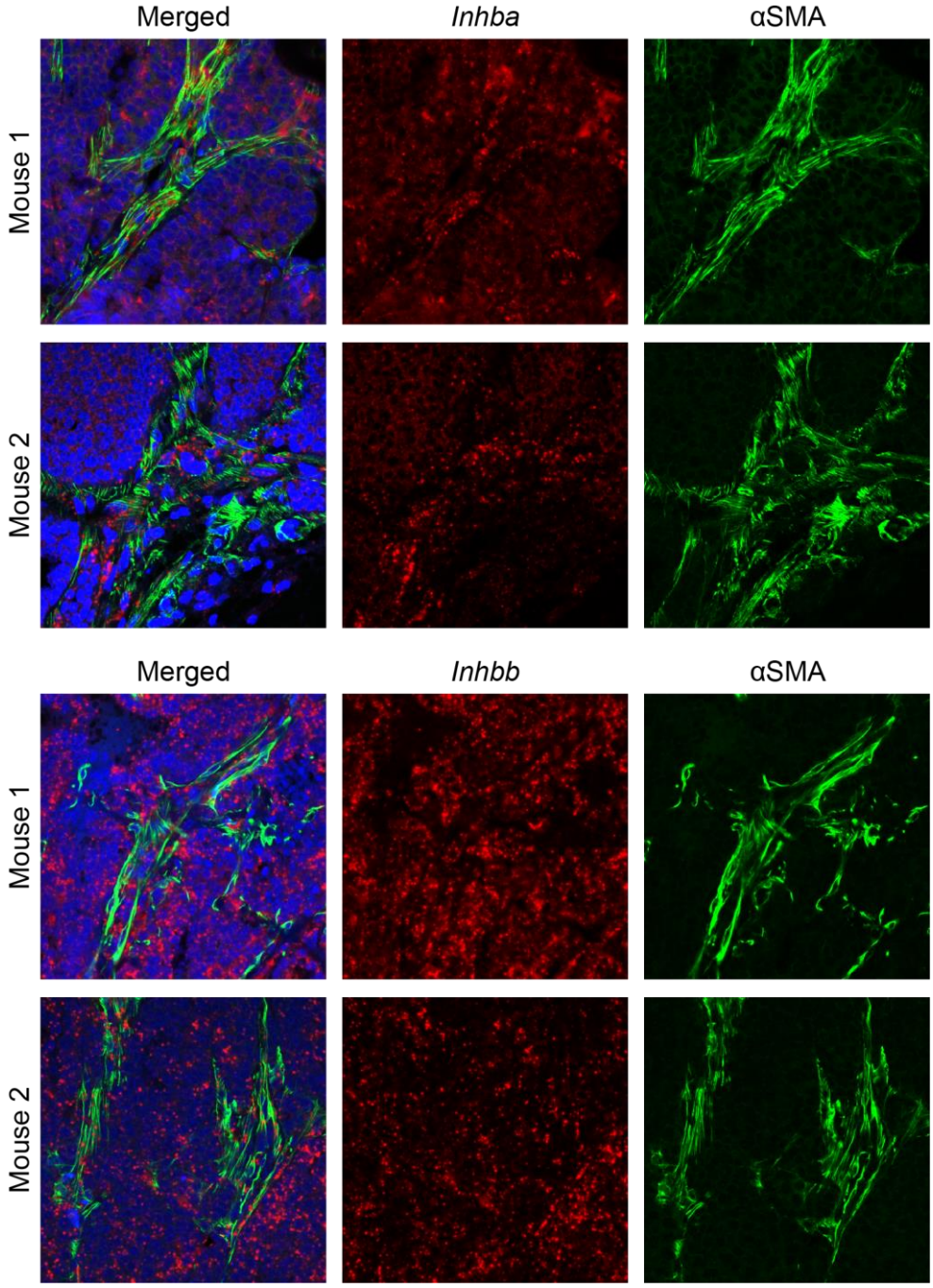

Figure 3.6. *Inhba* and *Inhbb* co-staining with αSMA in sections from MMTV-PyMT tumours. Sections taken from MMTV-PyMT tumours from 2 different mice probed for either *Inhba* or *Inhbb* transcripts using RNAScope (red). Subsequently, they were probed for αSMA using IF (green). Images taken are representative of at least 4 fields of view from 3 different mice. Merged images have DAPI stain.

I next investigated whether this phenomenon could be observed in other cancer types. Daniel had observed strong Activin A and B staining in mouse and human PDAC samples, as well as in skin cancer (data not shown). I sought to corroborate this finding. I conducted RNAScope staining against *Inhba* and *Inhbb* in

combination with αSMA IF on mouse pancreatic tumour samples. Specifically, I probed sections from Pan02 mouse xenograft tumours (Partecke et al., 2011) (Figure 3.7).

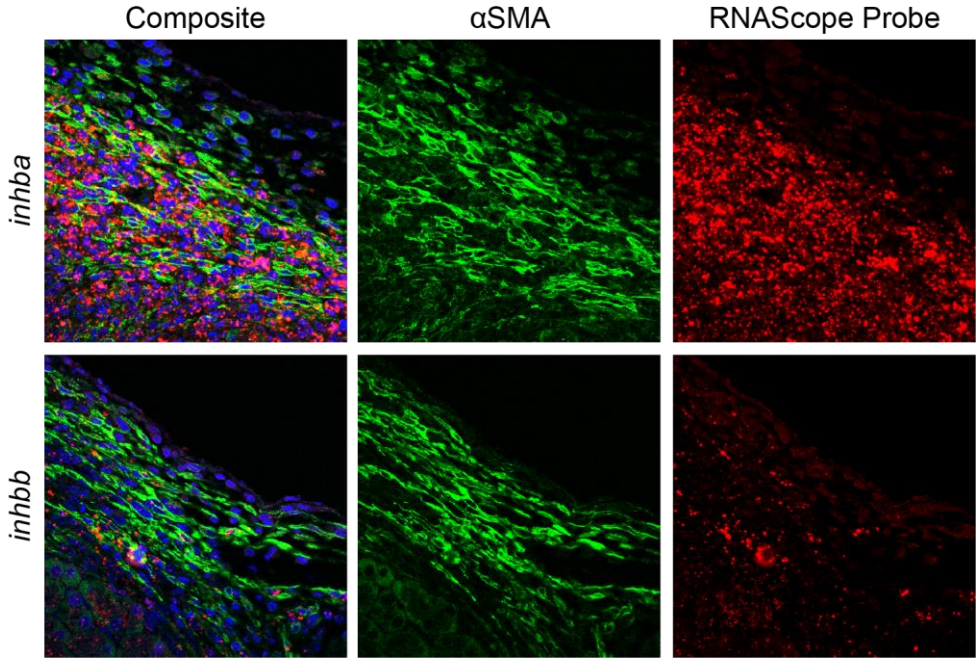

Figure 3.7. *Inhba* and *Inhbb* co-stain with αSMA on Pan02 mouse pancreatic tumour slices. Sections taken from a highly transformed Pan02 tumour were probed for *Inhba* and *Inhbb* using RNAScope (red) and a subsequent IF against αSMA (green). Images taken are representative of 4 distinct fields of view from one transformed pancreatic tumour sample.

There appears to be a very strong correlation between positive staining of αSMA and *Inhba* transcripts in these transformed pancreatic tumour samples. Additionally, some positive *Inhba* staining can be seen in αSMA-negative cells. The staining for *Inhbb* is not as strong as that seen for *Inhba* (Figure 3.7). However, areas of positive staining do co-localise with αSMA-positive cells. These observations are similar to those seen in Figure 3.6.

In this section colleagues and I have demonstrated that CAFs sourced from different tumour types produce Activin A and B. Moreover, the levels of Activin expression may correlate with poor prognosis in certain cancer types. This corroborates with published works (Seachrist and Keri, 2019; Staudacher et al., 2017b). Because of these observations, I sought to ablate Activin expression in a CAF cell line to determine its effect on signalling and function.

3.2.2 Knockout of Activin in CAFs

I chose to knock out expression of Activin A and B in a clonal CAF cell line using CRISPR/Cas9 technology. I aimed to obtain two cell lines for each of the following genotypes: *Inhba*$^{-/-}$, *Inhbb*$^{-/-}$ as well *Inhba*$^{-/-}$/*Inhbb*$^{-/-}$, referred to as Activin A-null, Activin B-null and Activin A/B-null lines respectively from herein. Figure 3.8 shows a schematic detailing the knockout strategy I employed.

Figure 3.8. CRISPR targeting region in INHBA (Activin A) and INHBB (Activin B). Schematic shows the structure of Activin A/B monomers as well as the accompanying nucleotide and amino acid sequences of the targeted region. Guides were designed against the start of the mature domain. The red line denotes the region to be targeted. Green letters in the nucleotide sequence denote the PAM site.

Activin dimers consist of 2 monomers. Each monomer contains a pro-domain and a mature region connected by a flexible linker (Figure 3.8) (Morikawa et al., 2016). During secretion, this linker is cleaved by Furin and the mature region leaves the cell non-covalently bound to its pro-domain. The mature region is then responsible for receptor binding and signal induction (Wang et al., 2016). I chose to target the mature region as truncation there should cause loss of downstream signalling. Single guide RNAs (sgRNAs) were generated using this strategy for each of Activin A and B. Subsequently, they were cloned into the px458 vector which also encodes Cas9 protein and GFP as a positive selection tool. The Cas9 and GFP sequences are segregated by a 2A sequence, encoding a self-cleaving peptide. The 2A component allows each of these 2 proteins to be synthesised from the same mRNA, meaning cells expressing GFP will also express the Cas9 protein (Radcliffe and Mitrophanous, 2004). This increases the chances of GFP positive cells harbouring the desired mutations. Following transfection of this construct, GFP-positive single cells can be sorted and, theoretically, would harbour mutations for appropriate proteins.

Before transfecting CAFs with each of these constructs, I isolated a parental CAF clone that was representative of the polyclonal pool. The population described thus far is an immortalised heterogeneous pool isolated from the MMTV-PyMT mouse model. Because of the heterogeneous and plastic nature of CAFs (see Section 1.5.4), there was a risk that a target clone isolated during the CRISPR/Cas9 knockout process may not be representative of the polyclonal pool. Utilising a parental clone would ensure that any clone selected downstream of CRISPR/Cas9 transfection would represent the initial heterogeneous pool and results generated thereafter would not be caused by clonal artefacts. Figure 3.9 shows a schematic for this clonal selection strategy and results from the mRNA screen. I chose to look at mRNA levels of each target gene as well as Follistatin. Knocking out Activins A and B in a clone that has high levels of each transcript may result in a more dramatic effect than the biological reality. Conversely, ablating their expression in a low expressing clone may have an inconsequential effect that is equally misrepresentative. For this same reason, I looked at expression of Activin antagonist Follistatin, which is also an Activin A/B target (Welt et al., 2002).

There is great variation across all clonal cell lines relative to the polyclonal pool (Figure 3.9). For example, clones 1 and 2 exhibit high expression of each of *Inhba* and *Inhbb*. Clones 3 and 4 show high expression of *Fst* relative to the polyclonal pool, 5 and 3-fold higher respectively. Conversely, clone 7 displays extremely low levels of *Inhbb* and *Fst* relative to the polyclonal pool. Of all clones, 5 and 6 appear to best represent the polyclonal pool in terms of expression of the transcripts of interest. However, clone 5 was selected for further experiments as expression levels were a slightly better representation of the polyclonal pool. From herein, CAF1 clone 5 is referred to as ‘parental CAF’.

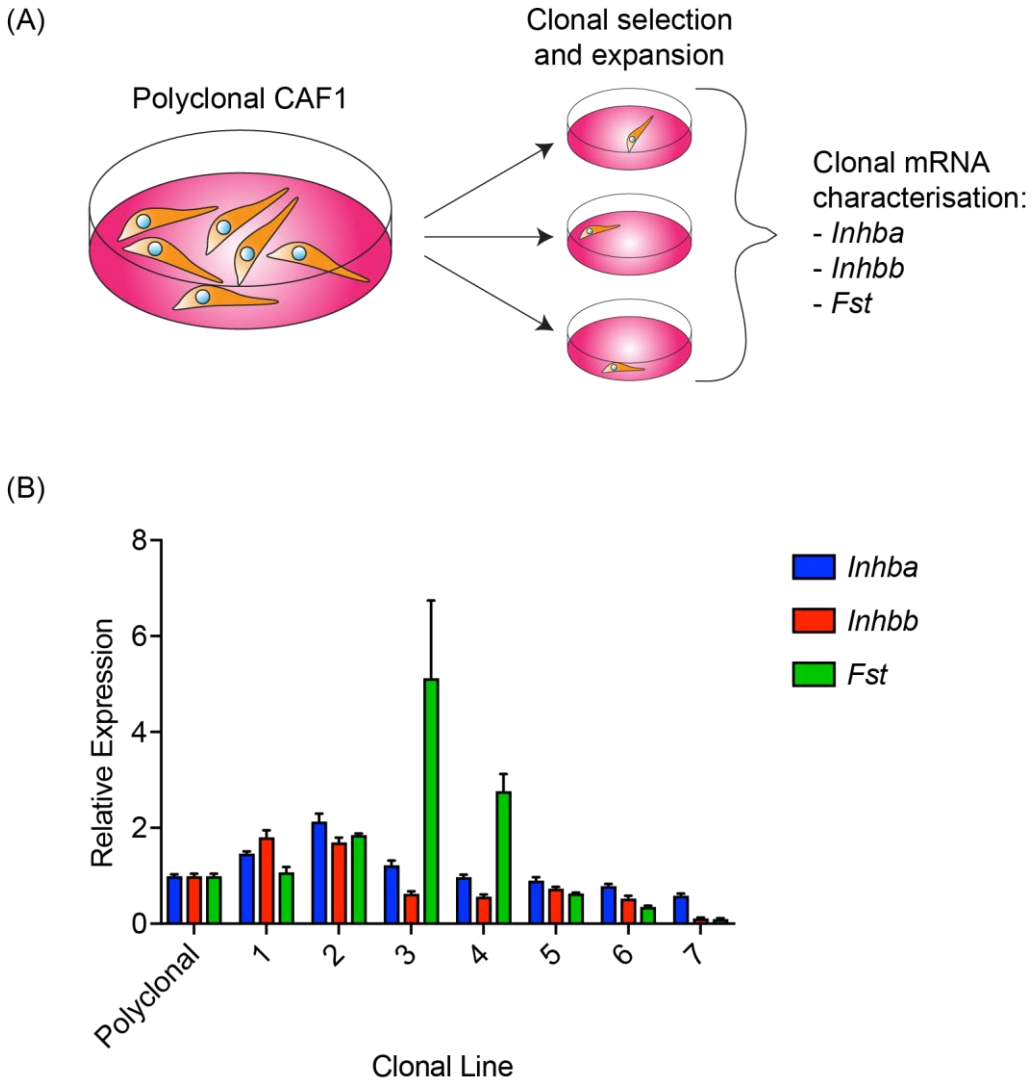

Figure 3.9. Parental CAF clone selection prior to CRISPR/Cas9 transfection. (A) Schematic detailing strategy to obtain a parental CAF clonal line. Polyclonal CAFs are seeded sparsely, clonal populations are taken and expanded before measuring transcripts of interest. (B) Results of qPCR mRNA analysis for 7 clonal lines relative to the polyclonal population. Results are of 3 technical replicates. Error bars represent SD.

Once I had determined the parental CAF clone for use, I conducted an initial transfection with guides against *Inhba*. Once I had obtained some Activin A null clones, I conducted a subsequent transfection with guides targeting *Inhbb* in both parental CAFs and Activin A-null clones to obtain Activin B-null and Activin A/B-null lines respectively. Clones obtained downstream of CRISPR/Cas9 transfection were expanded. I harvested protein for each clone and probed for Activin A and B expression.

(A)

Target	Activin A	Activin B	Activin A/B
Clones Screened	48	16	27
Negative Clones	8	5	9

(B)

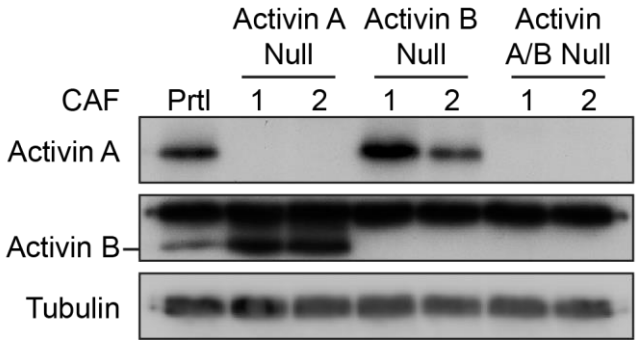

Figure 3.10. CAF Activin knockout clonal screen. (A) Table showing the number of clones screened for each target as well as the number that returned negative expression. (B) Western blot shows Activin A and B expression of the knockout clones selected for further experiments. Activin B band is denoted by black line to the left of blot. The band directly above is non-specific.

Forty-eight, 16 and 27 clones were screened for Activin A, Activin B and Activin A/B-null target populations respectively (Figure 3.10A). Varying percentages of clones were returned as successful knockouts based on a broader protein screen (data not shown), with 8, 5 and 9 negatives for Activin A only, Activin B only and both together respectively. The blot shows successful loss of protein expression for specific targets in appropriate populations (Figure 3.10B). Interestingly, Activin A-null cells appear to show enhanced levels of expression of Activin B when compared to levels in parental CAFs. The reverse phenomenon is not true in the case of Activin B null cells.

To confirm these clones as true knockouts, I sequenced the DNA encoding *Inhba* and *Inhbb* in relevant clones. Specifically, the region around the PAM site was sequenced, where I expected to see interruptions in the sequence (Figure 3.11).

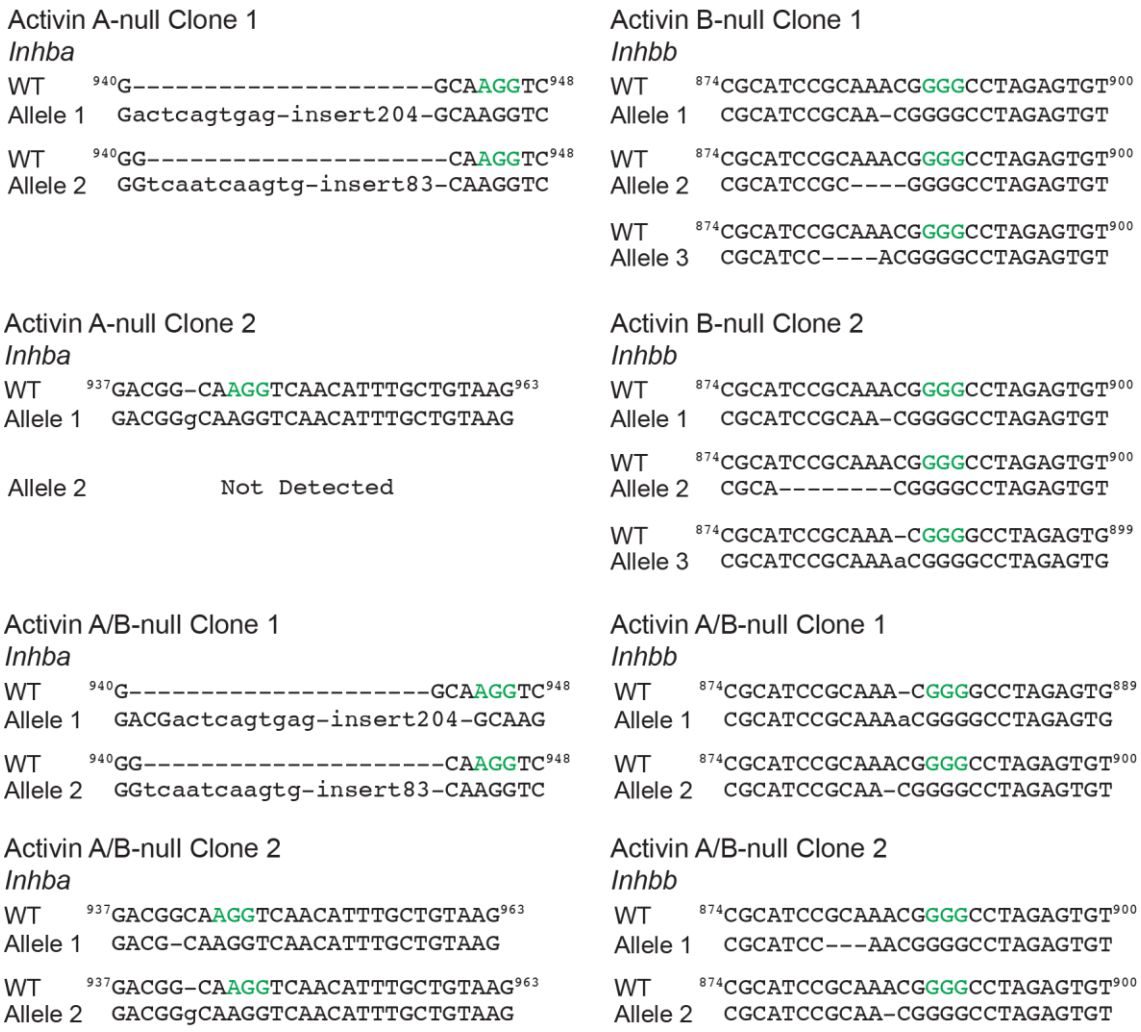

Figure 3.11. *Inhba* and *Inhbb* sequences in Activin knockout cells. DNA encoding Activin A (left) and Activin B (right) sequences in respective knockout clones aligned against the wildtype sequence. Lower case letters and '-' in allele sequences of knockout clones denote insertions and deletions respectively. Green font in the WT sequence indicates the PAM site.

Sequences were determined using distinct methods of MiSeq and PGemT cloning and sequencing (see Section 2.2.4). All targeted clones have indels in 100% of their alleles. The mutations are largely compound heterozygous with the exception of the Activin A sequence in Activin A-null clone 1. This has a homozygous single bp insertion. The majority of clones have out of frame mutations causing a frameshift and, therefore, truncation of the protein. One allele of the Activin B sequence in Activin A/B-null clone 2 is an exception to this, with allele 1 containing a 3-bp deletion. This could, theoretically, cause loss of just one amino acid, and the protein may remain functional. However, protein expression is lost (Figure 3.10B), and so a critical amino acid evidently has been deleted. The targeted region is within the furin

processing site. Loss of this amino acid may make it impossible for the protein to be processed and functionally expressed. Most clones have small indel mutations. However, Activin A-null clone 1 and Activin A/B-null clone 1 both have large insertions (totalling 216 bp and 96 bp for each allele) in the Activin A coding region. Not only are these large, but also out of frame, ensuring a loss of function truncation. Activin A null 1 is the clone of origin for the Activin A/B-null 1 line, hence the identical mutation for Activin A. Interestingly, there appears to be up to 3 alleles for Activin B, with each of the Activin B-null clones returning 3 mutated sequences in both MiSeq and PGemT methods. This could be because 2 clonal populations may have been sorted together with distinct mutations. Alternatively, one heterozygous WT clone may have been sorted initially. This may have undergone a division in which each daughter cell still had transiently active Cas9 protein. The Cas9 may then have mutated the remaining WT allele in each daughter cell with a distinct mutation. Finally, there may in fact be 3 alleles for Activin B in these CAFs. For the instances where 2 alleles are detected, there may be a large undetectable deletion, or the same mutation may occur in 2 alleles. In any case, the clone harbours no WT allele. A combination of the data in Figure 3.10 and Figure 3.11 confirm loss of expression of Activin A and B in the appropriate cell lines.

Once I had generated Activin A/B-null CAFs, I conducted another CM experiment with the knockout clones (Figure 3.12). I wanted to determine if the complete PSMAD2 induction through CAF CM seen in naïve HaCaTs was solely due to the Activin they secrete. As expected, HaCaT cells treated with recombinant Activin show similar levels of PSMAD2 induction to cells treated with CM from the parental CAF population (Figure 3.12). Additionally, the negative controls, NF1 CM and parental CAF CM with Follistatin, show little to no induction of PSMAD2 over untreated cells. Levels of PSMAD2 are significantly lower in Activin A-null CM ($P=0.0003$) and Activin B-null CM ($P=0.0008$) than parental CM-treated HaCaTs. CM from these clones exhibit a similar lack of induction seen in the negative controls. This effect is more pronounced in cells treated with CM from Activin A/B-null CAF clones ($P<0.0001$). Interestingly, PSMAD2 levels in cells treated with Activin A/B-null CM show lower levels of PSMAD2 than untreated cells, although this difference is not significant (Figure 3.12). These data suggest that the component within CAF CM that activates PSMAD signalling in HaCaTs is exclusively Activin A/B.

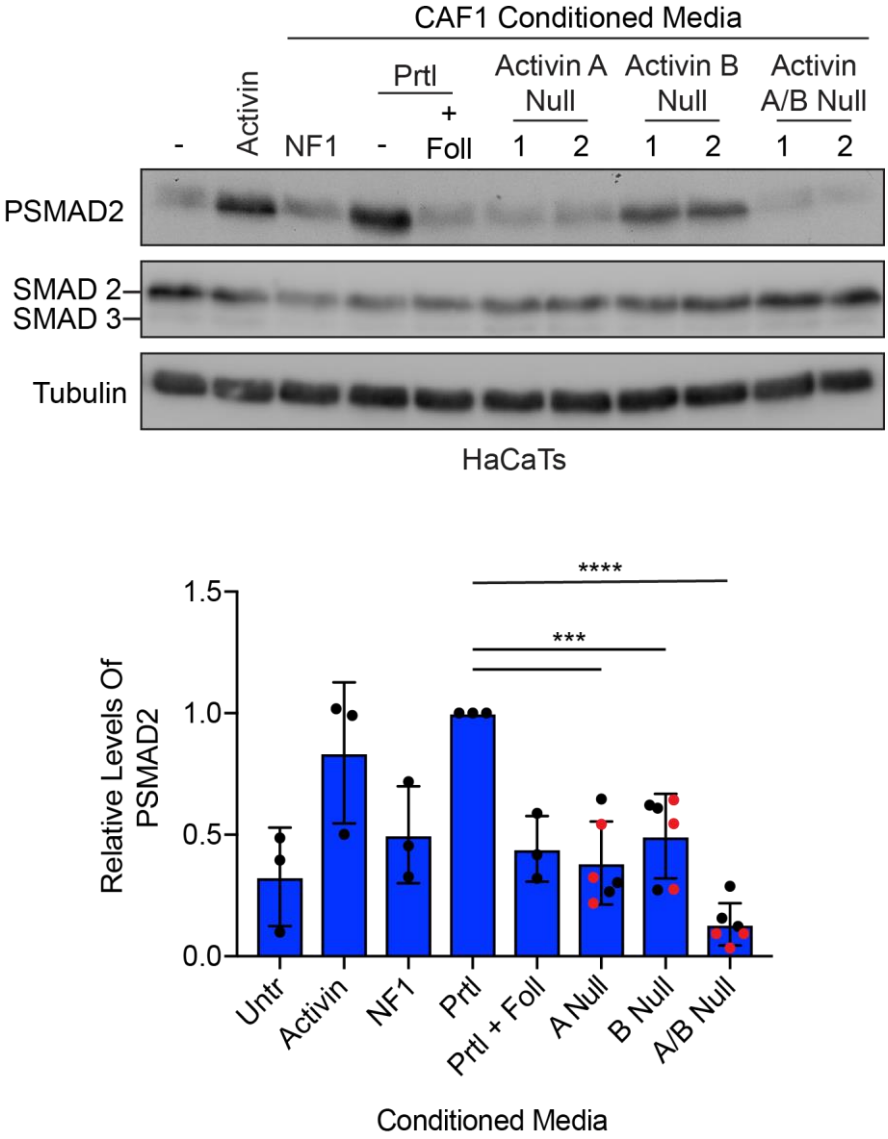

Figure 3.12. PSMAD2 induction in HaCaTs treated with clonal CAF CM. Levels of PSMAD2 in HaCaTs treated with CM from parental and knockout CAF clones alongside untreated, recombinant Activin treated and NF1 CM treated HaCaTs. Quantification is of 3 biological replicates and relative to HaCaTs treated with CM from parental CAFs. For knockout clones, each biological replicate of the 2 clones for each target population have been combined. Black dots denote clone 1 and red dots denote clone 2 replicates. Error bars denote SD. The statistical tests conducted were unpaired t-tests.

As well as PSMAD induction in naïve cells, I wanted to determine if basal PSMAD2 levels are affected across my Activin knockout clones (Figure 3.13).

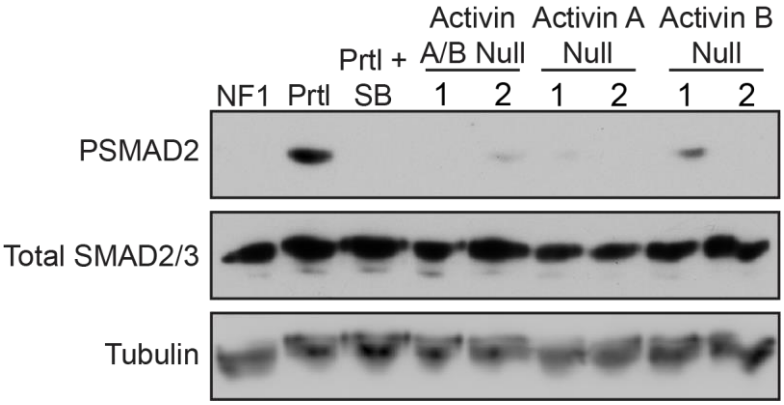

Figure 3.13. Basal PSMAD2 levels in CAF clonal populations. Lysates taken from respective CAF clonal populations were probed for levels of PSMAD2 and total SMAD2/3. Blot is representative of 2 biological replicates.

Strikingly, all knockout clones have much lower levels of basal PSMAD2. Parental CAFs exhibit by far the greatest levels of PSMAD2, whilst the negative controls NF1 and parental CAFs treated with type I receptor inhibitor SB show no PSMAD2. Interestingly, there is some clonal variability among each knockout population. Activin A/B-null 1 has no observable PSMAD2 compared to the small levels observed in Activin A/B-null 2. Similarly, Activin A-null 1 and Activin B-null 1 exhibit low levels of PSMAD2 whilst Activin A-null 2 and Activin B-null 2 show no observable levels. Of the knockout clones positive for PSMAD2, Activin B-null 1 shows the highest levels. In any case, all clones exhibit PSMAD2 levels significantly lower than the parental CAF population. This suggests that autocrine signalling has been dramatically affected in all knockout populations.

The experiments detailed in this section show that I successfully knocked out expression of Activin A and B alone and in combination. I have characterised these clones and demonstrated their autocrine signalling has been affected. Therefore, it was important to determine how this alteration manifested itself at a transcriptional and proteomic level to understand what CAF behaviours may be affected. I was interested in investigating the core CAF functionalities. Specifically, ECM remodelling, immune cell modulation, cancer cell invasion and angiogenesis.

3.2.3 Transcriptional characterisation of Activin null CAFs

To determine transcriptional changes genome wide in CAFs lacking Activin expression, RNA-Sequencing (RNA-Seq) was conducted on basal parental CAFs

and each of the Activin A/B-null lines. This aimed to provide unbiased insights into the type of CAF functionalities that may be affected by loss of Activin expression. Additionally, genes associated with the four core CAF functions of interest could also be interrogated. All data analysis and Figure curation in this section was conducted in collaboration with Stephanie Strohbuecker of the Bioinformatics facility at the Crick.

3.2.3.1 First pass analysis

Initially, a principal component analysis (PCA) plot was generated (Figure 3.14). This was done to determine variability among samples. All three technical replicates cluster very closely within distinct CAF clonal populations. This suggests the data obtained for each biological group is robust. However, there is greater variation between the distinct CAF populations themselves, including between each of the Activin A/B-null CAF populations. However, the most profound differences are observed when comparing the parental CAF samples with each of the Activin A/B-null cell lines. The variation between the parental CAFs and each of the Activin A/B-null lines is much more moderate. As a first pass analysis, this plot suggests that loss of Activin expression greatly affects the CAFs' transcriptome.

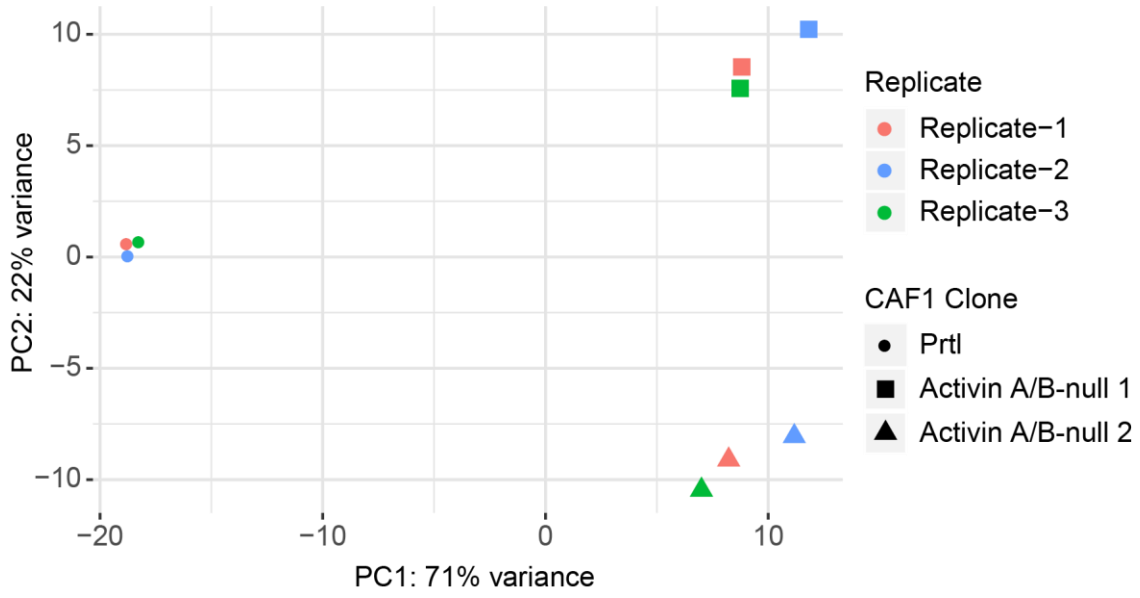

Figure 3.14. Principal component analysis of samples submitted for RNA-Seq. All 3 technical replicates for each of parental (Prtl) (circle), Activin A/B-null 1 (square) and Activin A/B-null 2 (triangle) were plotted for principal component analysis to show degrees of separation between biological groups and technical replicates within.

Further analysis was conducted to determine the number of genes affected by loss of Activin expression. A Venn diagram detailing the total number of genes with significantly altered log_2 fold change (log_2Fc) expression in Activin A/B-null cells when compared to parental CAFs was generated (Figure 3.15).

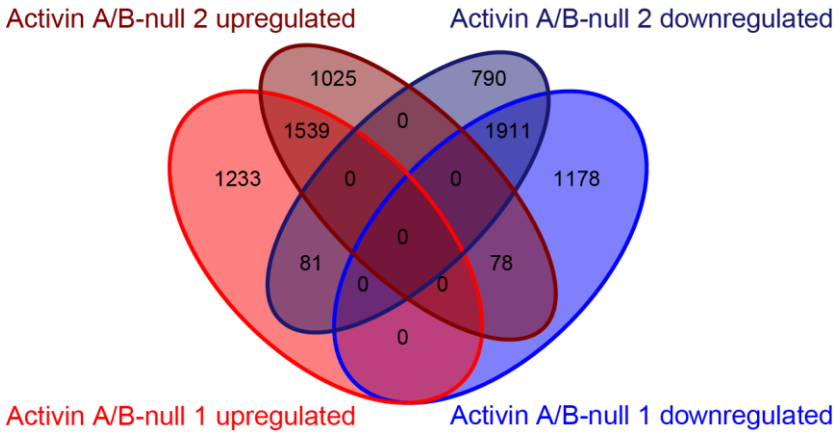

Figure 3.15. Venn diagram of all genes in which expression has been significantly affected in Activin A/B-null lines. Numbers of genes with significantly different levels of fold change expression in each Activin A/B-null cell line against the parental CAF clone ($P<0.05$).

All genes with a significant ($P<0.05$) log_2Fc of any value between each of the Activin A/B-null lines and the parental CAF line have been included in this Venn diagram and termed significantly differentially expressed genes. A total of 6020 and 5424 genes are significantly differentially expressed in Activin A/B-null 1 and 2 clonal lines respectively when compared to the parental CAF clone. Of these differential genes, 2853 and 2642 are upregulated for Activin A/B-null lines 1 and 2 respectively, whilst 3167 are downregulated in Activin A/B-null 1 and 2782 for Activin A/B-null 2. In total, 59.5% of genes differentially expressed in Activin A/B-null 1 are shared with Activin A/B-null 2. Similarly, 66.54% of differential Activin A/B-null 2 genes are shared with Activin A/B-null 1. Interestingly, 159 genes show inverse differential expression between Activin A/B-null 1 and 2 lines. Eighty-one genes that are upregulated in Activin A/B-null 1 are downregulated in Activin A/B-null 2. The corresponding inverse relationship can be seen for 78 genes upregulated in Activin A/B-null 2 cells. This data shows that a large number of genes demonstrate significant differential expression in CAFs upon loss of Activin A/B expression. A complete list of significantly differentially expressed genes is shown in Appendix 1.

For all analysis described herein, we focussed on comparing differences between the parental CAFs and a combination of the two Activin A/B-null CAFs. Results from such analysis would provide more robust conclusions as to the regulatory effects of Activin expression in CAFs rather than the subtle differences between the individual Activin A/B-null CAF lines. Additionally, for the analysis described in this paragraph, a log_2Fc expression cut-off was implemented. Only genes with a log_2Fc expression change greater than 2 are included. A total of 1648 significantly differentially expressed genes between the combined Activin A/B-null CAFs and parental CAFs met this threshold. The majority of these genes show similar levels and directions of change in expression (Figure 3.16). This demonstrates not only the massive effect loss of expression of Activin A/B has on CAFs, but also the robustness of the dataset generated.

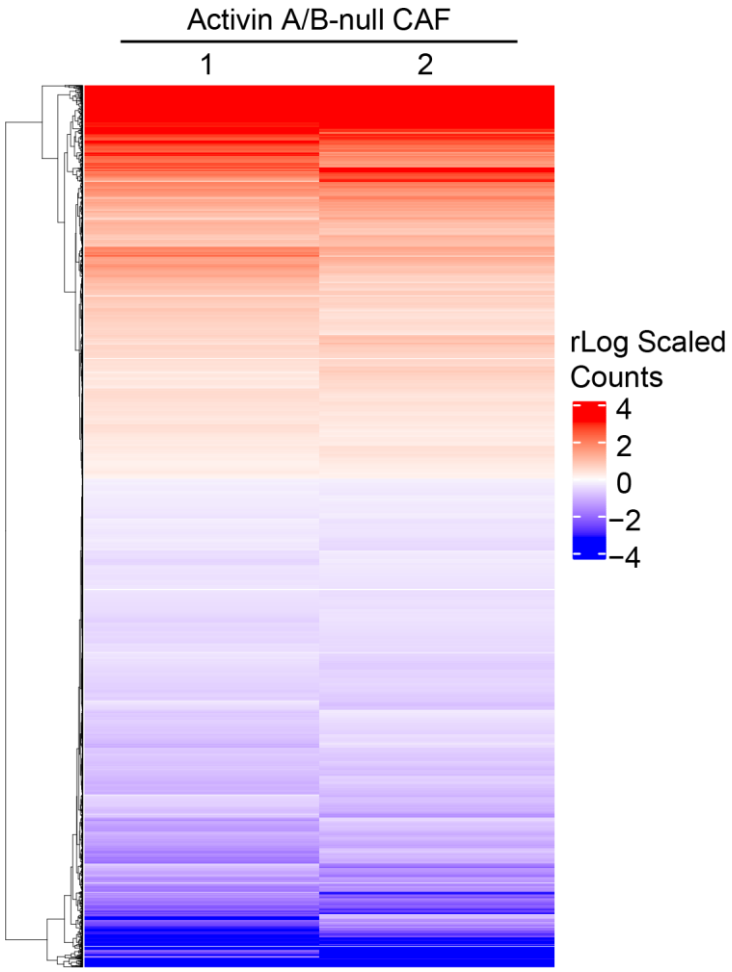

Figure 3.16. Heatmap showing grades of differential expression of genes in Activin A/B-null cells. Heatmap of all significantly differentially expressed genes that average a Log_2Fc greater than +/- 2. Red and blue shading denote degrees of up and downregulation respectively. The counts are regularised log transformed and scaled so the expression in the parental line equals zero.

3.2.3.2 Target validation

Before conducting any further analysis, I decided to investigate whether the significantly differentially expressed genes used in this analysis with low levels of expression, as measured by transcripts per million (TPM) values, could be validated using qPCR. I was concerned that genes with lower TPM values may have been noise that could invalidate the analysis and ensuing conclusions. I selected a cut-off of <1 as a threshold for low-expressing genes. If I could detect mRNA of these genes using qPCR, it would add validity to the mRNA-seq analysis.

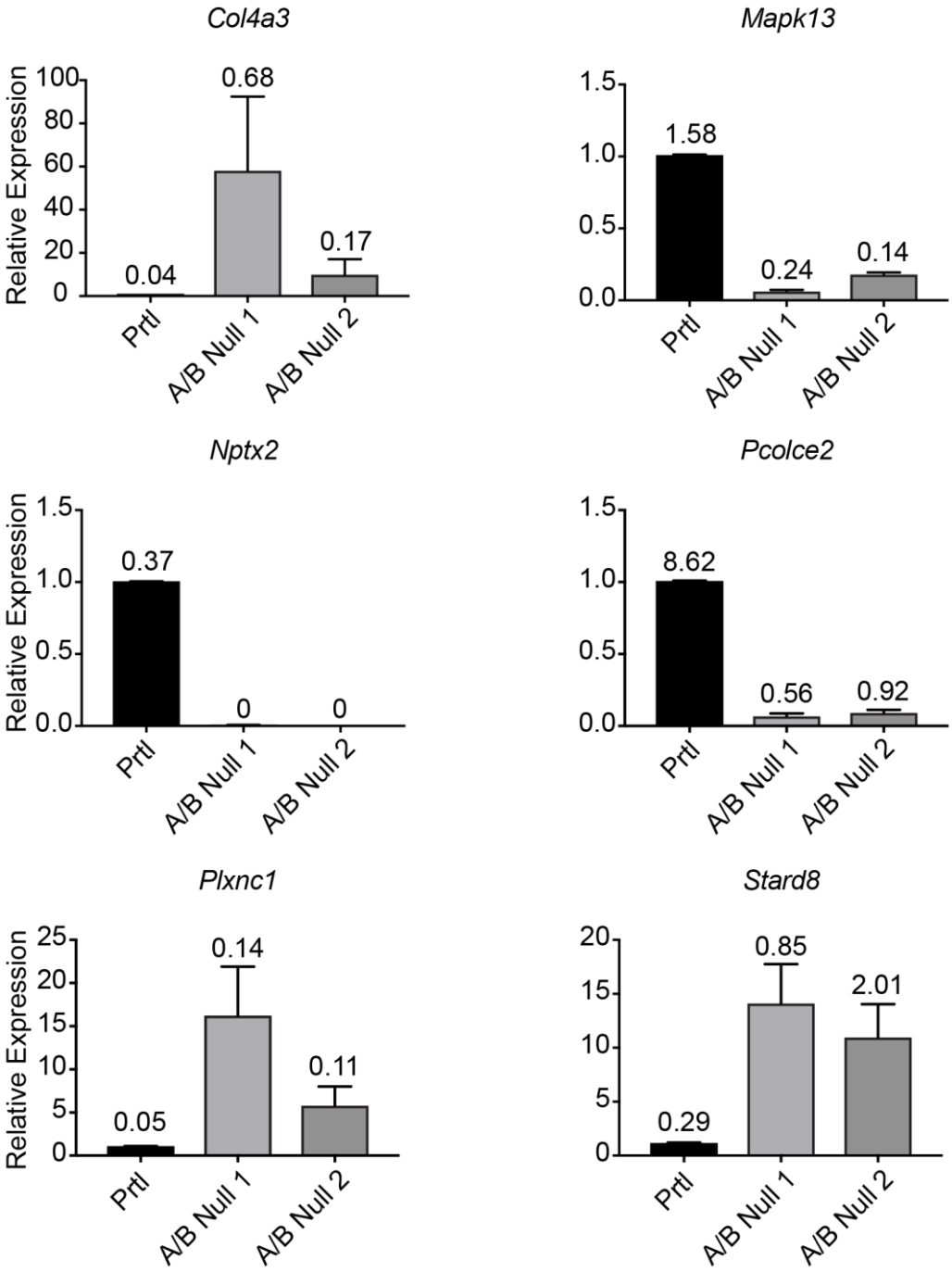

Figure 3.17. qPCR of low expressing significantly differentially expressed genes from RNA-seq analysis. Six genes with TPM values <1 were assessed using qPCR. The same RNA samples submitted for RNA-Seq were used in this experiment. Averages are of 3 biological replicates. Error bars denote the SEM. Values above each bar indicate the returned average TPM value from the RNA-Seq analysis. Expression is relative to the parental group for all genes.

Genes with TPM values as low as 0.04 (*Col4a3* expression in parental CAFs) are detectable using qPCR (Figure 3.17). Additionally, the vast majority of genes exhibit the same trends in expression as measured using TPM values. Exceptions

to this are *Stard8* and *Mapk13*. In the case of *Mapk13*, the TPM value for Activin A/B-null 1 is 0.24 whilst Activin A/B-null 2 it is 0.14. Whilst Activin A/B-null 1 and 2 lines exhibit TPM values of 0.85 and 2.01 respectively for *Stard8*. In each case, the cell line with the lower TPM value shows higher levels of expression as detected by qPCR for the gene in question. In any case, patterns of fold change expression are consistent between RNA-seq and qPCR detection in all cases, despite the low TPM value for each gene. This suggests the detection levels for significantly differentially expressed genes determined by RNA-seq are robust and the dataset is reliable.

3.2.3.3 Reactome pathway analysis

Following this first pass analysis, further analysis was conducted to determine the types of signalling pathways and functions that may be affected by loss of Activin A/B expression. All significantly differentially expressed genes between the combination of both Activin A/B-null CAF lines and parental CAFs were submitted for Reactome pathway analysis (Figure 3.18). No cut-off based on TPM values or standard deviations was applied, as this risked limiting the information available during this analysis. Many of the pathways listed are associated with interactions with and remodelling of the extracellular matrix such as 'Non-integrin membrane-ECM interactions', 'Collagen biosynthesis and modifying enzymes' and 'Collagen formation'. Additionally, propagation of 'Signalling by receptor tyrosine kinases' is associated with interactions with the extracellular matrix (Hastings et al., 2019). Furthermore, the 'Rho GTPase cycle' (4th in the list) is strongly associated with a contractile CAF phenotype (Calvo et al., 2015). This subtype is responsible for actively altering the extracellular and promoting cancer cell invasion (Calvo et al., 2015). Interestingly, axon guidance and other related pathways, such as Ephrin signalling, are highly significantly enriched. These pathways are associated with cellular migration, suggesting the motility of the CAFs may be affected (Aberle, 2019; Huot, 2004). Taken together, the Reactome pathway enrichment suggests that loss of Activin A/B may affect the way CAFs interact with and alter the extracellular matrix as well as their migratory capacity. A complete list of significantly enriched pathways is shown in Appendix 2.

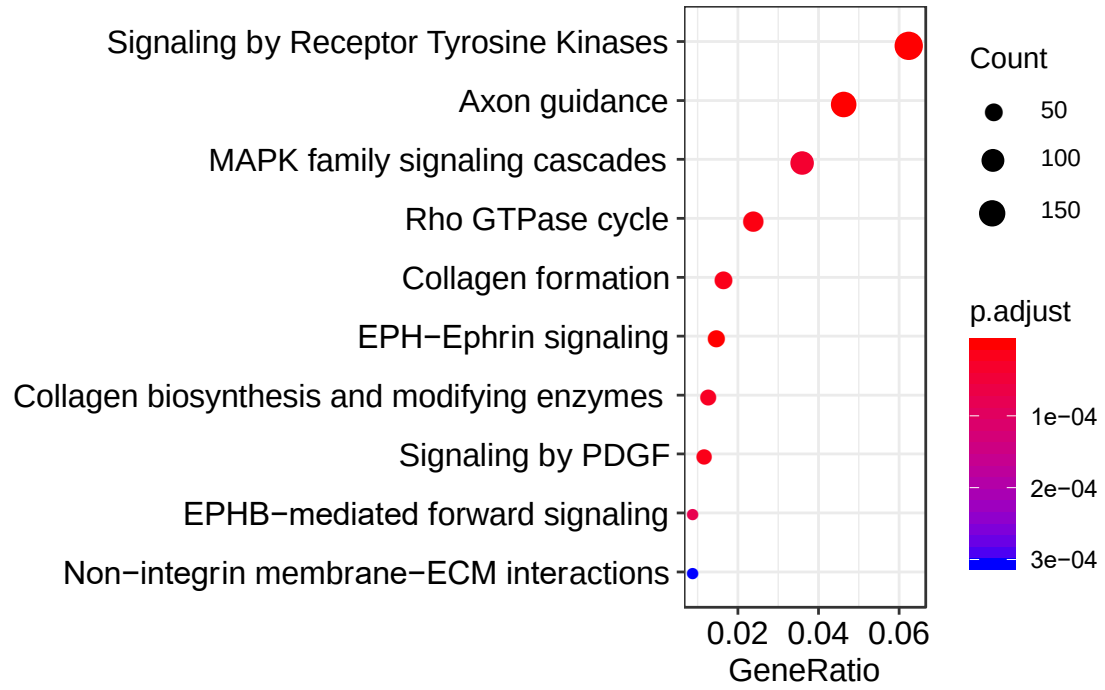

Figure 3.18. Top 10 significantly enriched terms in Reactome pathway analysis. Significantly differentially expressed genes between Activin A/B-null and parental CAFs were submitted for Reactome pathway analysis to determine pathway enrichment. Reactome pathway hits are ordered in terms of GeneRatio, with the highest at the top of the list.

Following this, I decided to look more closely at the genes associated with some of these pathways. Specifically, whether certain genes integral for pathway activity are up or downregulated. I chose to look specifically at 'Rho GTPase Cycle' (Figure 3.19), due to the pathway's association with CAF functionality, as well as 'Signalling by TGF-β family members' (Figure 3.20). This pathway was not in the top 10 most significantly enriched, however it is of interest due to the direct connotations with loss of Activin signalling as well as the strong functional association CAFs have with TGF-β family signalling (Calon et al., 2012, 2014).

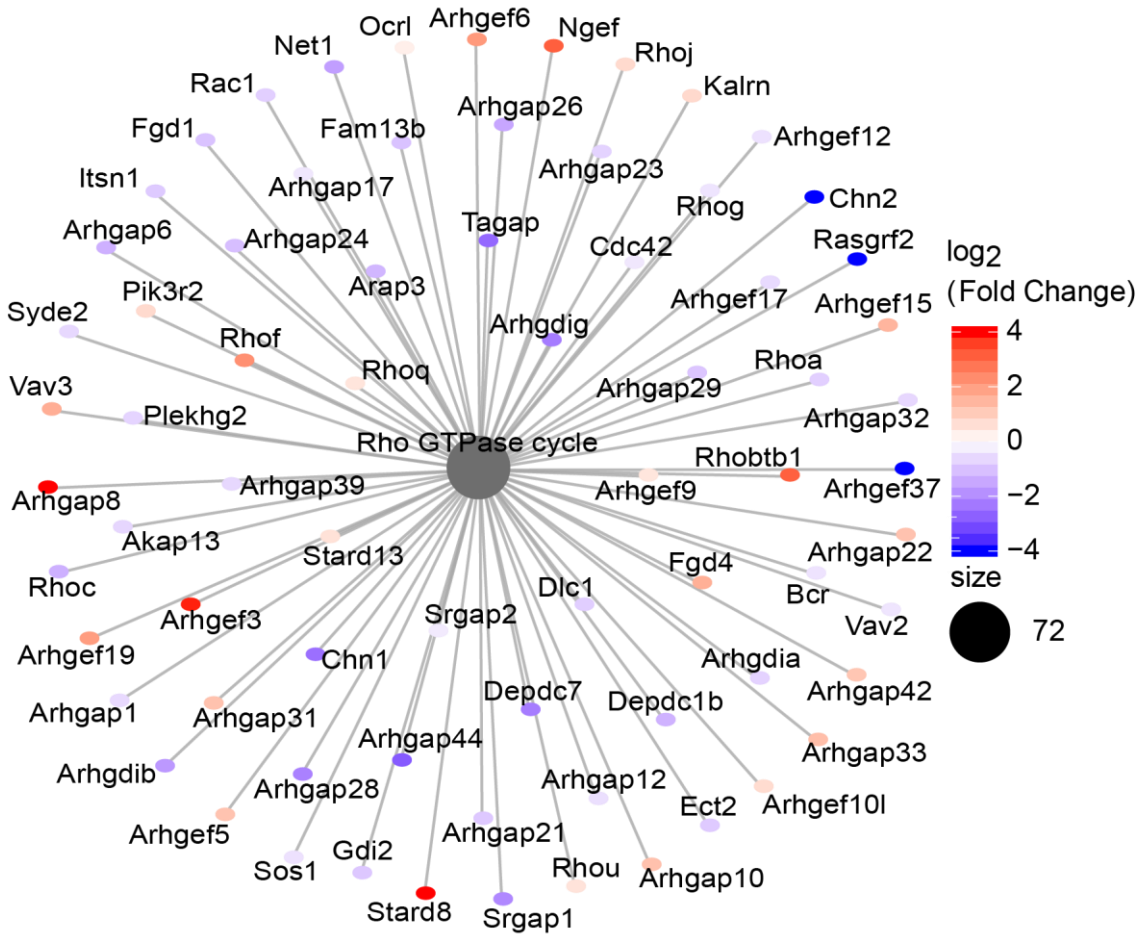

Figure 3.19. Spiderplot of significantly differentially expressed genes associated with Reactome pathway 'Rho GTPase cycle'. Genes associated with the 'Rho GTPase cycle' that are significantly differentially expressed upon loss of Activin expression in Activin A/B-null CAFs. Degrees of red and blue shading denote up- and downregulation respectively.

Investigating the effect of Activin A/B on expression of genes associated with the Rho GTPase cycle in CAFs lacking Activin expression is of great interest. Activation of this pathway leads to a phosphorylation of myosin light chain proteins and a contractile CAF phenotype. This is associated with promoting tumourigenesis and metastasis through extracellular matrix remodelling (Gaggioli et al., 2007). A general downregulation of genes associated with activation of the pathway was observed in Activin A/B-null CAFs (Figure 3.19). For example, Rho GTPases *Rhoa*, *Cdc42* and *Rac1* are significantly downregulated (Log2Fc of -0.7 -1.0 and -0.7 respectively). Interestingly, there is great variation of both up and downregulation in expression of the GEF and GAP proteins, responsible for activating and inactivating pathway activity respectively (Ungefroren et al., 2018). No consistent pattern of up or down

regulation can be observed for either of these family of proteins. Intriguingly however, *Net1* expression is significantly downregulated (Log2Fc -1.7). *Net1*, a direct SMAD3 target, is a GEF critical for RhoA activation and downstream cytoskeletal reorganisation and stress fibre induction (Lee et al., 2010).

The same analysis was conducted for the Reactome pathway 'Signalling by TGF-β family members'. A number of key mediators and regulators of the TGF-β pathway exhibit significant differential expression in CAFs lacking Activin A/B expression. Interestingly, inhibitors of the pathway, specifically *Grem2*, *Smad7*, *Fst* and *Bambi* show downregulation (Hill, 2016; Sanders et al., 2016; Shangguan et al., 2012; Welt et al., 2002). Additionally, transcripts that encode receptors and SMAD proteins show a general pattern of upregulation, including *Bmpr1b*, *Bmpr2*, *Smad1*, *Smad3*, *Smad4*, *Tgfbr1* and *Tgfbr2*. *Acvr1c* and *Acvrl1* are exceptions to this, exhibiting downregulation. No ligands show significant upregulation in expression upon loss of Activin expression. CAFs lacking Activin expression could be upregulating receptors and pathway mediators in an attempt to 'sense' signalling that has been lost by Activin autocrine signalling. This is compounded by the observation that pathway inhibitors are downregulated.

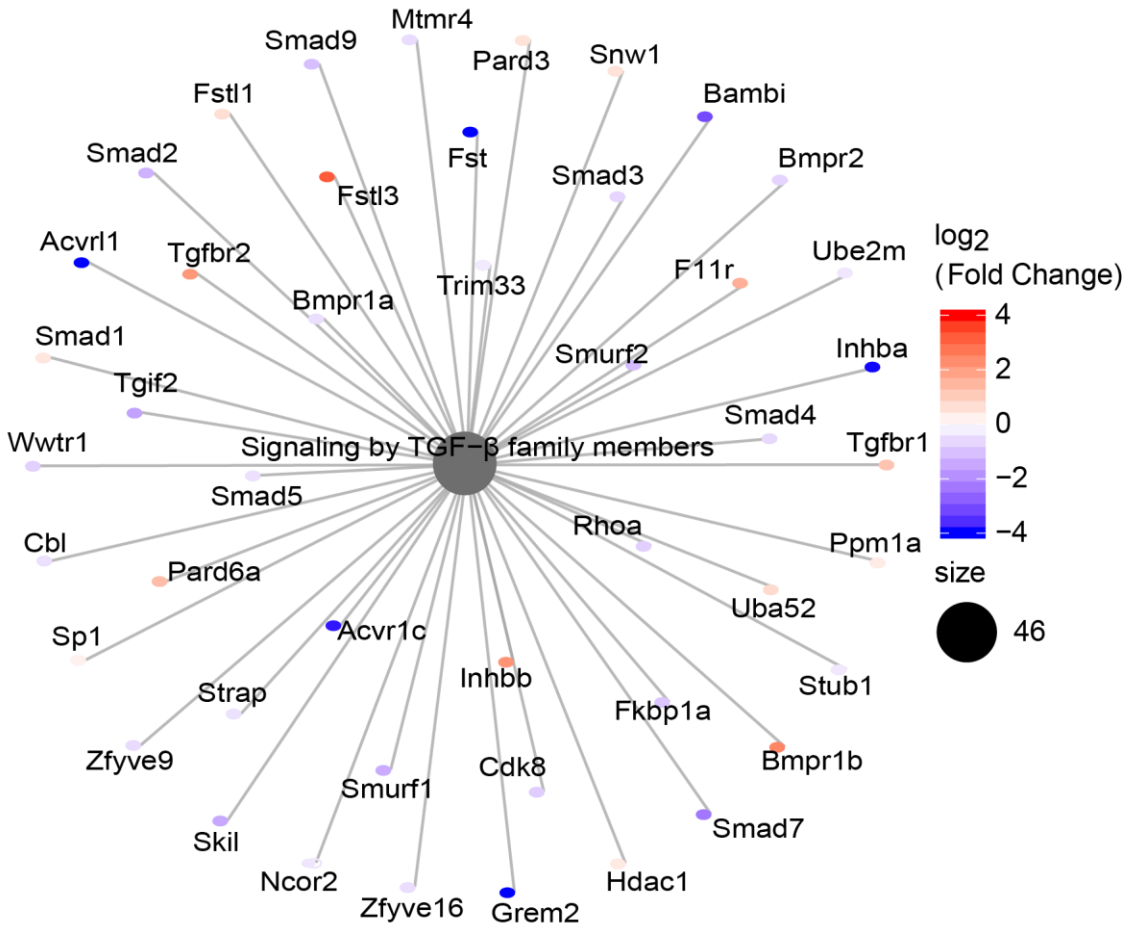

Figure 3.20. Spiderplot of significantly differentially expressed genes associated with Reactome pathway 'Signalling by TGF-β family members'. Genes associated with pathways 'Signalling by TGF-β family members' that are significantly differentially expressed in Activin A/B-null CAFs. Degrees of red and blue shading denote up and downregulation respectively.

The analysis above was a very unbiased approach to determine critical genes and pathways that are affected upon loss of Activin expression in CAFs. Further to this, I chose to look at curated lists of genes associated with 3 of the 4 critical functionalities; ECM remodelling, immune cell modulation and angiogenesis. Cancer cell invasion was not investigated. It was difficult to find a robust gene list for genes and cytokines associated with CAF-mediated cancer cell invasion. Any manually curated list may have not been comprehensive enough or risked introducing bias.

3.2.3.4 ECM Remodelling

For ECM remodelling, I adopted a previously curated list of 'ECM modulator proteins' established in Naba et al., 2012. These proteins are responsible for remodelling the extracellular matrix and include MMPs and their regulators. A heatmap was curated of 45 significantly differentially expressed genes with the highest log_2Fc between Activin A/B-null and parental CAFs (Figure 3.21).

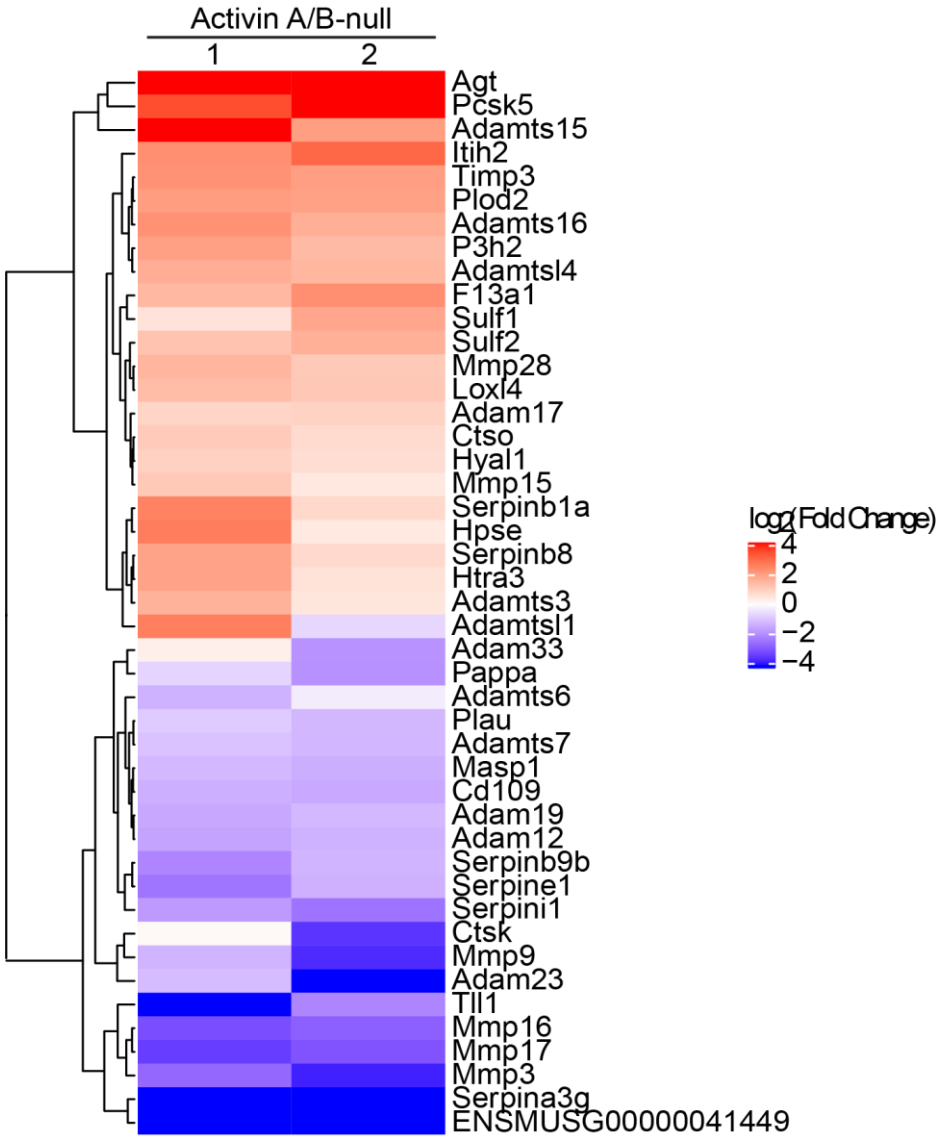

Figure 3.21. Differentially expressed genes in Activin A/B-null CAFs encoding ECM modulators. Heatmap of significantly differentially expressed known ECM modulators (Naba et al. 2012) between Activin A/B-null and parental CAFs. The genes with the top 45 absolute log_2Fc are shown.

The heatmap shows that, generally, genes encoding proteins responsible for degradation of the ECM are downregulated in Activin A/B-null CAFs. With the exception of *Mmp15*, all MMPs returned from this list are downregulated. These include *Mmp3*, *Mmp9*, *Mmp16* and *Mmp17*. MMPs are a family of zinc-dependent endopeptidases that are capable of degrading many components of the ECM. Such degradation is associated with enhanced cancer cell invasion (Itoh and Nagase, 2002). In fact, increased expression of MMP3 and MMP9 strongly correlates with increased invasion and poor prognosis in a variety of cancers, including breast cancer (Gobin et al., 2019). The genes encoding each of these are downregulated in Activin A/B-null CAFs. Additionally, many members of the ADAM (a disintegrin and metalloproteinase) and ADAMTS (a disintegrin and metalloproteinase with thrombospondin motifs) family of proteins, which are known to have protease and degradative properties (Edwards et al., 2009; Kelwick et al., 2015), appear to be downregulated, specifically, *Adam12, Adam19, Adam23, Adamts6* and *Adamts7*. However, this trend is less robust as many of these proteins are also upregulated in Activin A/B-null CAFs, namely: *Adam17, Adamts3, Adamts15, Adamts16* and *Adamtsl4*. Of the ADAMTS proteins, two have currently unknown substrates and functions (*Adamts6* and *Adamts16*) (Kelwick et al., 2015). Whilst *Adamts3* and *Adamts7* have documented associations with promoting lymphangiogenesis and thrombospondin cleavage respectively (Jeltsch et al., 2014; Liu et al., 2006). Interestingly, silencing of *Adamts15* is associated with enhanced tumour growth in colorectal cancer. It is thought that *Adamts15* may work to inhibit pro-proliferative P-ERK signalling (Viloria et al., 2009). Its elevated expression in Activin A/B-null CAFs may result in a similar phenomenon. Interestingly, with respect to the ADAM family, *Adam12* and *Adam19* show downregulation upon loss of Activin A/B expression. ADAM12 and ADAM19 are associated with enhanced cancer cell invasion and exhibit increased expression in breast cancer and glioma patients respectively (Duhachek-Muggy et al., 2017; Wildeboer et al., 2006). Conversely, ADAM17 is upregulated in Activin A/B-null CAFs. Its increased expression is observed in metastatic breast cancers (McGowan et al., 2007). In any case, these ECM remodelling proteins show great variations in expression upon loss of Activin A/B expression. Furthermore, genes encoding proteins that inhibit metalloproteinase like enzymes show altered expression. For example, the Serpin family of proteins and *Timp3*. Interestingly, *Timp3* (Log_2Fc of 4.2) has been shown to inhibit the oncogenic

Adam12 protein (Roy et al., 2004). Taken together, this data suggests expression of genes associated with remodelling the ECM are greatly affected in CAFs lacking Activin expression. Interestingly, there is a trend in decreased expression, and possibly activation, of degradative enzymes.

3.2.3.5 Immunomodulatory genes

From the Reactome pathway analysis, there was not great enrichment of genes associated with immune-modulatory cytokines. However, I identified a list of secreted inflammatory cytokines that are significantly differentially expressed in either Activin A/B-null cell line. A heatmap was then curated using this list to help visualise differential expression of these cytokines.

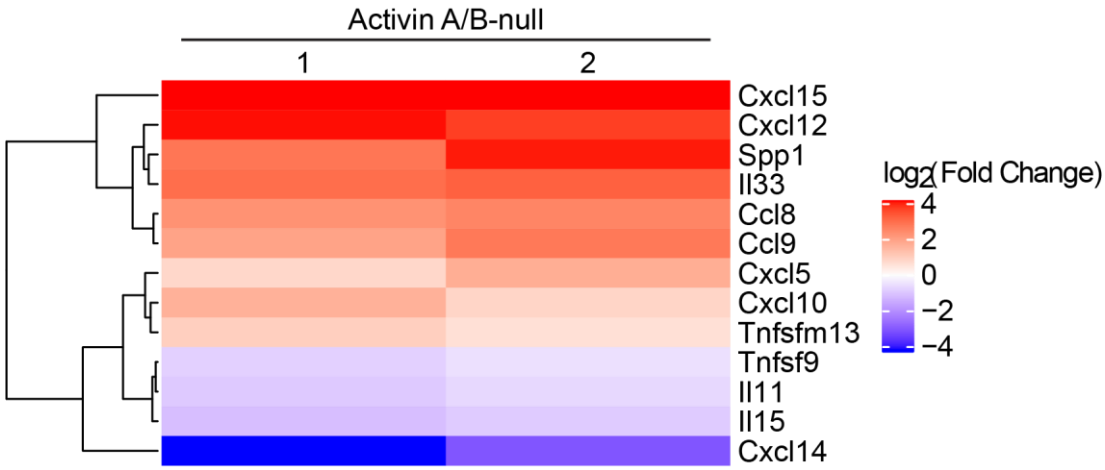

Figure 3.22. Immunomodulatory cytokines showing significant differential expression in Activin A/B-null CAFs. A manually created list of 13 genes associated with immune cell modulation that showed significant differential expression between Activin A/B-null and parental CAFs was curated. The heatmap shows the Log_2Fc expression of these genes in each Activin A/B-null CAF line.

Many of the genes in the heatmap are associated with monocyte and macrophage infiltration and activation. For example, *Spp1*, *Ccl8*, *Ccl9* and *Cxcl14* have all been demonstrated to act as monocyte and macrophage chemotractants (Halvorsen et al., 2016; Icer and Gezmen-Karadag, 2018; Kortlever et al., 2017; Lu et al., 2016). Each exhibit log_2Fc levels of expression of 6.5, 4.7, 4.6 and -7.0 respectively. Additionally, *Il11* (log_2Fc -0.4) signalling prevents macrophage activation (Schwertschlag et al., 1999). Genes associated with modulating lymphocyte responses within tumours also exhibit significant differences in

expression in Activin A/B-null CAFs. For example, *Cxcl12* (log_2Fc 7.5), *Cxcl10* (log_2Fc 2.4) and *Spp1* (log_2Fc 6.5) are lymphocyte chemotractants (Balabanian et al., 2005; Karin and Razon, 2018). Conversely, *Ccl9* (log_2Fc 4.6) has been shown to exclude T cells from the tumour microenvironment (Kortlever et al., 2017). Beyond migration, many of the genes are associated with promoting activation and differentiation of lymphocytes. For example *Il33* (log_2Fc 6.0) and *Il11* (log_2Fc -0.4) have been shown to promote a Th2 response (Bozza et al., 2001; Yagami et al., 2010). Additionally, *Il15* (log_2Fc -0.4) promotes a cytotoxic CD8 phenotype (Robinson and Schluns, 2017). Genes associated with modulating other immune cell populations are also differentially expressed. For example *Cxcl15* (log_2Fc 12.3), *Spp1* (log_2Fc 6.5) and *Cxcl5* (log_2Fc 2.4) promote neutrophil migration (Icer and Gezmen-Karadag, 2018; Schmitz et al., 2007; Zhang et al., 2020b). Finally, *Cxcl14* (log_2Fc -2.9) is a strong chemotractant for natural killer cells (Lu et al., 2016).

Taken together, the data in this heatmap suggests loss of Activin expression in CAFs may affect their immune modulatory functions. However, it is unclear whether this effect works to promote or diminish migration and activation of immune cell populations.

3.2.3.6 Angiogenesis

Gene ontology (GO) term analysis highlighted angiogenesis as a significantly overrepresented term ($P<2x10^{-16}$) among the significantly differentially expressed genes between Activin A/B-null and parental CAFs (GO term ‘0001525 angiogenesis) (a complete list of significantly overrepresented GO terms are shown in Appendix 3). A total of 241 genes from the GO term are significantly differentially expressed in Activin A/B-null CAFs. The top 45 most differentially expressed in terms of log_2Fc have been curated into a heatmap (Figure 3.23). Many of the genes listed in the heatmap are associated with embryogenesis and cardiac tissue development. However, several are implicated in promoting angiogenesis in adult tissue and during disease. These genes include: *Ccn3* (log_2Fc 15.8), the phosphoinositides *Pik3r6* and *Pik3cg* (log_2Fc 11.8 and 7.0 respectively), *Sfrp2* (log_2Fc 10.7), *Cxcl12* (log_2Fc 3.2), *Ccbe1* (log_2Fc 6.2), *Aqp1* (log_2Fc 5.4), *Pparg* (log_2Fc 4.7) and *Hgf* (log_2Fc 4.1) (Crowley et al., 2016; Davies et al., 2019; Gao et al., 2019; Jeltsch et al., 2014; Lin et al., 2005a; Saadoun et al., 2005; Vattulainen-Collanus et al., 2016). These genes

either work to promote migration of endothelial cells, enhance expression of endothelial growth factors or show significant correlative expression in tumours with high degrees of angiogenesis. Conversely, one of the upregulated genes, *Dcn* (log_2Fc 7.5) is a critical inhibitor of angiogenesis specifically within the tumour stroma. It directly inhibits VEGFR2 and cross-links type I collagen proteins to create a rigid environment that is less permissive for angiogenesis (Yamaguchi et al., 1990).

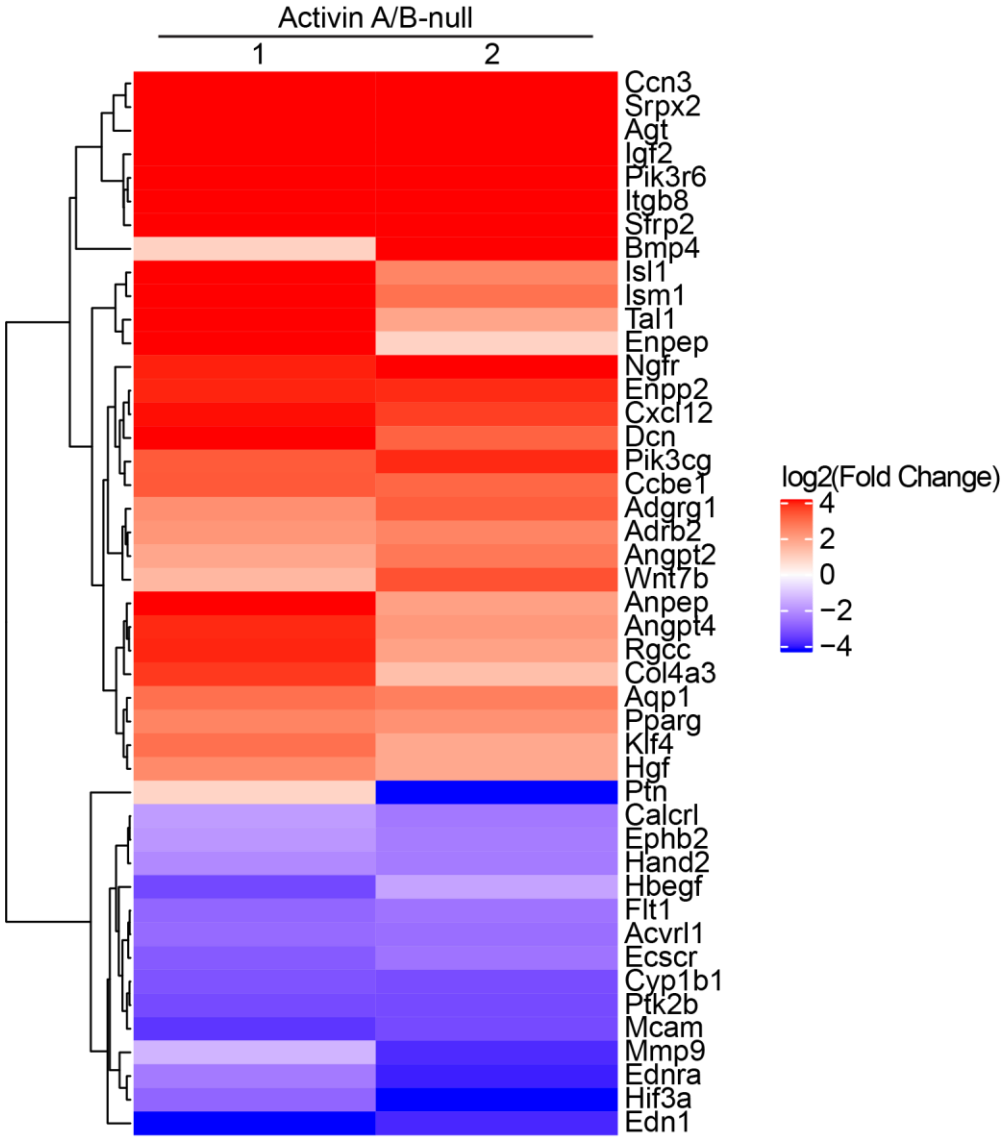

Figure 3.23. Heatmap showing expression of genes associated with angiogenesis. The dataset for significantly differentially expressed genes in Activin A/B-null CAFs was submitted for GO analysis for term '0001525 angiogenesis'. The top 45 most differentially expressed genes in terms of log_2Fc were curated into this heatmap.

Many of the downregulated genes are markers of endothelial cells with little known of their function in other cell populations. However, similarly to the

upregulated genes, many appear to be associated with enhancing angiogenesis. For example, *Calcrl* (log_2Fc -4.0), *Ephb2* (log_2Fc -4.0), *Hbegf* (log_2Fc -4.7) and *Flt1* (log_2Fc -5.0) have all been shown to promote angiogenesis specifically in tumour contexts. For example, extracellular vesicles containing Ephb2 promote angiogenesis in solid tumours (Sato et al., 2019). Hb-egf is a potent mitogen that has been shown to promote motility in multiple populations, including endothelial cells and cancer cells, promoting angiogenesis and metastasis (Ongusaha et al., 2004).

Taken together, these data suggest that loss of Activin expression in CAFs may affect the ability of CAFs to modulate angiogenesis. However, it is unclear whether the change in gene expression has functional relevance to either promote or inhibit this process.

3.2.4 Protein expression analysis

Following the transcriptome analysis, I decided to investigate whether some of these findings could be observed at the proteomic level. A pathway of particular interest was Rho GTPase signalling. As well as being a prominent hit in the RNA-Seq analysis, it is integral in establishing a CAF contractile phenotype (Calvo et al., 2015). I therefore investigated levels of PMLC, specifically PMYL9, as a readout of pathway activity in the parental CAFs and Activin A/B-null populations. Levels of both P-MYL9 and total MYL9 appear to be much higher in the parental cells compared to the NF1 negative control population. Levels of each of the proteins in the CAF Activin A/B-null clones reflect those seen in NF1. When averaged, levels of P-MYL9 in both of the Activin A/B-null clones are significantly lower than those observed in parental CAFs ($P<0.0001$), with levels dropping approximately 4-fold. This is relative to the tubulin loading control. Additionally, levels of total MLC protein appear to have dropped at the protein level, explaining why there is significantly less P-MYL9. This implies that Rho GTPase pathway activity is reduced in CAFs lacking Activin expression.

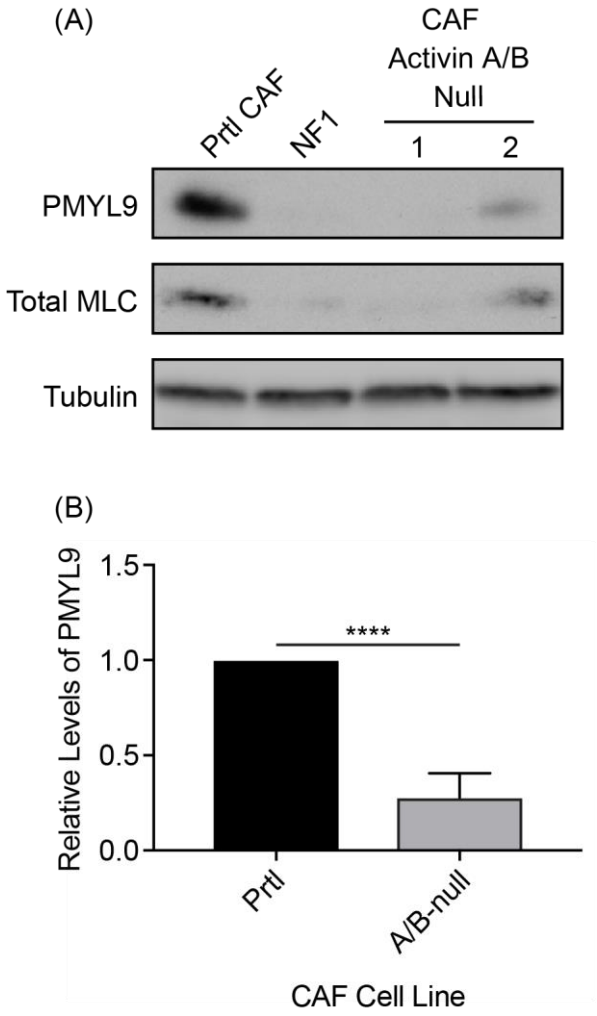

Figure 3.24. Levels of PMYL9 in CAF clones and NF1. Respective cell lines were cultured in 5% FBS DMEM for 72 hours before lysis and protein extraction. Protein lysate was then probed for PMYL9 as well as total levels of MYL9 in CAF parental clones, NF1 and each of the Activin A/B-null CAFs. Western blot is representative of 3 biological replicates. Quantification is average of 3 biological replicates relative to the parental CAF clone levels. Error bars represent SEM.

In addition to active Rho GTPase signalling, I also investigated the CAF secretome in Activin A/B-null CAF clones. Cytokines secreted by CAFs are integral in instigating the core CAF functionalities. To determine any changes in secreted cytokines, I used CM from CAFs on a cytokine array (Figure 3.25). This would determine the presence and relative levels of distinct secreted factors.

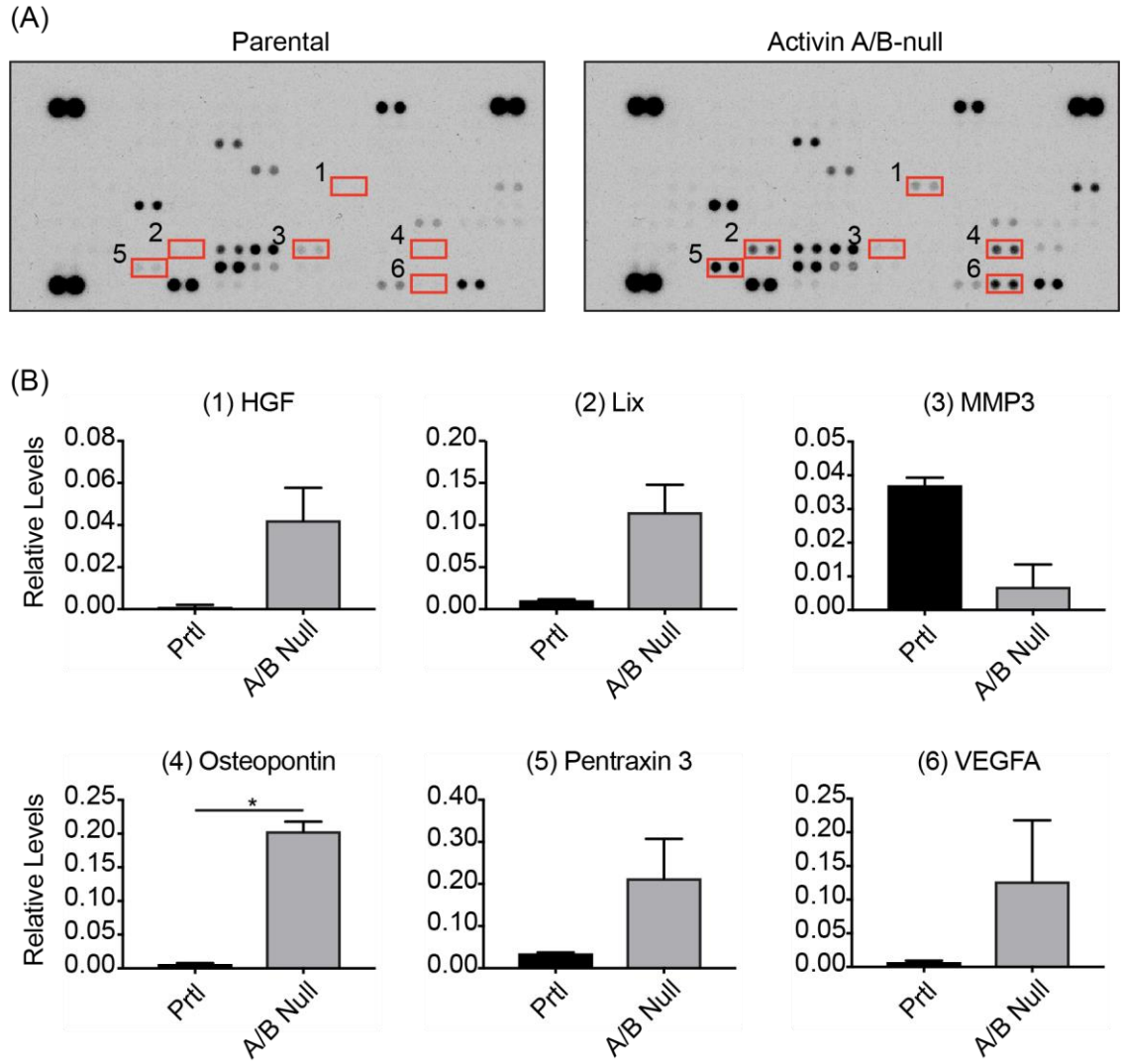

Figure 3.25. Cytokine array to assess CAF clone secretome. (A) Representative arrays for parental CAF and Activin A/B-null CAF CM. Each set of 2 dots represent one protein. Dots in each corner represent reference points and technical controls. Six differentially expressed proteins are highlighted with red boxes. (B) Quantification for each of the 6 highlighted genes relative to the reference points. Quantification for parental CAFs is of 2 biological replicates. Quantification of Activin A/B-null CAFs is a combination of a single biological replicate for each A/B-null line.

A total of 6 genes exhibit a consistent pattern of differential expression, relative to parental CAFs, in each Activin A/B-null line. These are HGF, Lix (CXCL5), MMP3, Osteopontin, Pentraxin 3 and VEGFA. These proteins are upregulated upon Activin knockout excluding MMP3, which is downregulated. Each of these proteins, in certain contexts, are documented to be involved in critical CAF functionalities. For example, HGF, Lix and VEGFA have been associated with angiogenesis (Gao et al., 2019; Shibuya and Claesson-Welsh, 2006; Zhang et al., 2020b). MMP3 is responsible for degrading the extracellular matrix (Banik et al., 2015). In terms of

immune cell modulation, Osteopontin, Lix and Pentraxin 3 have been demonstrated to be immune cell attractants and activators. Osteopontin has been shown to attract a range of immune cells, specifically, macrophages and T cells (specifically T_H1 and T_H17 cells). It has also been demonstrated to attract neutrophils, NK cells and dendritic cells (Icer and Gezmen-Karadag, 2018). However, it has also been linked with enhanced cancer cell motility and metastasis (Wai and Kuo, 2004). Lix functions as a neutrophil attractant (Zhang et al., 2020b), whilst Pentraxin 3 expression is associated with suppressing M2 macrophage activation and promoting M1 polarisation (Bonavita et al., 2015). These results corroborate earlier findings in the RNA-seq analysis. All protein targets discussed here show similar patterns of expression at an RNA level. Specifically, Osteopontin (*Spp1*), Lix (*Cxcl5*) and HGF (*Hgf*) all appeared as significantly upregulated in the RNA-seq analysis, with Log_2Fc values of 6.5, 2.4 and 4.1 respectively. Additionally, MMP3 shows a similar pattern of downregulation at the RNA level, specifically a Log_2Fc value of -6.3.

Following this finding, I investigated whether this expression could be validated at an RNA level (Figure 3.26). Additionally, I investigated RNA levels in Activin A-null and Activin B-null cells to determine whether these patterns occur in these cells. As observed in both the RNA-seq and secretome analysis, increased mRNA expression of genes encoding HGF, Lix (*Cxcl5*), Ostepontin (*Spp1*), PTX3 and VEGFA can be seen in the Activin A/B-null population as well as a decrease in expression of MMP3. This pattern is largely observed for every gene in each of the Activin A-null, B-null and parental + SB populations. Generally, Activin A-null cells are a closer representation of the A/B-null levels than B-null, excluding MMP3 which is marginally closer to A/B-null levels than A-null cells. Interestingly, levels of *Ptx3* are higher in Activin A-null CAFs than A/B-null population. This data validates observations seen in the secretome analysis. Moreover, it suggests that, in most cases, loss of both Activin A and B results in the most extreme differences from parental CAFs.

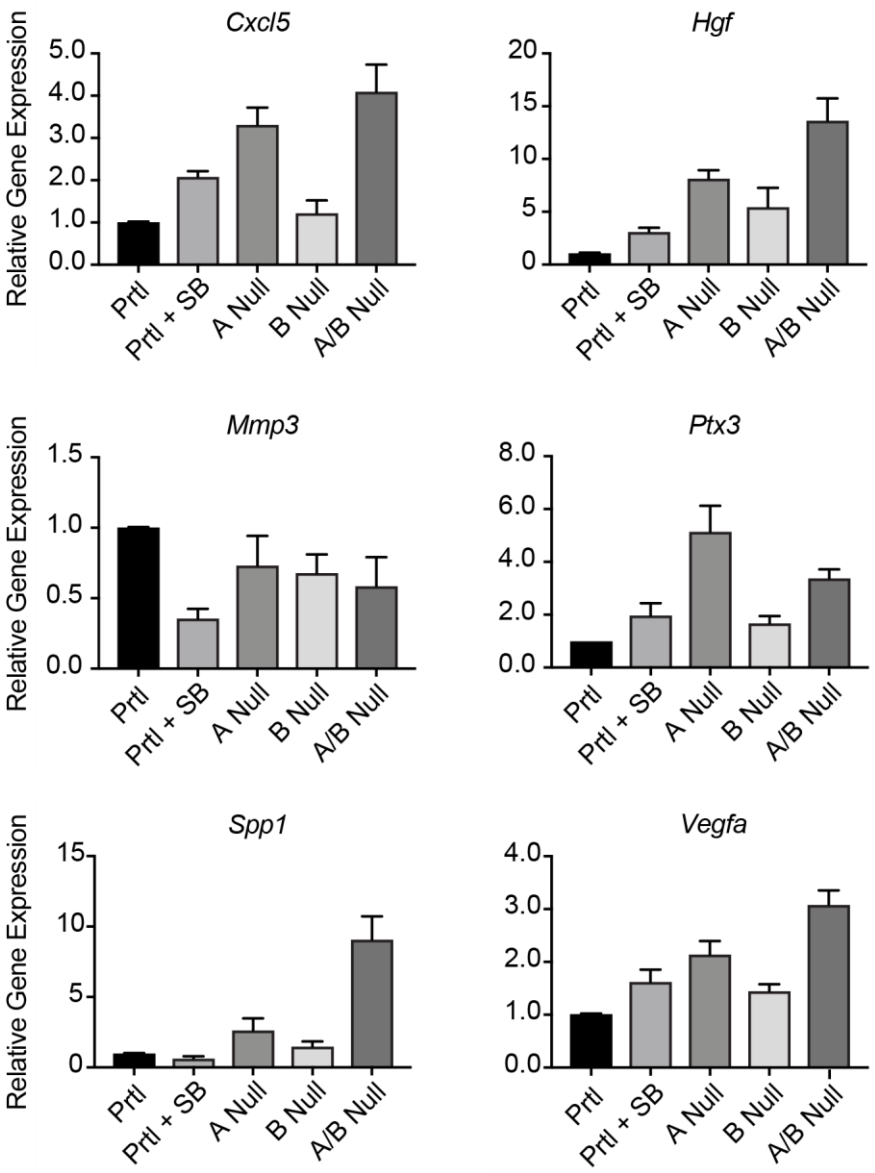

Figure 3.26. mRNA levels of positive hits from the secretome analysis in CAF clones. Expression of specific targets relative to the parental CAF clone. Data for each of the Activin A null, B null and A/B null lines consist of 6 biological replicates, 3 for each clone corresponding to the appropriate genotype. Error bars represent SEM. Prtl + SB corresponds to parental CAFs treated overnight with 10µM SB505124.

Data presented in this section suggests that many of the core CAF functionalities are affected upon loss of Activin expression at a transcriptomic and proteomic level. However, whether these can be translated into directly affecting function remains to be seen.

3.3 Discussion

3.3.1 Summary of results

- Activin A and B are produced by CAFs within the tumour stroma. Higher circulating levels correlate with poor prognosis in various tumour types.
- I successfully ablated expression of Activin A and B individually and together in distinct CAF clonal populations.
- Loss of Activin expression affects autocrine and paracrine signalling in CAFs.
- Activin signalling in CAFs substantially affects the transcriptome and secretome of CAFs. Affected RNA and protein expression is associated with core CAF functionalities including ECM remodelling, immune cell modulation and angiogenesis.

3.3.2 Activin vs TGF-β expression in the tumour stroma

TGF-β family signalling is strongly associated with certain pro-tumourigenic functionalities. These include EMT, immune cell suppression, angiogenesis and metastasis (Colak and ten Dijke, 2017). TGF-β ligand itself is frequently determined to be responsible for this. However, in many cases, these oncogenic phenotypes are attributed to 'TGF-β pathway activation' or 'TGF-β gene signatures' that are not exclusive to TGF-β ligand and could be perpetuated by Activin or other TGF-β family members including certain GDFs, such as GDF9, which are able to phosphorylate SMAD2 and induce transcription of the same target genes (Kaivo-Oja et al., 2003). For example, it has been published that a TGF-β gene signature in CAFs is strongly associated with poor disease outcome (Calon et al., 2015). Similarly, it has been demonstrated that immune cell exclusion in tumours is significantly associated with expression of TGF-β family components, including Activin receptor ACVR1B (Mariathasan et al., 2018). In each of these cases, it could be reasoned that Activin may be responsible for the detailed observations. Indeed, there is a growing body of evidence that implicates Activin in enhancing tumourigenesis. Specifically, data produced by the Werner lab has shown that Activin promotes an immune suppressive environment to promote skin tumourigenesis (Antsiferova et al., 2011, 2017). Additionally, a study has shown correlation of levels of Activin expression with

poor survival in mouse models of pancreatic cancer as well as a cohort of pancreatitis patients (Staudacher et al., 2017b). Data presented in section 3.2.1 supports the argument that Activin signalling may be partially or entirely responsible for many of the observed oncogenic phenotypes attributed to TGF-β family signalling seen in the literature.

Colleagues and I have demonstrated that Activin and not TGF-β is present in the CM of an immortalised CAF population. Additionally, co-localisation of Activin A and B with CAF marker αSMA can be observed in tumours of MMTV-PyMT mice. I have also demonstrated that these tumours are positive for PSMAD signalling. The combination of these data suggests that, at least in this context, Activin signalling is responsible for perpetuating TGF-β family signalling rather than TGF-β ligand itself. I have also observed this phenomenon in mouse Pan02 pancreatic tumour models. However, it will be important to demonstrate these findings more broadly in models beyond MMTV-PyMT into other breast cancer models and other tumour types in mice. Critically, it will be important to translate this into human cell lines. Colleagues have shown that Activin expression correlates with poor prognosis in various human cancer types. However, the source of this ligand and the nature of this correlation remain a mystery. CAFs from human cancers can be isolated and interrogated in a similar fashion. Additionally, organoid culture systems could be exploited to study the potential source of Activin signalling in human cancer models.

Interestingly, however, not all CAFs within PyMT tumours appear to be PSMAD2 positive. CAFs are highly heterogeneous, with an increasing number of studies showing that different subtypes with distinct functions exist. Specifically, one group has shown that immunosuppressive and contractile CAFs exist within the same tumour stroma (Bartoschek et al., 2018). Perhaps PSMAD2 positive and negative CAFs exhibit similar degrees of heterogeneity. Indeed, I have shown that loss of PSMAD2 signalling through Activin knockout does dramatically affect the CAFs at a signalling level. It would be interesting to investigate this in PSMAD2 positive and negative primary CAFs isolated from tumours.

3.3.3 CRISPR/Cas9 knockout of Activin

I chose to knock out expression of Activin A and B individually and in combination in distinct CAF populations. I excluded Activins C and E as little is known of their functional relevance in adult tissues and appear to be exclusively expressed in liver cells (Seachrist and Keri, 2019; Vejda et al., 2003). I generated all knockout lines from the same parental clone. The process of generating knockout clones involves sorting single cells before expanding them. If single cells are sorted from a heterogeneous population, there would be a risk that selected clones are not representative of the original polyclonal population (Stockholm et al., 2007). This would mean results generated could be clonal artefacts rather than biologically real. My decision to first isolate a homogenous parental clone ensures all downstream results are more reliable. I characterised parental clones exclusively by expression of *Inhba* and *Inhbb* transcripts as well as Activin inhibitor and target gene *Fst*. Ideally, further characterisation would have involved functional analysis, such as contraction assays (Calvo et al., 2015). However, I believed this signalling characterisation was sufficient. In any case, all downstream knockout clones would be compared against this parental clone. Therefore, any observed differences in the knockouts would be valid.

CRISPR/Cas9 technology was utilised over siRNA knockdowns as it results in complete and permanent deletion of the target gene (Ran et al., 2013). This means results generated downstream are more robust and conclusions drawn more valid. Despite this, CRISPR targeting shows varying degrees of success. In certain cases, some targets are easier to knock out for a number of reasons, such as genomic locus (Ran et al., 2013). In this case, however, all targets were successfully disrupted at a genomic level and protein expression was lost in appropriate populations. Interestingly though, one of the targets, specifically *Inhbb* in Activin A/B-null 2, shows an in-frame deletion of 3bps in one allele. This could potentially result in a silent mutation and successful expression of the protein. However, since there is no protein expression, a critical residue has likely been removed. Specifically, it resides within the Furin processing site. A mutation here may mean the protein is not processed properly and therefore not expressed (Stenvers and Findlay, 2010). Furthermore, the use of 2 distinct clones per experimental condition adds reliability to the data. This provides additional assurances that any observed results would not be due to clonal

artefacts. Similar trends between clones indicates that the data can be relied upon as biologically real.

It is important to note the constraints of an *in vitro* system when asking any research question. These constraints are particularly pronounced when investigating CAF biology because of their inherent heterogeneity and plasticity (see Section 1.5.4). Whilst the data I obtain using these cell lines have great biological value, they may not be entirely representative of an *in vivo* system. Isolation of a clonal line was an attempt to mitigate the loss of accurate biological representation. However, even the phenotype and morphology of polyclonal CAF lines isolated from tumours are less representative of CAFs *in vivo*. It will be important to determine the role of Activin signalling on CAFs *in vivo*, this is explored in Chapter 4.

3.3.4 Clonal characterisation and relative contribution of each Activin

Following successful generation of Activin A/B-null CAFs I sought to characterise these clones on a signalling level. I investigated levels of basal PSMAD2 in CAFs and the ability of conditioned media from these clones to induce signalling in naïve cells.

Strikingly, loss of Activin A/B completely negates PSMAD2 induction properties of CAF CM. Additionally, basal levels of PSMAD2 are dramatically reduced across all Activin knockout clones. However, basal levels of PSMAD2 are not entirely depleted upon loss of any one of the Activin dimers. This would suggest that a separate family ligand is responsible for sustaining the residual levels of PSMADs observed in Activin-null CAFs. One possible explanation is that HaCaTs do not express the corresponding receptors to the upregulated ligand. However, this seems unlikely, as these cells have been shown to express the requisite receptors for PSMAD2 induction (Levy and Hill, 2005). Another possible explanation is intracellular signalling in CAFs may be responsible for residual PSMAD2. Finally, the ligand responsible may remain membrane associated, perhaps even TGF-β. In any case, it is clear that autocrine and paracrine signalling in CAFs has been significantly affected upon loss of Activin expression.

Another interesting observation is the relative contributions of each Activin ligand. Within mammalian cells, Activin A and B homodimers exist as well as Activin

A/B heterodimers (Wang et al., 2016). Generally, throughout the chapter, it appears that Activin A contributes more than Activin B in terms of signalling output. Specifically, in terms of PSMAD induction and transcriptional output. However, a combination of the two is required for complete signalling. For example, there is no signal induction in naïve cells when treated with CM from Activin A/B-null CAFs. A small induction of PSMAD2 can be seen in cells treated with Activin A-null CM whilst the greatest, but not complete, induction is observed when treated with CM from Activin B-null CAFs. Additionally, this phenomenon can be seen in the qPCR analysis of the proteome targets. The most substantial effect is seen in Activin A/B-null CAFs in the majority of cases. These findings suggest a combination of Activin A and Activin B homodimers are required for complete signalling output and the effect of heterodimers is negligible. Loss of either Activin A or B would affect heterodimer formation. If heterodimers were required for signalling, then loss of Activin B would be more representative of loss of Activin A in terms of signalling output. Intriguingly, Activin B expression increases in Activin A-null cells in what appears to be a compensation mechanism. The reverse phenomenon is not true. Activin A may be the most prominent player in signalling output in terms of transcription and PSMAD2 induction, but subsequent upregulation in Activin B could be why the most dramatic changes are seen in Activin A/B-null cells.

Similar trends in results are always observed between clonal populations of the same knockout cohort, strongly suggesting that the results are not due to a clonal artefact. Because of this, the conclusions drawn have greater validity. Findings here suggest that, if Activin is a worthwhile therapeutic target, a dual specific approach against Activins A and B may be the most prudent approach. Because of this conclusion, future analysis focussed primarily on Activin A/B-null CAFs for the greatest biological effect.

3.3.5 Activin expression dramatically affects CAFs' transcriptome

The transcriptome of a CAF population can be very revealing with regards to its phenotype and potential influence in the tumour microenvironment. For example scRNA-seq analysis of CAFs isolated from human breast cancer samples revealed that distinct transcriptomic profiles correspond with separate functionalities (Costa et

al., 2018). Therefore, profiling the transcriptome of Activin A/B-null CAFs using RNA-seq was of great interest.

The data generated from the RNA-seq analysis is very robust and reliable for a number of reasons. Firstly, the use of three technical replicates from two separate Activin A/B-null CAF lines allows us to average six separate instances of RNA against the parental population. This means any observed differences will be highly robust and conclusions drawn can be made with great confidence. Furthermore, the data itself was of high quality, with >98% of reads aligning. The data itself shows there are substantial differences between CAFs that express Activin A/B and those that do not. A global analysis shows that a total of 7,835 genes are significantly differentially expressed in CAFs lacking Activin A/B expression. Reactome pathway analysis reveals that differentially expressed genes are significantly enriched for in many pathways that could critically influence core CAF functionalities. However, there are large numbers of genes that show significant differential expression in only one of the Activin A/B-null lines. The difference between each Activin A/B-null line is also shown in the PCA plot, where a degree of variance is evident. This may simply be due to clonal variance or possibly off-target effects of the CRISPR/Cas9 knockout process. It would be interesting to profile the genes that are uniquely expressed in each cell line. Perhaps many of them are close to significance in the other cell line or at least follow the same pattern of altered expression. Indeed, very few genes show conflicting patterns of significant differential expression.

Ultimately, I chose to utilise a dataset containing all genes that are significantly differentially expressed between the Activin A/B-null cell lines and the parental CAFs. I chose to do this because the focus of my analysis was to determine what type of pathways and behaviours are affected upon loss of Activin expression using Reactome pathway and Gene Ontology. In this instance, utilising a large and robust dataset makes this analysis more informative. Applying a stringent cut-off based on TPM values may have resulted in biologically relevant genes being omitted, resulting in a loss of potentially meaningful information from the analysis.

This dataset utilised also provides a wealth of information that can be compared to other publicly available datasets. In collaboration with Stephanie, I attempted to map the generated dataset onto existing CAF RNA-seq datasets. For example, various public datasets attribute specific transcriptional profiles to contractile, immune suppressive and pro-angiogenic CAFs (Bartoschek et al., 2018;

Costa et al., 2018). We attempted to map my dataset onto these profiles to reveal whether the transcriptional profile of Activin A/B-null CAFs correlates with the profile of any one of these functional phenotypes. We anticipated that this analysis would reveal potential functional associations the changes in expression seen in Activin A/B-null CAFs may have. However, we were unable to detect any instances where the dataset matched or opposed the specific gene expression profiles of functional CAF subtypes with any degree of confidence. This may be due to the inherent heterogeneity of CAF populations, which is well documented (Öhlund et al., 2014). Intriguingly, it may also indicate that the Activin A/B-null CAFs represent a unique CAF population that may influence the tumour microenvironment in a previously undocumented way.

As mentioned above, as mentioned above, I did not implement any stringent cut-offs to my dataset, all significantly differentially expressed genes between Activin A/B-null CAFs and parental CAFs were explored. However, an interesting possibility that could be explored is to use this dataset to generate an Activin signalling gene signature. One could be generated in a variety of ways; for example, one could apply stringent cut-offs and utilising either the top 100–200 most significantly differentially expressed genes between each of the Activin A/B-null CAFs and the parental CAF population. This can then be compared with other publicly available gene signatures, including TGF-β gene signatures; for example one generated using transcriptomic data from colorectal samples (Guinney et al., 2015). Such a refined gene signature could also be mapped onto TCGA datasets to reveal if the expression of the genes is associated with poorer or better survival in a variety of cancer types. Furthermore, such an Activin gene signature could be utilised in more personalised medicines. Patient tumour samples could be analysed at a transcriptomic level and compared against TGF-β and Activin gene signatures to determine tumours that are ‘hot’ for either ligand. Targeted therapies could then be utilised against either ligand to potentially provide optimal patient treatment and outcome.

It is important to note that any conclusions drawn using observations from RNA-Seq analysis may not be entirely biologically real. It will be vital to validate these findings both at the protein expression level and the functional level. Importantly, I validated many of the hits from the RNA-Seq analysis at a protein level using an antibody array. However, this was a restricted analysis, and more robust conclusions could be drawn regarding CAF functionality if a more wide-scale proteomic analysis

is conducted. In any case, the functional behaviours of these CAF populations are explored in more detail in the following chapter. In any case, there are many inferences, with regards to how functionality may be affected, one can make. As mentioned, I am primarily interested in the CAF functionalities, ECM remodelling, angiogenesis, immune cell modulation and cancer cell invasion. Based on all the data in this chapter, the theorised effects of Activin on each of these functionalities will be discussed in the following sections.

3.3.6 Loss of Activin may alter CAFs ability to remodel the ECM

CAFs are well documented in their ability to remodel the extracellular matrix. They do so by synthesising specific components of the ECM, as well as secreting degradative or cross-linking enzymes (Sahai et al., 2020). This remodelling can either enhance or inhibit tumour progression. For example, degradation of the ECM could lead to a more permissive environment for cancer cells to invade and spread. Conversely, a more rigidly organised ECM can prevent cancer cell migration and compress surrounding blood vessels that may prevent access of therapeutic agents (Park et al., 2020a). The RNA-seq data we have generated shows that pathways associated with these functionalities has been greatly affected. For example, ‘Collagen formation’ and ‘Collagen biosynthesis and modifying enzymes’ are two of the most significantly enriched for pathways in the reactome pathway analysis. This strongly indicates that the ability of CAFs to remodel and structure the ECM may be greatly affected. However, it is unclear whether this could lead to a more or less permissive ECM for tumourigenesis. Further analysis showed that many protease enzymes associated with degrading the ECM and generating a more permissive ECM for cancer cell invasion exhibit decreased expression at a transcriptomic and proteomic level, specifically MMP3. Expression of MMP3 in tumours promotes metastasis through its ability to remodel the ECM, consequently its expression correlates with poor prognosis (Banik et al., 2015; Gobin et al., 2019). This strongly suggests that the CAFs inherent ability to remodel the ECM and promote cancer cell invasion may be reduced. However, it will be important to demonstrate this *in vitro* and *in vivo*.

Furthermore, a contractile CAF subtype is strongly associated with remodelling the ECM and generating tracks by which cancer cells can invade (del Pozo Martin et al., 2015). Active Rho GTPase signalling is critical for this contractile CAF phenotype (Gaggioli et al., 2007). Reactome pathway analysis shows a large proportion of genes associated with Rho GTPase signalling are significantly differentially expressed in CAFs that lack Activin expression. Specifically, the Rho GTPases *Rac1*, *Cdc42* and *RhoA*, responsible for pathway activation, are downregulated. I later showed that this results in loss of active Rho GTPase signalling through ablation of P-MYL9. This strongly suggests that CAFs' ability to remodel its surrounding extracellular matrix is significantly reduced. However, it is of importance to test this at a functional level, which is explored in the following chapter.

The connection between TGF-β family and Rho GTPase signalling is well documented (Ungefroren et al., 2018). The mechanism by which Activin regulates this pathway is not definitive in this context. However, data here suggests it could be at a transcriptional level as certain key regulators of the pathway are downregulated such as *Cdc42*. Recombinant TGF-β induces *Cdc42* expression in normal fibroblasts to directly promote a contractile phenotype (Calvo et al., 2015). Therefore, it could be possible that autocrine Activin in CAFs may be responsible for maintaining a contractile CAF phenotype by means of elevating levels of Rho GTPase signalling through *Cdc42*. Additionally, *Net1*, a published SMAD3 target and activator of the Rho GTPase RhoA, is downregulated. Downregulation of *Net1* through loss of SMAD3 signalling has been shown to inhibit Rho GTPase signalling and prevent cytoskeletal reorganisation in EMT (Lee et al., 2010). This could equate to a loss of a contractile phenotype in Activin A/B-null CAFs. It remains unclear if altered expression of any one of these genes is critical in ablating Rho GTPase signalling in this context, or whether it is a combination of several. It would be interesting to conduct some siRNA experiments to determine the factors critical for this observation. This type of investigation may shed further light on the crosstalk between TGF-β family and Rho-Rock signalling, which is critical in EMT and metastasis in several cancer contexts (Sanz-Moreno et al., 2011).

In any case, a combination of the transcriptomic and proteomic analysis strongly suggests Activin is required for CAFs' ability to alter and degrade their surrounding ECM. This transcriptomic and proteomic profile suggests that these CAFs may have reverted to a more quiescent and less myofibroblastic phenotype

that more closely resembles a normal fibroblast (Section 1.5.3; Sahai et al., 2020). Reverting CAFs to a more quiescent phenotype may be a prudent method of therapeutically targeting them (Section 1.5.5); for example, targeting the vitamin D ligand in a pancreatic cancer model reverted stellate cells to a more quiescent phenotype and reduced disease aggressiveness (Sherman et al., 2014). This possibility could be explored further by comparing the RNA-Seq dataset to one from normal fibroblast populations. The possibility that targeting Activin could lead to a more quiescent and less contractile phenotype is investigated in the following chapter.

3.3.7 Activin expression affects expression of immune cell modulators

Another core CAF functionality is immune cell modulation. CAFs are known to secrete a wide array of cytokines to exert these functions. Primarily, they do so by affecting lymphocyte numbers and phenotype within the stroma. An immune suppressive environment is created by preventing activation and infiltration of cytotoxic CD8+ T cells whilst enhancing levels of FoxP3+ regulatory T cells (Kato et al., 2018). Additionally, they have been shown to promote migration of macrophages and their subsequent polarisation to a tumour-promoting M2 phenotype (An et al., 2020). TGF-β pathway activation has been shown to be responsible for both of these phenotypes in other contexts. TGF-β ligand signalling and pathway activation in CAFs is associated with their effects on lymphocytes (Mariathasan et al., 2018; Tauriello et al., 2018), whilst TGF-β can directly activate M2-macrophages (Batlle and Massagué, 2019).

If TGF-β pathway activity is responsible for immune cell modulation then, logically, Activin may also be perpetuating this phenotype. Additionally, as previously mentioned, Activin ligand itself has been shown to promote an immune suppressive environment in models of skin cancer (Antsiferova et al., 2011). It was therefore of interest to investigate the effect of loss of Activin on CAFs ability to modulate the immune system, especially since I have demonstrated that certain CAF populations actively produce Activin A/B rather than TGF-β.

In this chapter, I have not directly shown the effect of Activin on immune cell migration or activation. However, I have demonstrated that a wide variety of factors

associated with lymphocyte migration have been affected at an RNA and protein level. For example, expression of *Cxcl12*, *Cxcl10* and *Spp1* (Osteopontin) have all been significantly affected. All of which are associated with attracting lymphocytes (Costa et al., 2018; Icer and Gezmen-Karadag, 2018; Karin and Razon, 2018). Each of these proteins are upregulated at an RNA level, with Osteopontin also upregulated at a protein level, suggesting that lymphocyte infiltration may be increased in tumours with reduced Activin expression. Additionally, factors associated with activating certain subtypes of lymphocytes are affected. However, there is no definitive pattern of expression for factors that promote or diminish any given lymphocyte phenotype. For example, there is upregulation of *Il33* and downregulation of *Il11*. Each of which are associated with promoting a Th2 response. Investigating the effect of Activin from CAFs on the activation status of lymphocytes became of interest to investigate *In Vivo*.

Beyond lymphocytes, expression of many factors associated with macrophage migration and activation are significantly affected in Activin A/B-null CAFs. For example, Osteopontin, *Ccl8* and *Ccl9* all exhibit increased expression at the mRNA level and have been demonstrated to attract monocytes and macrophages in different contexts (Halvorsen et al., 2016; Icer and Gezmen-Karadag, 2018; Yan et al., 2015). Several factors associated with macrophage activation are also significantly differentially expressed. Most notably Pentraxin 3, expression of which is affected at a protein level, is responsible for promoting M1 polarisation of macrophages (Giacomini et al., 2018). Levels of M1 macrophages correlate with better prognosis in non-small cell lung cancer (Jackute et al., 2018). This suggests that loss of Activin in CAFs may have an indirect and beneficial effect on prognosis. However, the role of M1 vs M2 polarisation in macrophages is a contentious question, with each phenotype exhibiting opposing effects in distinct contexts (Sica et al., 2008). It will be important to determine if loss of Activin expression has any effect on macrophage infiltration and activation *in vivo* as well as any ultimate effect on tumour progression.

Finally, factors that have been documented to affect neutrophil migration are affected in Activin A/B-null CAF populations. Specifically, *Cxcl5* (Lix) is upregulated at the mRNA and protein level. *Cxcl5* has been shown to promote neutrophil migration (Zhang et al., 2020b). This suggests Activin produced by CAFs may

indirectly enhance neutrophil infiltration. However, the influence of neutrophils on the tumour microenvironment is unclear (Singel and Segal, 2016).

Taken together, these findings suggest Activin A/B produced by CAFs within a tumour may work to indirectly exclude infiltration of lymphocytes, macrophages and neutrophils. Additionally, it may be responsible for indirectly generating a tumour suppressive M1 macrophage phenotype. However, it is important to emphasise that it is unclear whether altered expression of these factors will have any significant biological impact. Furthermore, it is uncertain how or even whether these effects will alter tumour progression. Additionally, all of these observations represent indirect ways in which Activin may modulate immune cells. Activin itself has been shown to promote accumulation of tumour promoting Langerhans cells and regulatory T cells in models of skin cancer (Antsiferova et al., 2011, 2017). It will be important to explore any implications of the differential expression of the cytokines detailed above, as well as Activin itself, on immune cell migration and activation functionally both *in vitro* and *in vivo*

3.3.8 Activin signalling may affect angiogenesis

Another core CAF functionality is angiogenesis. Certain CAF subtypes can promote angiogenesis through secretion of a variety of cytokines and growth factors including HGF and VEGF proteins (Park et al., 2020a). Interestingly, each of these factors show elevated expression at protein and mRNA levels. Additionally, many other factors associated with promoting angiogenesis are upregulated at an RNA level. This shows that Activin expression in CAFs may work to indirectly inhibit angiogenesis. However, the data from the RNA-seq dataset is not conclusive in this respect, as many factors associated with promoting angiogenesis are also significantly downregulated in Activin A/B-null CAFs. In any case, the gene ontology term for angiogenesis is significantly enriched in the RNA-seq dataset. This strongly suggests that Activin A/B influences angiogenesis. It will be important to determine, at a functional level, the nature of this effect.

Similar to other functionalities of interest, this chapter has not determined any contribution that CAF-produced Activin A/B has directly on angiogenesis. Studies investigating the direct effects of Activin A/B on angiogenesis in other systems are

not comprehensive. However, it has been shown that Activin A/B may reduce proliferation of endothelial cells through activation of SMADs and suppress angiogenesis in glioblastomas (Panopoulou et al., 2005).

Whilst the role of Activin A/B in CAFs' ability to affect angiogenesis remains unclear in this chapter, the increased expression of VEGFA and HGF at a protein level is a strong indicator that angiogenesis may be elevated in tumours that lack Activin A/B expression. Angiogenesis correlates with poor prognosis as it is required for metastatic spread (Claesson-Welsh and Welsh, 2013). It will be important to determine any effect loss of Activin A/B has on CAFs' ability to promote angiogenesis at a functional level, as well as any tumour promoting effect this may have.

Chapter 4. The Role of Activin on CAF Functionality

4.1 Introduction

In the previous chapter, I demonstrated that Activin A and B are expressed by CAFs and that loss of Activin A/B in a clonal CAF1 cell line severely affects their transcriptome and proteome. However, whether these dramatic changes lead to any functional consequences remains unclear. CAF functionalities of particular interest are ECM remodelling, cancer cell invasion, immune cell modulation and angiogenesis. These functionalities play integral roles during tumour development and metastasis (Hanahan and Weinberg, 2011; Park et al., 2020a). As discussed in the previous chapter, a significant proportion of the altered transcriptomic profile in Activin A/B-null CAFs is associated with ECM remodelling, migration, immune cell modulation and angiogenesis.

I investigated whether the dramatic changes observed in Chapter 3 translate to altered CAF functionality. I have shown that Rho GTPase signalling is diminished in Activin A/B-null CAFs. CAFs with inactive Rho GTPase signalling have impaired contractility and are less able to remodel the extracellular matrix (Calvo et al., 2013). The ability of CAFs to remodel the extracellular matrix was assayed using gel contraction assays. In addition, I have shown that genes associated with axonal guidance are significantly different, suggesting that the migratory capacity of CAFs may be affected (Aberle, 2019). Therefore, I assessed the motility of Activin A/B-null CAFs by means of a scratch assay. More contractile and migratory CAFs are able to promote invasion of cancer cells through the generation of tracks in which the cancer cells can more easily migrate (Gaggioli et al., 2007). Therefore, I investigated the influence of Activin A/B-null CAFs on cancer cell invasion using co-culture spheroid invasion assays.

Furthermore, these parameters, as well as angiogenesis and immune cell modulation, were assessed *in vivo* using tumours generated by co-injection of cancer cells and CAF clonal populations. Tumour progression was monitored and their composition interrogated to determine any distinctions in immune cell infiltrate, altered ECM and blood vessel formation. Additionally, I conducted CAF only injections into the mammary fat pad of mice to further investigate their chemotactic, angiogenic and ECM influencing properties.

Assays conducted as part of this chapter have focussed on comparing Activin A/B-null CAFs with parental CAF populations. Data presented in the previous chapter suggested that the most profound biological effect would be observed in the Activin A/B-null populations.

4.2 Results

4.2.1 Activin signalling is critical for a contractile phenotype in CAFs

As discussed above, it was of great interest to determine if the contractile properties of the CAF clonal populations were influenced by Activin A/B signalling. Therefore, I asked whether loss of Activin A/B had any effect on the propensity of the CAFs to contract a collagen gel. Previous unpublished work within the lab has shown that treatment with the TGF-β family receptor inhibitor SB-505124 works to largely ablate contraction of CAFs in a collagen gel. SB-505124 is a chemical inhibitor of Activin and TGF-β type I receptors (DaCosta Byfield et al., 2004). Since I have demonstrated that these CAFs do not produce TGF-β, addition of this inhibitor would only block autocrine Activin signalling. This strongly suggested that loss of autocrine Activin signalling in these CAFs would ablate CAF contractility. Therefore, I sought to demonstrate that Activin A/B-null CAFs could not contract a collagen gel. Due to signalling-independent variations observed during optimisation of this assay, treatment with SB-505124 was used as a positive control (Figure 4.1).

Gels containing untreated parental CAFs show significant levels of collagen contraction over 72 hours, as expected. Treatment with SB-505124 largely ablates this. Strikingly, untreated Activin A/B-null CAFs show minimal levels of contraction at day 3, largely reflecting their SB-505124-treated counterparts. Percentage gel contraction is significantly less in Activin A/B-null CAFs compared to parental CAFs ($P<0.05$). I wanted to determine if this phenotype could be rescued through addition of recombinant Activin. Indeed, Activin A/B-null CAF containing collagen gels treated with recombinant Activin show similar levels of contraction to parental CAFs. These data suggest that Activin expression is critical for CAFs' ability to contract a collagen gel.

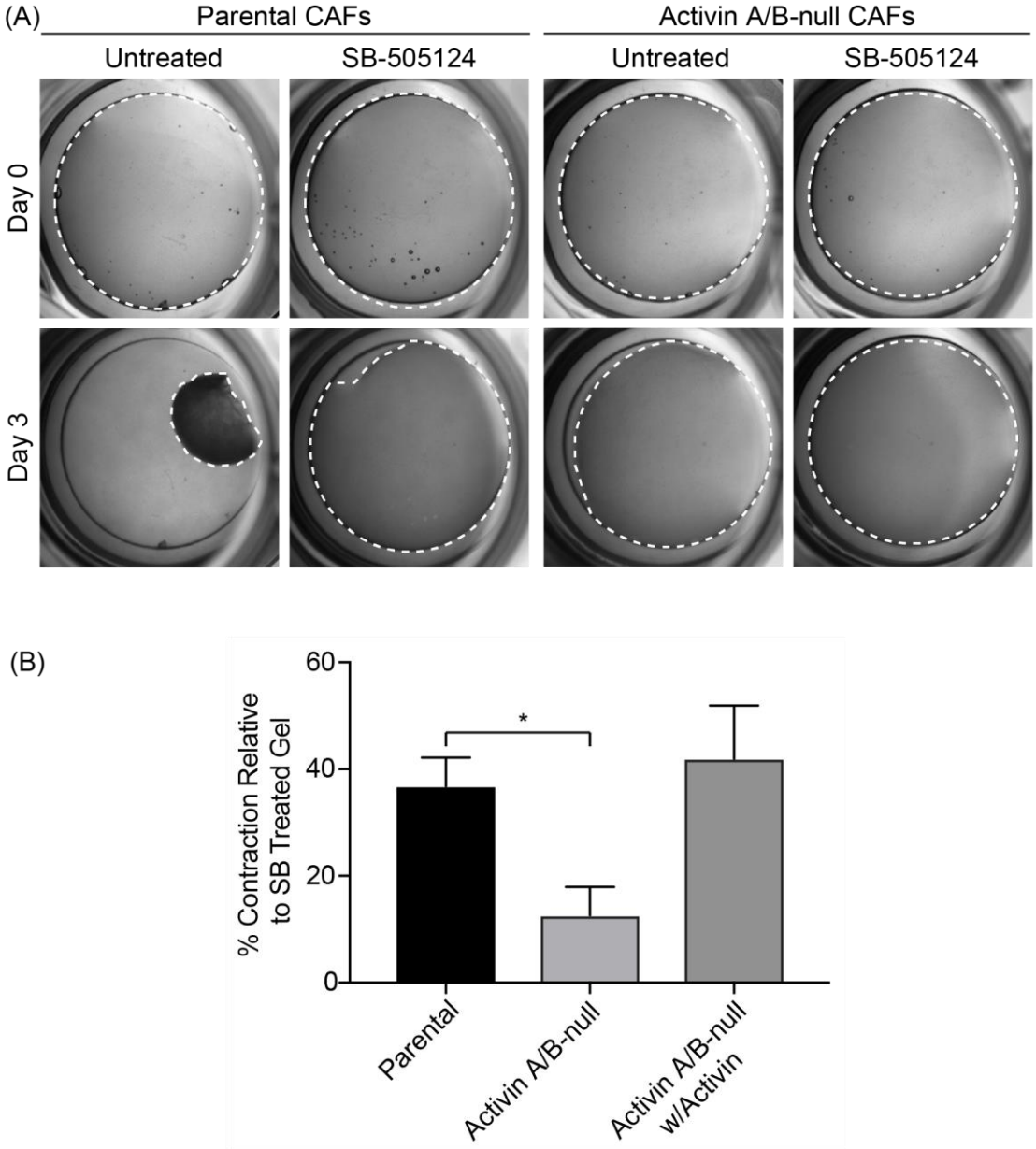

Figure 4.1. Contraction assay of CAFs embedded in collagen gel. (A) Representative images of parental CAFs and Activin A/B-null CAFs embedded in an untreated collagen gel or one supplemented with 10µM of SB-505124. (B) Quantification of % contraction of respective gels at day 3 relative to their SB-505124 treated counterparts. Averages are of 3, 6 and 2 biological replicates for parental CAFs, Activin A/B-null CAFs (3 for each clonal population) and Activin treated Activin A/B-null CAFs respectively. Error bars represent the SEM. Statistical analysis conducted was an unpaired t-test.

To rule out the possibility that the results observed in Figure 4.1 were an artefact of differential proliferation rates, I conducted a proliferation assay using the IncuCyte system. Lower proliferation would lead to fewer cells within the collagen gel over a 3-day period and, ultimately, a lower degree of contraction. Based on the

Incucyte proliferation assay, there appears to be no significant change in the growth rate between parental CAFs and Activin A/B-null populations. In fact, there is a slight increase in growth rate of double null CAFs. This suggests that the reduction in contractility of double null CAFs observed in Figure 4.1 is not an artefact of lower cell number within the gel.

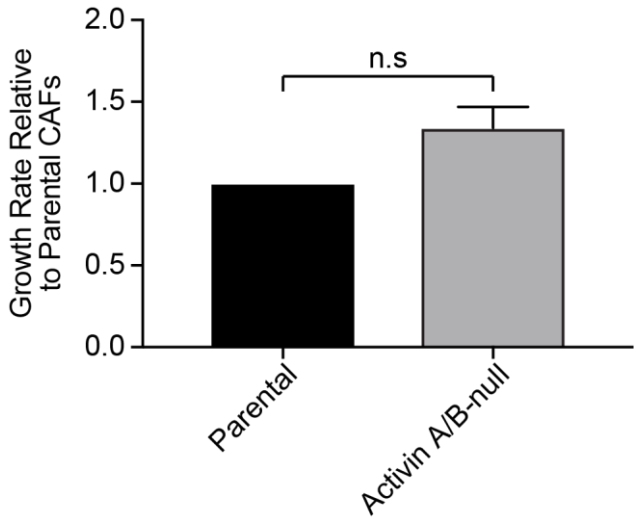

Figure 4.2. Proliferation of clonal CAF populations. Phase contrast images were taken 5 times a day over a 6-day period of parental CAFs (n=3) and double null CAFs (n=6, 3 for each clonal population). Growth rates were calculated based on the area occupied by cells over time. Growth rates were made relative to parental CAFs cells. Error bars represent the SEM.

In addition to contractility, I was interested in testing the migration of each CAF population. This is because the reduction in Rho GTPase activity and affected expression of axonal guidance genes observed in Chapter 3 suggested motility of Activin A/B-null CAFs may be affected. Additionally, more migratory CAFs have been shown to enhance cancer cell invasion (Henke et al., 2016). Therefore, I conducted scratch assays with parental CAFs and each Activin A/B-null CAF clonal line (Figure 4.3).

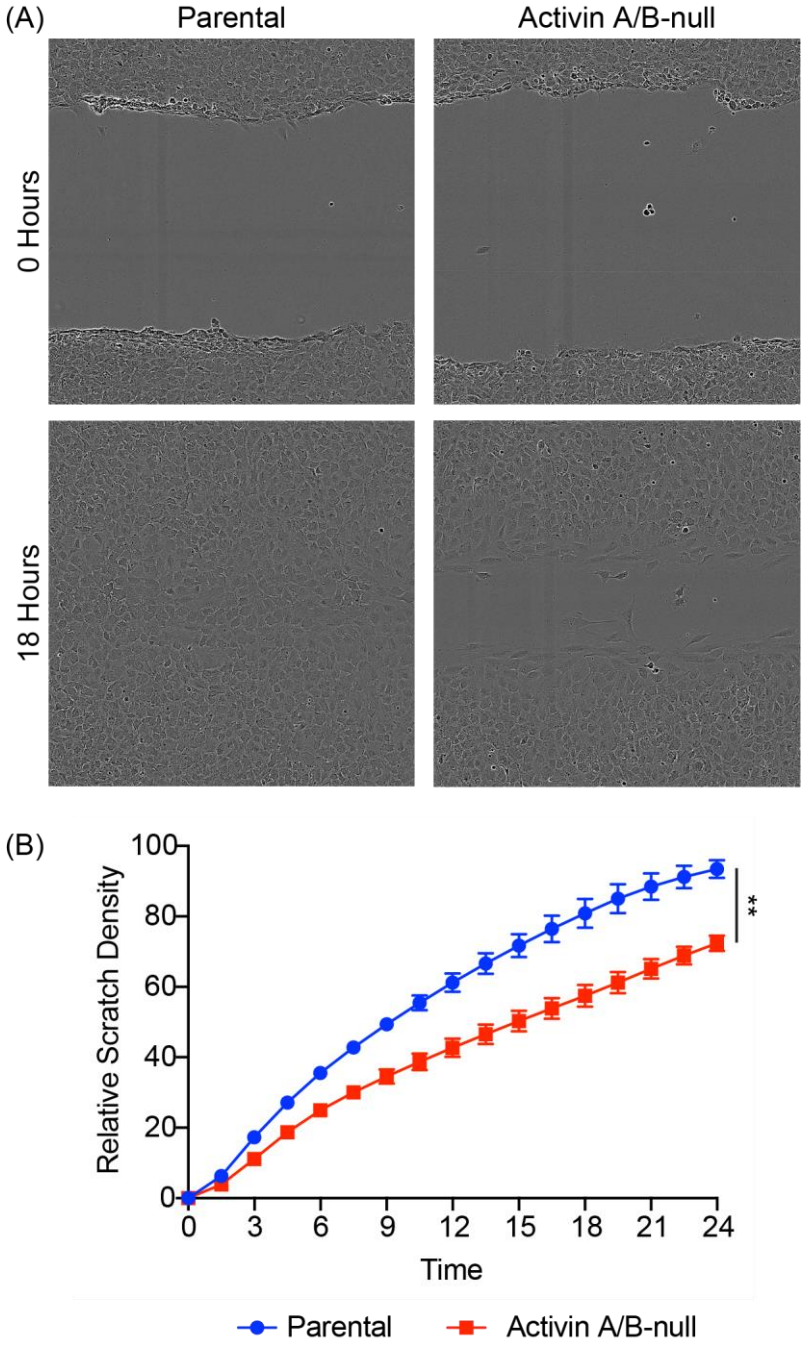

Figure 4.3. Scratch assay of clonal CAF populations. Uniform scratches were introduced into each CAF population. Phase contrast images were taken every 45 minutes over 24 hours. (A) Representative images of wound density at 0 hours and 18 hours for each CAF population. (B) Graph showing relative scratch density over time for parental CAFs (blue) (n=2) and Activin A/B-null CAFs (n=4, 2 for each clonal population). Statistical test conducted was an unpaired t-test. Error bars represent the SEM.

The relative scratch density, specifically the density of cells occupying the initial scratch, increases at a faster rate in parental CAFs than Activin A/B-null CAFs. Scratches are almost completely closed within 24 hours in parental CAFs (94%)

compared to double null CAFs, where the scratches are still partially open (73%). This difference in closure efficiency at 24 hours is statistically significant ($p<0.043$). This demonstrates that Activin expression in CAFs enhances their migration. Additionally, the rate at which the scratch closes could be influenced by proliferation. Despite the moderate increase in proliferation, Activin A/B-null CAFs were unable to close the scratch at an increased rate.

In this section, I have shown that Activin expression promotes CAF contractility and motility, suggesting parental CAFs have enhanced ECM remodelling capability, compared to Activin A/B-null CAFs. As discussed above, this strongly suggests that cancer cell invasion may also be affected in co-cultures of cancer cells. I therefore sought to assay the ability of my clonal CAF populations to propagate cancer cell invasion.

4.2.2 Interaction between CAFs and cancer cells

I first aimed to determine the effect of each CAF population on cancer cell invasion using an *in vitro* system. I chose to co-culture them with cancer cells isolated from the MMTV-PyMT mouse model of cancer. This is the same model from which the CAF clones originated. However, my RNAScope results in Chapter 3 show that these cancer cells produce Activin A and B within the tumour. Additionally, former PhD student Daniel Miller showed that conditioned media taken from these cells is able to induce PSMAD2 activity in naïve HaCaTs (Figure 4.4). This induction is largely diminished when PyMT cancer cell CM is added with Follistatin. The induction is also reduced, albeit to a lesser extent, when cancer cell CM is added in the presence of TGF-β ligand blocking antibody, LY. Finally, there is no observable induction of PSMAD2 in HaCaTs treated with a combination of cancer cell CM and both Follistatin and TGF-β blocking antibody (Figure 4.4). A combination of mine and Daniel's data show that these cancer cells produce functional Activin ligand.

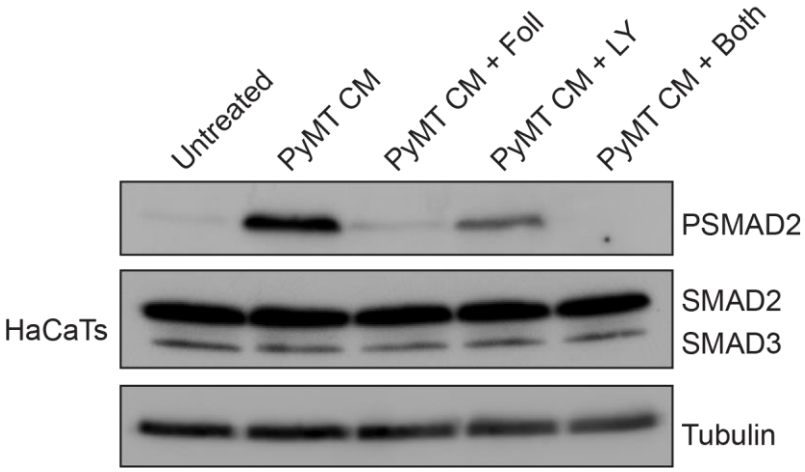

Figure 4.4. PSMAD2 induction in HaCaTs treated with PyMT CM. CM was taken from primary PyMT cells and added to naïve HaCaTs in the presence or absence of Activin antagonist follistatin (500ng/ml), TGF-β blocking antibody LY or a combination of the two. Western blot is representative of 3 biological replicates. Figure is adapted from data produced by Daniel Miller.

Because of this, any co-culture system with these cancer cells would expose my CAF populations to Activin ligand. This may result in recovery of any observable phenotype. Therefore, I decided to produce an Activin A/B-null CAF line that produced Follistatin to act as a dominant negative. I anticipated this would negate any Activin produced by the cancer cells in co-culture. This would allow me to truly determine the role of Activin signalling on CAFs' influence over cancer cell invasion.

Each Activin A/B-null CAF line was transfected with either a pcDNA3.1-FST or blank pcDNA3.1 control construct. Each construct contained hygromycin resistance as a positive selection tool. Cells were expanded following positive selection. I then measured relative levels of Follistatin gene expression using qPCR.

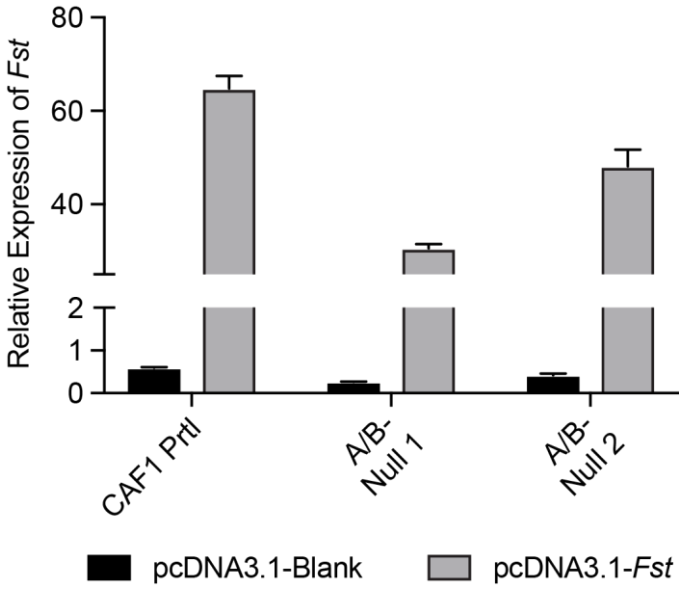

Figure 4.5. qPCR of *Fst* expression in transfected CAF clones. Expression of *Fst* transcripts in transfected CAF populations as measured by qPCR relative to un-transfected parental CAFs. Black bars represent clones transfected with a blank control construct. Grey bars represent clones transfected with the Follistatin overexpression construct. Graph is the average of three technical replicates. Error bars represent the standard deviation.

Levels of *Fst* expression are generally low in populations transfected with the blank control construct and equate to levels of un-transfected CAFs (bar not shown). Conversely, levels of *Fst* are much higher in cells transfected with pcDNA3.1-*Fst,* between 30 and 60-fold. However, increased mRNA expression does not necessarily translate to an enhanced Activin neutralising. Therefore, I aimed to determine each populations' Activin neutralising capacity using a $CAGA_{12}$-luciferase (CAGA-Luc) assay (see Section 2.3.10). In this assay, cells expressing a CAGA-Luc express luciferase under the control of SMAD binding element 'CAGA'. SMAD binding and transcription at these sites results in measurable luciferase production. The greater the Activin induction, the greater the luciferase output. For this assay, I utilised HEK293T cells that stably express the CAGA-Luc construct (HEK293T-CAGA-Luc).

CM from each cell line was added to HEK293T-CAGA-Luc cells in combination with recombinant Activin to determine their neutralising capacity. Levels of luciferase in HEK293T-CAGA-Luc cells are indicative of TGF-β family activity, specifically Activin induction in this instance. Cells were serum starved prior to induction to ensure that it is only factors within the CM that could be inducing pathway activity.

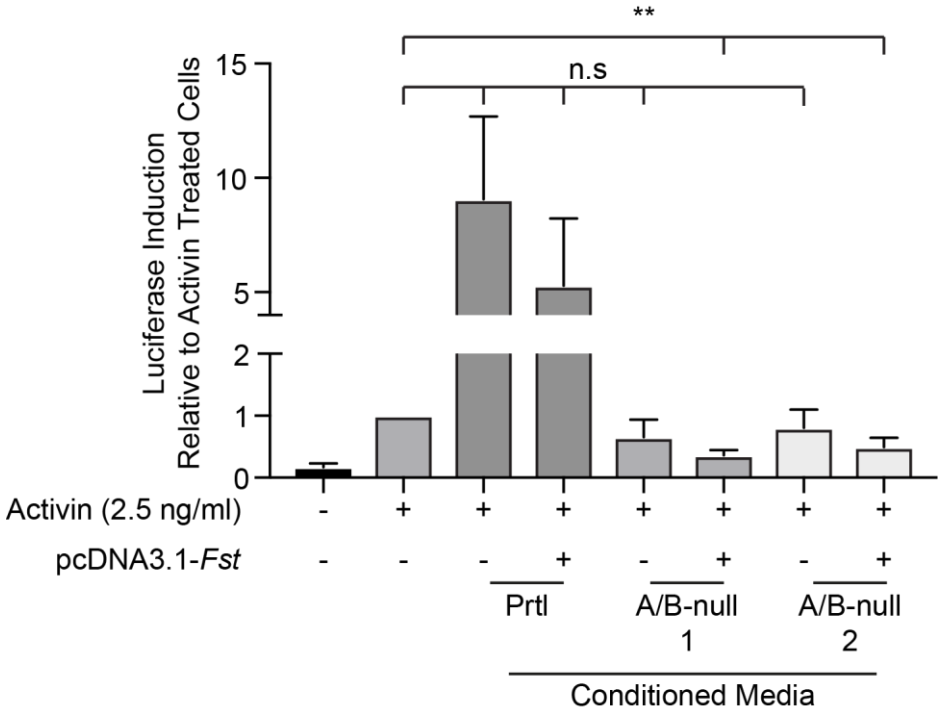

Figure 4.6. $CAGA_{12}$-Luc assay with transfected CAF CM. Quantification of luciferase induction in HEK293T-CAGA-Luc cells treated with CM from CAF clones transfected with a blank or pcDNA3.1-*Fst* overexpression construct in combination with a low dose of Activin (2.5 ng/ml). Untreated and recombinant Activin treated HEK293T CAGA-Luc were used as negative and positive controls respectively. Levels of luciferase induction is relative to recombinant Activin treated cells. Averages are of 5 biological replicates. Error bars represent SEM. Statistical analysis conducted was an unpaired t-test.

HEK293T-CAGA-Luc cells treated with recombinant Activin show a large increase in the luciferase reporter over untreated cells (6.5-fold) (Figure 4.6). HEK293T-CAGA-Luc cells treated with CM from parental CAFs show even higher levels of luciferase activity in both the blank (9-fold) and *Fst* (5-fold) transfected cells. This is likely due to their own production of Activins A and B. However, this increase is slightly lower in FST-expressing cells. Strikingly, luciferase levels are much lower than the Activin treated control in cells treated with CM from either Activin A/B-null CAF population. The reduction is most prominent in cells treated with CM from Activin A/B-null cells overexpressing FST This difference is significant for each population ($P<0.05$). CM from cells transfected with the blank construct show no significant difference in luciferase induction from the recombinant treated cells. These data suggest that the FST-overexpressing double null CAFs are able to neutralise Activin. Activin A/B-null/FST 1 clone induces lower levels of luciferase activity than Activin A/B-null/FST 2 clone. This implies this population may have

slightly better Activin neutralising properties. Henceforth, this dominant negative cell line is referred to as Activin A/B-null/FST.

Following this result, I sought to make mCHR fluorescent cell lines for parental CAFs, Activin A/B-null and Activin A/B-null/FST populations. This would ultimately help with quantification in any co-culture assays. A GFP fluorescent MMTV-PyMT cancer cell line already existed for use within the lab. The CAF mCHR populations were generated using a PiggyBack construct and sorted using flow cytometry before expansion (data not shown).

After I had generated fluorescent CAF populations, I finally sought to assay their influence on cancer cell invasion using a spheroid co-culture assay. Spheroids were generated at a 50:50 CAF:cancer cell ratio and embedded in a type I collagen matrix. This assay replicates the interaction of these cells in a tumour context. It measures the effect of direct interaction between these cells within an ECM matrix (Friedl et al., 2012). Spheroids were then imaged after 72 hours and quantified.

For this assay, I was interested in several features of cancer cell invasion. Specifically, the total area the cancer cells and CAFs ultimately cover. This indicates how invasive each population is within each experimental group. Additionally, I was interested in the gross shape the cancer cells exhibit. Specifically, whether it was rounded or an irregular ‘starfish-like’ shape. A more irregular shape indicates more invasive cancer cells (De Wever et al., 2010). Finally, I wanted to determine whether cancer cells detach and fragment from the spheroid bulk. This is an indicator of their single cell or collective invasive capabilities. Invasion of cancer cells collectively or as multi-cellular clusters correlates with a poorer prognosis in many types of cancer (Aceto et al., 2014; Cheung and Ewald, 2016).

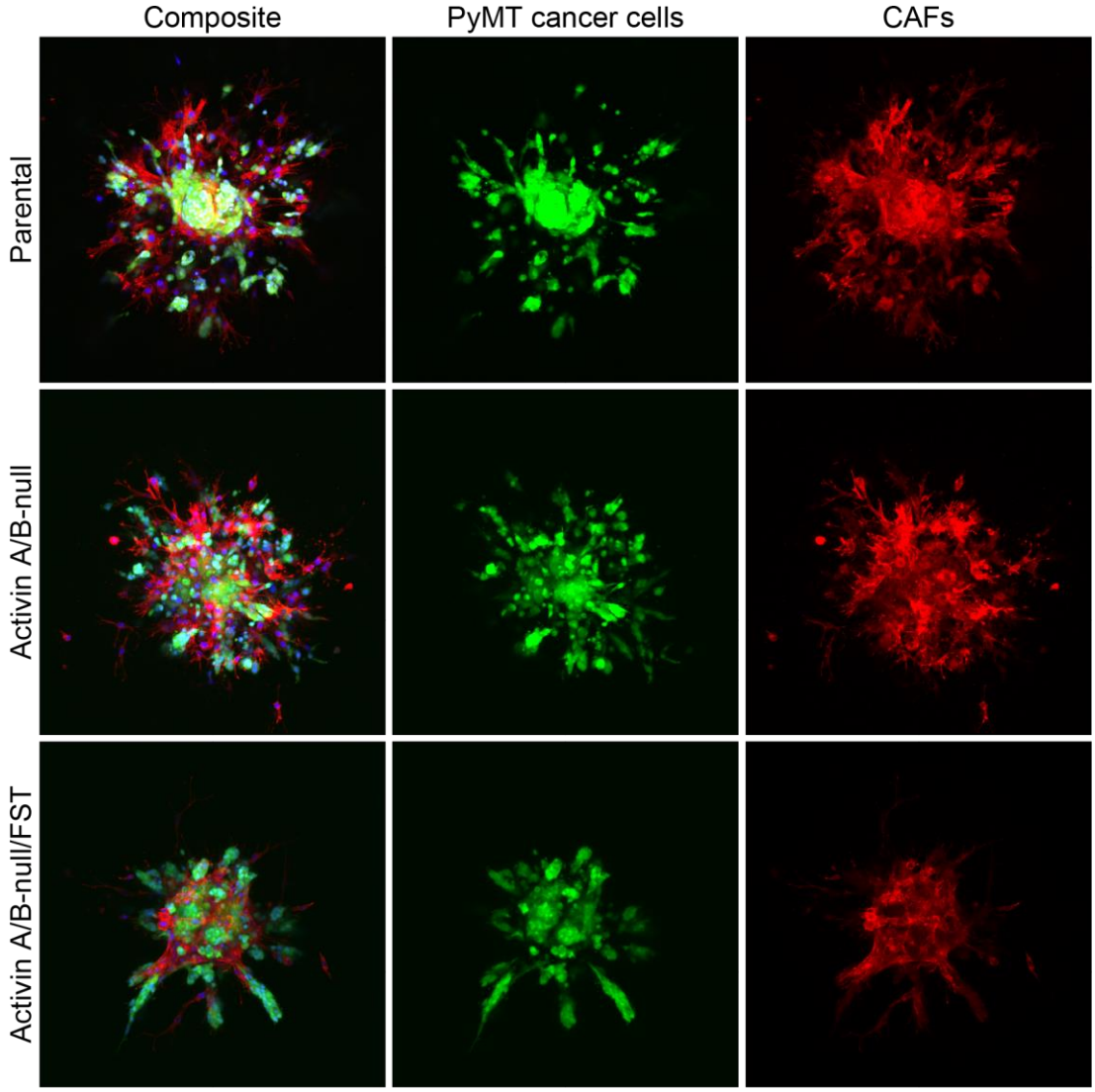

Figure 4.7. CAF and PyMT cancer cell co-culture spheroid invasion assay. Images of spheroids containing respective mCHR CAF populations and GFP MMTV-PyMT cancer cells at 72 hours after embedding. Nuclei are stained with DAPI (blue). Images are representative of three biological replicates.

Firstly, the total area covered by spheroids containing parental CAFs appears to be the most expansive, followed by Activin A/B-null CAFs with the Activin A/B-null/FST CAF containing spheroids appearing to cover the smallest amount of space (Figure 4.7). Cancer cells within parental CAF-containing spheroids exhibit more single and multicellular clusters of invasive cancer cells than those containing Activin A/B-null and Activin A/B-null/FST CAFs. Cancer cells in parental CAF-containing spheroids also exhibit collective strands of cancer cells. Those within Activin A/B-null and Activin A/B-null/FST-containing spheroids show a shift away from invasion as

clusters, appearing to exclusively invade as collective strands, especially within spheroids containing Activin A/B-null FST CAFs.

The most uniform and circular spheroids appear to be those containing the dominant negative Activin A/B-null/FST CAFs (Figure 4.7). This observation has been quantified using the factor shape equation (Figure 4.8). Using this equation, spheroids with a low factor shape represent a more uniform circular shape, whilst a higher factor shape denotes a more irregular and 'starfish' like structure, indicating a greater degree of invasion (De Wever et al., 2010). The difference in factor shape between parental CAF-containing spheroids and each of Activin A/B-null and Activin A/B-null/FST CAF-containing spheroids is significant ($P<0.04$ and $P<0.02$ respectively). Quantification was conducted based solely on the cancer cell spheroid core and not the fragmented cancer cells that appear to have detached. In fact, the levels of fragmentation appear to be distinct between experimental groups. As mentioned, parental CAF-containing spheroids seem to have more detached invasive clusters of cancer cells migrating away from the spheroid core. I quantified this by dividing the area of 'released' clusters of cancer cells, by the total area covered by the cancer cells. This '% fragmentation' quantification indicates that, on average, around 16% of all quantifiable cancer cell regions are detached from the spheroid core in parental CAF-containing spheroids. This same calculation shows that Activin A/B-null and Activin A/B-null/FST CAF-containing spheroids have 6% and 3% fragmentation respectively (Figure 4.8). The difference between parental CAF- and Activin A/B-null/FST CAF-containing spheroids is significant ($P<0.02$). These data suggest that parental CAF-containing spheroids may be invading as single cells or multicellular clusters, whilst those lacking Activin may be invading more as collective strands (Cheung and Ewald, 2016; Friedl et al., 2012).

Finally, the area covered by the CAFs themselves appears to be much smaller in both Activin A/B-null and Activin A/B-null/FST CAF-containing spheroids compared to parental CAF-containing spheroids. Quantification indicates the difference between Activin A/B-null/FST and parental CAF-containing spheroids is significant ($P<0.04$) (Figure 4.8). This suggests that CAFs may be either less migratory in the matrix or less able to remodel it. Furthermore, CAFs seem to be preceding or leading invasive cancer cell strands in parental CAF- and Activin A/B-null CAF-containing spheroids. This is not observed in spheroids containing Activin

A/B-null/FST spheroids, and thus suggests they may have reduced potency in leading cancer cell invasion.

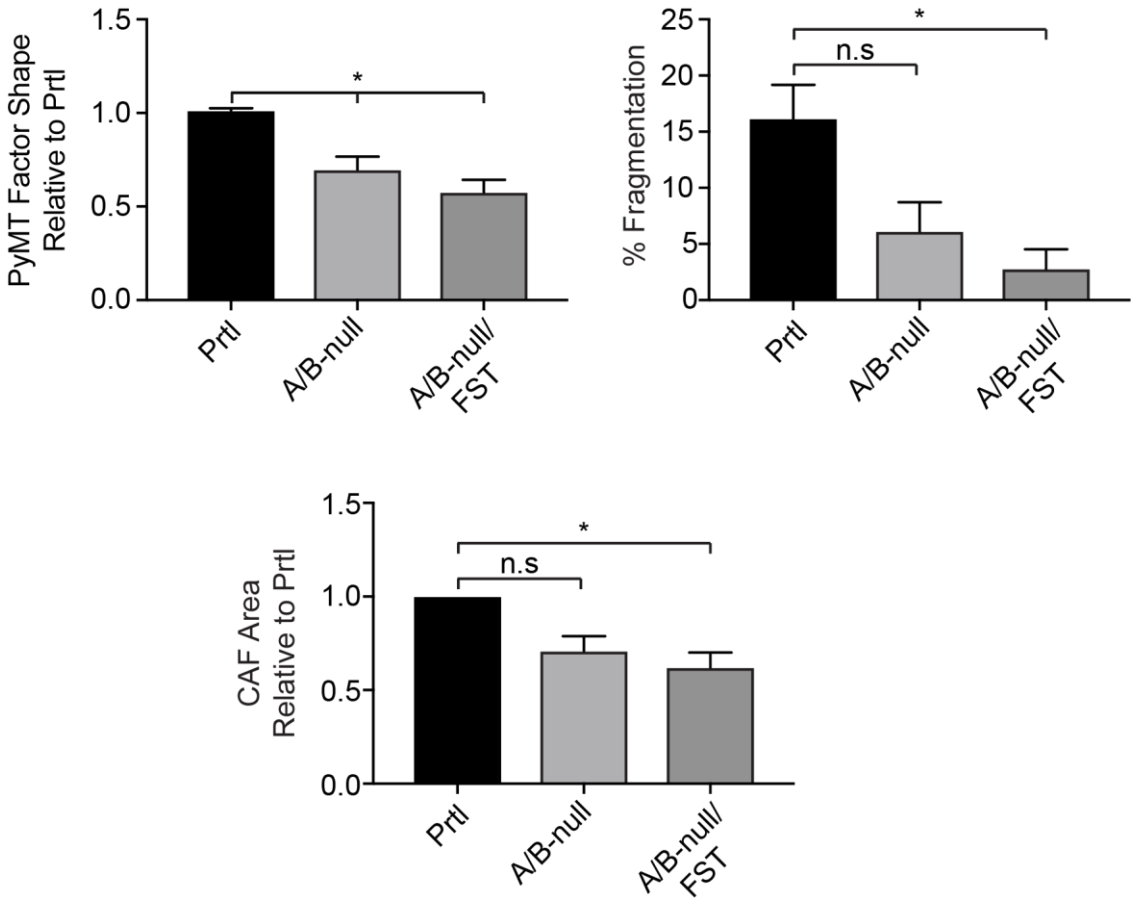

Figure 4.8. Quantification of CAF and PyMT co-culture spheroid invasion assay. Top left – PyMT cancer cell factor shape relative to respective parental biological average. Statistical analysis conducted was a paired t-test. Top right – % fragmentation. Statistical analysis conducted was an unpaired t-test. Bottom – CAF area relative to respective parental biological average. Statistical analysis conducted was a paired t-test. All quantifications are an average of 3 biological replicates each containing 3 technical replicates per condition. Error bars represent SEM.

Overall, these data suggest that cancer cells within spheroids lacking Activin are less invasive. This is observable in both Activin A/B-null and Activin A/B-null/FST CAF-containing spheroids, with the most profound effect seen in the latter. The extent to which differences in each CAF populations contractility, cytokine production or proteolysis contribute to this observation is unclear. Additionally, it is uncertain whether this phenomenon can be replicated *in vivo*. I therefore sought to conduct various *in vivo* experiments to test this effect as well as other functionalities of interest.

4.2.3 CAF functionality *in vivo*

So far, I have demonstrated, *in vitro*, that Activin expression has a profound effect on CAF signalling and function. Specifically, on their ability to remodel the ECM and promote cancer cell invasion. However, it is imperative to determine the role of Activin signalling in CAFs *in vivo*. To do this, I chose to conduct co-injections of my CAF populations with cancer cells from the MMTV-PyMT breast cancer model (Figure 4.9). Such a set-up would allow for the interrogation of the effect specific CAF populations have on tumour establishment, growth and composition. Specifically, I was interested in immune cell infiltrate, the vasculature as well as ECM structure and organisation.

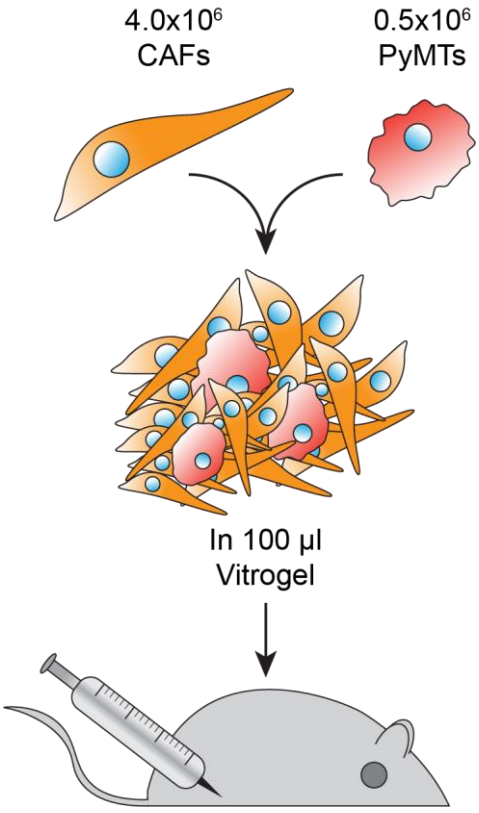

Figure 4.9. Schematic of CAF-PyMT co-injections. A combination of CAFs and cancer cells are re-suspended at a ratio 8:1 in a Vitrogel-PBS mix. The mixture is injected unilaterally into the mammary fat pad of female FvB mice.

Co-injections were conducted with either parental, Activin A/B-null or Activin A/B-null/FST CAFs. Additionally, an injection of cancer cells alone was used. To be able to accurately discern any differences between experimental groups, I decided

to overwhelm the co-injection system with CAFs, at a ratio of 8:1, CAF:cancer cells. Co-injection mixtures were suspended in a Vitrogel matrix, a solution composed of organic basement membrane proteins. This solution was selected over others, such as Matrigel, as it is free from growth factors, including all TGF-β family ligands (The Well Biosceince, 2019). I was concerned that the presence of these growth factors may compensate for loss of Activin signalling within the experimental set-up, negating any differences between experimental groups. Following injection, tumours, once established, were measured twice weekly. At the end of the experiment, tumours were harvested, and histopathological analysis of H&E stains conducted to determine immune cell and vascular infiltration into the tumour body. Additionally, Massons' Trichome staining was performed to determine any differences in fibrotic regions and ECM structure. Finally, IHC staining for various specific immune markers of interest was conducted to specifically immunophenotype the tumours. Experiments in this section were designed and analysed in collaboration with Alejandro Suarez-Bonnet and Simon Priestnall at the Royal Veterinary College.

The initial co-injection experiment was designed to run until measured tumours reached the permitted severity threshold (approximately 1.4mm in diameter). As soon as one mouse reached this threshold, all tumours were harvested so they could be time matched. The first mouse reached the tumour size threshold at day 29. Tumours were then excised, processed and H&E stained to interrogate their gross structures (Figure 4.10A). Additionally, tumours were measured twice weekly and volumes were calculated and plotted as a growth curve (Figure 4.10B).

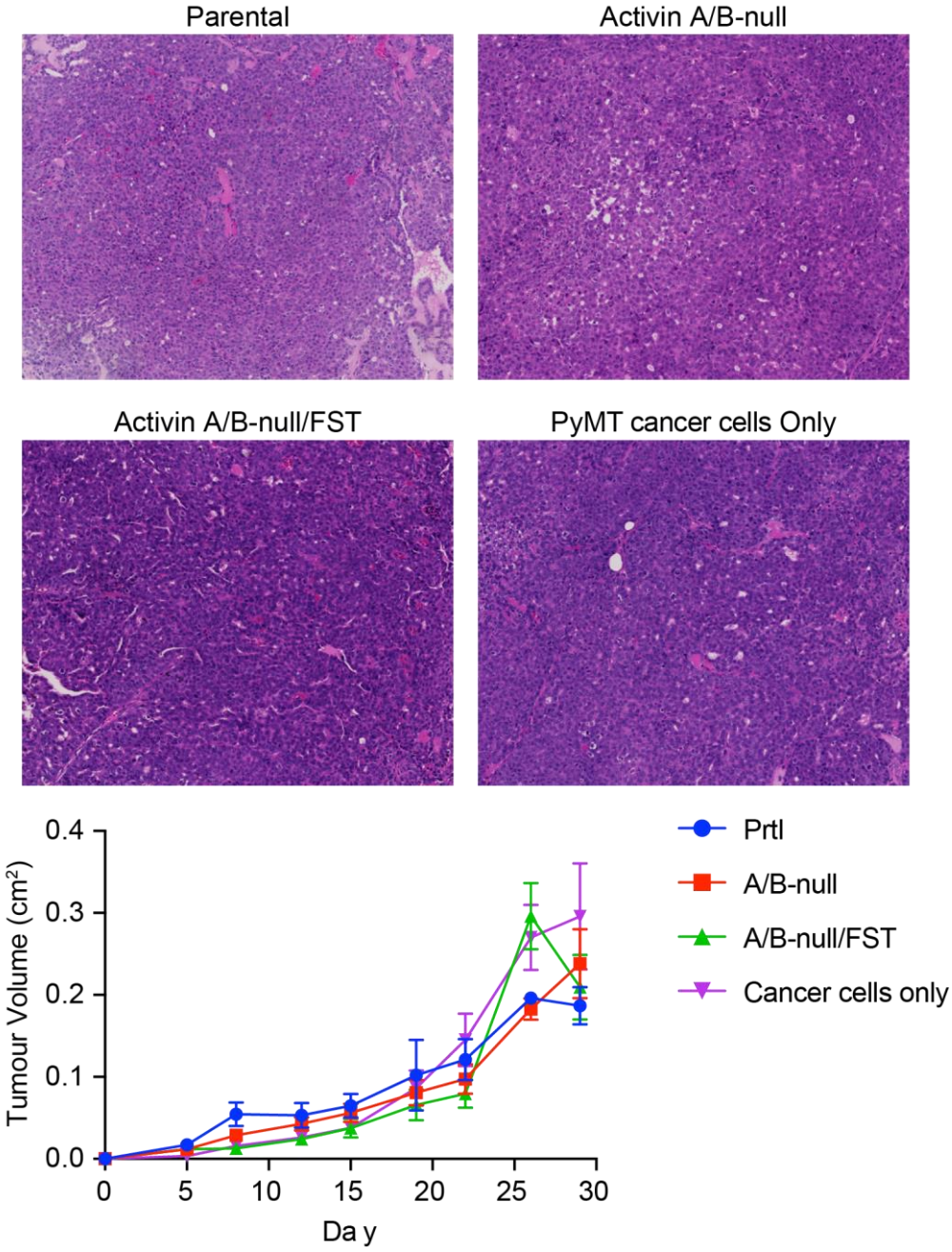

Figure 4.10. H&E sections and growth curves of CAF:PyMT co-injections. H&E images are representative of 3 distinct whole tumours for each respective experimental cohort. Images are at 10x magnification. Graph shows growth curve of tumour volumes for each experimental group. Each data point is an average of 4 different tumour measurements. Error bars represent SEM. Images labelled 'parental' 'Activin A/B-null' and 'Activin A/B-null/FST' represent injections containing respective CAF populations injected with cancer cells.

Tumours at this timepoint, in all experimental groups, were composed almost entirely of neoplastic cells, approximately 95% based on histopathological grading. Very few elongated cells resembling fibroblasts, if any, can be observed. Due to the

highly proliferative nature of the cancer cells and migratory nature of the CAFs, it may be the case that the CAFs had migrated away from the tumour and the cancer cells had begun to dominate. Based on this data and my colleagues' own observations, these tumours appear to be able to grow independently of a significant stromal compartment. There were no observable immune cell populations or blood vessels based on histopathological analysis. I concluded it was not possible to determine any influence the injected CAFs may have had on the tumour at this stage. Additionally, it was noted that harvesting additional normal mammary fat pad tissue around the tumour may be prudent, allowing analysis of tissue surrounding the node itself. Beyond histological features, there were negligible differences in tumour growth at all stages of development (Figure 4.10).

Based on the above observations, I decided to set up two additional experiments to harvest tumour samples at earlier timepoints. I used the same experimental set-up, but harvested tumours at days 15 and 19. I believed these timepoints would be late enough for the CAFs to establish any notable effects on the tumour and prior to the CAFs migrating away and neoplastic cells beginning to dominate. At these timepoints, tumours containing parental CAFs were 1.3, 1.6 and 1.2-fold larger than those containing Activin A/B-null CAFs, Activin A/B-null/FST CAFs and PyMT only tumours respectively.

Interestingly, tumour samples harvested at day 19, have varying degrees of neoplasm within tumour nodules between samples (Figure 4.11). Some nodules resemble those observed in Figure 4.10, almost entirely neoplastic. The remaining samples exhibit smaller, dispersed regions of neoplasm (between 5% and 40% of the node) embedded in a diffuse matrix (Figure 4.11). Additionally, within this matrix, several different immune cell populations appear to be embedded. Furthermore, there is no difference in tumour volume between experimental groups at the majority of timepoints measured.

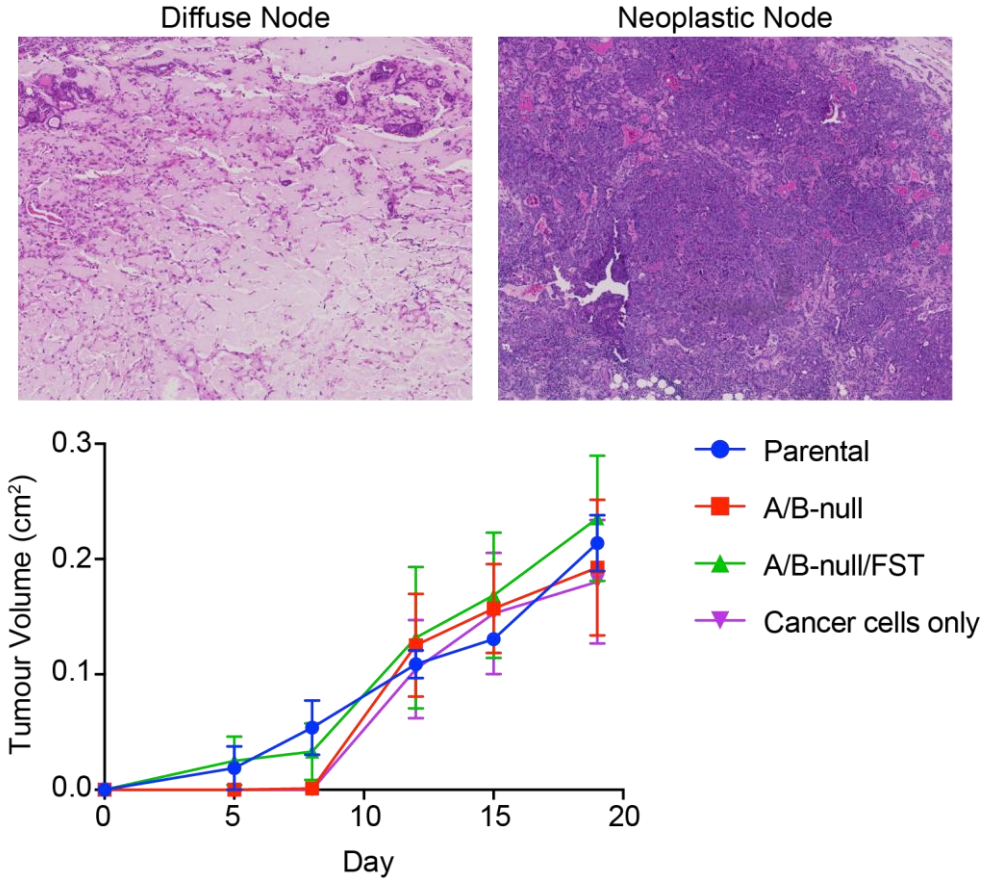

Figure 4.11. H&E sections and growth curves of co-injection experiments ending at day 19. H&E images show examples of entirely neoplastic tumour nodes alongside more diffuse nodes composed of a diffuse matrix and other stromal components. Images are at 4x magnification. Growth curve is the average tumour volume for 4 mice (parental and Activin A/B-null groups) or 5 mice (Activin A/B-null/FST and PyMT only n=9 groups). Error bars represent SEM.

Samples from the 15-day experiment consist entirely of the diffuse nodes observed in Figure 4.11. Additionally, the amount of neoplastic material within each node has been analysed using an objective semi-quantitative approach.

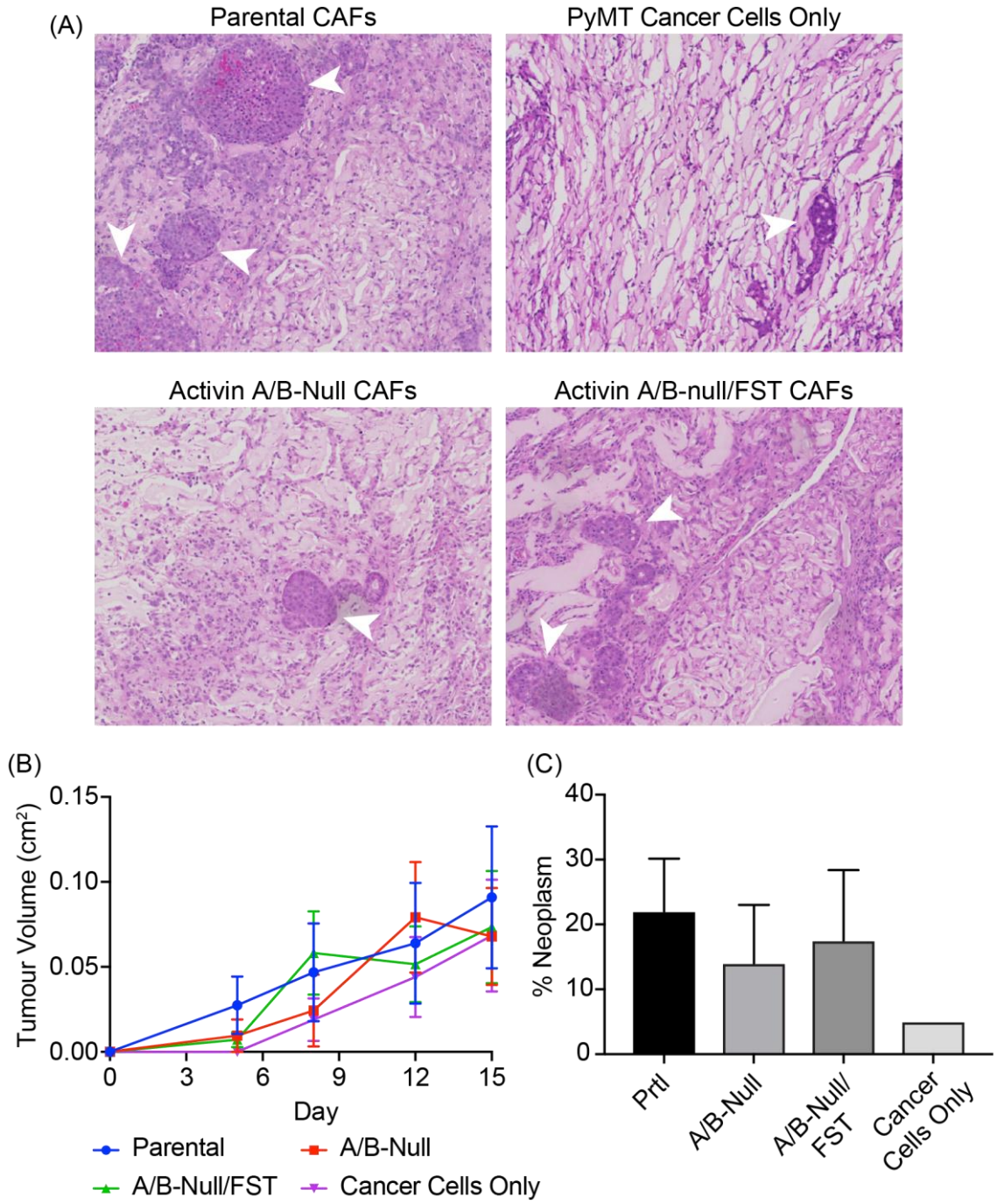

Figure 4.12. H&E sections and quantifications of co-injection experiment ending at day 15. (A) Representative H&E images of tumour nodules across 5 mice per experimental group. White arrows indicate regions of neoplasm (B) Average tumour volume growth curve of all tumour nodules (n=5 for each experimental condition. Error bars represent SEM. (C) Percentage neoplasm quantification conducted blind and independently by a pathologist. Quantification is the average of all samples deemed by the pathologist to contain neoplastic material; n=5 for parental and A/B-null samples, n=4 for A/B-null/FST samples and n=2 for PyMT only samples. Samples classified as normal mammary gland were omitted from the quantification.

Once more, there is minimal difference in volume between tumour nodules containing any one of the different CAF populations (Figure 4.12B). At day 15, tumour nodules containing parental CAFs are the largest. At this stage, they are 1.3 times larger than both PyMT only and A/B-null CAF-containing tumour nodules; and 1.2 times larger than A/B-null/FST CAF-containing tumour nodules. This difference is not significantly different. Additionally, tumour nodules containing parental CAFs exhibit the highest percentage neoplasm on average (22%) compared to each of A/B-null, A/B-null/FST and PyMT cancer cell only-containing tumour nodules (14%, 17.5% and 5% respectively) (Figure 4.12C). The H&E images shown reflect the average percentage neoplastic quantification (Figure 4.12A). The dark purple regions embedded within the diffuse white material are regions of neoplasm (indicated by white arrows). Additionally, a complete lack of lymphatic and angiogenic invasion was noted across all samples.

Measurements from all mice, up to day 15, were averaged from all experiments to obtain a more robust comparison of rates of growth between each experimental group (Figure 4.13).

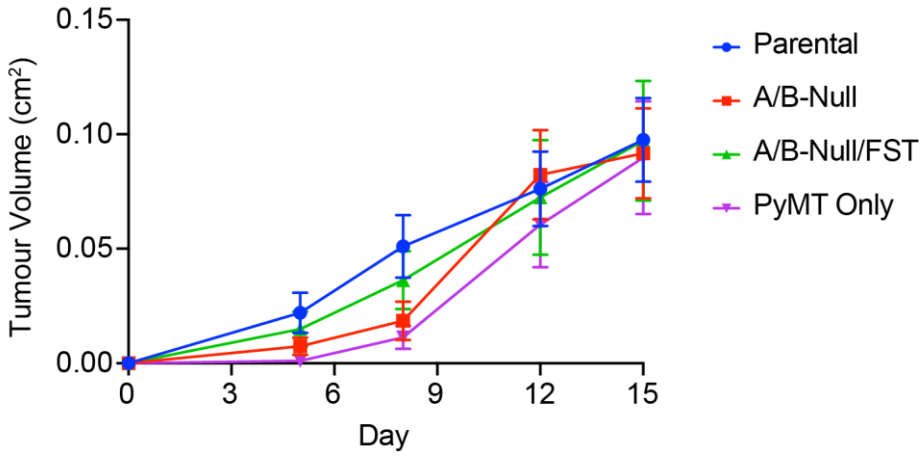

Figure 4.13. Average tumour volume growth curve for all co-injection experiments. Average tumour nodule volume growth curve of all individual mice across all 3 experiments up to day 15. Averages were of 12 and 13 mice (for parental and A/B-null mice respectively) and 14 mice for each of A/B-null/FST and PyMT only samples.

At day 15 and throughout tumour development, tumours are approximately the same size across all experimental groups (Figure 4.13). The largest difference in tumour volume can be seen at Day 8, when nodules containing parental CAFs are largest. Specifically, at day 8, tumours containing parental CAFs are, on average, 2.9, 1.5

and 4.4 times larger than double null, double null FST and PyMT only tumours respectively (Figure 4.13). This observation is partially reflected in the % neoplasm quantification of samples from the 15-day experiment (Figure 4.12C). However, this difference is negligible and not statistically significant.

Due to greater levels of consistency between samples in the 15-day experiment, I elected to conduct more rigorous analysis on these samples. Analysis of the 19-day experiment would be more difficult as comparisons between diffuse and neoplastic nodules may result in less valuable and robust conclusions. First, I investigated any differences in ECM composition between experimental groups. I conducted a Massons' Trichome stain to see any fibrotic, collagen rich regions within each sample as well as their organisation (Figure 4.14).

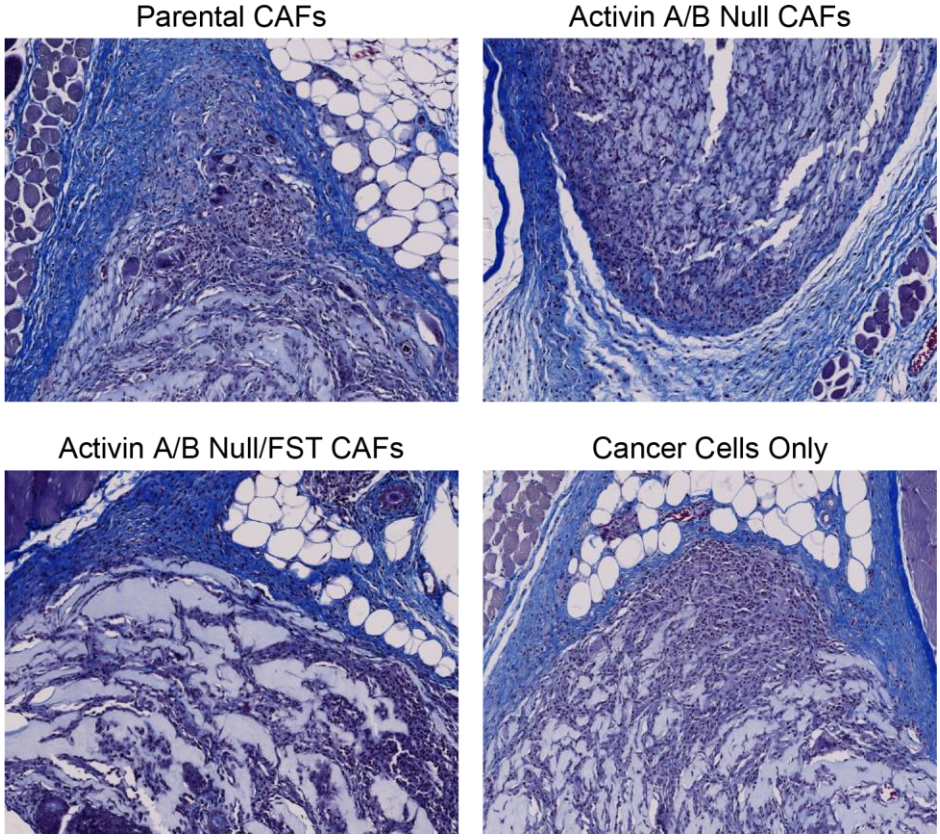

Figure 4.14. Massons' Trichome stain of 15-day co-injection samples. Representative images of Massons' Trichome stain for each experimental group. Blue stain denotes connective tissue including collagen. Darker blue and brown stains denote nuclei.

Examination of Massons' Trichome stains shows minimal presence of collagen deposition within each tumour nodule. A ring of collagen can be observed

surrounding each nodule in the majority of cases (Figure 4.14). However, this could be an inflammatory reaction from the host in response to the injected nodule to barricade the foreign substrate rather than any deposition by CAF populations. In any case, there appears to be no distinction between the organisation of these collagen rings between biological groups.

Furthermore, I conducted IHC analyses to determine the amount and phenotype of infiltrating immune cells within each tumour nodule. Specifically, I stained for CD4, CD8 and FoxP3 positive lymphocytes as well as F4/80 (macrophages) and S100a9 (neutrophils). Figure 4.15 shows the quantification for each population between samples. Representative images for each of these stains are shown in Figure 4.16.

Between experimental groups, there was negligible difference in the number of cells that were positive for each lymphocyte marker (CD4, CD8 and FoxP3). The highest levels for all three markers are observed in the parental CAF co-injection samples. However, there was variability between samples within the same experimental population and there are no significant differences between any sample for each lymphocyte marker.

There is a significant decrease in F4/80 positive cells (macrophages) in both Activin A/B-null and A/B-null/FST CAF-containing spheroids compared to parental CAF-containing spheroids ($P<0.05$ and $P<0.01$ respectively). Additionally, absolute numbers of F4/80 positive cells are higher than any other immune cell marker across all experimental groups. Finally, there is no difference in the numbers of s100a9 positive cells (neutrophils) between nodules containing any one of the CAF populations. However, there is a slight increase, on average, in s100a9 positive cells in nodules containing PyMT cancer cells only. The absolute numbers of s100a9 positive cells are lower than any other immune cell marker investigated.

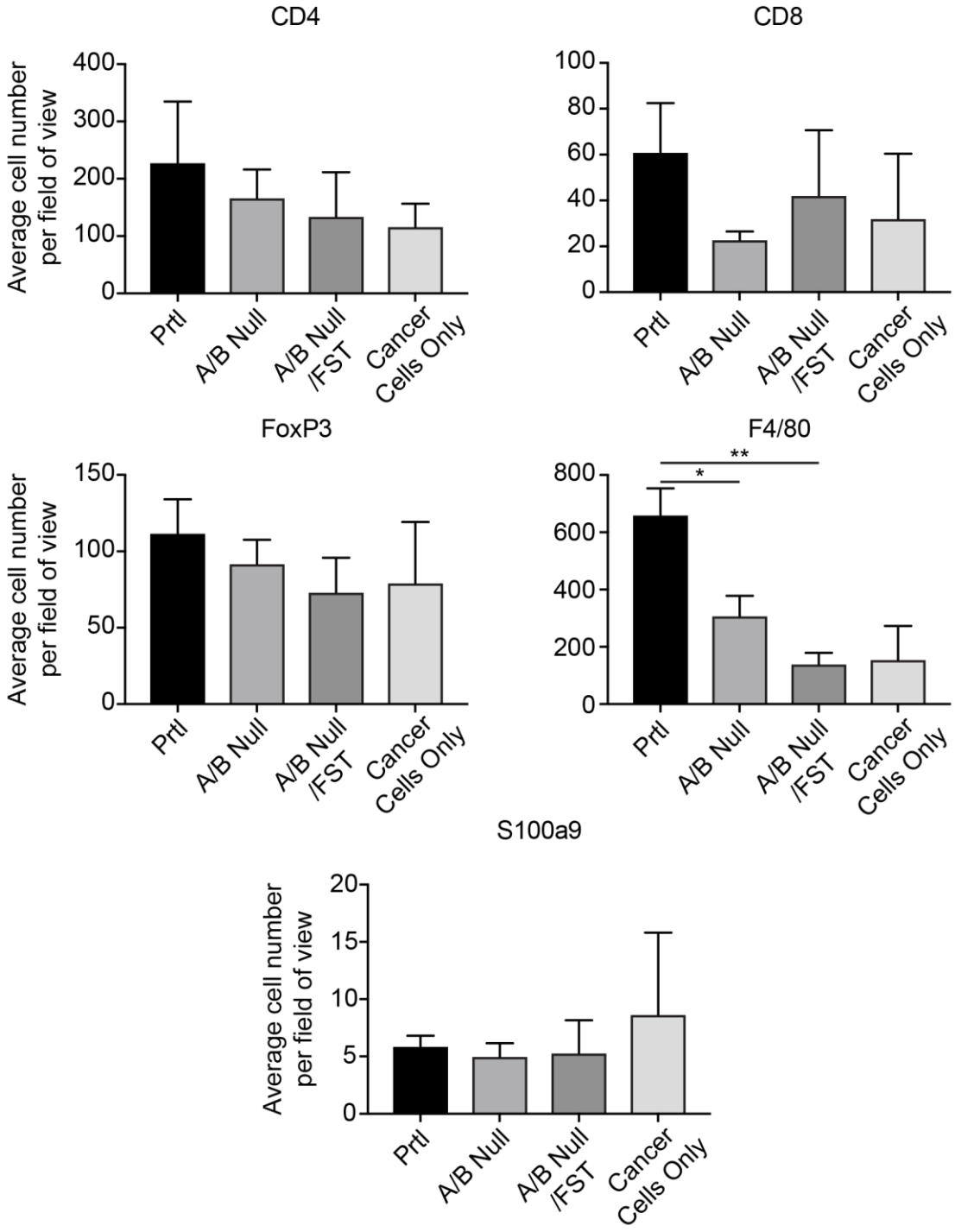

Figure 4.15. Quantification of immune cell markers in 15-day co-injection tumour nodules. Quantification was done using the QuPath positive cell detection tool. Cells reaching a set threshold for levels of DAB staining were deemed positive for the respective marker. For each sample, several distinct fields of view were captured and quantified in this way. Fields of view were averaged for each sample and all averages were plotted (n=5 for parental and Activin A/B-null CAF-containing samples, n=4 for Activin A/B-null/FST CAF-containing samples and n=2 for PyMT only samples). Each field of view equates to a 10x objective field. Error bars represent SEM.

Images of these samples reflect this quantification (Figure 4.15). The images shown exhibit a close representation of the average number of positive cells seen for each marker. Generally, numbers of CD4 and FoxP3 cells are high across all samples and appear to be at similar levels. Numbers of CD8 positive cells are generally low across all experimental groups. The number of F4/80 positive cells is high between experimental groups and appears to be highest in parental-CAF containing tumour nodules.

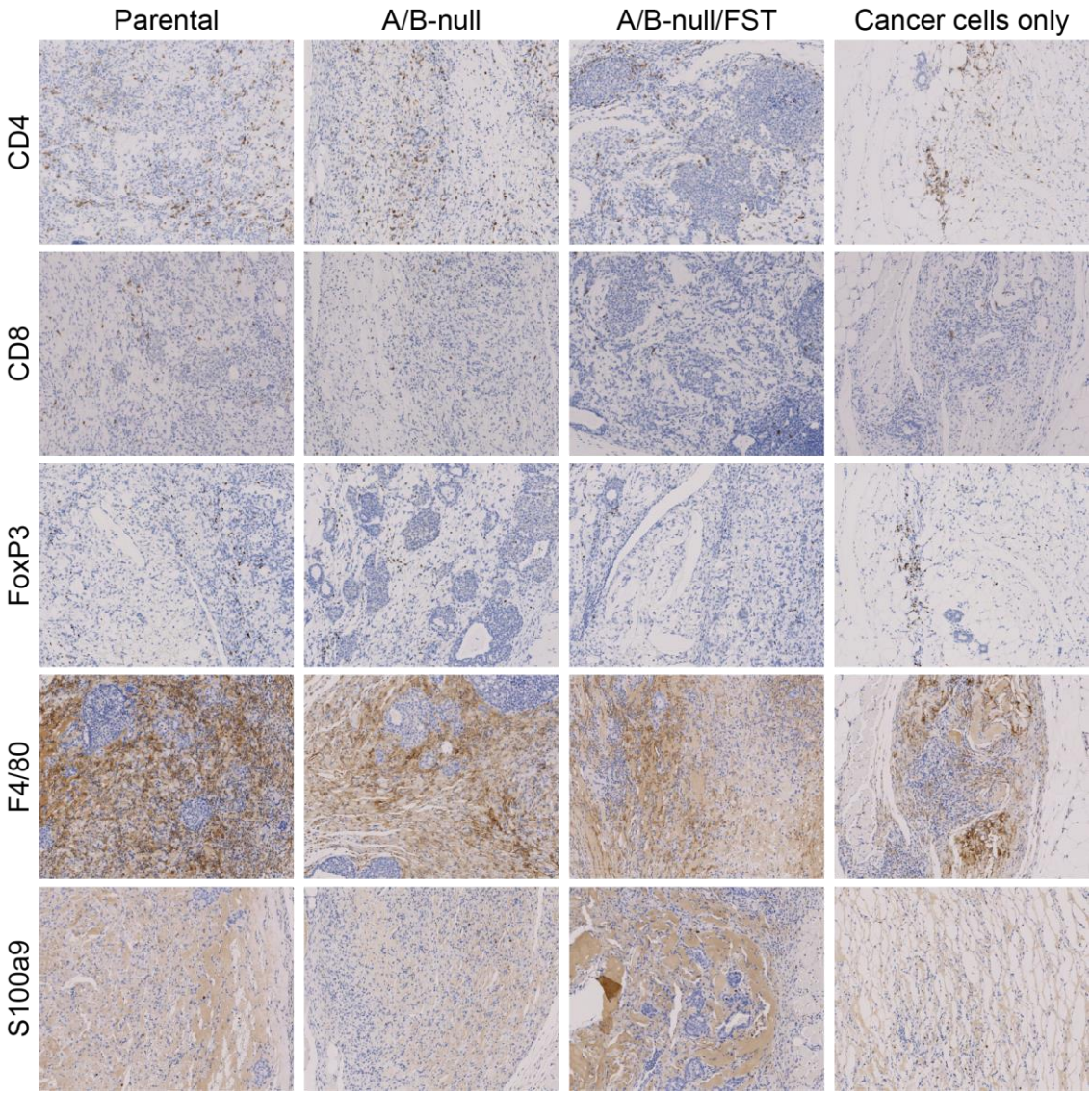

Figure 4.16. IHC staining for immune cell markers in 15-day co-injection tumour nodes. Images are representative of at least 3 fields of view for 5 distinct mice per experimental group. Positive DAB staining for respective markers is shown in brown. Nuclear stains are haematoxylin blue.

It was also important to demonstrate that the injected CAFs were present within the tumour nodules, eliciting the effects observed above. Since the cells initially injected were unlabelled, I conducted staining for a CAF marker, αSMA (Figure 4.17).

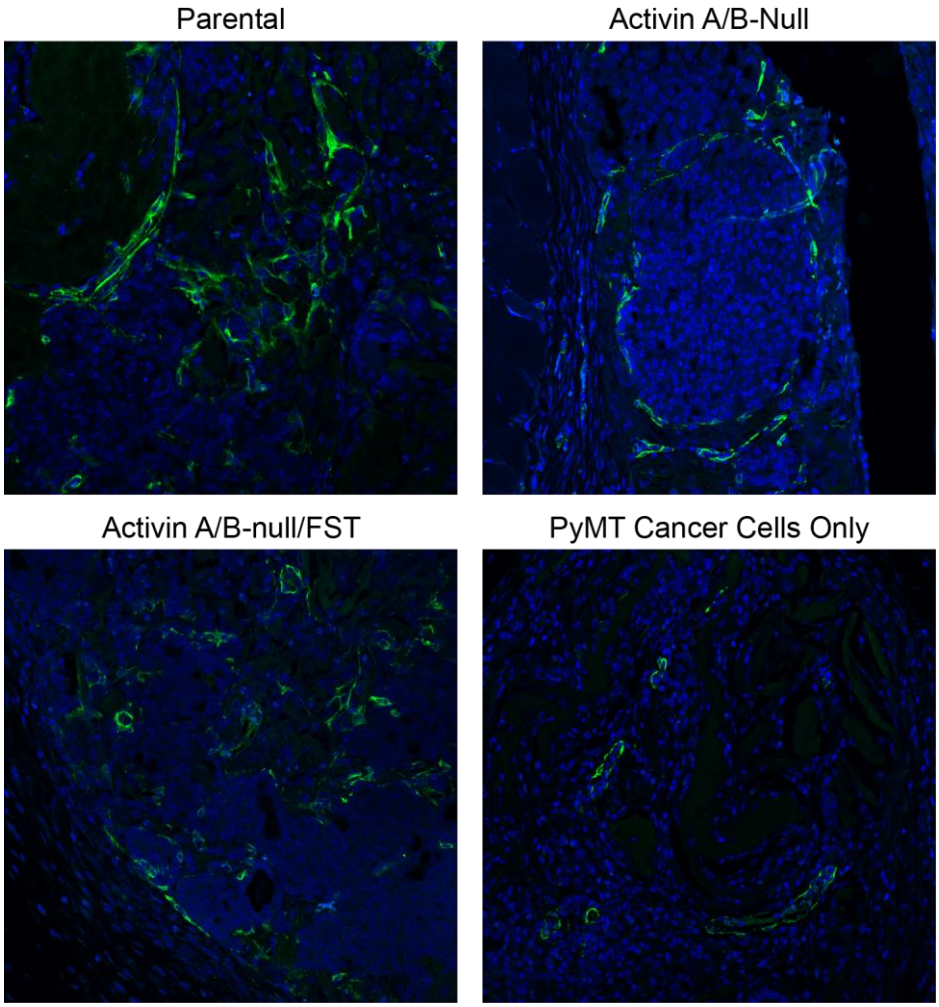

Figure 4.17. αSMA staining of nodules from 15-day co-injection experiment. αSMA (green) and DAPI (blue) IF staining conducted on sections from the 15-day co-injection experiment. Images are representative of 5 separate mice for each experimental group.

Samples from all mice show a degree of positive αSMA staining. It is unclear if these cells are tissue resident αSMA cells or the injected CAFs. However, the PyMT only samples show less positive staining, suggesting that some of the cells observed in the parental, Activin A/B-null and Activin A/B-null/FST CAF-containing samples are likely to be those that were initially injected. Positive staining of samples shows fibroblasts are present and possibly responsible for the observations detailed previously.

In addition to these co-injection experiments, I set-up CAF only injections into the mammary fat pad. This would allow me to directly ask whether distinct CAF populations influence immune cell infiltration and angiogenesis, as well as their capacity to alter the ECM. Since this is independent of a cancer cell compartment, I could harvest the injected plug at an earlier stage, before the CAFs begin to migrate away.

Initially, a short-term experiment was set-up (5 days) using Vitrogel as the injection suspension. However, samples at this stage showed no immune cell compartment, except neutrophils. Additionally, no angiogenic infiltrate was observed (data not shown). Based on this experiment and observations from the co-injection experiment, I decided that a change of injection suspension matrix to growth-factor reduced Matrigel (GFR Matrigel) may be beneficial. I reasoned that Vitrogel was less appropriate for establishing a biological plug, in which cells can efficiently grow and penetrate. This observation is supported by data within the lab that shows tumours establish and develop at a quicker rate when cancer cells are injected in GFR Matrigel compared to Vitrogel (Figure 4.18).

GFR Matrigel tumours exhibit a rapid growth rate when compared to Vitrogel tumours. By the first timepoint (day 12) GFR Matrigel tumours are approximately 0.09cm^2, whilst the Vitrogel tumours have failed to establish. Vitrogel tumours do not reach sizes any larger than this until day 26, when tumours measure, on average, 0.17 cm^2. Moreover, tumours within GFR Matrigel reach the severity threshold permitted within the protocol at day 21, measuring, on average, 0.57 cm^2. At the same timepoint, Vitrogel tumours measure just 0.05 cm^2 on average, approximately 11-fold smaller than the GFR Matrigel tumours. Vitrogel tumours themselves do not reach the severity threshold until day 31. This shows a marked decrease in tumour growth for samples injected in Vitrogel. This indicates that cells are possibly less viable in Vitrogel suspension compared to GFR Matrigel.

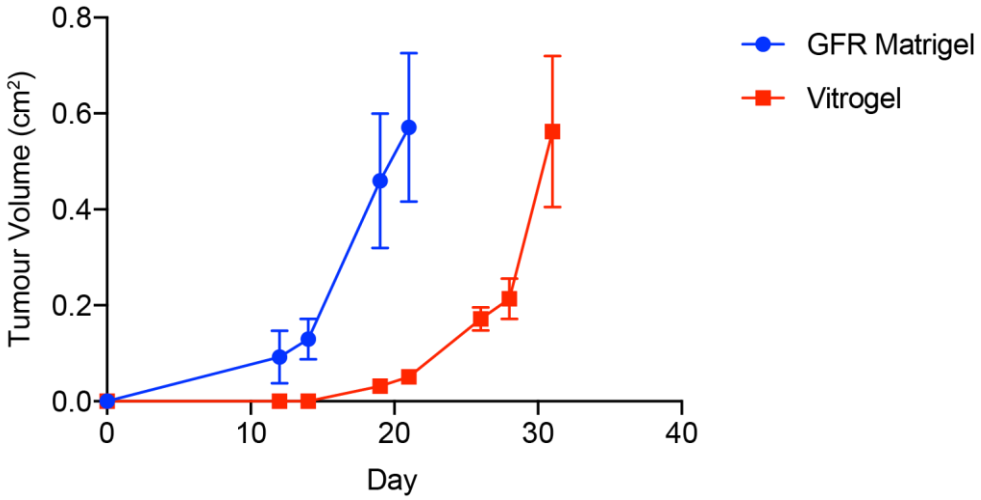

Figure 4.18. Growth curve of tumours originating from cancer cells injected in GFR Matirgel or Vitrogel. Tumours were measured twice weekly and tumour volume calculations conducted for GFR Matrigel (blue) and Vitrogel (red) injected tumours. Datapoints are an average of 2 biological replicates. Error bars represent the SEM. The data in this figure was produced by Danielle Park.

4.3 Discussion

4.3.1 Summary of results

- CAFs lacking Activin expression are unable to contract a collagen gel and are less migratory than their wildtype parental counterparts.
- Activin A/B-null CAFs have reduced ability to promote cancer cell invasion *in vitro.*
- I have begun to optimise *in vivo* models to interrogate the role of Activin expression in CAFs on tumour development.
- There is a reduction in F4/80 positive cell infiltrate in tumour nodes containing Activin A/B-null or Activin A/B-null FST CAFs compared to those containing parental CAFs.

4.3.2 Activin expression greatly affects the ECM remodelling capacity of CAFs

The ability of CAFs to remodel the extracellular matrix within and surrounding the tumour stroma is one of their prominent tumourigenic properties (Östman and Augsten, 2009). Contraction assays are a robust method of measuring the capacity

of cells to remodel and degrade the ECM (Ngo et al., 2006). Using this assay, I have demonstrated that CAFs lacking Activin expression are unable to contract a collagen gel. These data indicate that the ability of Activin A/B-null CAFs to remodel their surrounding ECM is markedly reduced. This result correlates with observations in the previous chapter which showed that Activin A/B-null CAFs have lower levels of Rho GTPase activity. Active Rho GTPase signalling is strongly associated with enhanced CAF contractility and remodelling capacity (Calvo et al., 2015; Wilkinson and Frame, 2016). Additionally, reduced levels of expression of ECM degradative proteins, specifically MMP3, seen in the previous chapter may also be contributing to the reduction in contractility. The relative contributions of each of these observations on the reduced contractility in Activin A/B-null CAFs has not been determined in this body of work. It will be important to conduct knockdown/knockout experiments of MMP3 and Rho GTPase regulators alongside these CAF populations to determine their relative contributions to this phenotype. Alternatively, rescue experiments in which MMP3 is overexpressed in the Activin A/B-null populations may answer this question.

In addition to ECM remodelling, an elevation in CAFs' motility and migratory capacities could enhance cancer cell invasion. More motile CAFs migrate away from the tumour bulk, generating tracks in which cancer cells can collectively invade (Gaggioli et al., 2007; Henke et al., 2016). I have shown, using a scratch assay, that CAFs lacking Activin A/B expression have reduced motility. In the context of a tumour, this may result in CAFs remaining within the tumour bulk and not generating tracks in which cancer cells can migrate away and metastasise. However, additional controls as part of this assay (including inhibition of proliferation and cell-cell interactions) would have added further validity to this result. Indeed, Activin A/B-null and Activin A/B-null/FST CAFs exhibit reduced migration away from spheroid co-cultures of 3 days when compared to the parental CAFs. This, in addition to the scratch assay, suggests the motility of these CAFs is reduced. Therefore, a combination of reduced ECM remodelling and motility could explain why cancer cell invasion in Activin A/B-null containing spheroids is reduced. Additionally, the scratch assay is analogous to wound closure. Reduction in wound closure observed in my Activin A/B-null CAFs correlates with published literature that Activin overexpression results in more rapid wound closure (Cangkrama et al., 2020b).

Whilst these *in vitro* assays show dramatic alterations in the behaviour of Activin A/B-null CAFs, it was important to demonstrate that these observations could be seen in a more biologically representative *in vivo* model. My co-injections were inconclusive in this respect. Massons' Trichome stains showed no observable distinctions in connective tissue and collagen bundle organisation between different CAF populations. Additionally, there appeared to be no regions of fibrosis across the samples. This may be biologically real, however, based on the robust and dramatic *in vitro* results, it seems likely that there should be changes in ECM remodelling capacity within the tumour stroma between these different CAF populations. These investigations may be conducted at inappropriate timepoints. Additionally, the set-up of the *in vivo* experiments may be inadequate (discussed below in Section 4.3.6).

Nevertheless, the *in vitro* results strongly suggest CAFs lacking Activin expression are unable to remodel the surrounding ECM. This may result in a less permissive environment for cancer cells to invade. Additionally, the dramatic changes observed in proteomic and transcriptomic analysis of different CAF populations indicate changes in cytokine expression may alter cancer cell invasion, in a manner that may be independent of ECM alteration. Investigating cancer cell invasion was therefore of great interest.

4.3.3 Activin and cancer cell invasion

There is currently minimal evidence that directly links Activin to promoting cancer cell invasion. One study has shown that overexpression of Follistatin can reduce levels of lung metastasis in a mouse model of breast cancer (Seachrist et al., 2017). This implies that Activin may promote cancer cell invasion and extravasation. Here, I have demonstrated using CAF and cancer cell spheroid co-culture models, that Activin secretion by CAFs acts to promote cancer cell fragmentation and invasion away from the spheroid.

For each method of quantifying invasion, factor shape and percentage fragmentation, cancer cells from parental CAF-containing spheroids show the greatest degrees of invasive behaviour, whilst the dominant negative CAF spheroids exhibit the least. However, the role of Activin A/B in eliciting these effects has not been determined in this body of work. Elevated levels of percentage fragmentation

are indicative of a more extravasation-type behaviour (Friedl et al., 2012). Existence of these fragmented cancer cell clusters has been shown to be partially dependant on ECM proteolysis (Sanz-Moreno and Marshall, 2010). I have shown that CAFs lacking Activin A/B expression produce less ECM remodelling proteins, such as MMP3, and have also demonstrated they are unable to contract a collagen gel. Therefore, this may be the cause of the increased cancer cell fragmentation in the parental CAF-containing spheroids. The contribution of degradative proteins to this phenomenon could be tested by using a Transwell invasion assay. In these assays, CAFs are seeded beneath Transwells harbouring cancer cells growing on a collagen matrix (Marshall, 2011). Secretion of degradative proteins by the CAFs influences the extent of invasion of the cancer cells through the Transwells.

Additionally, an elevation in invasion may result from an enhanced mesenchymal phenotype. Cancer cells in the Activin A/B-null/FST CAF-containing spheroids appear to invade more locally and collectively as a cluster. This type of behaviour suggests stable expression of adherens junction proteins (Rørth, 2009). Cancer cells within parental CAF-containing spheroids may have adopted a more mesenchymal phenotype, losing their adherens junctions and allowing them to invade as single cells and multi-cellular clusters away from the spheroid core. The published role of Activin A/B in promoting EMT is ambiguous. It has been shown to promote EMT, specifically by stabilising CDKN1A (p21), as well as promoting a migratory and mesenchymal phenotype in colon cancer through pAkt signalling (Bauer et al., 2015). It would be interesting to test whether this invasive phenotype is partially dependant on loss of adherens junctions. One could treat cancer cells from the MMTV-PyMT mice with CM from each CAF population and measure E-cadherin (CDH1) and vimentin protein levels. Loss of the junctional protein E-cadherin and gain of vimentin expression would suggest a more migratory phenotype.

Importantly, however, I have not determined the degree to which the cancer cells invade as single cells or collectively. The detached clusters may be single cells rather than collective multi-cellular groups. This is important as collective invasion correlates with a poorer prognosis in many cancer types (Aceto et al., 2014; Cheung and Ewald, 2016). Invasion as multicellular clusters would more likely result in polyclonal metastatic niches, whereas single cell invasion would result in clonal niches (Cheung and Ewald, 2016). One could quantify this phenomenon by defining

distinct invasive clusters, through the distance between neighbouring clusters, and subsequently counting the individual DAPI stained cells within each of those clusters. Due to difficulties with DAPI staining between replicates, I was unable to do this quantification in a robust way.

I believe the bulk of the evidence presented in this chapter indicates that the altered CAF migratory and contractile properties of Activin A/B-null CAF-containing spheroids has the most substantial effect on the observed moderation of cancer cell invasion. Through their proclivity for remodelling the ECM, CAFs generate tracks in which cancer cells follow and invade (Gaggioli et al., 2007). To this end, I have shown that the area in which CAFs expand and grow is diminished in Activin A/B-null and A/B-null/FST CAF-containing spheroids. Additionally, Activin A/B-null/FST CAFs no longer appear to lead cancer cells in these spheroids. Conversely, parental CAFs always appear to be leading the cancer cell invasion in these spheroids. These observations, combined with the result that Activin promotes CAF contractility, suggests that Activin A/B-null and Activin A/B-null/FST CAFs may be producing less tracks in which cancer cells can migrate. A more elegant experimental set-up in which cancer cells are tracked live microscopically would help determine whether cancer cell invasion is dependent on CAFs' generation of these tracks. Additionally, organotypic invasion assays may help to answer this question (Kramer et al., 2013). In any case, it is clear that CAFs lacking Activin expression have a lower propensity to promote cancer cell invasion than their wildtype parental counterparts.

4.3.4 The effect of Activin A/B-null CAFs on immune cell infiltration

The immune cell component of tumours is increasingly being shown to have a critical influence during tumourigenesis (Lei et al., 2020). Activin A/B has previously been shown to have a range of effects on various immune cell populations. Different studies show Activin to have either pro- or anti-inflammatory effects (Morianos et al., 2019). In skin cancer, Activin has been shown to create an oncogenic anti-inflammatory niche (Antsiferova et al., 2017). Therefore, it was vital to determine whether CAF secreted Activin had a similar effect on immune cell infiltration and phenotype.

I investigated the effect of each CAF population on the numbers of infiltrating cells positive for lymphocyte markers, including CD4+, CD8+ and FoxP3+ lymphocytes. No substantial or significant differences between each experimental cohort was observed. The variability within the data makes it difficult to draw any robust conclusions from these results. Additionally, it is also unclear whether the immune cell infiltration observed is an effect of the distinct CAF populations, or just an immune response to the injection.

There is a statistically significant reduction in numbers of F4/80 positive cells (macrophages) in tumour nodules containing both Activin A/B-null and A/B-null/FST CAFs compared to parental CAF-containing nodules. More tumour-associated macrophages (TAMs) in breast tumours are associated with poorer prognosis (Qiu et al., 2018). This suggests Activin may be enhancing tumour-promoting macrophage infiltrate. However, it is important to note that the phenotype of these infiltrating macrophages is crucial to determine disease outcome. Macrophages can elicit tumour-promoting or suppressive functions depending on their phenotype (Guerriero, 2018; Lin et al., 2019). I have not shown whether these infiltrating macrophages work to promote tumourigenesis. Published data shows that Activin overexpression correlates with enhanced macrophage infiltration in HPV8 induced skin lesions. Macrophages isolated form this model expressed a pro-tumourigenic phenotype (Antsiferova et al., 2017). However, it is difficult to make comparisons between this work and my own as experimental set-ups are distinct and the cancer type is different. It will be important to conduct further investigations to determine the role of Activin on immune cell activation and infiltration in breast cancer.

In any case, the observations discussed above appeared to have minimal impact on the ultimate development of the tumours, as they grew at similar rates at later stages. It may be valuable to conduct *in vitro* assays to determine the role each CAF population may have on immune cell activation and migration. For example, Transwell assays could be conducted with RAW264.7 macrophages to determine the influence each CAF population has on their migratory capacity. Additionally, CM from CAFs could be used to treat these immune cells before immunophenotyping them for tumour-promoting or suppressive markers, such as CD206 and CD80 respectively (Haque et al., 2019; Pinto et al., 2019). However, this is not an ideal approach as there is no definitive way to distinguish tumour-promoting and tumour-suppressive TAMs (Guerriero, 2018).

4.3.5 Activin and tumour growth

Activin has been shown to promote tumour growth and metastasis in a variety of cancer types, its inhibition results in smaller and less metastatic tumours (Loomans and Andl, 2014; Seachrist et al., 2017). I was unable to determine the effect (if any) of Activin A/B-null CAFs on tumour growth *in vivo*. Any observed differences in tumour size and percentage neoplasm was negligible at most stages. The largest observed difference in measured tumour size was at the earlier 8-day timepoint, when nodules containing parental CAFs were the largest. However, tumours ultimately grow to similar sizes at later stages. This may be because the injected cancer cells reach a certain threshold of cell number before their growth accelerates, seemingly independent of any other stromal compartment. The use of the co-injection experimental set-up utilised during this work may not have been the best approach to determine the role of Activin on CAF-mediated behaviours *in vivo*. Developing a model that uses cancer cells more dependent on stromal input may help better determine the effect of different CAF populations on cancer cell growth and tumour development.

4.3.6 Optimisation of *in vivo* experimental design

One of the major aims of the work described in this chapter was to determine the role of Activin A/B expressed by CAFs on tumour development and architecture *in vivo*. The experimental design aimed to answer these questions whist minimising the input of other TGF-β family signals that may compromise any biologically relevant observations. For example, Activin A/B-null Follistatin expressing CAFs were used to neutralise any circulating endogenous Activin in host mice. Additionally, Vitrogel was utilised as a suspension matrix for the injections over GFR Matrigel. Despite its reduced levels of growth factors, GFR Matrigel generally contains what is deemed a saturating dose of TGF-β, 2.0 ng/ml (Vizán et al., 2013). However, this approach carried its own disadvantages. Following the first co-injection, it became apparent that I should conduct these experiments at earlier timepoints. The injected CAFs appeared to migrate away from the tumour itself, meaning any influence they may have is not being observed. However, looking at earlier timepoints was problematic when using Vitrogel as an injection substrate. My colleague in the lab, Danielle Park,

demonstrated that tumour growth is substantially slower when using Vitrogel compared to GFR Matrigel. Therefore, tumours have had insufficient time to develop at these early timepoints before the influence of the injected CAFs is lost. To overcome this issue, I believe co-injections with GFR Matrigel should be implemented in future experiments. Additionally, since the cancer cell component is almost absent at the early timepoints I investigated, CAF only injections can be conducted to ask similar questions. Another advantage of CAF-only injections is I can look at earlier timepoints whilst CAFs are still abundant within the injected node as there is no interest in allowing time for cancer cells to embed within the host tissue and form a tumour. However, the caveat of this set-up is that any conclusions drawn would then have to be extrapolated to the context of a tumour, which may not necessarily translate.

An additional drawback of the co-injection experiments was the choice to use non-fluorescent cells. Using fluorescent CAFs and cancer cells would allow for more accurate localisation of each population. Additionally, it would allow distinction of tissue resident CAFs from the injected populations. However, injecting fluorescent cells in immune competent mice has been shown to generate an immune response against the fluorophore (Steinbauer et al., 2003), interfering with the results. The use of immune competent mice was necessary to determine the effect of Activin on CAFs ability to modulate the immune system. Ideally, these experiments would be conducted in the ‘Glowing Head’ mouse model. This model does not generate an immune response against fluorophores, including eGFP (Day et al., 2014). Conducting co-injection experiments using this mouse model would allow the use of fluorescent cells and intravital imaging for more accurate tumour monitoring *in vivo*.

Ideally, a conditional knockout mouse model would be utilised to study these effects. A Cre-Lox recombinase mouse could be used to conditionally knock Activin out in specific cell types (Zheng et al., 2000). For example, a conditional *Ccn2* knockout in COL1A2 positive fibroblasts has been generated (Hutchenreuther et al., 2018). In another study, BMPR2 was knocked out under the control of FSP1 (Pickup et al., 2015). A similar set-up could be implemented targeting Activin A and Activin B in cells expressing fibroblast markers, such as COL1A2. This model could then be used for injection experiments or crossed with a mouse model of spontaneous breast cancer. The tumour volume and number could be measured over time in mice with and without Activin expression in their resident fibroblasts. The same tumours can

then be excised and their structure interrogated. This would be the most unbiased and robust method of determining the role of Activin expression in CAFs during tumourigenesis. The observations from my *in vivo* experiments have biological merit in their own right and can be used to further optimise more robust *in vivo* experiments in the future.

Chapter 5. ESCRT Machinery Regulates Long-term Signalling Dynamics of TGF-β

5.1 Introduction

Many tumours present with active and prolonged PSMAD2/3 signalling (see Chapter 3 and Giampieri *et al.*, 2009). As discussed in the Introduction, cells exposed to sustained levels of TGF-β ligand become unresponsive to ligand in terms of levels of PSMAD induction (Vizán et al., 2013). This presents us with a dilemma. Either another family ligand is responsible for perpetuating this signal (as outlined in Chapters 3 and 4) and/or there is re-wiring of established TGF-β dynamics, allowing TGF-β ligand to prolong active signal. This second possibility is explored in this chapter.

A genome-wide siRNA screen was conducted by former PhD student Daniel Miller, to determine factors responsible for controlling the signalling dynamics of TGF-β ligand. HaCaT cells were plated in triplicate in a 1536-well plate and transfected with a Dharmacon whole genome SMARTpool siRNA library for 72 hours. Cells were then treated with TGF-β for either 1 hour or 20 hours. After which time they were fixed, stained and imaged for SMAD2. Levels of nuclear SMAD2 was the indicative marker of active signalling. Positive hits were considered to be those that led to elevated nuclear SMAD2 at 20 hours, relative to the non-targeting control, but unaltered levels at the 1-h time point (Figure 5.1). Several distinct components of the ESCRT machinery were identified as positive hits that maintain the established TGF-β dynamics. Specifically, VPS28, UBAP1, VPS4B and PTPN23. The ESCRT family consists of 4 subunits: ESCRT-0, ESCRT-I, ESCRT-II and ESCRT-III. ESCRT-0 and ESCRT-I recognise and bind ubiquitinated cargo. ESCRT-II then binds ESCRT-I and ESCRT-III subunits which facilitates the incorporation of the targeted cargo into intra-luminal vesicles. This leads to the generation of MVBs that fuse with the lysosome, degrading the cargo within (Campsteijn et al., 2016; Wollert et al., 2009). Daniel validated the findings of this screen, proving, in various cell lines, that loss of function of the ESCRT machinery resulted in sustained TGF-β pathway activation. Loss of ESCRT function resulted in no degradation of internalised TGF-β

receptors, meaning they could continue to propagate signalling intracellularly (Miller et al., 2018).

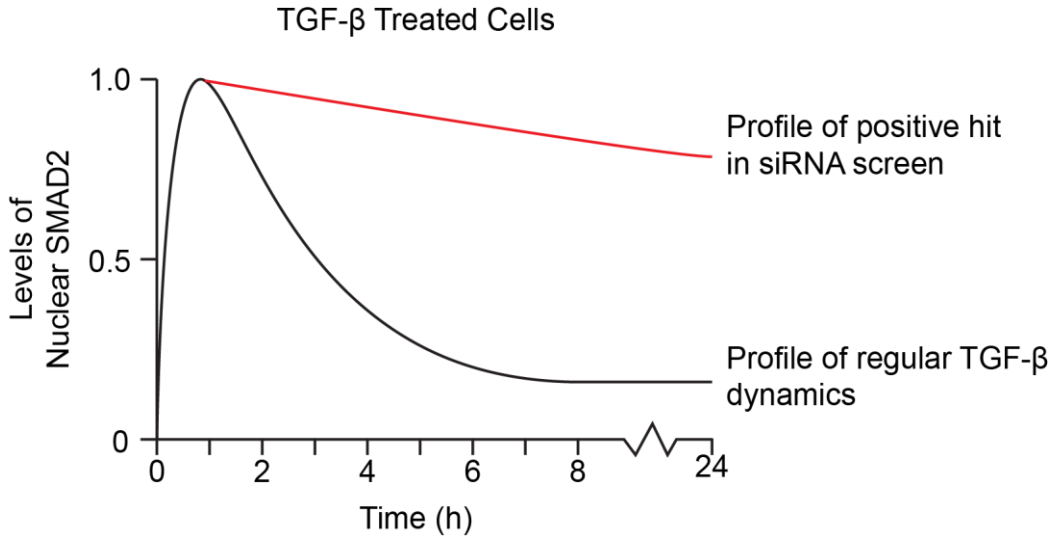

Figure 5.1. Schematic to show profile of positive hits in siRNA screen. The black line denotes the type of profile we expect to see for pathway activity over respective periods of TGF-β treatment. The red line shows the type of profile we expect to see when expression for a gene regulating normal TGF-β dynamics is lost, denoting a positive hit in the screen.

However, work had yet to be done to determine whether these findings had any functional consequences. Do sustained levels of PSMADs, caused by loss of function of the ESCRT machinery, lead to enhanced TGF-β-mediated functionality that can be observed in tumours? I aimed to knockdown expression of *Vps28*, a core component of the ESCRT machinery and a significant hit in the siRNA screen, in a mouse epithelial cell line (NMuMGs) and assess the effect on TGF-β-mediated EMT. The role of TGF-β in causing EMT is well established (Massagué, 2008). Additionally, EMT is a critical step in the process of metastasis and fibrosis (Ye and Weinberg, 2015).

This work shows, in addition to active pools of Activin, that re-wiring of mechanisms maintaining TGF-β signalling dynamics could be responsible for propagating active and functional PSMAD signalling seen in tumours and other diseases.

5.2 Results

5.2.1 Knockdown of ESCRT components leads to sustained PSMAD signalling

To validate Daniels' findings at a functional level, I investigated the effect of loss of ESCRT functionality on TGF-β-mediated EMT in NMuMGs. This cell line was chosen as the model as they show a complete EMT in response to TGF-β (Valcourt et al., 2004). Additionally, NMuMGs undergo a rapid EMT (48 h) versus other systems such as EpRas cells. EpRas cells can take up to 6 days to undergo a complete EMT (Daly et al., 2010). A more rapid EMT was desirable as longer experimental times may reduce the effectiveness of siRNA knockdowns. First, I aimed to demonstrate that the phenomenon observed in HaCaTs could be seen in NMuMGs. The same experimental set-up was utilised, but as well as PSMAD2, levels of PSMAD1/5 were also measured. Although TGF-β primarily signals via SMAD2/3, activation of PSMAD1/5 signalling has also been demonstrated. Indeed, PSMAD1/5 signalling is required for a complete TGF-β-mediated EMT. TGF-β activates SMAD1/5 through transphosphorylation of ACVR1 receptors by active TGFBR1 (Ramachandran et al., 2018). In turn, ACVR1 then phosphorylates and activates SMAD1/5, which form complexes with SMAD4 that induce target genes such as *ID1* which are necessary for a complete TGF-β-mediated output.

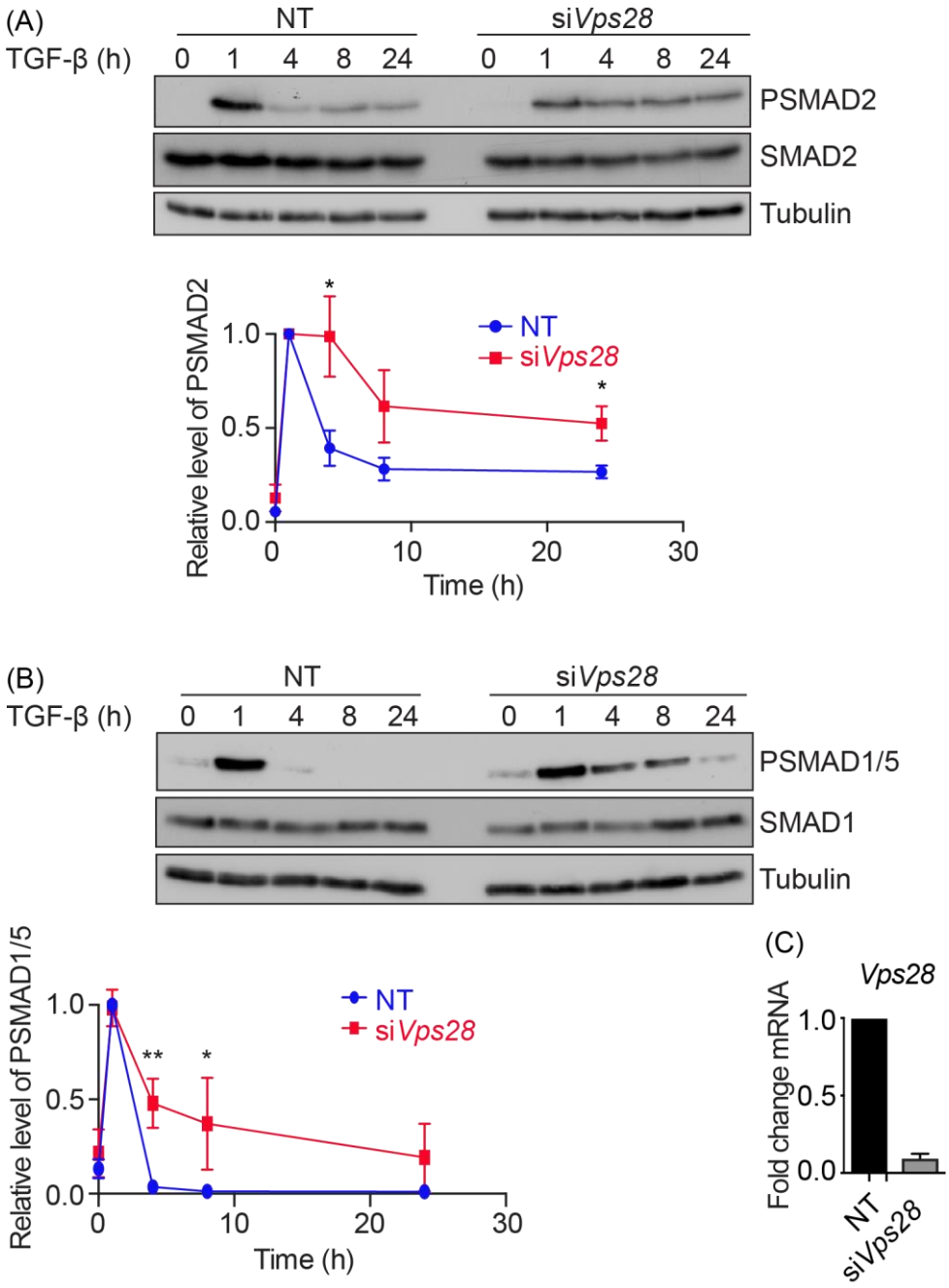

Figure 5.2. Levels of PSMADs in *Vps28* knockdown NMuMG cells. Western blot and quantification of PSMAD2 (A) and PSMAD1/5 (B) levels in si*Vps*28 and siNT cells. Quantifications are the average of 3 biological replicates normalised to the 1-hour timepoint. Error bars denote SD. (C) Levels of *Vps28* transcript in the same biological replicates.

In a similar fashion to HaCaT cells, knockdown of *Vps28* leads to more sustained levels of PSMAD2 over 24 h (Figure 5.2A). Interestingly, levels of PSMAD2 at the 1-h timepoint in knockdown cells appear to be slightly lower than those seen in NT cells. However, PSMAD2 levels at every subsequent timepoint are greater than

those in NT cells. This elevation is significant at the 4-h timepoint ($P<0.05$). The effect on levels of PSMAD1 over time is more profound. Levels of PSMAD1/5 are reduced almost to zero in control cells beyond 1 h of TGF-β treatment. Conversely, high levels persist at most subsequent time points during TGF-β treatment in *Vps28* knockdown cells before falling at 24 h (Figure 5.2B). This difference is significant at the 4- and 8-h timepoints ($P<0.05$ and $P<0.01$ respectively). I confirmed the knockdown had worked by performing qPCR for *Vps28* (Figure 5.2C) These results show that loss of ESCRT machinery results in sustained TGF-β signalling over prolonged periods in NMuMG cells, with the PSMAD1/5 pathway being affected more profoundly than the PSMAD2 pathway.

5.2.2 Loss of ESCRT machinery expression sensitises cells to TGF-β-mediated EMT

Once I had established that loss of expression of ESCRT components leads to sustained signalling, I aimed to determine whether this resulted in enhanced TGF-β-mediated EMT. I transfected NMuMGs with the same experimental set-up seen in Figure 5.2 before treatment with TGF-β at a saturating dose of 2.0 ng/ml or a lower dose of 0.5 ng/ml for 24- and 48-h timepoints, alongside an untreated control. The lower dose of TGF-β was employed to detect any enhanced sensitivity to ligand due to prolonged signalling. Cells were fixed and the degree of EMT assessed through localisation of junctional proteins (Figure 5.3) as well as actin fibre alignment via phalloidin staining (Figure 5.4). These parameters are indicative markers of EMT.

In cells transfected with a non-targeting control, a saturating dose of TGF-β over a 48-h treatment period is required for a complete EMT, as seen by total delocalisation of junctional proteins (CDH1 [E-cadherin] and TJP1 [ZO1]) and loss of epithelial morphology. A lesser degree of this phenotype is observed at the 24-h timepoint. Cells closely resemble untreated conditions when treated with the lower dose of 0.5 ng/ml for 24 h with only a slight increase in delocalisation at the 48-h time point (Figure 5.3). Conversely, in cells transfected with si*Vps28*, delocalisation of junctional proteins can be seen more profoundly at 48 h with the lower dose of TGF-β. A higher degree of delocalisation is observed with the same dose at 24 h relative to control cells. Additionally, a more complete EMT occurs at the earlier timepoint of

24 h at the saturating does rather than the 48 h required in control cells (Figure 5.3). This suggests that loss of ESCRT machinery sensitises cells to TGF-β.

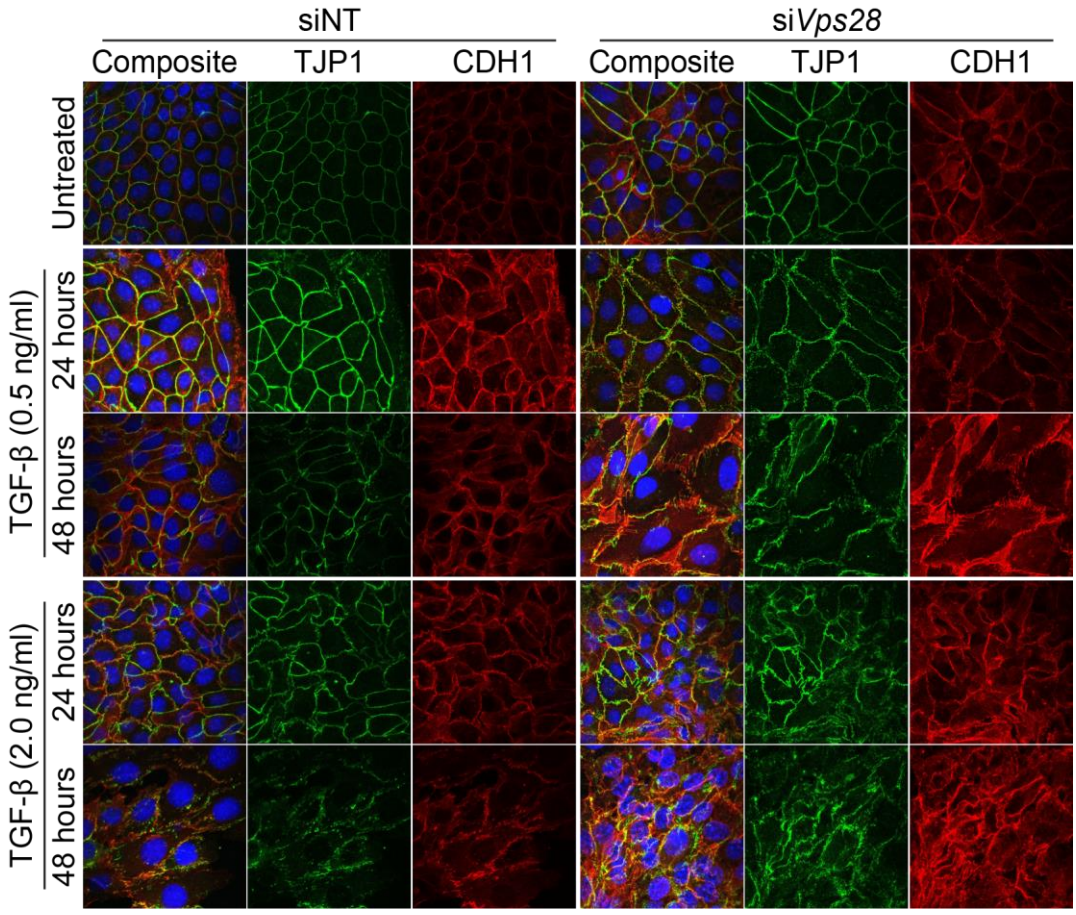

Figure 5.3. Expression of junctional proteins in NMuMGs following *Vps28* knockdown. Panels show cells stained for CDH1 (red) and TJP1 (green) following transfection with a NT siRNA or siRNA against *Vps28*. Cells were then treated with a low (0.5 ng/ml) or a saturating (2.0 ng/ml) dose of TGF-β for 24 or 48 hours. Each experimental group had an untreated set of cells. Images shown are representative of respective treatments.

A similar phenomenon was observed when using actin fibre alignment as the EMT readout (Figure 5.4). For the low dose of TGF-β, actin stress fibres only just begin to form at 48 h in control cells. Conversely, completely aligned actin stress fibres are seen in si*Vps28* cells at the same timepoint. There is also an increase in fibre alignment at the earlier 24-h timepoint in *siVps28* cells relative to control cells. A similar trend is seen in cells treated with the saturating dose of TGF-β. At 24 h of TGF-β treatment at 2.0 ng/ml, completely aligned actin stress fibres are observed in *siVps28* cells. Comparatively, actin stress fibres are only beginning to form in control

cells. Taken together, these data suggest that cells lacking ESCRT machinery result in an enhanced and more sensitised TGF-β-mediated EMT.

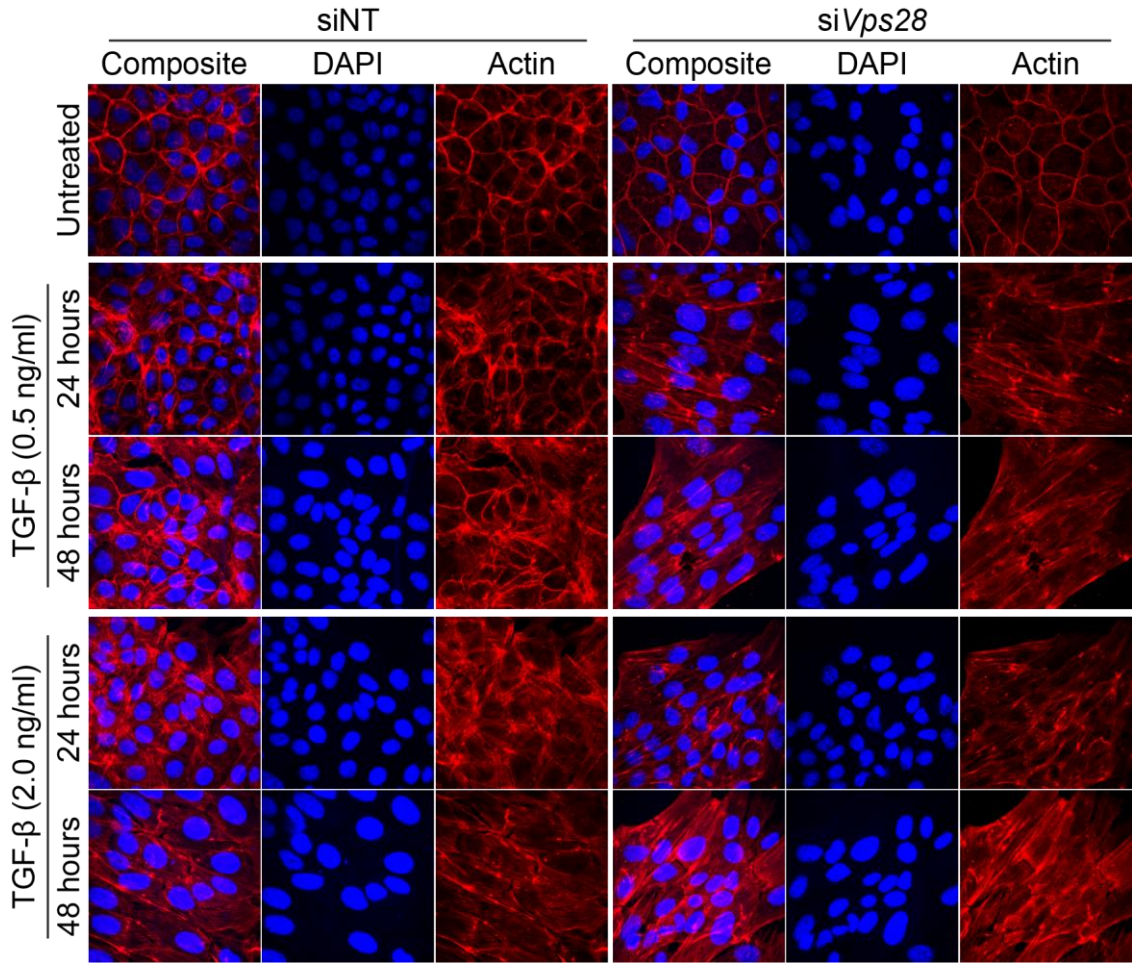

Figure 5.4 Actin fibre alignment in TGF-β treated NMuMGs following *Vps28* knockdown. Panels show cells stained with phalloidin to detect actin fibres following transfection with si*Vps28* or siNT. Cells were then treated with either 0.5 ng/ml or 2.0 ng/ml of TGF-β for 24 and 48 hours. Each experimental group had an untreated set of cells. Images shown are representative of respective treatments.

5.2.3 Enhanced TGF-β-mediated EMT in ESCRT knockdown cells is caused by elevated and prolonged PSMAD1/5 signalling

As previously mentioned, PSMAD1/5 is required for a complete TGF-β-mediated EMT through upregulation of the *ID* genes (Ramachandran et al., 2018). This signalling is mediated by transphosphorylation of ACVR1 by TGF-β's type I receptor (TGFBR1) following ligand binding (Figure 5.5).

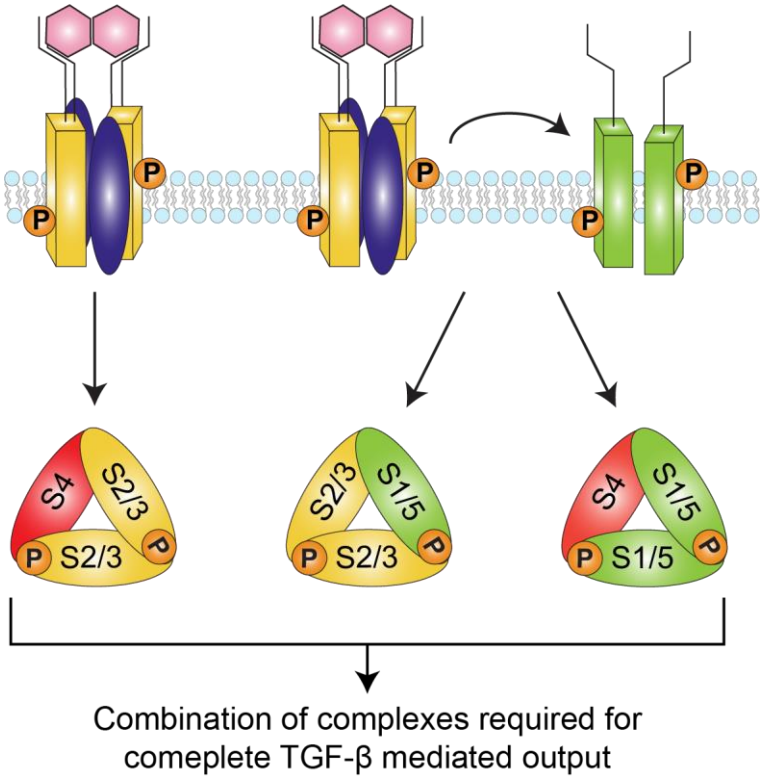

Figure 5.5. PSMAD1/5 as well as PSMAD2 is required for a complete TGF-β-mediated EMT. Figure modified from Ramachandran *et al.* 2018. TGF-β ligand binding to respective type I and type II receptors leads to canonical activation of SMAD2/3 signalling. Additionally, TGFBR1 can phosphorylate and activate ACVR1, resulting in downstream activation of PSMAD1/5. This arm of signalling is necessary for TGF-β-mediated EMT (Ramachandran et al., 2018).

Based on this mechanism, I aimed to determine whether the enhanced TGF-β-mediated EMT seen in Figure 5.3 and Figure 5.4 was due to prolonged PSMAD1/5 signalling. To test this, I treated NMuMGs with TGF-β, at a saturating or low dose, alone or in combination with BMP4 for a 48-h period (Figure 5.6). Treatment with BMP4 was used to increase PSMAD1/5 levels as a surrogate for loss of ESCRT expression.

Treatment with either BMP4 or 0.5 ng/ml of TGF-β alone fails to induce actin stress fibres, as seen in non-targeting siRNA transfected cells treated with the low TGF-β dose in Figure 5.4. However, when combined, actin stress fibres were induced to a greater degree (Figure 5.6). This resembles something similar to the phenotype observed in *Vps28* knockdown cells treated with the low dose of TGF-β (Figure 5.4). Additionally, there appears to be a slight increase in actin stress fibre formation in cells treated with a combination of saturating TGF-β and BMP4 ligands, as opposed to saturating TGF-β alone (Figure 5.6). This suggests that a slight

elevation in levels of PSMAD1/5, as seen in *Vps28* knockdown cells treated with TGF-β (Figure 5.2), is sufficient to induce a greater degree of EMT in terms of actin stress fibres.

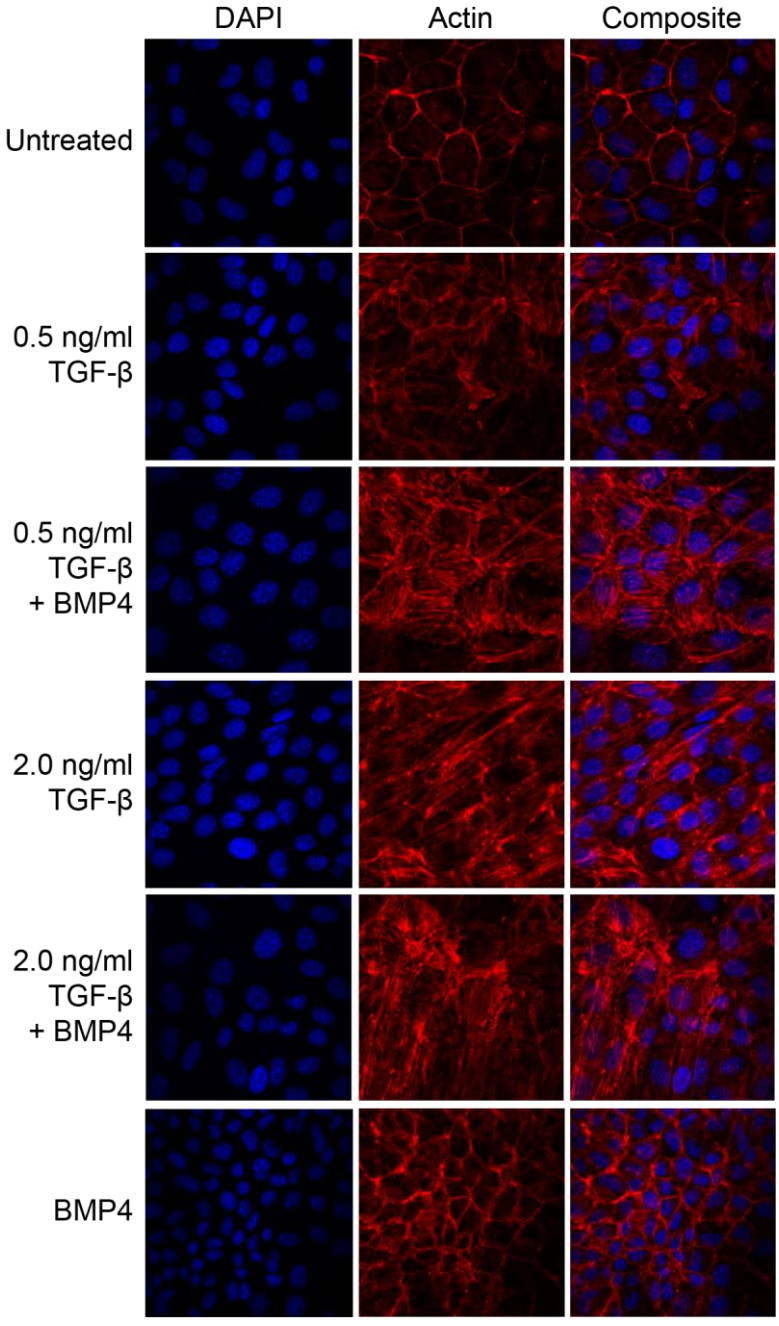

Figure 5.6. Actin fibre alignment in cells treated with a combination of BMP4 and TGF-β. NMuMGs were left untreated or treated with BMP4 (10 ng/ml), a low dose or high dose of TGF-β alone or in combination for 48 hours. Cells were then fixed and stained with phalloidin for actin stress fibres. Images shown are representative of respective experimental groups.

To corroborate this finding, I also probed for global levels of αSMA via western blot, using the low dose of TGF-β alone or in combination with BMP4 against BMP4 alone (Figure 5.7).

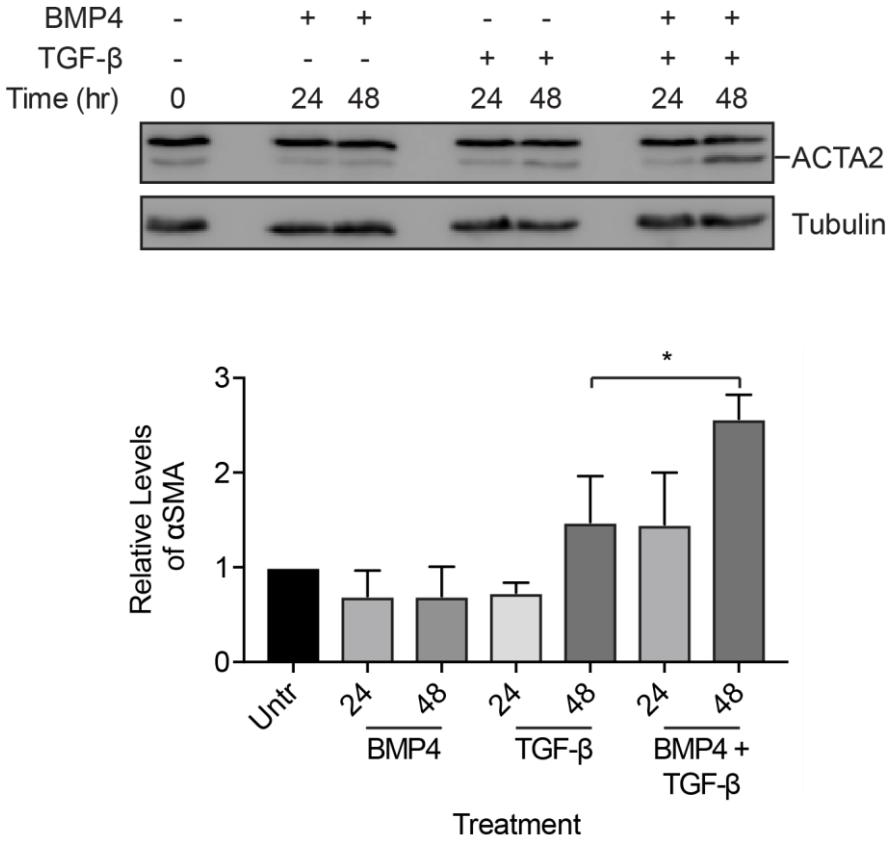

Figure 5.7. Levels of αSMA in NMuMGs following BMP4 and TGF-β treatments. Cells were treated with the same experimental set-up seen in Figure 5.6, excluding high doses of TGF-β and with an additional timepoint at 24 hours. Following treatment, cells were harvested and levels of ACTA2 (αSMA) were probed for. Accompanying quantification is the average of 3 biological replicates. Error bars represent SD.

Levels of αSMA were unaffected following BMP4 only treatment at either timepoint as well as a low dose of TGF-β only treatment at 24 h. A marginal increase is observed following treatment with a low dose of TGF-β for 48 h. However, the biggest elevation in αSMA levels is seen in the combination treatment at the 48-h timepoint, a significant increase relative to TGF-β alone at the same timepoint ($P<0.05$). Taken together, these data confirm the hypothesis that the enhanced TGF-β-mediated EMT seen in ESCRT knockdown cells is due to the prolonged levels of PSMAD1/5 signalling.

5.3 Discussion

5.3.1 Summary of results

- Loss of expression of components of the ESCRT machinery leads to elevated levels of PSMAD2 and PSMAD1/5 during continued exposure to TGF-β.
- Loss of ESCRT components leads to enhanced TGF-β-mediated EMT in NMuMGs.
- ESCRT knockdown cells have enhanced sensitivity to TGF-β. Outputs of signalling occur at lower doses of TGF-β stimulation.
- The elevated levels of PSMAD1/5 in ESCRT knockdown cells is the underlying mechanism for the enhanced TGF-β-mediated EMT.

5.3.2 Model of role of ESCRT machinery in regulating TGF-β signalling dynamics and functional output

Based on the data presented in this chapter, I propose the following model for the role of ESCRT proteins in maintaining TGF-β signalling dynamics (Figure 5.8). Upon ligand binding, TGFBR1 is phosphorylated by TGFBR2. Following activation of this receptor complex, TGFBR1 goes on to phosphorylate and activate ACVR1. These activated receptors are then internalised into early endosomes where they are able to phosphorylate and activate SMAD complexes, including SMAD2/3 and SMAD1/5. The complexes go onto propagate TGF-β-mediated outputs. ESCRT-0 and -I complexes target ubiquitinated cargo within internalised endosomes. ESCRT-II forms membrane invaginations within these endosomes which are then constricted and ‘cut’ by helical formations of ESCRT-III monomers to form MVBs. MVBs ultimately fuse with the lysosome, where the contents are degraded (Campsteijn et al., 2016). This process terminates actively signalling receptors. It follows, as part of this model, that if ESCRT function is lost, no MVBs would be formed and the receptors would either continue to signal from internalised endosomes or be recycled back to the membrane. Therefore, internalised receptors are forced into the active signalling arm of the model, propagating active signalling for prolonged periods of time and enhancing TGF-β-mediated output.

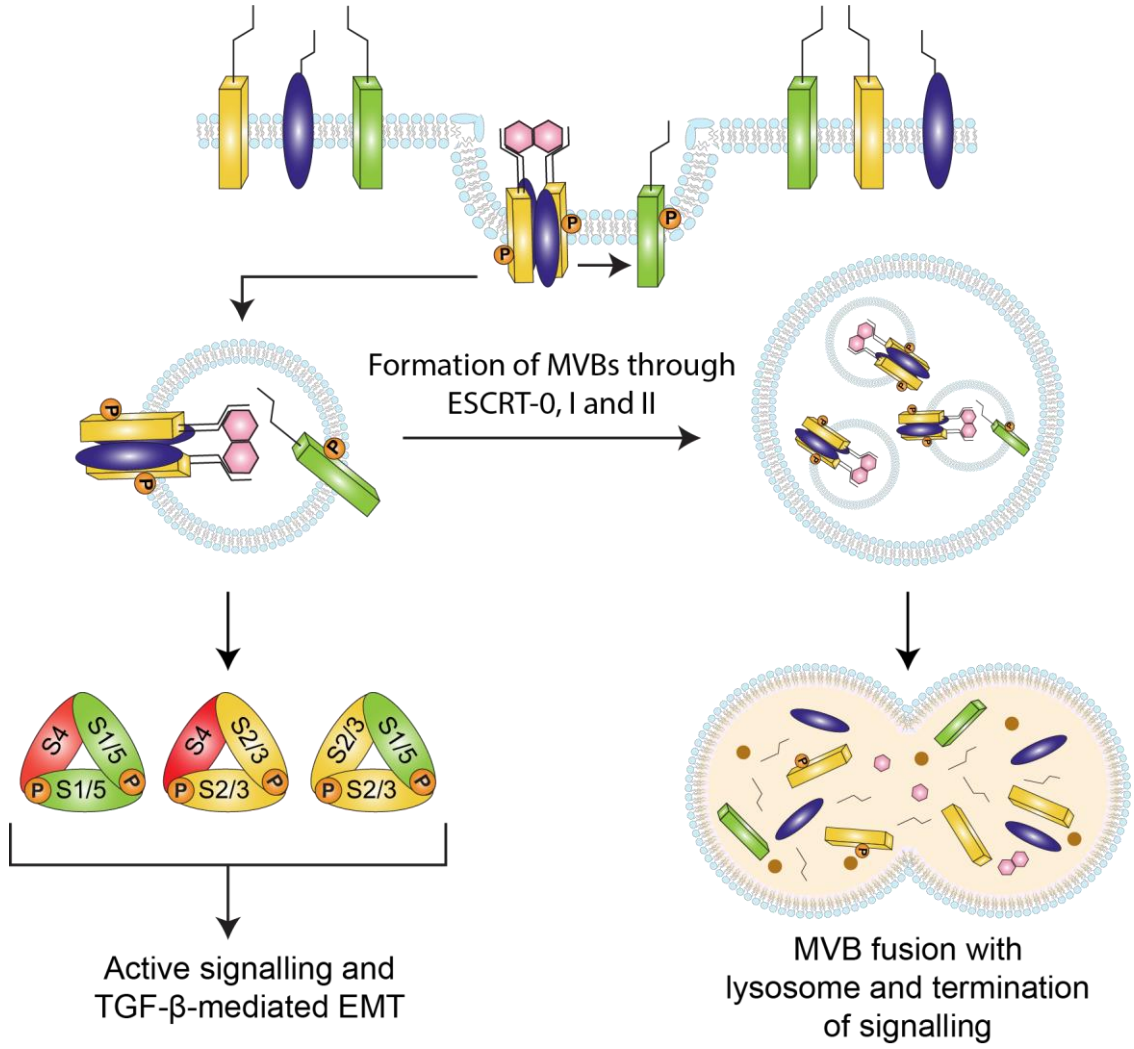

Figure 5.8. Schematic of model of ESCRT regulation of TGF-β signalling. Ligand binds appropriate receptors before internalisation into early endosomes where they are able to phosphorylate SMAD complexes. MVBs are then formed, mediated by ESCRT proteins, before fusing with the lysosome, degrading receptors.

5.3.3 ESCRT machinery terminates actively signalling receptors resulting in moderated TGF-β functionality

If signalling continues to propagate, it follows that downstream functional output would be enhanced. I have demonstrated this in the form of TGF-β-mediated EMT in NMuMGs. Additionally, it has been shown that ESCRT proteins are responsible for repairing internalised endosomes that have been breached by sheer stress (Skowyra et al., 2018). If this function is also impeded, it is possible the cargo within,

in this case signalling receptors, would be released rather than degraded. This is another possible explanation for the observed sustained TGF-β-mediated signalling.

Additionally, this finding was validated in a further model of EMT, namely EpRas cells. Following my own initial validation, former PhD student Daniel Miller showed that loss of *Vps28* in EpRas cells resulted in a similar enhancement of TGF-β-mediated EMT (Miller et al., 2018). Moreover, he showed that other TGF-β functional outputs are affected, specifically, growth arrest in HaCaTs. Treatment of serum starved HaCaTs with TGF-β prevents release into G1/S phase once serum is added (Levy and Hill, 2005). A higher degree of TGF-β-mediated cell cycle arrest is observed in HaCaTs lacking ESCRT component expression. Additionally, expression of TGF-β target genes are elevated in ESCRT knockdown cells following stimulation with ligand (Miller et al., 2018). This truly demonstrates the functional relevance of ESCRT proteins in relation to TGF-β signalling.

In addition to these functional observations, a substantial result seen in this chapter is the contribution of both PSMAD1/5 and PSMAD2 to TGF-β-mediated function. It is well established that TGF-β can phosphorylate both SMAD2/3 and SMAD1/5 arms of the pathway (Daly et al., 2008). Beyond this, it has been shown the SMAD1/5 phosphorylation is dependent on cross-activation of the ACVR1 receptor, a process which is critical for complete TGF-β functional output (Ramachandran et al., 2018). I have corroborated these observations and shown an elevation of PSMAD1/5 levels, mediated by either loss of ESCRT function in TGF-β treatment or increased BMP4, is critical alongside PSMAD2 signalling for enhancing TGF-β-induced EMT.

These findings contribute to addressing the initial issue posed at the start of this chapter. Observed levels of sustained PSMAD activity seen in functional contexts, such as cancer, could be due to re-wiring of mechanisms that establish TGF-β signalling dynamics. These observations could have wide-ranging and significant implications for TGF-β outputs more globally. Abrogation of ESCRT components could be detrimental to many of the critical TGF-β outputs during development and adult tissue homeostasis.

5.3.4 Loss of ESCRT function could contribute to disease progression and perturb other TGF-β functions

The association between TGF-β and EMT is well established. TGF-β signalling controls the expression of critical EMT regulators including *SNAIL*, *TWIST* and the *ID* genes (Massagué, 2008; Miettinen et al., 1994; Thuault et al., 2006). Additionally, the role of EMT during metastasis is equally well-established. Cells undergoing EMT lose the epithelial markers that keep cells in a rigid and organised formation, creating a more motile system resulting in migration of cells beyond their niche (Derynck and Akhurst, 2007; Ye and Weinberg, 2015). The data presented here show that abrogation of ESCRT proteins enhances TGF-β-mediated EMT. In the context of a tumour, this would result in enhanced motility, extravasation and metastasis of cancer cells, promoting tumorigenesis. Additionally, the enhanced sensitivity of ESCRT knockdown cells would result in tumourigenic EMT at much lower doses of TGF-β. Beyond EMT, loss of ESCRT machinery could enhance other known pro-tumorigenic functions of TGF-β. These include the exclusion of tumour suppressive cytotoxic T cells (Mariathasan et al., 2018) and pro-proliferative transcriptional programmes. Specifically, TGF-β has been shown to induce proliferation in glioma cells by promoting expression of *PDGF* genes (Jennings and Pietenpol, 1998).

In relation to this, it has been demonstrated, using TCGA datasets, that loss of expression of certain critical ESCRT components correlates with poorer prognosis in multiple tumour types, including breast and prostate cancers (Miller et al., 2018). However, it should be noted this correlation is exclusively made between ESCRT expression and survival, rather than TGF-β associated ESCRT abrogation. Moreover, this information does not take into account the cell type in which expression is lost. It would be interesting to see whether loss of expression in any one of epithelial cells, immune cells or fibroblasts contributes more significantly to the poorer prognosis.

Another classical example of excess TGF-β signalling contributing to disease is fibrosis and ensuing organ failure. For example, in some cases of kidney failure, TGF-β signalling causes elevated levels of ECM to be deposited whilst also inhibiting collagen lysis. This is largely due to the role of TGF-β in activating myofibroblasts, but this behaviour has also been attributed to TGF-β's action on epithelial and endothelial cells (Meng et al., 2016). Theoretically, enhanced sensitivity to TGF-β caused by loss of ESCRT function in any of these cell types could lead to the

elevated levels of fibrosis seen in kidney failure. It would be interesting to look at ESCRT pathways within different cell types in fibrotic tissue.

Beyond disease, it would be interesting to determine the importance of ESCRT proteins in other TGF-β related functions. I have clearly established loss of ESCRT function enhances EMT in adult cells. However, TGF-β-mediated EMT is also critical during embryonic development. For example, several rounds of EMT and MET occur during development of the heart, specifically valve formation (Nieto et al., 2016). My findings here suggest this process could be perturbed if there is loss of ESCRT function, potentially resulting in malformation of the heart.

5.3.5 Other TGF-β family ligands and the ESCRT pathway

Beyond TGF-β ligand itself, the dynamics of other family ligands are, at least partially, under the control of the ESCRT machinery, specifically BMP4 and Activin (Miller et al., 2018). Generally, cells respond distinctly when treated with any one of these 3 ligands in terms of pathway activity over time (Miller et al., 2019). Similar experiments were conducted to investigate if the ESCRT-related findings detailed in this chapter could be extended to Activin and BMP4. Following *VPS28* knockdown, HaCaTs treated with either ligand demonstrated a similar phenomenon to those treated with TGF-β. For Activin, levels of pathway activity were generally elevated at each individual timepoint in ESCRT knockdown cells compared to the controls. For BMP, baseline signalling increased (Miller et al., 2018).

Beyond ESCRT regulation, it would be interesting to investigate other factors involved in determining the distinct pathway activity profiles cells exhibit when treated with other family ligands. Mathematical modelling of TGF-β signalling shows that parameters such as rates of receptor internalisation, degradation and maturation are critical for the establishment of the signalling profile for the ligand (Vizán et al., 2013). This model provides substantial information as to the behaviour of cells in response to TGF-β over time. Such information does not exist for other ligands. Furthermore, the parameters mentioned above have not actually been imaged and tracked live for any of the family ligands, including TGF-β. In the case of TGF-β, these parameters were measured using snapshots of global protein levels over time. Chapter 6 details experiments and results that aimed to develop and validate a model that is able to

track family receptors live in real time. Such a model that could shed light on factors beyond the ESCRT machinery that are vital for regulating the dynamics of family ligands in a novel way.

Chapter 6. HALO Technology as a Tool for Tracking TGF-β Family Receptors

6.1 Introduction

As shown in the previous chapters, studying signalling dynamics and their underlying mechanisms can lead to work identifying potential therapeutic targets. Therefore, further work investigating the mechanisms underlying TGF-β family signalling is crucial to understand how cells respond to family signals in both health and disease. Receptor dynamics are critical in determining the degree of signalling output for the TGF-β family ligands. The pathway activity is distinct when cells are treated with either TGF-β or Activin (see Section 1.3.2). The signalling profiles for these ligands are reflected in the levels of their surface receptors. TGF-β receptors at the cell surface, specifically TGFBR2, are depleted within 5 minutes of signalling and do not reaccumulate to saturated levels while ligand remains in the extracellular space. In the case of Activin A, receptors remain at steady levels at the cell surface. This allows cells to monitor levels of ligand and incorporate active signalling over longer periods of time, with pathway activity diminishing when ligand has been depleted (Miller et al., 2019). This implies mechanisms are in place for Activin signalling, that do not exist for TGF-β, that ensure there is maintenance of steady levels of receptor at the cell surface.

The findings detailed above are based on global levels of receptor pools at specific snapshots during TGF-β/Activin A treatment. Little work has been conducted to track these receptors live at an endogenous level. Such work could determine the mechanisms that regulate distinct receptor dynamics and, therefore, the differing signalling output between ligands. Our current understanding of the recycling routes of family receptors is limited to the TGF-β receptors (Di Guglielmo et al., 2003). These authors show that TGFBR2 co-localises with markers indicative of caveolin and clathrin mediated endocytosis using cells expressing an HA-tagged TGFBR2 construct. This study was limited by the use of an overexpression construct. Therefore, results may not represent the biological reality. The technology for tracking and distinguishing surface and cytoplasmic receptor populations at endogenous levels with bright enough fluorophores has not yet been established.

HALO technology is an emerging tool for tracking protein localisation at an endogenous level. The HALO-tag is a catalytically inactivated version of the bacterial enzyme haloalkane dehalogenase (Los et al., 2008). The resulting enzyme covalently binds its respective ligand rather than cleaving it. Various dyes can then be appended to these ligands. The HALO-tag itself can be integrated to the protein of interest and probed with these HALO specific fluorescent ligands. Different fluorescent ligands are available, including cell permeable and impermeable (Grimm et al., 2017). If the HALO tag is expressed at the N-terminus of TGF-β family receptors, downstream of the signal peptide, then, theoretically, successive probing with impermeable and then permeable dyes could be added to distinctly stain surface and intracellular receptor pools. These receptors could then be tracked and localised from timepoint zero to observe the routes they take during a treatment time course.

In the work described in the following chapter I aimed to validate HALO technology for the use of tracking TGF-β family receptors in this way. As a proof of concept, I tagged ACVR1B, the type 1 receptor for Activin, with the HALO-tag at its N-terminus. This work can then form the foundation for a project that aims to track family receptors more broadly.

6.2 Results

6.2.1 Construct design and generation

Before any attempts to knock in the HALO-tag endogenously, I aimed to generate an ACVR1B-HALO overexpression construct in pcDNA3.1, a mammalian overexpression construct, for validation purposes. The design of the construct had to be intelligent to ensure the technology could be harnessed appropriately to target distinct populations of ACVR1B receptors (Figure 6.1).

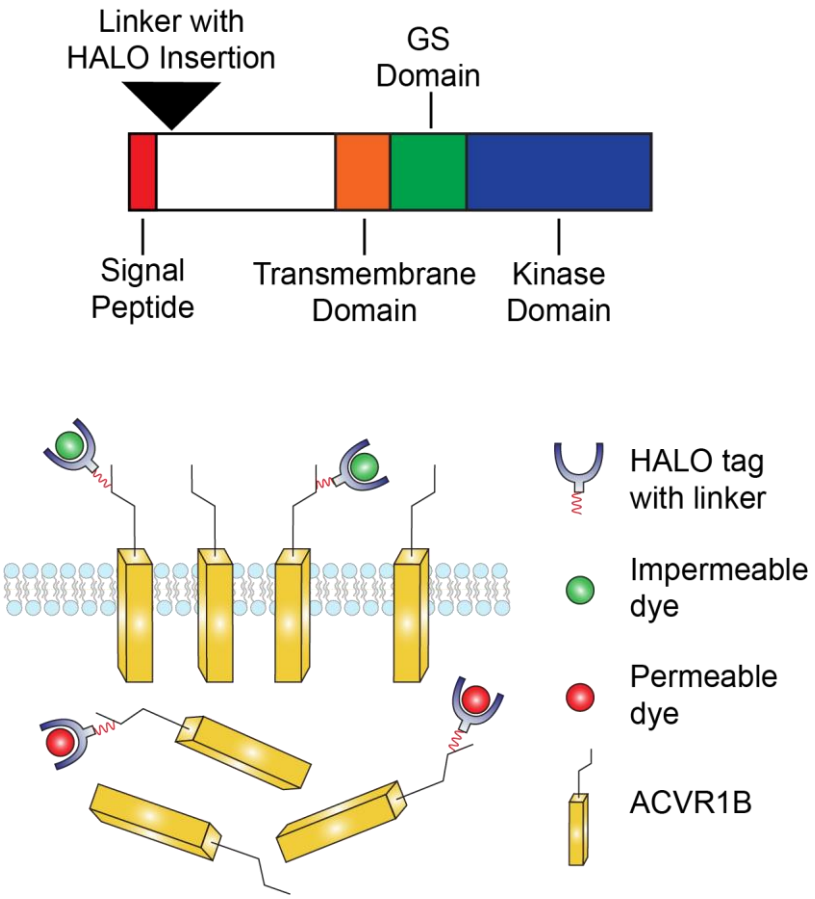

Figure 6.1. Schematic outlining ACVR1B-HALO design and implementation. Top - Schematic detailing different regions of the ACVR1B protein and where I aimed to insert the HALO-tag with a flexible linker. Bottom - How ACVR1B-HALO will be utilised in conjunction with various HALO specific ligand dyes to stain distinct receptor pools.

ACVR1B consists of five different domains. The signal peptide is responsible for ensuring the receptor successfully navigates and inserts into the plasma

membrane (Nickel and Seedorf, 2008). However, in the case of TGF-β family receptors, this is cleaved once receptors reach the membrane (Gray and Mason, 1990). Therefore, it was imperative to design the construct to ensure the HALO-tag was inserted downstream of the signal peptide. A flexible linker was also included in the insertion. This would ensure the HALO-tag was not rigidly attached to the receptor. In such a case, both HALO ligand binding and Activin binding to ACVR1B proper could be perturbed. Additionally, it was essential to ensure the insertion site was still within the extracellular region. This would allow distinct staining of both surface and intracellular receptor pools. Impermeable HALO ligand dyes could be added in the first instance before washing out and subsequent staining with a different coloured permeable dye. Time course experiments can then be conducted with Activin A and receptors can be tracked from the surface and cytoplasm independently.

For the cloning, the *Mus Musculus* (*Mm)* ACVR1B coding sequence was amplified with flanking restriction sites and ligated into pcDNA3.1. A KPN1 restriction site was then inserted 3bp downstream of the signal peptide. *Mm* DNA was selected as the downstream model for mechanistic investigations and functional validation in a cell line of mouse origin. The HALO-tag sequence was amplified with flanking KPN1 sites as well as a flexible linker of 18bps at its N-terminus. Restriction digests with KPN1 were then conducted using the pcDNA3.1-Avcr1b-KPN1 and the HALO-tag amplified region. The digests were subsequently ligated and sequenced to identify constructs with the desired sequence. An additional ACVR1B-HALO construct was made with the HALO-tag at the C-terminus of the receptor to act as a comparator. The construct generation followed a similar process, with the HALO-tag sequence being inserted immediately upstream of the stop codon of the ACVR1B coding sequence.

Once successfully generated, constructs were transfected into HEK293Ts to test their expression and functionality alongside an untagged ACVR1B WT construct. Successful expression of ACVR1B in cells transfected with respective constructs was observed via western blot (Figure 6.2). PNGase treatment was used to de-glycosylate proteins from control cells. Such treatment results in a ‘band-shift’ that helps identify the specific band of interest on the western blot. In order to prevent overexposure, only 1 µg of lysate was run for cells transfected with a construct containing any one of the overexpressed ACVR1B constructs. This allowed

comparison of the molecular weight of ACVR1B constructs against WT receptors in cells transfected with an empty vector.

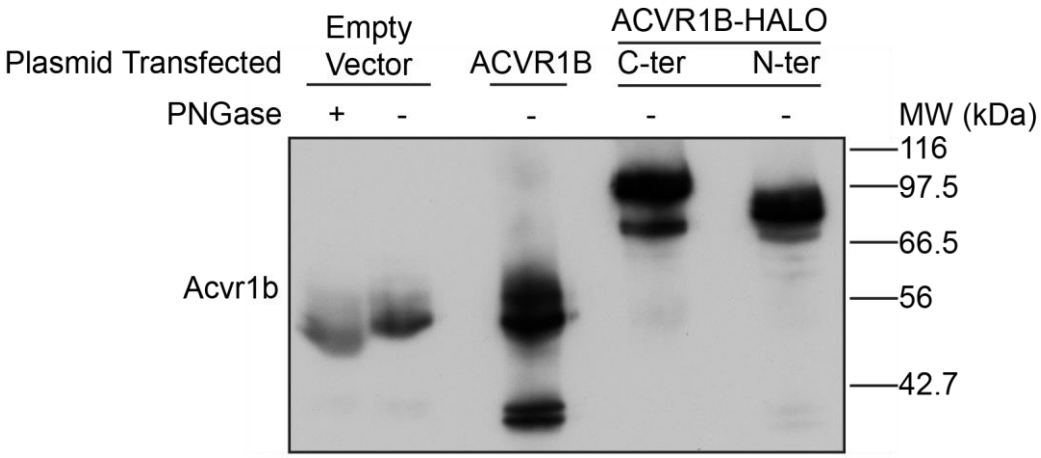

Figure 6.2. Western blot showing expression of ACVR1B in cells transfected with respective constructs. HEK293T cells were transfected with 2 µg of empty pcDNA construct, WT ACVR1B, ACVR1B-HALO C-terminally tagged or ACVR1B-HALO N-terminally tagged. Fifty micrograms of lysate from cells transfected with an empty vector lysate were run across each of two separate lanes, one lysate was treated with PNGase and the other without. All other lysates were run at 1 µg. Numbers on the right of the blot denote molecular weights (MW) (KDa). No loading control is shown due to varying amounts of lysate loaded.

The coding sequence for ACVR1B is 506 amino acids and an expected molecular weight of approximately 56kDa. This molecular weight is observed in both empty vector and WT ACVR1B construct transfected cells. The HALO-tag and linker sequence inserted in each of the ACVR1B-HALO constructs is 307 amino acids. The total length of the C-terminally tagged and N-terminally tagged constructs are 818 and 817 amino acids respectively. This should have a molecular weight of approximately 91 kDa for each construct. However, a molecular weight of approximately 96 kDa is observed for the C-terminal construct and 89 kDa for the N-terminal construct. It is unclear what has caused this discrepancy between each of the constructs. It could be due to distinct post-translational modifications, such as glycosylation. However, both constructs are within a reasonable range of the expected molecular weight to suggest the construct has been successfully expressed.

6.2.2 Testing functionality of ACVR1B and HALO-tag receptors in constructs

Once I had demonstrated successful expression of WT ACVR1B and ACVR1B-HALO constructs, it was crucial to test if the expressed ACVR1B is still able to bind ligand and activate downstream signalling. Due to the large size of the HALO tagged receptor and its localisation to the ligand binding domain, I was concerned it may interfere with Activin ligand binding in the N-terminally tagged construct. In initial experiments, I transfected HEK293T cells directly with the construct, treated them with Activin A at various timepoints and checked levels of PSMAD2. However, it was not possible to discern whether saturated levels of PSMAD2 were reached due to activation of endogenously expressed receptors, rather than the transfected construct (data not shown).

Therefore, I knocked out expression of ACVR1B in HEK293T cells. I reasoned that this would result in loss of endogenous induction of PSMAD2 following Activin treatment. ACVR1B constructs could then be transfected into ACVR1B-null cells, which could be assayed for PSMAD2 induction after Activin A stimulation. Rescue would indicate receptors are able to bind ligand and activate downstream signalling. CRISPR/Cas9 technology was utilised to knock out ACVR1B expression. A guide was designed targeting exon 4. The SMAD2/3 binding region and kinase domains are downstream of this exon (Hedger et al., 2011). Therefore, introduction of a frameshift here would nullify ACVR1B's ability to bind and phosphorylate SMAD2/3. Following guide transfection, GFP-positive transfected cells were sorted individually and expanded for screening. The screening strategy was to check induction of PSMAD2 following Activin treatment (Figure 6.3). A direct measure of ACVR1B protein expression could not be used as commercially available antibodies also bind another TGF-β family receptors, namely, ACVR1C. The antibodies specifically target the C-terminus of ACVR1B, which shares homology with ACVR1C.

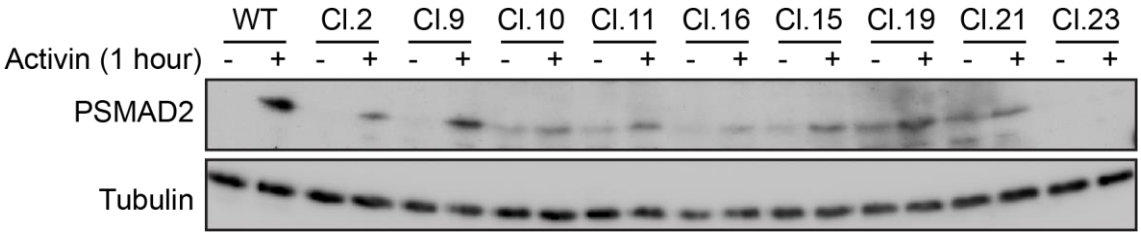

Figure 6.3. PSMAD2 induction screen for potential ACVR1B knockout clones. Western blot shows PSMAD2 induction following treatment with Activin (+) against untreated controls (-). Nine of 23 possible ACVR1B knockout clones were tested in this way against the WT parental clone.

The WT parental clone shows strong PSMAD2 induction when treated with Activin A. Indeed, PSMAD2 induction is the greatest in WT parental cells than all other clones. The remaining clones from the screen demonstrate much weaker levels of induction, with Clones 10 to 23 exhibiting almost no induction. Of the clones screened, Clone 9 exhibits the greatest levels of PSMAD2 induction when treated with Activin. The remaining clones show lower levels of PSMAD2 induction. Interestingly, basal levels of PSMAD2 seem to be higher in the clones that have lost Activin A-induced PSMAD2. However, induction beyond these elevated basal levels is almost zero. I selected Clone 10 for further investigation as it appeared to have the lowest levels of induction. Clone 23 was omitted as I was concerned the lack of any band was an artefact of the blot itself.

These knockout cells were then used to test the functionality of the ACVR1B constructs. ACVR1B knockout cells (clone 10) were transfected with each of the ACVR1B constructs. Following transfection, cells were treated with SB-431542, a type I receptor kinase inhibitor, to abolish basal levels of PSMAD2 before a subsequent wash out and Activin treatment (Inman et al., 2002). The difference in PSMAD2 levels between SB-431542 with a washout and Activin A-treated cells is the comparison of interest (Figure 6.4).

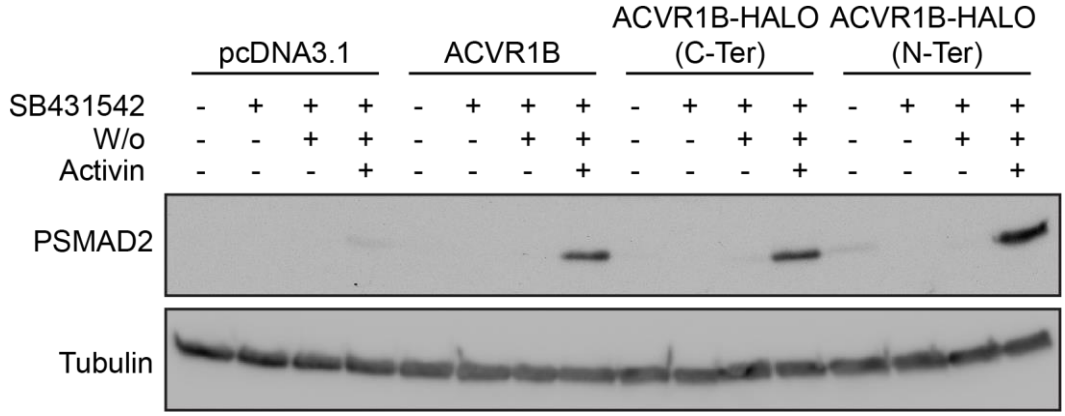

Figure 6.4. PSMAD2 induction in ACVR1B knockout cells transfected with ACVR1B constructs. ACVR1B knockout cells were transfected with 50 ng of respective constructs for 24 hours. Cells were left untreated, treated with SB (10 µM) only, SB with a washout (W/o) or SB with a washout followed by Activin treatment (20 ng/ml) for 1 hour.

ACVR1B null cells transfected with an empty vector (pcDNA3.1) exhibit no induction of PSMAD2 following Activin treatment when compared to SB-431542 treatment only (Figure 1.5). Conversely, cells transfected with any one of the three ACVR1B constructs show higher levels of PSMAD2 following Activin treatment. This recovery of PSMAD2 induction demonstrates that the receptor constructs are able to bind Activin ligand and activate downstream signalling. Both HALO tagged constructs exhibit similar levels of PSMAD2 induction to the wildtype ACVR1B construct. This demonstrates the HALO-tagged receptor does not impair ligand binding in the case of the N-terminal construct; or the SMAD binding domain, or kinase activity, in the case of the C-terminal construct.

Once receptor functionality had been established, it was important to determine whether the HALO tag itself was able to bind its respective ligand. If successful, this would allow us to label both surface and cytoplasmic pools of receptors using subsequent impermeable and permeable fluorescent ligands, as described in Figure 6.1. I focused exclusively on the N-terminal construct, as the C-terminal construct would not bind the impermeable ligands and so is less useful.

Cells expressing ACVR1B-HALO N-terminal constructs show bright staining for both impermeable and permeable fluorescent ligands. Additionally, these fluorescent ligands are specific to the surface and cytoplasm respectively (Figure 6.5). Conversely, cells expressing WT ACVR1B constructs show no positive staining for either HALO fluorescent ligand. Additionally, based on the distribution of positive staining, there appears to be heterogenous expression of the ACVR1B-HALO N-

terminal construct between cells. Fluorescence levels range from no observed levels to very bright in separate cells.

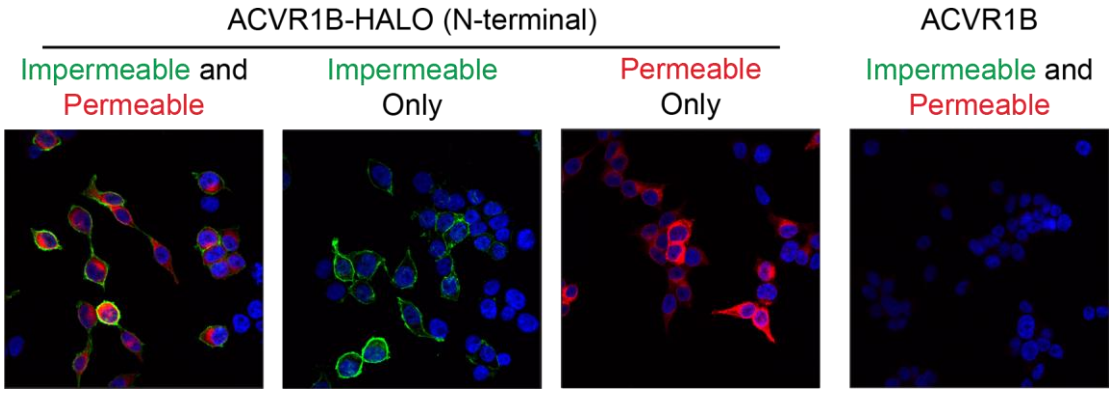

Figure 6.5. Test of HALO ligand dyes on HEK293Ts transiently expressing receptor constructs. ACVR1B-null HEK293T cells were transiently transfected with respective constructs. Cells were fixed 48 hours after transfection. Impermeable fluorescent HALO ligand (JF-546) was added at room temperature for 30 minutes followed by 3 subsequent PBS washes and a 30-minute stain with a permeable fluorescent HALO ligand (JF647). Two further groups of fixed cells were treated with either ligand dye. Images shown are representative of 3 distinct fields of view. Green and red colours represent impermeable and permeable ligands respectively.

Data presented in this section shows that ACVR1B-HALO constructs are able to bind Activin A and HALO ligands. This validates their prospective use as a tool for tracking functional receptors. In order to obtain biologically relevant data using the ACVR1B-HALO N-terminal construct, I aimed to generate a stable cell line with homogenous expression. From herein, the ACVR1B-HALO N-terminal construct will be referred to as ACVR1B-HALO.

6.2.3 Generating and characterising stable ACVR1B-HALO expressing cells

Once I had generated a functioning ACVR1B-HALO construct, I aimed to test if this tool could be used to track localisation of surface and cytoplasmic receptors live during an Activin A induction time course. In order to achieve this, I wanted to generate cells stably expressing the ACVR1B-HALO construct at a homogenous level. I aimed to generate cells expressing receptor levels that resemble endogenous amounts of ACVR1B, as well as a clone expressing higher levels. The latter could be used for optimising quantification of receptor levels and tracking techniques. I transfected ACVR1B null HEK293T cells (Clone 21; see Figure 6.3), with a low

amount of ACVR1B-HALO construct (50 ng). I applied positive selection media, containing hygromycin, to generate a pool of expressing clones.

From this pool I isolated 27 clones that I subjected to various screening methods. First, I checked both positive expression and levels of the ACVR1B-HALO construct at an mRNA level (Figure 6.6). Oligos used in this screen were specific for the unique ACVR1B-HALO sequence. Wildtype ACVR1B oligos could not be used to compare transfected cells with wildtype endogenous levels. The construct contains *Mus Musculus Acvr1b*, whilst the HEK293T cells are of human origin. Therefore, the levels detected would not be comparable. Heterogeneity of expression of ACVR1B-HALO is observed between clones (Figure 6.6). Expression is absent from negative controls; the WT parental clone and ACVR1B null cell line. All selected clones demonstrate some degree of expression. Clones with equal expression to, or lower than the ACVR1B-HALO pool were considered clones of interest, such as Clones 1, 4, 10, and 22. Additionally, a high-expressing clone was considered for further screening, Clone 20.

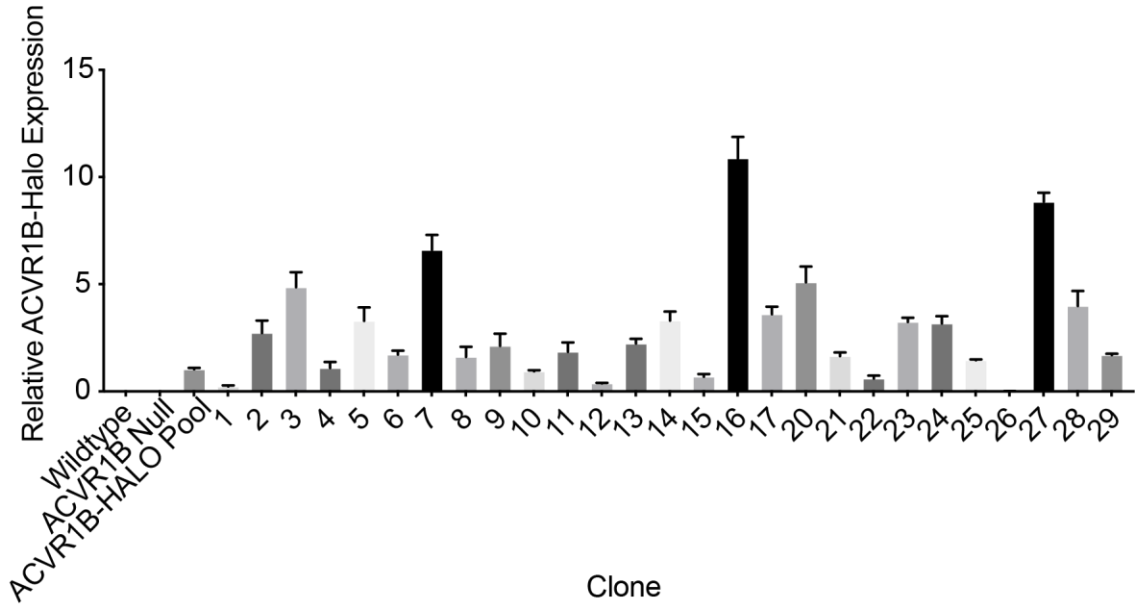

Figure 6.6. qPCR screen of ACVR1B-HALO expressing clones. Graph shows levels of expression of ACVR1B-HALO mRNA in respective cell lines. Oligos used for the screen targeted the specific genetic region encoding the transition between ACVR1B and HALO-tag sequences within the construct. Data consists of 3 technical replicates. Error bars represent the SD. Expression is relative to the ACVR1B-HALO pool population.

Following the qPCR screen, a number of clones were then taken forward for a HALO ligand staining screen (Figure 6.7). Selected clones aimed to represent the heterogeneity seen in the mRNA screen, with both low expressing and high expressing clones included. These were either low or high ACVR1B-HALO expressing clones as well as a middle range level of expression. I selected a single clone for low expression (Clone 1), three clones with expression slightly less than or equal to the parental pool (Clones 4, 10, and 22) as well as one high-expressing clone (Clone 20).

The parental ACVR1B-HALO pool shows heterogeneous levels of positive staining between cells. Conversely, each clonal cell line shows homogenous levels of positive HALO ligand staining (Figure 6.7). Clone 1 exhibits lower levels of staining when compared to the other clones. Interestingly, Clone 4 shows no staining with the impermeable dye. This suggests the clone may be aberrantly expressing the construct. Therefore, it was not considered for use in future experiments. Clone 10 shows positive staining in both channels, but to a very low degree. The clone with the greatest degree of positive staining was clone 20, which was selected for high expression of the ACVR1B-HALO construct. Generally, the mRNA expression levels of the construct (Figure 6.6) are reflected in the amount of observed staining. Based on these results, clone 20 was selected for future optimisation experiments as it showed homogenous levels of bright staining. From herein, this clone will be referred to as ‘stable ACVR1B-HALO’. Clone 10 was selected as a ‘low expressing’ clone that could eventually be used in experiments to obtain more biologically representative data. However, this was beyond the scope of my project timeline.

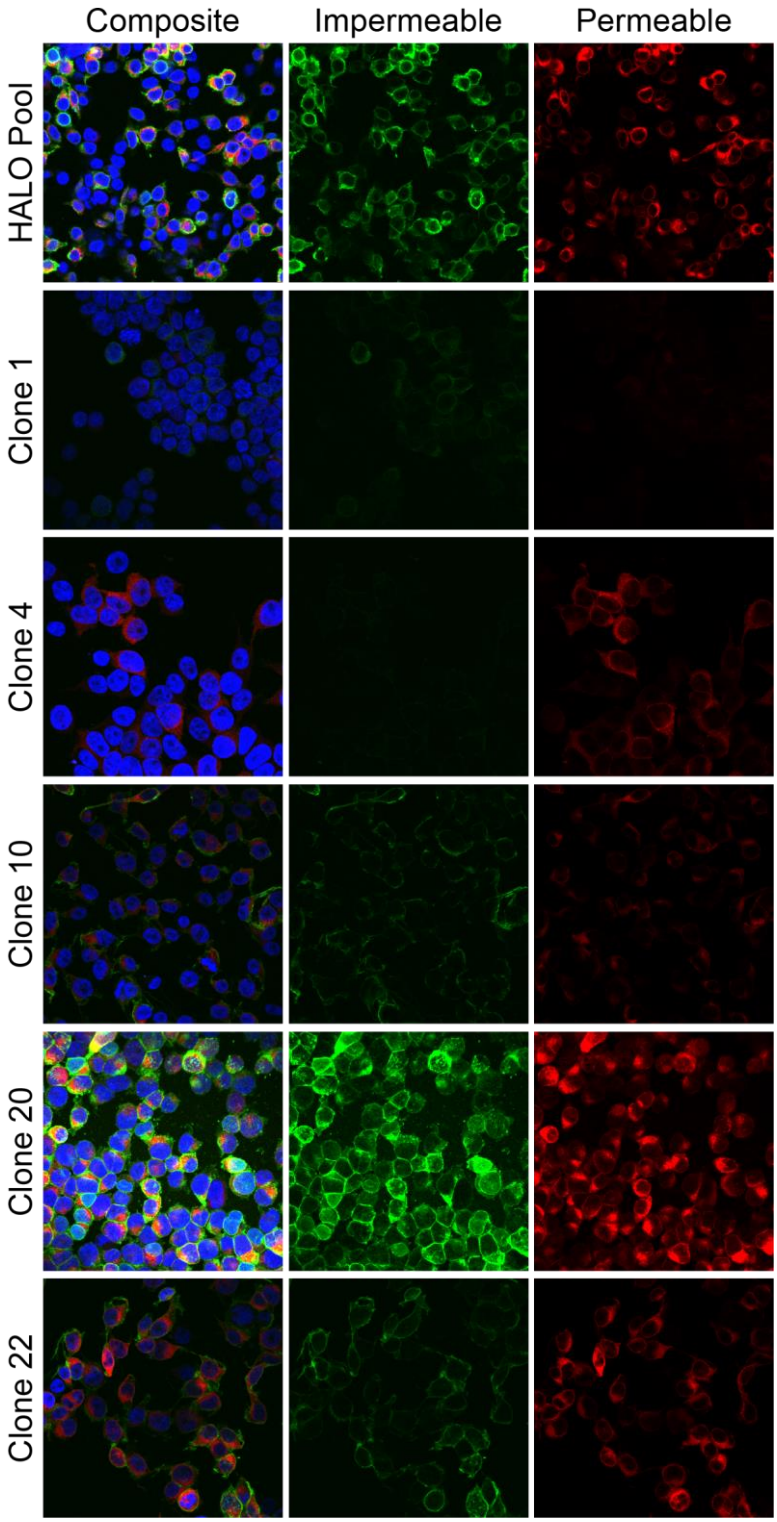

Figure 6.7. HALO ligand dye staining of ACVR1B expressing clones. Clones stably expressing ACVR1B-HALO to various degrees were grown on coverslips for 48 hours before fixation. Cells were then stained with impermeable and subsequent permeable ligand dyes. Images shown are representative of 3 fields of view.

6.2.4 Tracking ACVR1B-HALO localisation live during Activin treatment

I then utilised the stable ACVR1B-HALO cell line to investigate if it was possible to track ACVR1B localisation both basally and during Activin A treatment. To do this, I seeded the stable ACVR1B-HALO cell line on Mattek dishes and imaged them live using a spinning disc microscope (Figure 6.8).

Figure 6.8. QR codes for video files of ACVR1B-HALO localisation in stable cell lines. Scan the above codes using a smartphone for respective video files. Top – Untreated cells. Bottom – Activin treated cells. Each file is representative of 4 distinct fields of interest.

The impermeable and permeable fluorescent ligands appear to be specific to the surface and cytoplasmic pools respectively at the zero-h time point. Over time, these receptors are visibly dynamic in their localisation. The impermeable fluorescent ligand disappears from the cell surface during the time course in both treatment groups. The staining for the cytoplasmic pool remains strong and possibly more localised to the surface as time progresses, compared to the surface staining.

Interestingly, there does not appear to be a great degree of distinction between the localisation of each receptor pool over time between treatment conditions. Additionally, punctate regions appear over time for each labelled receptor, some of which appear to be yellow. This suggests that the distinct receptor pools are clustering and co-localising at specific regions within the cell. These observations are reflected in still images taken at the start and end time points of this same experiment (Figure 6.9).

A combination of these observations suggest that Activin receptors are dynamic in their movement regardless of the treatment they have been subjected to. However, it should be noted that, due to technical restrictions, each group was imaged on distinct days. This makes direct comparisons less robust due to variations in time taken to set-up the assay. However, these data demonstrate that distinct receptor pools can indeed be tracked live with a high degree of accuracy utilising the HALO technology.

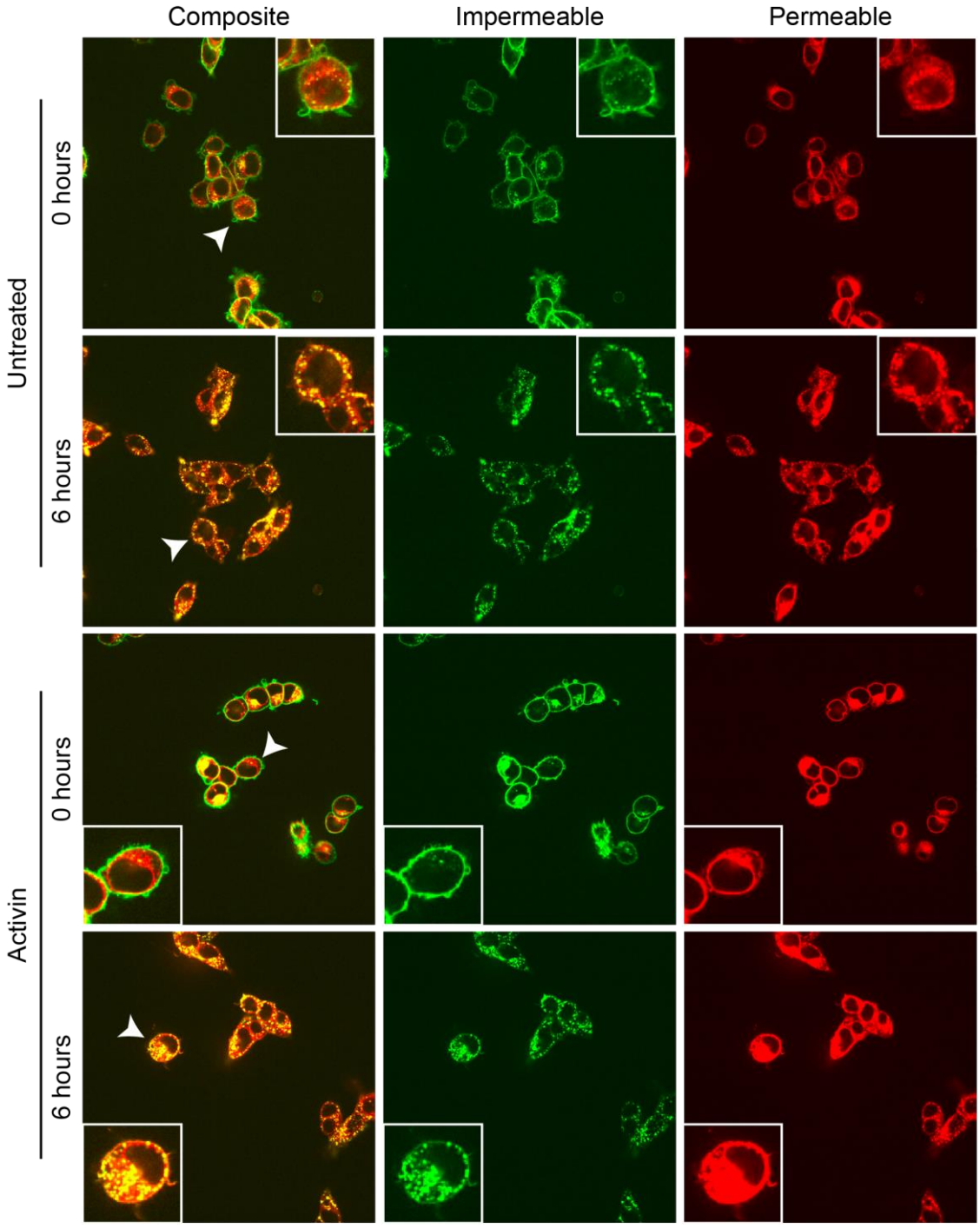

Figure 6.9. Still images of start and end timepoints of stable ACVR1B-HALO cells. Stable ACVR1B-HALO cells stained with respective fluorescent HALO ligands and imaged over the course of 6 hours for untreated (top) and Activin A treated (bottom). Untreated and Activin A-treated groups were imaged on separate days. Images represent start and end time points for each experiment. Fields selected are representative of four regions of interest. Cells in the white box are magnified versions of cells indicated by white arrows.

In addition to tracking receptor localisation live, this technology allows us to track and quantify global levels of receptor pools in individual cells at distinct time points. Following staining with fluorescent HALO ligands, I treated groups of cells with Activin A alongside an untreated control. I then fixed the labelled cells at various time points throughout an Activin A time course (Figure 6.10). This setup allowed the quantification of distinct receptor pools at various timepoints for each treatment regime.

At the zero-h time point, there is specific staining at the surface and cytoplasm by impermeable and permeable fluorescent ligands respectively. At the 1-h time point, labelling still appeared to be largely specific (Figure 6.10A). However, at the 8-h timepoint, the labels become intermingled and difficult to distinguish. Once again, as seen in Figure 6.9, punctate regions of positive staining become visible. Many of these regions appear to show co-localisation of receptors of surface and cytoplasmic origin. Receptors that cluster as part of these punctate regions could be vesicles or multi-vesicular bodies (MVBs) being shuttled to the lysosome for degradation. Alternatively, they could be co-localising with members of the RAB family of proteins to be recycled back to the cell surface. It will be interesting to probe what routes these apparent receptors are taking over time. To interrogate this, one could theoretically stain for different markers of subcellular compartments alongside fluorescent HALO ligand staining.

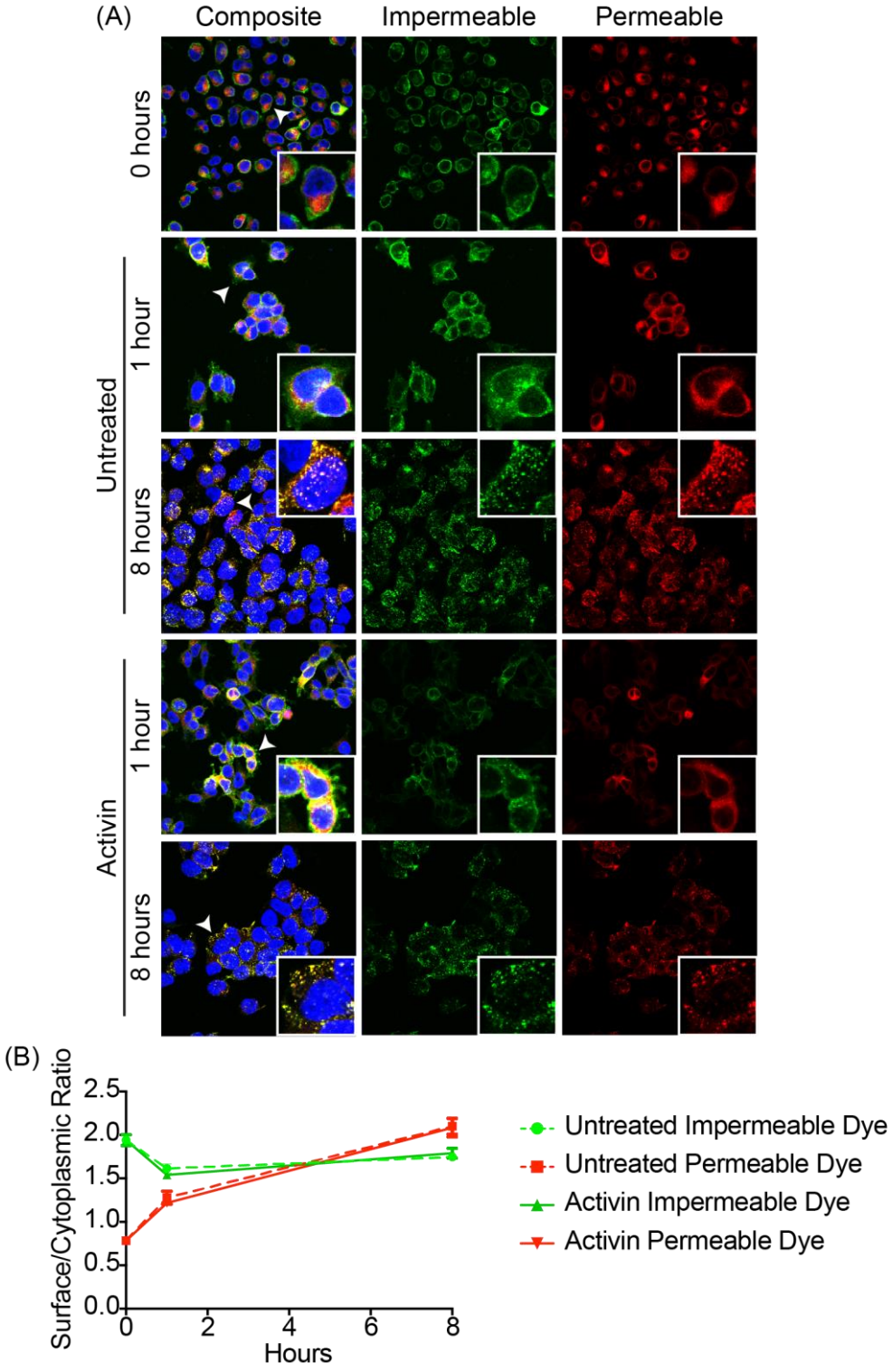

Figure 6.10. Images and quantification of HALO stained ACVR1B-HALO cells during an Activin A time course. Cells were labelled with fluorescent HALO ligands at 0 hours. All time points correlate with duration of respective Activin A treatment and time at fixation. Quantification represents the total surface to cytoplasmic ratio for respective dyes in single cells across 3 distinct fields of view. Error bars represent the SEM.

These observations are reflected in the accompanying quantification (Figure 6.10B). I quantified the global ratio of each fluorescent ligand at the surface versus the cytoplasm in single segmented cells. I hoped to gain an understanding of how distinct populations of receptors transition between the surface and the cytoplasm over time. Therefore, I quantified the surface:cytoplasmic ratio of each stain in each treatment group. At timepoint zero, there is approximately twice as much impermeable fluorescent ligand, at what is defined to be the surface, compared to the cytoplasm. This ratio is twice as high as that for the permeable fluorescent ligand, which shows just under a 1:1 ratio at the surface to cytoplasm. This is observed in both Activin A-treated and untreated conditions. At 4 h, this differential in ratio metric labelling is reduced, with a ratio of 1.5:1 for impermeable ligand and approximately 1.2:1 for permeable ligand. At around 8 h, the differential is almost entirely reversed. A surface:cytoplasmic ratio of 2:1 is observed for the permeable ligand and 1.5:1 for impermeable ligand. The same change in ratio over time is observed irrespective of Activin treatment. This shows that, regardless of Activin treatment, receptors that start at either the surface or cytoplasm at timepoint zero will eventually become intermingled. Surface receptors may become internalised, whilst intracellular receptors may be shuttled to the surface, resulting in an equilibrium.

The data shown here demonstrates the successful use and potential power in utilising HALO technology to track TGF-β family receptors. Ultimately, we would like to compare and contrast receptor localisation over time for TGF-β and Activin ligand receptors. To make direct comparisons, a model that responds to both ligands whilst exhibiting a dynamic range of quantifiable functional outputs is required.

6.3 Discussion

6.3.1 Summary of results

- I have successfully generated an ACVR1B-HALO construct that can be transiently or stably expressed in mammalian cells.
- I proved that the construct is able to bind Activin ligand and activate downstream signalling.
- I have demonstrated that surface and cytoplasmic pools of receptors tagged in such a way can be distinctly visualised and tracked in living cells for the first time.

6.3.2 HALO technology can be used as tool for tracking proteins of interest

The tracking of protein localisation and dynamics is vital to further our understanding of how proteins and the pathways they are responsible for mediating behave (Ohno et al., 2014). Efforts to accurately localise and track TGF-β family receptors at an endogenous level over time have remained elusive. In a bid to localise these receptors accurately, we turned to HALO technology.

In this chapter, I have demonstrated that HALO-tags can be utilised to visualise, for the first time, the localisation of surface and cytoplasmic pools of TGF-β family receptors distinctly. Crucially, I have demonstrated that, despite the HALO-tag's large size relative to the receptor (307 to 506 amino acids respectively), the receptor remains functional. This was a vital step in validating HALO technology for use in tracking these receptors. With any protein tag, there is an associated risk of multivalency causing oligomerisation of the protein of interest. Furthermore, there is a chance these tags may interfere with vital protein-protein interactions (Giepmans et al., 2006). Specifically, the HALO-tag may have interfered with the ligand binding domain, blocking interaction with the ligand. Additionally, it may have disrupted proper protein binding. To mitigate this, I cloned in a flexible linker so the HALO tag itself was not directly appended to the end of the receptor. Ultimately, I demonstrated the tag did not interfere with protein function. It will be important to see if this can be translated to other TGF-β family receptors, especially at an endogenous level.

However, it seems likely that the problem of multivalency will be even less likely at an endogenous level, since expression, and therefore proximity, would be lower.

However, a separate issue may arise when visualising these proteins endogenously using the HALO-tag. Specifically, whether the fluorescent HALO ligands will provide sufficient brightness to detect expression and accurate localisation. I have gone some way to answering this question by demonstrating positive staining in clones expressing 'low levels' of the ACVR1B-HALO construct. It should be noted it is unclear whether these levels are a close representation of endogenous levels. In any case, the staining is significantly weaker in these clones. This can therefore be expected at an endogenous level. However, I have employed just one labelling protocol throughout this chapter. Making alterations to the concentration and timings of the stains may enhance levels of brightness if this issue arises.

6.3.3 The advantages of HALO technology over other protein tags

HALO technology was initially employed over other available fluorescent and tracking methods for a variety of reasons. Primarily, if appropriate ligand dyes are used, it allows for distinct staining of surface and cytoplasmic pools of the same receptor population. This is a feature that is lacking in standard fluorescent protein tags such as GFP. Moreover, the organic dyes used for HALO labelling are much brighter and more stable than fluorescent proteins (Hänselmann and Herten, 2017). However, its size, approximately 33 kDa, is larger and potentially more problematic compared to the smaller fluorescent proteins such as GFP, which are usually around 25 kDa (Kremers et al., 2011). Despite this, I have managed to demonstrate, in this context, that the receptor can remain functional with the HALO-tag at its N-terminus.

Furthermore, HALO-tags were employed above standard antibody-fluorophore conjugate staining methods. Antibodies specific for TGF-β family receptors generally exhibit poor specificity against their targets. Additionally, these methods would require fixation and cell permeabilization for accurate staining, removing the option to track these cells live over time (Giepmans et al., 2006; Ohno et al., 2014). Furthermore, these receptors are expressed at very low levels with no effective way of amplifying the signal adequately. Another tag considered for use

was the SNAP-tag. This works based on similar principles to the HALO-tag (Juillerat et al., 2003). SNAP-tags are under 20 kDa in size and may therefore interfere less with protein function. However, it has been shown to require prolonged staining times to reach sufficient detection levels, sometimes requiring overnight staining protocols (Grimm et al., 2017; Hänselmann and Herten, 2017). For this reason, it was deemed a less viable option. The TGF-β family receptors are, as I have demonstrated for ACVR1B, very dynamic in their movements even under basal conditions. Rapid staining is required as certain receptors that initially stain as surface receptors using impermeable dyes may become cytoplasmic before imaging has begun. The required distinction between these pools may become lost. Overall, the HALO-tag was selected for its specific and bright staining capabilities. I have demonstrated that this decision was justified, and we are able to stain and track HALO tagged receptors over time in fixed and live cells. However, SNAP-tags could be utilised in addition to HALO to tag two separate receptors within the same population, such as Type I and Type II receptors, to track them independently of each other and within the same system.

6.3.4 Developing robust methods to quantify receptor localisation over time

Another important point to consider is the development of methods for accurate tracking and quantification of HALO tagged receptors over time. This issue has not been explored extensively in this chapter. For fixed cells, I have attempted quantification of distinct receptor pools over time at both the surface and cytoplasm. I segmented individual cells and defined their cytoplasm and surface through consistent degrees of erosion and subsequent subtracting of these regions from the whole cell during image processing. This technique worked to the extent of quantifying total amounts of distinct ligands in these regions and making comparisons. However, at later timepoints, the fluorescence disappears and defining the cell surface becomes more problematic. Developing a pipeline for tracking single fluorescent particles within single cells in this system would be a powerful tool to quantify receptor localisation accurately. These types of quantification are more accurate when dealing with low density staining in slow moving molecules (Chenouard et al., 2014). This may make endogenous labelling of these receptors a

more appropriate setting for optimising these quantification methods and obtaining salient data. Additionally, a separate stain to mark the cell membrane would make definition of the cell surface and downstream quantification simpler.

6.3.5 ACVR1B dynamics appear to be independent of ligand treatment

As discussed, quantification techniques have not been optimised over the course of this work. However, we are able to make some preliminary observations about the dynamics of ACVR1B over time. From the data in fixed and live cell staining, it appears that the ACVR1B-HALO proteins are very dynamic, moving between the surface and cytoplasm as time progresses. Interestingly, this dynamic movement does not appear to be dependent on the presence of Activin ligand. This phenomenon is observed for TGF-β receptors. TGFBRI and TGFBRII receptors undergo constant internalisation and recycling independent of ligand binding (Chen, 2009; Mitchell et al., 2004). The constant turnover of receptor between surface and cytoplasmic pools could explain how cells are able to monitor levels of ligand and integrate the signal over time (Miller et al., 2019). However, it is important to note, if the fluorescent HALO-ligand has been successfully washed out, that newly synthesised receptors are not stained for. The contribution of this pool is unknown in these experiments. Another interesting observation was the presence of yellow spots within cells over the timecourse, indicating that receptors that started at either the surface or the cytoplasm co-localise within the cell. Tracking the fate of receptors in these regions will be of interest to see if they are recycled to the surface or degraded. Comparisons can then be made to the ultimate fate of receptors within regions harbouring either one of the green or red markers.

Furthermore, co-staining of specific trafficking markers such as Rab5 (marker for early endosomes) (Sorkin and Von Zastrow, 2009) and Rab11 (marker for recycling endosomes) (Brunet et al., 2004) have not been used as part of these initial experiments. Therefore, no conclusions can be drawn in terms of trafficking routes and observations with regards to overall dynamics must be made cautiously. The ultimate aim of this section was not to draw any substantial conclusions in terms of receptor trafficking, but to determine whether the technology could be applied to answer these questions; an aim I have successfully achieved.

6.3.6 HALO technology could be utilised to track TGF-β family receptors for the first time

Despite its importance in determining signalling output (Vizán et al., 2013), little is known for certain in terms of TGF-β family receptor trafficking over time, especially for receptors beyond the TGF-β ligand. Ultimately, it is hoped the implementation of the technology utilised successfully as part of this chapter could be used to track TGF-β family receptors more broadly. Comparative studies for separate ligand and receptor combinations could answer vital questions about distinct receptor dynamics that can broaden our understanding of signalling output.

These receptors have never been visualised and tracked downstream of internalisation accurately live over time. HALO-tags could allow us to do this. The majority of existing knowledge for receptor dynamics focuses largely on TGF-β receptors. Furthermore, there are conflicting observations as to the relative distribution of distinct internalisation and recycling routes. For example, TGF-β receptors have been demonstrated to internalise through clathrin-coated pits as well as caveolae (Di Guglielmo et al., 2003). However, the relative distribution between each of these routes in an accurate biological context remains a mystery. This initial study suggests receptors internalise by each of these routes equally, whilst a conflicting study demonstrates clathrin-mediated endocytosis dominates (Brunet et al., 2004). Furthermore, the mechanism by which receptors are internalised by one method or the other is not known. Internalisation by each of these routes is crucial in determining downstream signalling output, with computational modelling suggesting that clathrin-mediated internalisation results in a sustained response against a more transient response for those internalised via caveolae (Zi and Klipp, 2007). By tracking TGFBR1 and TGFBR2 complexes with HALO-tags, combined with co-localisation of internalisation markers, we can more accurately determine the relative contribution for each of these pathways and, ultimately, what is responsible for the signalling output.

Beyond internalisation, the route for receptor complex degradation, as I have shown in Chapter 5, is through the ESCRT machinery. In terms of recycling receptors back to the surface, RAB11 has been demonstrated to be crucial (Brunet et al., 2004). A combination of these studies, whilst informative, provide a very fragmentary explanation as to how these receptors are internalised and trafficked. Additionally,

they are largely based on overexpression studies and may not be biologically relevant. No single study has tracked the receptors from internalisation and beyond continuously. HALO-tag technology may allow us to do this for the first time, providing a clear and robust picture as to the trafficking routes of the TGF-β receptors.

Beyond TGF-β ligand, even less is known with regards to other family member receptor dynamics. One study in *Xenopus* embryos has shown RAP2 to be crucial for Activin/Nodal receptor recycling (Choi et al., 2008). Again, this study did not directly visualise and track receptors. Furthermore, studies directly comparing receptor trafficking between family members are entirely absent.

By using separate self-labelling tags such as SNAP-tags, we may also be able to track both Type I and Type II receptors simultaneously for the first time. However, as discussed in Section 6.3.3, staining with SNAP ligands may be sub-optimal for this type of study and optimisation would be required (Hänselmann and Herten, 2017). HALO tagging these distinct family receptors within the same model will be a novel study that could answer questions with regards to the established dynamics of family ligands as well as signalling output more broadly.

6.3.7 E14Tg2a cells as a model for testing signalling output downstream of receptor localisation studies

In addition to validating the use of HALO-tags to track TGF-β family receptors, I have also established a model in which comparative studies between trafficking of TGF-β and Activin receptors can be made (data not shown). Cell lines that respond to each ligand with both signal induction and a downstream functional response are currently lacking within the field. I supervised a Masters student and together we demonstrated that the E14Tg2a embryonic stem (ES) cell line responds to both TGF-β and Activin ligands as measured by PSMAD2 induction. This cell line expresses RFP and GFP proteins under the control of endodermal markers hHEX and Goosecoid respectively (Rothová et al., 2016). Plans for future experiments involve tagging ACVR1B and TGFBR1 with HALO in distinct clonal E14Tg2a lines to directly compare localisation and dynamics in treated and untreated conditions. This cell line was favoured as it exhibits a quantifiable functional output in response to Activin, specifically endoderm differentiation (Rothová et al., 2016). I have established the use of an Activin-

dependant endoderm differentiation assay with these cells for the first time within the lab. In these experiments, expression of specific differentiation markers match expected levels at appropriate times at both an RNA and protein level (Morrison et al., 2008; Rothová et al., 2016). Any findings observed in tracking experiments can then be tested at a functional level in the differentiation protocol.

Chapter 7. Discussion

7.1 TGF-β family pathway signalling in cancer

The work that comprises this thesis aimed to determine why we see sustained PSMAD activation and downstream TGF-β family-mediated functional outputs, such as EMT, in certain disease contexts, specifically cancer (Nieto et al., 2016; del Pozo Martin et al., 2015). Such observations did not correlate with the finding that, during sustained exposure to ligand, cells become unresponsive to TGF-β (Vizán et al., 2013). Therefore, I investigated two possibilities that may explain the prolonged pathway activation and functional output. I have successfully shown that these signals and functions may be perpetuated by separate family ligands that signal through the same SMAD pathway as TGF-β, specifically Activin A/B, produced by CAFs. Additionally, I have added to existing work to show that perturbation of the mechanisms that dictate a cell's response to sustained TGF-β exposure results in enhanced sensitivity to ligand and an elevated functional output. Specifically, loss of ESCRT expression results in an enhanced TGF-β-mediated EMT. This work has helped us better understand how TGF-β family signals are perpetuated in disease states and how they can cause pathogenic outputs.

7.2 CAFs produce Activin A/B rather than TGF-β

Significantly, I have demonstrated that certain CAF populations may produce Activin A/B and not TGF-β. Much of the published literature identify CAFs as a source of TGF-β ligand within the tumour stroma that propagates oncogenic functionalities (Ao et al., 2007; Park et al., 2020a; Yu et al., 2014). For example, expression of a manually curated TGF-β gene signature set in fibroblast populations correlated with lower immune cell infiltrate, unresponsiveness to immunotherapy and poor patient survival in urothelial cancer patients (Mariathasan et al., 2018). This research, and others like it, use these gene signatures and SMAD pathway activation to justify targeting TGF-β ligand therapeutically. Indeed, in this example, researchers went on to target TGF-β ligand in mouse models. However, these gene signatures and pathway activation are not unique to TGF-β ligand. Other family members may be the source of this transcriptional output. My work indicates Activin could be the ligand

responsible for these gene signatures. In another example, a ‘Consensus Molecular Subtype’ (specifically termed CMS4) of colorectal cancer (CRC) was strongly associated with TGF-β family signalling (specifically gene signatures), invasive tumours and poor prognosis (Guinney et al., 2015). This finding, combined with an elevation of PSMAD3 signalling in mouse models of CRC, was used as justification for the targeting of TGF-β ligand in mouse models of CRC (Tauriello et al., 2018). Expression of these genes and PSMAD3 induction could be caused by Activin. My work indicates that Activin, instead of or in addition to TGF-β, should be considered for therapeutic targeting in some contexts.

Additionally, my work adds to a recently growing body of evidence of the significance between Activin signalling and CAFs. Recently, Activin has been implicated in the activation of fibroblasts to CAFs. In a mouse model of skin cancer, CAFs were generated by Activin A signalling through SMAD3 and mDia2 signalling (Cangkrama et al., 2020a). Additionally, Activin A secretion was observed in CAFs during colorectal cancer. This was associated with EMT and cancer cell invasion (Bauer et al., 2020).

I have demonstrated that CAFs isolated from the MMTV-PyMT mouse model of breast cancer express Activin A/B, rather than TGF-β. It will be vital to show this phenomenon exists in other CAF lines from breast cancer models as well as other cancer types. Additionally, demonstrating this in human CAF populations will be important.

7.3 Activins’ role on core CAF functionalities

Throughout Chapters 3 and 4 I investigated whether Activin A/B signalling may be responsible for propagating active TGF-β family signalling and output in tumour contexts. I showed that Activin A/B signalling in CAFs dramatically affects their transcriptome, secretome, contractility and ability to promote cancer cell invasion. Many of the significantly altered genes in Activin A/B-null CAFs are associated with several oncogenic CAF functions, specifically, ECM remodelling, cancer cell invasion, immune cell modulation and angiogenesis (Östman and Augsten, 2009).

7.3.1 ECM remodelling

Importantly, I have shown that Activin A/B signalling in CAFs is vital for their ECM remodelling and contractile properties. Activin A/B-null CAFs have reduced expression of many ECM degradative enzymes, specifically MMP3, and reduced Rho GTPase activity. This amounted to ablation of a contractile phenotype in these Activin A/B-null CAFs. This finding is novel, as Activin had not previously been considered to promote CAF contractility. Other signals have previously been reported as responsible for CAF contractility, notably Rho GTPase signalling; inhibition of which ablates their ability to contract a collagen gel and remodel their surrounding ECM (Calvo et al., 2015; Gaggioli et al., 2007). My work has shown that loss of Activin A/B reduces Rho GTPase activity in CAFs which may be the primary cause for loss of contractility in the Activin A/B-null CAFs. Other signals, specifically SRF/MRTF and Hippo/YAP pathways, are also associated with CAF contractility. Increased tissue stiffness and tension has been shown to activate these pathways in CAFs (Calvo et al., 2013; Foster et al., 2017). Consequently, their downstream gene expression programmes increase CAF contractility. These include prominent CAF marker *Acta2* (αSMA) and Rho GTPase regulator *Cdc42*. Loss of each of these signalling pathways also ablated CAF contractility. Determining the relationship between Activin, SRF/MRTF, Hippo/YAP and Rho GTPase signalling and their relative contributions to CAF contractility would be hugely interesting. SRF/MRTF and Hippo/YAP were shown to be mutually dependant for CAF contractility (Foster et al., 2017). However, their association with Activin A/B remains a mystery. It would be interesting to determine whether regulators of each pathway are targets of the other. Conducting ChIP-Seq experiments, or using publicly available datasets, could help answer this question. Additionally, it would be interesting to investigate SRF/MRTF and Hippo/YAP pathway activity in my Activin A/B-null CAFs. It does seem likely that Rho GTPase signalling is the most critical pathway for contractility as its activation is observed downstream of all the others. However, I have not determined if there is any feedback loop, whether Rho GTPase activity causes production of Activin A/B in CAFs. To summarise, data presented in Chapters 3 and 4 shows that Activin signalling is critical for the ECM remodelling capacity of CAFs. These findings are significant as less contractile CAF phenotypes have a favourable

prognosis. Generating more senescent CAFs through therapeutic targeting of Activin signalling in the tumour stroma may have beneficial effects.

7.3.2 Cancer cell invasion

Using spheroid co-culture systems, I have shown that Activin A/B expression in CAFs significantly enhances cancer cell invasion. CAFs have previously been shown to promote cancer cell invasion in a number of ways. These can be contact dependant. For example, CAFs have been shown to remodel the ECM through their contractility and secretion of ECM degradative proteins, such as MMPs, to generate tracks in which they can migrate away from the tumour body. Cancer cells then follow CAFs in these tracks in a contact dependant manner (Gaggioli et al., 2007). Additionally, contact mediated Eph–Ephrin between CAFs and cancer cells has been shown to promote their invasion (Astin et al., 2010). CAFs can also promote cancer cell invasion through cytokine secretion in a contact independent manner. For example, production of HGF, growth arrest-specific protein 6 (Gas6) and CXCL5 have been shown to promote cancer cell proliferation, migration and invasion (Gao et al., 2019; Park et al., 2020a; Sahai et al., 2020; Zhang et al., 2020b). Enhanced invasion in my parental CAF-containing spheroids could be contact dependant or independent. Specifically, I have shown Activin A/B-null CAFs have reduced migration, ECM remodelling capacity and altered cytokine expression. Determining the relative contributions of each of these phenomena to the observed reduction in cancer cell invasion caused by Activin A/B-null CAFs would be of great interest. Adding CM from CAFs to PyMT cancer cells and checking any loss of epithelial and gain of mesenchymal markers may determine if the enhanced invasion is partially cytokine dependant. Additionally, indirect co-cultures using CAFs and cancer cells separated by a Transwell would help answer this question. If less invasion is observed when CAFs are separated from cancer cells, then the phenomenon is likely to be contact dependant and a result of reduced migration and contractility in Activin A/B-null CAFs. I hypothesise the effect is largely contact dependant. CAF contractility is hugely influential in promoting cancer cell invasion. Additionally, I have shown parental Activin A/B expressing CAFs have largely increased expression of ECM degradative proteins such as MMP3. Moreover, Activin A/B-null CAFs actually have increased expression of cytokines documented to promote invasion, specifically

HGF and CXCL5. Despite this, they are less invasive, suggesting the observed result is indeed largely contact dependant.

Moreover, Activin secretion itself may be important in promoting cancer cell invasion. I have not conducted experiments that determine the direct effect of Activin signalling on cancer cell invasion. Published literature has shown that Activin A promotes cancer cell survival and invasion in separate models of lung adenocarcinoma and ovarian cancer (Seder et al., 2009; Steller et al., 2005). Moreover, Activin signalling causes loss of the epithelial marker E-cadherin and promotes expression of mesenchymal marker N-cadherin to drive cancer cell invasion (Li et al., 2014; Yi et al., 2019). The experiments described above would help determine any role Activin expression has directly on cancer cell invasion. Intriguingly, I observed further reductions in invasion in spheroids containing Activin A/B-null FST CAFs. The additional expression of FST would neutralise any Activin produced by the cancer cells themselves. The further reductions in invasion compared to Activin A/B-null CAFs indicate the residual Activin expression by cancer cells may indeed be playing a direct role on their invasive capacity. In any case, these findings add substance to the concept that therapeutically targeting Activin may have beneficial prognostic outcomes.

7.3.3 Immune cell modulation

Moreover, I have shown CAF-sourced Activin may affect immune cell modulation. CAFs have well-documented immune modulatory roles. Specifically, secretion of factors including, but not limited to, IL-6 and CXCL9 which have been shown to exclude T cells from the tumour stroma (Fearon, 2014). Notably, TGF-β secretion by CAFs, in certain contexts, has been shown to exclude T cells from the tumour stroma, resulting in poorer prognosis (Batlle and Massagué, 2019). My work has shown that Activin A/B-null CAFs have increased expression of a variety of known immune modulatory proteins. Notably, CXCL5 and Osteopontin expression are increased at an RNA and protein level. These factors are strong chemoattractants for macrophages and lymphocyte populations (Icer and Gezmen-Karadag, 2018; Speetjens et al., 2008). However, tumour nodules containing Activin A/B-null CAFs show a significant reduction in macrophage infiltrate. Infiltration of

tumour-associated macrophages correlates with poor prognosis in breast cancer (Qiu et al., 2018). However, it is unclear whether the macrophages observed in these experiments are tumour promoting or suppressive. Additionally, I have not determined whether this effect is Activin dependant or due to increased expression of other cytokines. One could conduct *in vitro* migration assays with macrophage populations and recombinant Activin to answer this question. Further investigations into the role of Activin on CAFs' immune modulatory capacity would be interesting. *In vivo* experiments provide the best platform to answer these questions as *in vitro* assays fail to recapitulate the true heterogeneity of the immune system. However, trying to decouple any effect of injected Activin A/B-null CAFs from endogenous Activin within an *in vivo* system is difficult. The *in vivo* set-up I leected to use to generate these data was not ideal. For example, it was unclear whether the observed infiltrate was due to an inflammatory reaction to the injection itself or caused by the cells within the injected substrate. Additionally, it appeared that the injected PyMT cells were able to grow independent of a stromal compartment. Any conclusions drawn need to be considered in light of these caveats. I believe the best set-up for these *in vivo* experiments would be conditional knockouts or by targeting global pools of Activin within these tumours. In one such example, FSP1 (fibroblast marker) driven expression of Cre recombinase was used to knockout expression of BMPRII in a cell specific manner. Researchers then discovered that loss of BMPRII in fibroblasts drove metastasis (Pickup et al., 2015). If time allowed, it would have been valuable to generate a cell-specific model to knock out Activin A/B expression. Such a model would help robustly answer questions regarding Activins' role on all the functionalities of interest.

7.3.4 Angiogenesis

I have shown that expression of genes associated with these functionalities are affected at an RNA and protein level. For example, VEGFA, known to promote angiogenesis, exhibits reduced expression at an RNA and protein level in Activin-expressing parental CAFs (Shibuya and Claesson-Welsh, 2006). Additionally, HGF, which shows the same pattern of reduced expression in Activin-expressing CAFs, is also associated with promoting angiogenesis (Khan and Kerbel, 2018; Park et al., 2020a). However, many other factors associated with promoting angiogenesis are

elevated in parental Activin-expressing CAFs, such as *Hbegf* and *Ephb2* (Ongusaha et al., 2004; Sato et al., 2019). My *in vivo* experiments did not show any evidence of angiogenic infiltration in tumour nodules in any of the experimental groups. I was therefore unable to test if Activin signalling in CAFs promotes or inhibits angiogenesis at a functional level. Given more time, I could conduct *in vitro* angiogenesis assays, such as a vascular tube formation assay. Specifically, I could treat endothelial cells, plated in Matrigel, with CM from different CAF populations and image their tube formation over time. Such a set-up was used to show VEGFA secreted by CAFs promoted angiogenesis through regulation of zeste homolog-2/vasohibin 1 pathway (Huang et al., 2019).

7.3.5 Activin signalling in CAFs and tumourigenesis

Based on the results presented in this thesis, I have generated a schematic detailing how Activin affects CAF signalling and functionality (Figure 7.1).

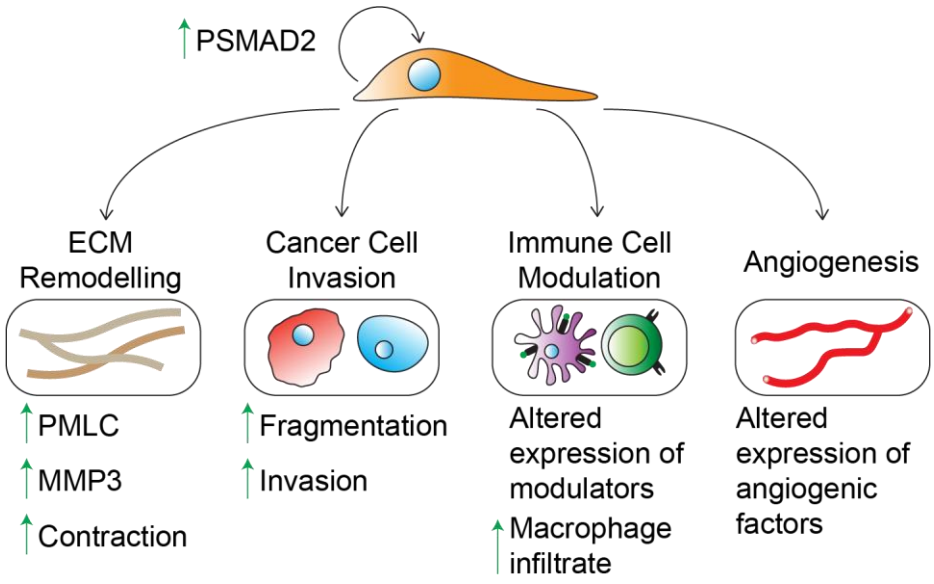

Figure 7.1. The role of Activin signalling in CAF functionality. The schematic details the proposed roles of Activin signalling on respective CAF functionalities based on data presented in this thesis.

I have shown, for the first time, that Activin signalling in CAFs alters their contractility, ability to promote cancer cell invasion; Activin may also affect CAFs' immune cell modulation (particularly their ability to promote macrophage infiltrate) and expression of angiogenic factors. The bulk of my data suggests that Activin A/B signalling in

CAFs would work to promote tumourigenesis. Activin expression enhances ECM remodelling and cancer cell invasion that may lead to metastatic spread. However, I have not been able to show this in the context of a tumour *in vivo*. This may be due to the suboptimal experimental design of the *in vivo* experiments. As mentioned above, I believe the best method of testing the effect of Activin signalling in CAFs *in vivo* would be a conditional knockout model of Activin A/B specifically in CAF populations. Even still, this approach is not ideal, as there is no unique marker for CAFs. Any conditional knockout could also non-specifically target pericytes, mesenchymal stem cells and resident tissue fibroblasts (Birbrair et al., 2015; Sahai et al., 2020; Shangguan et al., 2012).

However, it is vital to remember that when studying cell signalling in the context of cancer, there is invariably more than one signal responsible for perpetuating oncogenic phenotypes. Activin alone is not responsible for each of these phenotypes. It will be crucial to determine how Activin signalling associates with and affects other oncogenic signals, such as RhoGTPase, SRF/MRTF, Wnt and EGFR signalling (Avgustinova et al., 2016; Foster et al., 2017; Gaggioli et al., 2007; Liu et al., 2019). The work detailed in this thesis provides novel understandings as to the role of Activin in oncogenic processes. However, this is only one fragment of a massive network of signals, all interacting and affecting one another. It will be important to further elucidate how these signals cooperate during tumourigenesis. My work can form part of these investigations. In any case, my data have identified Activin as a potential therapeutic target.

7.4 Activin as a therapeutic target

Whilst CAFs are generally considered to promote tumourigenesis, removing them entirely from the tumour microenvironment has been shown to enhance tumour growth, resulting in poorer prognosis (Özdemir et al., 2014; Rhim et al., 2014). Therefore, targeting oncogenic signals in CAFs may be a more prudent approach. Reverting CAFs to a less contractile and more ‘normal’ phenotype is associated with a favourable prognosis (Sahai et al., 2020). For example, targeting vitamin D receptors of stellate cells resulted in more quiescent CAFs, reducing disease aggressiveness in pancreatic cancer patients (Sherman et al., 2014). As I have

shown, Activin A/B is critical in promoting a contractile CAF phenotype. Targeting and blocking Activin A/B signalling may revert CAFs to a similar quiescent state, improving prognosis. Additionally, it may also prevent further CAF activation as Activin A/B has been shown to activate fibroblasts to CAFs through SMAD2-mediated mDia2 signalling (Cangkrama et al., 2020a). The benefits may therefore be two-fold.

Inhibition of TGF-β ligand has shown promise as a therapeutic agent, with many TGF-β ligand inhibitors currently undergoing clinical trials. There are small molecule inhibitors targeting TGFBR1 kinase activity, such as Galunisertib, and anti-TGF-β ligand antibodies such as Fresolimumab. Galunisertib, in combination with gemcitabine, showed modest increases in patient survival in late stage pancreatic patients (8.9 months versus 7.1 months in placebo treated patients) (Melisi et al., 2018). Various pre-clinical models indicate its beneficial effects may be further enhanced when used in combination with checkpoint inhibitors. For example, in a mouse model of breast cancer, use of Galunisterab in combination with anti PDL1 in mice with showed greater reduction in tumour growth and enhanced survival than Galunisterab monotherapy (Holmgaard et al., 2018). However, total inhibition of this ligand has negative side effects. Specifically, induction of heart valve lesions (Anderton et al., 2011). Recent reports have renewed these safety concerns. Targeting TGF- β signalling caused cardiovascular toxicity and death in mice and monkeys (Mitra et al., 2020). Additionally, TGF-β blockade may inhibit its tumour-suppressive effects at early stages of cancer development, such as cell cycle arrest (Siegel and Massagué, 2003).

Targeting Activin may have similar or enhanced beneficial effects in certain cancer types, without the negative side effects. My data suggest that both ligands are required for complete signalling, in terms of pathway activity and transcriptional output in CAFs. Therefore, a dual specific approach of targeting Activin A/B may be the best approach. The best way to achieve this would be to have one agent that targets regions of INHBA and INHBB that share homology. However, none of my functional assays utilised Activin A-null or Activin B-null only CAFs. It would be interesting to conduct functional assays and RNA-Seq analysis on these populations to comprehensively determine the relative contributions of each ligand to signalling and functional output. This may better inform any downstream work conducted to target Activin signalling therapeutically.

However, in a similar way to TGF-β, targeting Activin systemically may also have negative side effects. For example Activin signalling is required for homeostasis of reproductive organs as well as wound healing (Antsiferova and Werner, 2012; Bilezikjian et al., 2006). Systemic targeting of Activin A/B may interfere with these processes. For example, in wound healing, Activin is expressed by keratinocytes and is responsible for the reepithelization of cutaneous wounds in the epidermis (Antsiferova and Werner, 2012; Munz et al., 1999). Loss of this signalling may cause delays in this wound healing process. This could predispose individuals to infection and development of chronic wounds (Rodrigues et al., 2019).

The RNA-Seq dataset detailed in this thesis could be used to generate an Activin signalling gene signature. Such a signature, as well as a specific TGF-β gene signature, could be utilised in personalised therapies for treating cancers. Expression of genes from these distinct signatures could be assessed in tumour samples to determine if they are TGF-β or Activin 'hot'. Drugs targeting each of these ligands specifically could then be implemented in a patients' treatment, and hopefully improve outcome. Personalised therapies can be less toxic and more efficacious in the treatment of cancer (Jackson and Chester, 2015). The RNA-Seq dataset I have generated in collaboration with Stephanie Strohbuecker, could form the foundation of a project that investigates the possibility of TGF-β and Activin personalised therapies.

7.5 ESCRT family regulates appropriate response to TGF-β

In addition to Activin signalling I have also demonstrated that enhanced TGF-β-pathway activation and functional output seen in disease contexts may be due to the de-regulation of mechanisms that determine the response of cells to TGF-β. I have demonstrated that loss of ESCRT function results in enhanced sensitivity and response to TGF-β ligand over prolonged periods. This amounted to an enhanced TGF-β-mediated EMT, an important feature in the progression of many diseases, such as cancer (Nieto et al., 2016). It would be interesting to explore the role of loss of ESCRT function and enhanced TGF-β-mediated disease progression *in vivo*. This would be particularly interesting in the context of cancer development. At early stages, TGF-β has a tumour suppressive effect; specifically, it causes cell cycle

arrest (Colak and ten Dijke, 2017; Heldin et al., 2009). An enhanced response of cells to TGF-β, caused by ESCRT depletion, at this stage may result in delayed tumour onset. However, at later stages, enhanced sensitivity to TGF-βs may result in enhanced EMT, causing cancer cell extravasation and metastasis, as well as immune cell exclusion, which may lead to more aggressive tumour growth. Investigating ESCRT depletion at distinct stages of tumour development would be greatly interesting. Loss of ESCRT component expression is associated with poor prognosis in a variety of cancer types (Miller et al., 2018). In fact, attempts were made to determine a correlation between TGF-β-mediated tumourigenesis and reduction of ESCRT function using TCGA datasets. However, it was not possible to correlate them robustly enough to obtain valid data. Moreover, it would be interesting to determine whether abrogation of ESCRT components affects Activin A/B signalling in the context of cancer. Depletion of ESCRT components has been shown to further prolong cells' response to Activin ligand in terms of PSMAD2 activation (Miller et al., 2018). This may work to enhance its pro-tumourigenic functions that are described throughout this thesis and published in the literature. Furthermore, it would be interesting to explore if these two phenomena, Activin signalling and re-wiring of cellular responses to TGF-β, could be acting concurrently within tumours to propagate the oncogenic effects of TGF-β family signalling. One could investigate levels of expression of ESCRT components, TGF-β ligand and Activin A/B ligands within tumour samples.

This work has helped identify a novel explanation as to why and how TGF-β signalling can switch from tumour suppressive, to tumour promoting. In certain tumours, loss of core TGF-β pathway components (such as SMAD4 in pancreatic and TGFBRII in ovarian cancers) promotes tumourigenesis, due to the loss of the tumour suppressive effects of TGF-β (Ahmed et al., 2017; Alvi et al., 2001; Levy and Hill, 2006). Here, I have shown that, in some contexts, loss of ESCRT expression or function may sensitise cells to TGF-β ligand and it's tumour promoting effects. Not only is this a novel finding for the field of TGF-β family signalling, but it may also have clinical relevance. For example, gene therapy could be implemented to compensate for loss of ESCRT function when its expression is lacking in certain tumours.

7.6 HALO technology as a powerful tool to track protein localisation

Beyond these functional investigations, I have also conducted work aimed at understanding why cells respond distinctly, in terms of pathway activation, to TGF-β and Activin ligands. It has been shown that Activin receptors remain at a steady level at the surface during Activin exposure, allowing cells to continually monitor and respond to the signal. Conversely, TGF-β receptors are internalised within the first 5 minutes of signalling (Miller et al., 2019). This extra regulatory mechanism may exist for TGF-β as there are no known biological antagonists of the ligand. TGF-β is activated where it is required, this refractory response of cells to TGF-β is possibly protective, to prevent hyperactivation (Koli et al., 2001). Such a system is less crucial for Activin, as Follistatin and inhibin expression serve to prevent hyperactivation (Stenvers and Findlay, 2010; Thompson et al., 2005). However, the mechanisms responsible for maintaining surface levels of Activin receptors are not known. I have shown that HALO technology can be used to answer this question. By co-staining cells with HALO ligands and various markers of recycling machinery, we would be able to track the routes these receptors take when they traffic within the cell. We can therefore determine what causes the maintenance of Activin receptors at the surface. By visualising Activin receptors live for the first time, I have confirmed earlier findings that the receptors remain at a steady level at the cell surface. It will be vital to do the same for TGF-β receptors. However, it will be crucial to validate and optimise this technique using HALO-tagged receptors at endogenous levels. Such investigations would be novel and powerful. No one has yet been able to track distinct clusters of TGF-β family receptors live and at an endogenous level. Receptor dynamics are pivotal in how a cell responds to a signal. My investigations can form the foundation of a project that will answer fundamental questions as to why cells respond as they do to TGF-β family ligands.

Additionally, this technology could be used to address other questions in this thesis. HALO-tagged TGF-β receptors could be tracked to determine, more precisely, the proportion of internalised receptors that are degraded, recycled or remain in actively signalling endosomes in WT and ESCRT knockdown cells.

7.7 Concluding remarks: The study of cell signalling mechanisms can identify therapeutic targets

Understanding how signalling operates in healthy cells can tell us how they can become deregulated and cause disease. A core theme of this thesis has been how mechanistic studies can be vital to inform downstream functional studies. These functional studies can lead to identification of therapeutic targets. Such a mechanistic study formed the questions at the foundation of this thesis; why do we see sustained TGF-β family pathway activation and functional outputs in disease contexts? What regulates receptor localisation during TGF-β and Activin treatment? By answering these questions, I have identified two possible therapeutic targets, specifically Activin A/B ligands in cancer and TGF-β signalling where ESCRT machinery has been depleted. Additionally, I have identified a powerful tool that can be used to answer fundamental questions about why TGF-β family receptors localise distinctly from one another during signalling. This mechanistic study could also result in the generation of further functional investigations with similar benefits.

I believe the future of these projects should focus on targeting Activin A/B signalling in the context of cancer. Such work could help us more comprehensively understand the role of Activin in cancer and be of translational benefit. Additionally, implementing HALO technology to track distinct receptor pools at an endogenous level could answer some fundamental questions about TGF-β family receptor dynamics and downstream signalling that have been unanswered until now.

Reference List

Aberle, H. (2019). Axon Guidance and Collective Cell Migration by Substrate-Derived Attractants. Front. Mol. Neurosci. *12*, 148.

Aceto, N., Bardia, A., Miyamoto, D.T., Donaldson, M.C., Wittner, B.S., Spencer, J.A., Yu, M., Pely, A., Engstrom, A., Zhu, H., et al. (2014). Circulating tumor cell clusters are oligoclonal precursors of breast cancer metastasis. Cell *158*, 1110–1122.

Ahmed, S., Bradshaw, A.-D., Gera, S., Dewan, M., and Xu, R. (2017). The TGF-β/Smad4 Signaling Pathway in Pancreatic Carcinogenesis and Its Clinical Significance. J. Clin. Med. *6*, 5.

Alt, E., Welte, G., Li, J., Hennessy, B.T., Devarajan, E., Krishnappa, S., Pinilla, S., Droll, L., and Jotzu, C. (2010). Adipose tissue-derived stem cells differentiate into carcinoma-associated fibroblast-like cells under the influence of tumor-derived factors. Anal. Cell. Pathol. *33*, 61–79.

Alvi, A.J., Rader, J.S., Broggini, M., Latif, F., and Maher, E.R. (2001). Microsatellite instability and mutational analysis of transforming growth factor β receptor type II gene (TGFBR2) in sporadic ovarian cancer. In Journal of Clinical Pathology - Molecular Pathology, (BMJ Publishing Group), pp. 240–243.

An, Y., Liu, F., Chen, Y., and Yang, Q. (2020). Crosstalk between cancer-associated fibroblasts and immune cells in cancer. J. Cell. Mol. Med. *24*, 13–24.

Anastas, J.N., and Moon, R.T. (2013). WNT signalling pathways as therapeutic targets in cancer. Nat. Rev. Cancer *13*, 11–26.

Anderton, M.J., Mellor, H.R., Bell, A., Sadler, C., Pass, M., Powell, S., Steele, S.J., Roberts, R.R.A.A., and Heier, A. (2011). Induction of heart valve lesions by small-molecule ALK5 inhibitors. Toxicol. Pathol. *39*, 916–924.

Annes, J.P. (2003). Making sense of latent TGFbeta activation. J. Cell Sci. *116*, 217–224.

Antsiferova, M., and Werner, S. (2012). The bright and the dark sides of activin in wound healing and cancer. J. Cell Sci. *125*, 3929–3937.

Antsiferova, M., Huber, M., Meyer, M., Piwko-Czuchra, A., Ramadan, T., MacLeod, A.S., Havran, W.L., Dummer, R., Hohl, D., and Werner, S. (2011).

Activin enhances skin tumourigenesis and malignant progression by inducing a pro-tumourigenic immune cell response. Nat. Commun. *2*, 576.

Antsiferova, M., Martin, C., Huber, M., Feyerabend, T.B., Förster, A., Hartmann, K., Rodewald, H.-R., Hohl, D., and Werner, S. (2013). Mast Cells Are Dispensable for Normal and Activin-Promoted Wound Healing and Skin Carcinogenesis. J. Immunol. *191*, 6147–6155.

Antsiferova, M., Piwko-Czuchra, A., Cangkrama, M., Wietecha, M., Sahin, D., Birkner, K., Amann, V.C., Levesque, M., Hohl, D., Dummer, R., et al. (2017). Activin promotes skin carcinogenesis by attraction and reprogramming of macrophages. EMBO Mol. Med. *9*, 27–45.

Ao, M., Franco, O.E., Park, D., Raman, D., Williams, K., and Hayward, S.W. (2007). Cross-talk between paracrine-acting cytokine and chemokine pathways promotes malignancy in benign human prostatic epithelium. Cancer Res. *67*, 4244–4253.

Astin, J.W., Batson, J., Kadir, S., Charlet, J., Persad, R.A., Gillatt, D., Oxley, J.D., and Nobes, C.D. (2010). Competition amongst Eph receptors regulates contact inhibition of locomotion and invasiveness in prostate cancer cells. Nat. Cell Biol. *12*, 1194–1204.

Attieh, Y., Clark, A.G., Grass, C., Richon, S., Pocard, M., Mariani, P., Elkhatib, N., Betz, T., Gurchenkov, B., and Vignjevic, D.M. (2017). Cancer-associated fibroblasts lead tumor invasion through integrin-β3-dependent fibronectin asse. J. Cell Biol. *216*, 3509–3520.

Augsten, M. (2014). Cancer-associated fibroblasts as another polarized cell type of the tumor microenvironment. Front. Oncol. *4*, 1–8.

Avery, D., Govindaraju, P., Jacob, M., Todd, L., Monslow, J., and Puré, E. (2018). Extracellular matrix directs phenotypic heterogeneity of activated fibroblasts. Matrix Biol. *67*, 90–106.

Avgustinova, A., Iravani, M., Robertson, D., Fearns, A., Gao, Q., Klingbeil, P., Hanby, A.M., Speirs, V., Sahai, E., Calvo, F., et al. (2016). Tumour cell-derived Wnt7a recruits and activates fibroblasts to promote tumour aggressiveness. Nat. Commun. *7*, 10305.

Balabanian, K., Lagane, B., Infantino, S., Chow, K.Y.C., Harriague, J., Moepps,

B., Arenzana-Seisdedos, F., Thelen, M., and Bachelerie, F. (2005). The chemokine SDF-1/CXCL12 binds to and signals through the orphan receptor RDC1 in T lymphocytes. J. Biol. Chem. *280*, 35760–35766.

Bamberger, C., Schärer, A., Antsiferova, M., Tychsen, B., Pankow, S., Müller, M., Rülicke, T., Paus, R., and Werner, S. (2005). Activin controls skin morphogenesis and wound repair predominantly via stromal cells and in a concentration-dependent manner via keratinocytes. Am. J. Pathol. *167*, 733–747.

Banik, D., Netherby, C.S., Bogner, P.N., and Abrams, S.I. (2015). MMP3-Mediated tumor progression is controlled transcriptionally by a novel IRF8-MMP3 interaction. Oncotarget *6*, 15164–15179.

Bartoschek, M., Oskolkov, N., Bocci, M., Lövrot, J., Larsson, C., Sommarin, M., Madsen, C.D., Lindgren, D., Pekar, G., Karlsson, G., et al. (2018). Spatially and functionally distinct subclasses of breast cancer-associated fibroblasts revealed by single cell RNA sequencing. Nat. Commun. *9*, 5150.

Batlle, E., and Massagué, J. (2019). Transforming Grown Factor-β Signaling in Immunity and Cancer. Immunity *50*, 924–940.

Bauer, J., Ozden, O., Akagi, N., Carroll, T., Principe, D.R., Staudacher, J.J., Spehlmann, M.E., Eckmann, L., Grippo, P.J., and Jung, B. (2015). Activin and TGFβ use diverging mitogenic signaling in advanced colon cancer. Mol. Cancer *14*, 1–14.

Bauer, J., Emon, M.A.B., Staudacher, J.J., Thomas, A.L., Zessner-Spitzenberg, J., Mancinelli, G., Krett, N., Saif, M.T., and Jung, B. (2020). Increased stiffness of the tumor microenvironment in colon cancer stimulates cancer associated fibroblast-mediated prometastatic activin A signaling. Sci. Rep. *10*, 1–11.

Bergeron, J.J.M., Di Guglielmo, G.M., Dahan, S., Dominguez, M., and Posner, B.I. (2016). Spatial and Temporal Regulation of Receptor Tyrosine Kinase Activation and Intracellular Signal Transduction. Annu. Rev. Biochem. *85*, 573–597.

Bettelli, E., Carrier, Y., Gao, W., Korn, T., Strom, T.B., Oukka, M., Weiner, H.L., and Kuchroo, V.K. (2006). Reciprocal developmental pathways for the generation of pathogenic effector TH17 and regulatory T cells. Nature *441*, 235–238.

Biffi, G., Oni, T.E., Spielman, B., Hao, Y., Elyada, E., Park, Y., Preall, J., and

Tuveson, D.A. (2019). Il1-induced Jak/STAT signaling is antagonized by TGFβ to shape CAF heterogeneity in pancreatic ductal adenocarcinoma. Cancer Discov. *9*, 282–301.

Bilezikjian, L.M., Blount, A.L., Donaldson, C.J., and Vale, W.W. (2006). Pituitary actions of ligands of the TGF-β family: Activins and inhibins. Reproduction *132*, 207–215.

Birbrair, A., Zhang, T., Wang, Z.M., Messi, M.L., Mintz, A., and Delbono, O. (2015). Pericytes at the intersection between tissue regeneration and pathology. Clin. Sci. *128*, 81–93.

Bonavita, E., Gentile, S., Rubino, M., Maina, V., Papait, R., Kunderfranco, P., Greco, C., Feruglio, F., Molgora, M., Laface, I., et al. (2015). PTX3 Is an Extrinsic Oncosuppressor Regulating Complement-Dependent Inflammation in Cancer. Cell *160*, 700–714.

Bozza, M., Bliss, J.L., Dorner, A.J., and Trepicchio, W.L. (2001). Interleukin-11 modulates Th1/Th2 cytokine production from activated CD4+ T cells. J. Interf. Cytokine Res. *21*, 21–30.

Brunet, S., Sardon, T., Zimmerman, T., Wittmann, T., Pepperkok, R., Karsenti, E., and Vernos, I. (2004). Characterization of the TPX2 Domains Involved in Microtubule Nucleation and Spindle Assembly in Xenopus. Mol Biol Cell *15*, 5318–5328.

Budi, E.H., Muthusamy, B.P., and Derynck, R. (2015). The insulin response integrates increased TGF-b signaling through Akt-induced enhancement of cell surface delivery of TGF-b receptors. Sci. Signal. *8*, 1–16.

Calon, A., Espinet, E., Palomo-Ponce, S., Tauriello, D.V.F.F., Iglesias, M., Céspedes, M.V., Sevillano, M., Nadal, C., Jung, P., Zhang, X.H.F.F., et al. (2012). Dependency of Colorectal Cancer on a TGF-β-Driven Program in Stromal Cells for Metastasis Initiation. Cancer Cell *22*, 571–584.

Calon, A., Tauriello, D.V.F.V.F., and Batlle, E. (2014). TGF-beta in CAF-mediated tumor growth and metastasis. Semin. Cancer Biol. *25*, 15–22.

Calon, A., Lonardo, E., Berenguer-Llergo, A., Espinet, E., Hernando-Momblona, X., Iglesias, M., Sevillano, M., Palomo-Ponce, S., Tauriello, D.V.F., Byrom, D., et al. (2015). Stromal gene expression defines poor-prognosis subtypes in

colorectal cancer. Nat. Genet. *47*, 320–329.

Calvo, F., Ege, N., Grande-Garcia, A., Hooper, S., Jenkins, R.P., Chaudhry, S.I., Harrington, K., Williamson, P., Moeendarbary, E., Charras, G., et al. (2013). Mechanotransduction and YAP-dependent matrix remodelling is required for the generation and maintenance of cancer-associated fibroblasts. Nat. Cell Biol. *15*, 637–646.

Calvo, F., Ranftl, R., Hooper, S., Farrugia, A.J., Moeendarbary, E., Bruckbauer, A., Batista, F., Charras, G., and Sahai, E. (2015). Cdc42EP3/BORG2 and Septin Network Enables Mechano-transduction and the Emergence of Cancer-Associated Fibroblasts. Cell Rep. *13*, 2699–2714.

Campsteijn, C., Vietri, M., and Stenmark, H. (2016). Novel ESCRT functions in cell biology: spiraling out of control? Curr. Opin. Cell Biol. *41*, 1–8.

Cangkrama, M., Wietecha, M., Mathis, N., Okumura, R., Ferrarese, L., Al-Nuaimi, D., Antsiferova, M., Dummer, R., Innocenti, M., and Werner, S. (2020a). A paracrine activin A–mDia2 axis promotes squamous carcinogenesis via fibroblast reprogramming. EMBO Mol. Med. *12*, e11466.

Cangkrama, M., Wietecha, M., and Werner, S. (2020b). Wound Repair, Scar Formation, and Cancer: Converging on Activin. Trends Mol. Med. *26*, 1107–1117.

Chacko, B.M., Qin, B., Correia, J.J., Lam, S.S., De Caestecker, M.P., and Lin, K. (2001). The L3 loop and C-terminal phosphorylation jointly define Smad protein trimerization. Nat. Struct. Biol. *8*, 248–253.

Chen, Y.G. (2009). Endocytic regulation of TGF-β signaling. Cell Res. *19*, 58–70.

Chenouard, N., Smal, I., De Chaumont, F., Maška, M., Sbalzarini, I.F., Gong, Y., Cardinale, J., Carthel, C., Coraluppi, S., Winter, M., et al. (2014). Objective comparison of particle tracking methods. Nat. Methods *11*, 281–289.

Cheung, K.J., and Ewald, A.J. (2016). A collective route to metastasis: Seeding by tumor cell clusters. Science (80-.). *352*, 167–169.

Choi, S.C., Kim, G.H., Lee, S.J., Park, E., Yeo, C.Y., and Han, J.K. (2008). Regulation of Activin/Nodal Signaling by Rap2-Directed Receptor Trafficking. Dev. Cell *15*, 49–61.

Cirri, P., and Chiarugi, P. (2012). Cancer-associated-fibroblasts and tumour cells: A diabolic liaison driving cancer progression. Cancer Metastasis Rev. *31*, 195–

208.

Claesson-Welsh, L., and Welsh, M. (2013). VEGFA and tumour angiogenesis. J. Intern. Med. *273*, 114–127.

Cohen, N., Shani, O., Raz, Y., Sharon, Y., Hoffman, D., Abramovitz, L., and Erez, N. (2017). Fibroblasts drive an immunosuppressive and growth-promoting microenvironment in breast cancer via secretion of Chitinase 3-like 1. Oncogene *36*, 4457–4468.

Colak, S., and ten Dijke, P. (2017). Targeting TGF-β Signaling in Cancer. Trends in Cancer *3*, 56–71.

Costa, A., Kieffer, Y., Scholer-Dahirel, A., Pelon, F., Bourachot, B., Cardon, M., Sirven, P., Magagna, I., Fuhrmann, L., Bernard, C., et al. (2018). Fibroblast Heterogeneity and Immunosuppressive Environment in Human Breast Cancer. Cancer Cell *33*, 463–479.

Crowley, R.K., O'Reilly, M.W., Bujalska, I.J., Hassan-Smith, Z.K., Hazlehurst, J.M., Foucault, D.R., Stewart, P.M., and Tomlinson, J.W. (2016). SFRP2 is associated with increased adiposity and VEGF expression. PLoS One *11*, p.e0163777.

DaCosta Byfield, S., Major, C., Laping, N.J., and Roberts, A.B. (2004). SB-505124 Is a Selective Inhibitor of Transforming Growth Factor-β Type I Receptors ALK4, ALK5, and ALK7. Mol. Pharmacol. *65*, 744–752.

Daly, A.C., Randall, R.A., and Hill, C.S. (2008). Transforming Growth Factor β-Induced Smad1/5 Phosphorylation in Epithelial Cells Is Mediated by Novel Receptor Complexes and Is Essential for Anchorage-Independent Growth. Mol. Cell. Biol. *28*, 6889–6902.

Daly, A.C., Vizán, P., and Hill, C.S. (2010). Smad3 protein levels are modulated by ras activity and during the cell cycle to dictate transforming growth factor-β responses. J. Biol. Chem. *285*, 6489–6497.

Daopin, S., Piez, K.A., Ogawa, Y., and Davies, D.R. (1992). Crystal structure of transforming growth factor-β2: An unusual fold for the superfamily. Science (80-.). *257*, 369–373.

Davies, E.M., Gurung, R., Le, K.Q., and Mitchell, C.A. (2019). Effective angiogenesis requires regulation of phosphoinositide signaling. Adv. Biol. Regul.

71, 69–78.

Day, C.-P., Carter, J., Ohler, Z.W., Bonomi, C., El Meskini, R., Martin, P., Graff-Cherry, C., Feigenbaum, L., Tüting, T., Van Dyke, T., et al. (2014). “Glowing Head” Mice: A Genetic Tool Enabling Reliable Preclinical Image-Based Evaluation of Cancers in Immunocompetent Allografts. PLoS One *9*, 1–13.

Derynck, R., and Akhurst, R.J. (2007). Differentiation plasticity regulated by TGF-β family proteins in development and disease. Nat. Cell Biol. *9*, 1000–1004.

Derynck, R., Lindquist, P.B., Lee, A., Wen, D., Tamm, J., Graycar, J.L., Rhee, L., Mason, A.J., Miller, D.A., and Coffey, R.J. (1988). A new type of transforming growth factor-beta, TGF-beta 3. EMBO J. *7*, 3737–3743.

Ten Dijke, P., and Arthur, H.M. (2007). Extracellular control of TGFβ signalling in vascular development and disease. Nat. Rev. Mol. Cell Biol. *8*, 857–869.

Dobin, A., Davis, C.A., Schlesinger, F., Drenkow, J., Zaleski, C., Jha, S., Batut, P., Chaisson, M., and Gingeras, T.R. (2013). STAR: Ultrafast universal RNA-seq aligner. Bioinformatics *29*, 15–21.

Donovan, P., Dubey, O.A., Kallioinen, S., Rogers, K.W., Muehlethaler, K., Müller, P., Rimoldi, D., and Constam, D.B. (2017). Paracrine Activin-A Signaling Promotes Melanoma Growth and Metastasis through Immune Evasion. J. Invest. Dermatol. *137*, 2578–2587.

Doré, J., Yao, D., Edens, M., Garamszegi, N., Sholl, E.L., and Leof, E.B. (2001). Mechanisms of transforming growth factor-β receptor endocytosis and intracellular sorting differ between fibroblasts and epithelial cells. Mol. Biol. Cell *12*, 675–684.

Dubois, C.M., Blanchette, F., Laprise, M.H., Leduc, R., Grondin, F., and Seidah, N.G. (2001). Evidence that furin is an authentic transforming growth factor-β1-converting enzyme. Am. J. Pathol. *158*, 305–316.

Duhachek-Muggy, S., Qi, Y., Wise, R., Alyahya, L., Li, H., Hodge, J., and Zolkiewska, A. (2017). Metalloprotease-disintegrin ADAM12 actively promotes the stem cell-like phenotype in claudin-low breast cancer. Mol. Cancer *16*, 32.

Dünker, N., Schmitt, K., and Krieglstein, K. (2002). TGF-β is required for programmed cell death in interdigital webs of the developing mouse limb. Mech. Dev. *113*, 111–120.

Dupont, S., Morsut, L., Aragona, M., Enzo, E., Giulitti, S., Cordenonsi, M., Zanconato, F., Le Digabel, J., Forcato, M., Bicciato, S., et al. (2011). Role of YAP/TAZ in mechanotransduction. Nature *474*, 179–184.

Dushyanthen, S., Beavis, P.A., Savas, P., Teo, Z.L., Zhou, C., Mansour, M., Darcy, P.K., and Loi, S. (2015). Relevance of tumor-infiltrating lymphocytes in breast cancer. BMC Med. *13*, 1–13.

Edwards, D.R., Handsley, M.M., and Pennington, C.J. (2009). The ADAM metalloproteinases. Mol. Aspects Med. *29*, 258–289.

Emon, B., Bauer, J., Jain, Y., Jung, B., and Saif, T. (2018). Biophysics of Tumor Microenvironment and Cancer Metastasis - A Mini Review. Comput. Struct. Biotechnol. J. *16*, 279–287.

Erez, N., Truitt, M., Olson, P., and Hanahan, D. (2010). Cancer-Associated Fibroblasts Are Activated in Incipient Neoplasia to Orchestrate Tumor-Promoting Inflammation in an NF-κB-Dependent Manner. Cancer Cell *17*, 135–147.

Evans, R.A., Tian, Y.. C., Steadman, R., and Phillips, A.O. (2003). TGF-β1-mediated fibroblast–myofibroblast terminal differentiation—the role of smad proteins. Exp. Cell Res. *282*, 90–100.

Faivre, S.J., Santoro, A., Kelley, R.K., Merle, P., Gane, E., Douillard, J.-Y., Waldschmidt, D., Mulcahy, M.F., Costentin, C., Minguez, B., et al. (2014). A phase 2 study of a novel transforming growth factor-beta (TGF-β1) receptor I kinase inhibitor, LY2157299 monohydrate (LY), in patients with advanced hepatocellular carcinoma (HCC). J. Clin. Oncol. *32*, 173.

Fazilleau, N., Mark, L., McHeyzer-Williams, L.J., and McHeyzer-Williams, M.G. (2009). Follicular Helper T Cells: Lineage and Location. Immunity *30*, 324–335.

Fearon, D.T. (2014). The carcinoma-associated fibroblast expressing fibroblast activation protein and escape from immune surveillance. Cancer Immunol. Res. *2*, 187–193.

Feng, X.H., and Derynck, R. (2005). Specificity and versatility in TGF-β signaling through smads. Annu. Rev. Cell Dev. Biol. *21*, 659–693.

Flier, J.S., Underhill, L.H., and Dvorak, H.F. (1986). Tumors: Wounds That Do Not Heal. N. Engl. J. Med. *315*, 1650–1659.

Formenti, S.C., Lee, P., Adams, S., Goldberg, J.D., Li, X., Xie, M.W., Ratikan,

J.A., Felix, C., Hwang, L., Faull, K.F., et al. (2018). Focal irradiation and systemic TGFb blockade in metastatic breast cancer. Clin. Cancer Res. *24*, 2493–2504.

Foster, C.T., Gualdrini, F., and Treisman, R. (2017). Mutual dependence of the MRTF-SRF and YAP-TEAD pathways in cancer-associated fibroblasts is indirect and mediated by cytoskeletal dynamics. Genes Dev. *31*, 2361–2375.

Friedl, P., Locker, J., Sahai, E., and Segall, J.E. (2012). Classifying collective cancer cell invasion. Nat. Cell Biol. *14*, 777–783.

Fukumura, D., Xavier, R., Sugiura, T., Chen, Y., Park, E.C., Lu, N., Selig, M., Nielsen, G., Taksir, T., Jain, R.K., et al. (1998). Tumor induction of VEGF promoter activity in stromal cells. Cell *94*, 715–725.

Gaggioli, C., Hooper, S., Hidalgo-Carcedo, C., Grosse, R., Marshall, J.F., Harrington, K., and Sahai, E. (2007). Fibroblast-led collective invasion of carcinoma cells with differing roles for RhoGTPases in leading and following cells. Nat. Cell Biol. *9*, 1392–1400.

Gao, L.M., Wang, F., Zheng, Y., Fu, Z.Z., Zheng, L., and Chen, L.L. (2019). Roles of Fibroblast Activation Protein and Hepatocyte Growth Factor Expressions in Angiogenesis and Metastasis of Gastric Cancer. Pathol. Oncol. Res. *25*, 369–376.

Giacomini, A., Ghedini, G.C., Presta, M., and Ronca, R. (2018). Long pentraxin 3: A novel multifaceted player in cancer. Biochim. Biophys. Acta - Rev. Cancer *1869*, 53–63.

Giampieri, S., Manning, C., Hooper, S., Jones, L., Hill, C.S., and Sahai, E. (2009). Localized and reversible TGFβ signalling switches breast cancer cells from cohesive to single cell motility. Nat. Cell Biol. *11*, 1287–1296.

Giepmans, B.N.., Adams, S.., Ellisman, M.., and Tsien, R.. (2006). The Fluorescent Toolbox for Assessing Protein Location and Function. Science (80-.). *312*, 217–225.

Gilbert, R.W.D., Vickaryous, M.K., and Viloria-Petit, A.M. (2016). Signalling by transforming growth factor beta isoforms in wound healing and tissue regeneration. J. Dev. Biol. *4*, 1–21.

Gilboa, L., Wells, R.G., Lodish, H.F., and Henis, Y.I. (1998). Oligomeric structure of type I and type II transforming growth factor β receptors: Homodimers form in

the ER and persist at the plasma membrane. J. Cell Biol. *140*, 767–777.

Gobin, E., Bagwell, K., Wagner, J., Mysona, D., Sandirasegarane, S., Smith, N., Bai, S., Sharma, A., Schleifer, R., and She, J.X. (2019). A pan-cancer perspective of matrix metalloproteases (MMP) gene expression profile and their diagnostic/prognostic potential. BMC Cancer *19*, 581.

Gok Yavuz, B., Gunaydin, G., Gedik, M.E., Kosemehmetoglu, K., Karakoc, D., Ozgur, F., and Guc, D. (2019). Cancer associated fibroblasts sculpt tumour microenvironment by recruiting monocytes and inducing immunosuppressive PD-1 + TAMs. Sci. Rep. *9*, 1–15.

Goumans, M.J., and Mummery, C. (2000). Functional analysis of the TGFβ receptor/Smad pathway through gene ablation in mice. Int. J. Dev. Biol. *44*, 253–265.

Gray, A.M., and Mason, A.J. (1990). Requirement for activin a and transforming growth factor-β1 pro-regions in homodimer assembly. Science (80-.). *247*, 1328–1330.

Green, J.B.A., and Smith, J.C. (1990). Graded changes in dose of a Xenopus activin A homologue elicit stepwise transitions in embryonic cell fate. Nature *347*, 391–394.

Grimm, J.B., Brown, T.A., English, B.P., Lionnet, T., and Lavis, L.D. (2017). Synthesis of Janelia Fluor HaloTag and SNAP-Tag Ligands Experiments, and Their Use in Cellular Imaging. In Methods in Molecular Biology (Clifton, N.J)., H. Erfle, and J.M. Walker, eds. (Springer Protocols), pp. 179–188.

Gu, Z., Nomura, M., Simpson, B.B., Lei, H., Feijen, A., Van Den Eijnden-Van Raaij, J., Donahoe, P.K., and Li, E. (1998). The type I activin receptor ActRIB is required for egg cylinder organization and gastrulation in the mouse. Genes Dev. *12*, 844–857.

Gu, Z., Eils, R., and Schlesner, M. (2016). Complex heatmaps reveal patterns and correlations in multidimensional genomic data. Bioinformatics *32*, 2847–2849.

Guerriero, J.L. (2018). Macrophages: The Road Less Traveled, Changing Anticancer Therapy. Trends Mol. Med. *24*, 472–489.

Di Guglielmo, G.M., Le Roy, C., Goodfellow, A.F., and Wrana, J.L. (2003).

Distinct endocytic pathways regulate TGF-β receptor signalling and turnover. Nat. Cell Biol. *5*, 410–421.

Guinney, J., Dienstmann, R., Wang, X., De Reyniès, A., Schlicker, A., Soneson, C., Marisa, L., Roepman, P., Nyamundanda, G., Angelino, P., et al. (2015). The consensus molecular subtypes of colorectal cancer. Nat. Med. *21*, 1350–1356.

Haertel, E., Joshi, N., Hiebert, P., Kopf, M., and Werner, S. (2018). Regulatory T cells are required for normal and activin-promoted wound repair in mice. Eur. J. Immunol. *48*, 1001–1013.

Halvorsen, E.C., Hamilton, M.J., Young, A., Wadsworth, B.J., LePard, N.E., Lee, H.N., Firmino, N., Collier, J.L., and Bennewith, K.L. (2016). Maraviroc decreases CCL8-mediated migration of CCR5+ regulatory T cells and reduces metastatic tumor growth in the lungs. Oncoimmunology *5*, 1–16.

Hanahan, D., and Weinberg, R.A. (2011). Hallmarks of cancer: The next generation. Cell *144*, 646–674.

Hänselmann, S., and Herten, D.P. (2017). Two-color single-molecule tracking in live cells. In Methods in Molecular Biology, (Humana Press Inc.), pp. 127–138.

Hao, Y., Baker, D., and Dijke, P. Ten (2019). TGF-β-mediated epithelial-mesenchymal transition and cancer metastasis. Int. J. Mol. Sci. *20*, 1–34.

Haque, A.S.M.R., Moriyama, M., Kubota, K., Ishiguro, N., Sakamoto, M., Chinju, A., Mochizuki, K., Sakamoto, T., Kaneko, N., Munemura, R., et al. (2019). CD206+ tumor-associated macrophages promote proliferation and invasion in oral squamous cell carcinoma via EGF production. Sci. Rep. *9*, 1–10.

Harrington, A.E., Morris-Triggs, S.A., Ruotolo, B.T., Robinson, C. V., Ohnuma, S.I., and Hyvönen, M. (2006). Structural basis for the inhibition of activin signalling by follistatin. EMBO J. *25*, 1035–1045.

Hartmann, N., Giese, N.A., Giese, T., Poschke, I., Offringa, R., Werner, J., and Ryschich, E. (2014). Prevailing role of contact guidance in intrastromal T-cell trapping in human pancreatic cancer. Clin. Cancer Res. *20*, 3422–3433.

Hastings, J.F., Skhinas, J.N., Fey, D., Croucher, D.R., and Cox, T.R. (2019). The extracellular matrix as a key regulator of intracellular signalling networks. Br. J. Pharmacol. *176*, 82–92.

He, K., Yan, X., Li, N., Dang, S., Xu, L., Zhao, B., Li, Z., Lv, Z., Fang, X., Zhang,

Y., et al. (2015). Internalization of the TGF-β type i receptor into caveolin-1 and EEA1 double-positive early endosomes. Cell Res. *25*, 738–752.

Hedger, M.P., Winnall, W.R., Phillips, D.J., and de Kretser, D.M. (2011). The Regulation and Functions of Activin and Follistatin in Inflammation and Immunity.

Heldin, C.H., Landström, M., and Moustakas, A. (2009). Mechanism of TGF-β signaling to growth arrest, apoptosis, and epithelial-mesenchymal transition. Curr. Opin. Cell Biol. *21*, 166–176.

Hellyer, N.J., Mantilla, C.B., Park, E.W., Zhan, W.Z., and Sieck, G.C. (2006). Neuregulin-dependent protein synthesis in C2C12 myotubes and rat diaphragm muscle. Am. J. Physiol. - Cell Physiol. *291*, 1–6.

Henke, A., Franco, O.E., Stewart, G.D., Riddick, A.C.P., Katz, E., Hayward, S.W., and Thomson, A.A. (2016). Reduced contractility and motility of prostatic cancer-associated fibroblasts after inhibition of heat shock protein 90. Cancers (Basel). *8*, 77.

Hill, C.S. (2016). Transcriptional control by the SMADs. Cold Spring Harb. Perspect. Biol. *8*, a022079.

Hill, C.S. (2018). Spatial and temporal control of NODAL signaling. Curr. Opin. Cell Biol. *51*, 50–57.

Hinck, A.P., Mueller, T.D., and Springer, T.A. (2016). Structural biology and evolution of the TGF-β family. Cold Spring Harb. Perspect. Biol. *8*, 1–52.

Hinz, B. (2016). The role of myofibroblasts in wound healing. Curr. Res. Transl. Med. *64*, 171–177.

Holmgaard, R.B., Schaer, D.A., Li, Y., Castaneda, S.P., Murphy, M.Y., Xu, X., Inigo, I., Dobkin, J., Manro, J.R., Iversen, P.W., et al. (2018). Targeting the TGFβ pathway with galunisertib, a TGFβRI small molecule inhibitor, promotes anti-tumor immunity leading to durable, complete responses, as monotherapy and in combination with checkpoint blockade. J. Immunother. Cancer *6*, 1–15.

Hong, S., Lim, S., Li, A.G., Lee, C., Lee, Y.S., Lee, E.K., Park, S.H., Wang, X.J., and Kim, S.J. (2007). Smad7 binds to the adaptors TAB2 and TAB3 to block recruitment of the kinase TAK1 to the adaptor TRAF2. Nat. Immunol. *8*, 504–513.

Huang, F., and Chen, Y.G. (2012). Regulation of TGF-β receptor activity. Cell Biosci. *2*, 1–10.

Huang, B., Huang, M., and Li, Q. (2019). Cancer-Associated Fibroblasts Promote Angiogenesis of Hepatocellular Carcinoma by VEGF-Mediated EZH2/VASH1 Pathway. Technol. Cancer Res. Treat. *18*, 1–12.

Huber, S., Stahl, F.R., Schrader, J., Lüth, S., Presser, K., Carambia, A., Flavell, R.A., Werner, S., Blessing, M., Herkel, J., et al. (2009). Activin A Promotes the TGF-β-Induced Conversion of CD4 + CD25 − T Cells into Foxp3 + Induced Regulatory T Cells . J. Immunol. *182*, 4633–4640.

Hübner, G., Qianjin, H., Smola, H., and Werner, S. (1996). Strong induction of activin expression after injury suggests an important role of activin in wound repair. Dev. Biol. *173*, 490–498.

Huot, J. (2004). Ephrin signaling in axon guidance. Prog. Neuro-Psychopharmacology Biol. Psychiatry *28*, 813–818.

Huse, M., Chen, Y.G., Massagué, J., and Kuriyan, J. (1999). Crystal structure of the cytoplasmic domain of the type I TGFβ receptor in complex with FKBP12. Cell *96*, 425–436.

Hutchenreuther, J., Vincent, K., Norley, C., Racanelli, M., Gruber, S.B., Johnson, T.M., Fullen, D.R., Raskin, L., Perbal, B., Holdsworth, D.W., et al. (2018). Activation of cancer-associated fibroblasts is required for tumor neovascularization in a murine model of melanoma. Matrix Biol. *74*, 52–61.

Icer, M.A., and Gezmen-Karadag, M. (2018). The multiple functions and mechanisms of osteopontin. Clin. Biochem. *59*, 17–24.

Inman, G.J., Nicolás, F.J., Callahan, J.F., Harling, J.D., Gaster, L.M., Reith, A.D., Laping, N.J., and Hill, C.S. (2002). SB-431542 Is a Potent and Specific Inhibitor of Transforming Growth Factor-beta Superfamily Type I Activin Receptor-Like Kinase (ALK) Receptors ALK4, ALK5, and ALK7. Mol. Pharmacol. *62*, 65–74.

Itoh, Y., and Nagase, H. (2002). Matrix metalloproteinases in cancer. Essays Biochem. *38*, 21–36.

Jackson, S.E., and Chester, J.D. (2015). Personalised cancer medicine. Int. J. Cancer *137*, 262–266.

Jackute, J., Zemaitis, M., Pranys, D., Sitkauskiene, B., Miliauskas, S., Vaitkiene, S., and Sakalauskas, R. (2018). Distribution of M1 and M2 macrophages in tumor islets and stroma in relation to prognosis of non-small cell lung cancer. BMC

Immunol. *19*, 1–13.

Jang, C.W., Chen, C.H., Chen, C.C., Chen, J.Y., Su, Y.H., and Chen, R.H. (2002). TGF-β induces apoptosis through Smad-mediated expression of DAP-kinase. Nat. Cell Biol. *4*, 51–58.

Jaźwińska, A., Badakov, R., and Keating, M.T. (2007). Activin-βA Signaling Is Required for Zebrafish Fin Regeneration. Curr. Biol. *17*, 1390–1395.

Jeltsch, M., Jha, S.K., Tvorogov, D., Anisimov, A., Leppänen, V.-M., Holopainen, T., Kivelä, R., Ortega, S., Kärpanen, T., and Alitalo, K. (2014). CCBE1 Enhances Lymphangiogenesis via ADAMTS3-Mediated VEGF-C Activation. Circulation *129*, 1962–1971.

Jennings, M.T., and Pietenpol, J.A. (1998). The role of transforming growth factor β in glioma progression. J. Neurooncol. *36*, 123–140.

Jiang, H., Hegde, S., Knolhoff, B.L., Zhu, Y., Herndon, J.M., Meyer, M.A., Nywening, T.M., Hawkins, W.G., Shapiro, I.M., Weaver, D.T., et al. (2016). Targeting focal adhesion kinase renders pancreatic cancers responsive to checkpoint immunotherapy. Nat. Med. *22*, 851–860.

Jones, R.L., Findlay, J.K., Farnworth, P.G., Robertson, D.M., Wallace, E., and Salamonsen, L.A. (2006). Activin A and inhibin a differentially regulate human uterine matrix metalloproteinases: Potential interactions during decidualization and trophoblast invasion. Endocrinology *147*, 724–732.

Juillerat, A., Gronemeyer, T., Keppler, A., Gendreizig, S., Pick, H., Vogel, H., and Johnsson, K. (2003). Directed evolution of O6-alkylguanine-DNA alkyltransferase for efficient labeling of fusion proteins with small molecules in vivo. Chem. Biol. *10*, 313–317.

Kaivo-Oja, N., Bondestam, J., Kämäräinen, M., Koskimies, J., Vitt, U., Cranfield, M., Vuojolainen, K., Kallio, J.P., Olkkonen, V.M., Hayashi, M., et al. (2003). Growth Differentiation Factor-9 Induces Smad2 Activation and Inhibin B Production in Cultured Human Granulosa-Luteal Cells. J. Clin. Endocrinol. Metab. *88*, 755–762.

Kalluri, R., and Zeisberg, M. (2006). Fibroblasts in cancer. Nat. Rev. Cancer *6*, 392–401.

Kang, Y., Chen, C.R., and Massagué, J. (2003). A self-enabling TGFβ response

coupled to stress signaling: Smad engages stress response factor ATF3 for Id1 repression in epithelial cells. Mol. Cell *11*, 915–926.

Karin, N., and Razon, H. (2018). Chemokines beyond chemo-attraction: CXCL10 and its significant role in cancer and autoimmunity. Cytokine *109*, 24–28.

Karnoub, A.E., Dash, A.B., Vo, A.P., Sullivan, A., Brooks, M.W., Bell, G.W., Richardson, A.L., Polyak, K., Tubo, R., and Weinberg, R.A. (2007). Mesenchymal stem cells within tumour stroma promote breast cancer metastasis. Nature *449*, 557–563.

Kato, T., Noma, K., Ohara, T., Kashima, H., Katsura, Y., Sato, H., Komoto, S., Katsube, R., Ninomiya, T., Tazawa, H., et al. (2018). Cancer-associated fibroblasts affect intratumoral CD8 and Foxp3 T cells via IL6 in the tumor microenvironment. Clin. Cancer Res. *24*, 4820–4833.

Kelwick, R., Desanlis, I., Wheeler, G.N., and Edwards, D.R. (2015). The ADAMTS (A Disintegrin and Metalloproteinase with Thrombospondin motifs) family. Genome Biol. *16*, 113.

Khan, K.A., and Kerbel, R.S. (2018). Improving immunotherapy outcomes with anti-angiogenic treatments and vice versa. Nat. Rev. Clin. Oncol. *15*, 310–324.

Kholodenko, B.N. (2006). Steady state Cell-signalling dynamics in time and space. Nat. Rev. Mol. Cell Biol. *7*, 165–176.

Kiecker, C., Bates, T., and Bell, E. (2016). Molecular specification of germ layers in vertebrate embryos. Cell. Mol. Life Sci. *73*, 923–947.

Kim, S.W., Yoon, S.J., Chuong, E., Oyolu, C., Wills, A.E., Gupta, R., and Baker, J. (2011). Chromatin and transcriptional signatures for Nodal signaling during endoderm formation in hESCs. Dev. Biol. *357*, 492–504.

Kim, Y.W., Park, J., Lee, H.J., Lee, S.Y., and Kim, S.J. (2012). TGF-β sensitivity is determined by N-linked glycosylation of the type II TGF-β receptor. Biochem. J. *445*, 403–411.

Koli, K., Saharinen, J., Hyytiäinen, M., Penttinen, C., and Keski-Oja, J. (2001). Latency, activation, and binding proteins of TGF-β. Microsc. Res. Tech. *52*, 354–362.

Kortlever, R.M., Sodir, N.M., Wilson, C.H., Burkhart, D.L., Pellegrinet, L., Brown Swigart, L., Littlewood, T.D., and Evan, G.I. (2017). Myc Cooperates with Ras by

Programming Inflammation and Immune Suppression. Cell *171*, 1301–1315.

Kramer, N., Walzl, A., Unger, C., Rosner, M., Krupitza, G., Hengstschlager, M., and Dolznig, H. (2013). In vitro cell migration and invasion assays. Mutat. Res. *752*, 10–24.

Kremers, G.J., Gilbert, S.G., Cranfill, P.J., Davidson, M.W., and Piston, D.W. (2011). Fluorescent proteins at a glance. J. Cell Sci. *124*, 157–160.

Labernadie, A., Kato, T., Brugués, A., Serra-Picamal, X., Derzsi, S., Arwert, E., Weston, A., González-Tarragó, V., Elosegui-Artola, A., Albertazzi, L., et al. (2017). A mechanically active heterotypic E-cadherin/N-cadherin adhesion enables fibroblasts to drive cancer cell invasion. Nat. Cell Biol. *19*, 224–237.

Landis, M.D., Seachrist, D.D., Montañez-Wiscovich, M.E., Danielpour, D., and Keri, R.A. (2005). Gene expression profiling of cancer progression reveals intrinsic regulation of transforming growth factor-β signaling in ErbB2/Neu-induced tumors from transgenic mice. Oncogene *24*, 5173–5190.

Latres, E., Mastaitis, J., Fury, W., Miloscio, L., Trejos, J., Pangilinan, J., Okamoto, H., Cavino, K., Na, E., Papatheodorou, A., et al. (2017). Activin A more prominently regulates muscle mass in primates than does GDF8. Nat. Commun. *8*, 1–13.

Lee, J., Moon, H.J., Lee, J.M., and Joo, C.K. (2010). Smad3 regulates Rho signaling via NET1 in the transforming growth factor-β-induced epithelial-mesenchymal transition of human retinal pigment epithelial cells. J. Biol. Chem. *285*, 26618–26627.

Lee, S.-J., Reed, L.A., Davies, M. V, Girgenrath, S., P Goad, M.E., Tomkinson, K.N., Wright, J.F., Barker, C., Ehrmantraut, G., Holmstrom, J., et al. (2005). Regulation of muscle growth by multiple ligands signaling through activin type II receptors.

Leedham, S.J., and Chetty, R. (2016). Wnt disruption in colorectal polyps - the traditional serrated adenoma enters the fray. J. Pathol. *239*, 387–390.

Lei, X., Lei, Y., Li, J.K., Du, W.X., Li, R.G., Yang, J., Li, J., Li, F., and Tan, H.B. (2020). Immune cells within the tumor microenvironment: Biological functions and roles in cancer immunotherapy. Cancer Lett. *470*, 126–133.

Levy, L., and Hill, C.S. (2005). Smad4 Dependency Defines Two Classes of

Transforming Growth Factor (TGF-) Target Genes and Distinguishes TGF- -Induced Epithelial-Mesenchymal Transition from Its Antiproliferative and Migratory Responses. Mol. Cell. Biol. *25*, 8108–8125.

Levy, L., and Hill, C.S. (2006). Alterations in components of the TGF-β superfamily signaling pathways in human cancer. Cytokine Growth Factor Rev. *17*, 41–58.

Levy, L., Howell, M., Das, D., Harkin, S., Episkopou, V., and Hill, C.S. (2007). Arkadia Activates Smad3/Smad4-Dependent Transcription by Triggering Signal-Induced SnoN Degradation. Mol. Cell. Biol. *27*, 6068–6083.

Li, B., and Dewey, C.N. (2011). RSEM: Accurate transcript quantification from RNA-Seq data with or without a reference genome. BMC Bioinformatics *12*, 1–16.

Li, M.O., and Flavell, R.A. (2008). TGF-β: A Master of All T Cell Trades (NIH Public Access).

Li, M.O., Sanjabi, S., and Flavell, R.A.A. (2006). Transforming Growth Factor-β Controls Development, Homeostasis, and Tolerance of T Cells by Regulatory T Cell-Dependent and -Independent Mechanisms. Immunity *25*, 455–471.

Li, Y., Klausen, C., Cheng, J.C., Zhu, H., and Leung, P.C.K. (2014). Activin A, B, and AB increase human trophoblast cell invasion by up-regulating N-cadherin. J. Clin. Endocrinol. Metab. *99*, 2216–2225.

Lin, C.G., Chen, C.C., Leu, S.J., Grzeszkiewicz, T.M., and Lau, L.F. (2005a). Integrin-dependent functions of the angiogenic inducer NOV (CCN3): Implication in wound healing. J. Biol. Chem. *280*, 8229–8237.

Lin, E.Y., Jones, J.G., Li, P., Zhu, L., Whitney, K.D., Muller, W.J., and Pollard, J.W. (2003). Progression to Malignancy in the Polyoma Middle T Oncoprotein Mouse Breast Cancer Model Provides a Reliable Model for Human Diseases. Am. J. Pathol. *163*, 2113–2126.

Lin, J.T., Martin, S.L., Xia, L., and Gorham, J.D. (2005b). TGF-β1 Uses Distinct Mechanisms to Inhibit IFN-γ Expression in CD4 + T Cells at Priming and at Recall: Differential Involvement of Stat4 and T-bet . J. Immunol. *174*, 5950–5958.

Lin, Y., Xu, J., and Lan, H. (2019). Tumor-associated macrophages in tumor metastasis: Biological roles and clinical therapeutic applications. J. Hematol.

Oncol. *12*, 1–16.

Liu, C., Kong, W., Ilalov, K., Yu, S., Xu, K., Prazak, L., Fajardo, M., Sehgal, B., Di Cesare, P.E., Liu, C., et al. (2006). ADAMTS-7: a metalloproteinase that directly binds to and degrades cartilage oligomeric matrix protein. FASEB J. *20*, 988–990.

Liu, Y.L., Chou, C.K., Kim, M., Vasisht, R., Kuo, Y.A., Ang, P., Liu, C., Perillo, E.P., Chen, Y.A., Blocher, K., et al. (2019). Assessing metastatic potential of breast cancer cells based on EGFR dynamics. Sci. Rep. *9*, 1–13.

Locci, M., Wu, J.E., Arumemi, F., Mikulski, Z., Dahlberg, C., Miller, A.T., and Crotty, S. (2016). Activin A programs the differentiation of human T FH cells. Nat. Immunol. *17*, 976–984.

Loomans, H., and Andl, C. (2014). Intertwining of Activin A and TGFβ Signaling: Dual Roles in Cancer Progression and Cancer Cell Invasion. Cancers (Basel). *7*, 70–91.

Los, G. V, Encell, L.P., McDougall, M.G., Hartzell, D.D., Karassina, N., Zimprich, C., Wood, M.G., Learish, R., Ohana, R.F., Urh, M., et al. (2008). HaloTag: A novel protein labeling technology for cell imaging and protein analysis. ACS Chem. Biol. *3*, 373–382.

Love, M.I., Huber, W., and Anders, S. (2014). Moderated estimation of fold change and dispersion for RNA-seq data with DESeq2. Genome Biol. *15*, 1–21.

Lu, J., Chatterjee, M., Schmid, H., Beck, S., and Gawaz, M. (2016). CXCL14 as an emerging immune and inflammatory modulator. J. Inflamm. (United Kingdom) *13*, 1–8.

Luo, W., Xia, T., Xu, L., Chen, Y.G., and Fang, X. (2014). Visualization of the post-Golgi vesicle-mediated transportation of TGF-β receptor II by quasi-TIRFM. J. Biophotonics *7*, 788–798.

Mailliard, R.B., Egawa, S., Cai, Q., Kalinska, A., Bykovskaya, S.N., Lotze, M.T., Kapsenberg, M.L., Storkus, W.J., and Kalinski, P. (2002). Complementary dendritic cell-activating function of CD8 + and CD4 + T cells: Helper role of CD8 + T cells in the development of T helper type responses. J. Exp. Med. *195*, 473–483.

Marchant, L., Linker, C., and Mayor, R. (1998). Inhibition of mesoderm formation

by follistatin. Dev. Genes Evol. *208*, 157–160.

Margadant, C., and Sonnenberg, A. (2010). Integrin-TGF-B crosstalk in fibrosis, cancer and wound healing. EMBO Rep. *11*, 97–105.

Mariathasan, S., Turley, S.J., Nickles, D., Castiglioni, A., Yuen, K., Wang, Y., Kadel, E.E., Koeppen, H., Astarita, J.L., Cubas, R., et al. (2018). TGFβ attenuates tumour response to PD-L1 blockade by contributing to exclusion of T cells. Nature *554*, 544–548.

Marie, J.C., Letterio, J.J., Gavin, M., and Rudensky, A.Y. (2005). TGF-β1 maintains suppressor function and Foxp3 expression in CD4 +CD25+ regulatory T cells. J. Exp. Med. *201*, 1061–1067.

Marshall, C.J. (1995). Specificity of Receptor Tyrosine Kinase Signaling: Transient versus Sustained Extracellular Signal-Regulated Kinase Activation Review. Cell *80*, 179–185.

Marshall, J. (2011). Transwell ® invasion assays. Methods Mol. Biol. *769*, 97–110.

Massagué, J. (2008). TGFβ in Cancer. Cell *134*, 215–230.

Massagué, J. (2012). TGFβ signalling in context. Nat. Rev. Mol. Cell Biol. *13*, 616–630.

Matzuk, M.M., Kumar, T.R., Vassalli, A., Bickenbach, J.R., Roop, D.R., Jaenisch, R., and Bradley, A. (1995). Functional analysis of activins during mammalian development. Nature *374*, 354–357.

McGowan, P.M., Ryan, B.M., Hill, A.D.K., McDermott, E., O'Higgins, N., and Duffy, M.J. (2007). ADAM-17 expression in breast cancer correlates with variables of tumor progression. Clin. Cancer Res. *13*, 2335–2343.

Melisi, D., Garcia-Carbonero, R., Macarulla, T., Pezet, D., Deplanque, G., Fuchs, M., Trojan, J., Oettle, H., Kozloff, M., Cleverly, A., et al. (2018). Galunisertib plus gemcitabine vs. gemcitabine for first-line treatment of patients with unresectable pancreatic cancer. Br. J. Cancer *119*, 1208–1214.

Meng, X.M., Nikolic-Paterson, D.J., and Lan, H.Y. (2016). TGF-β: The master regulator of fibrosis. Nat. Rev. Nephrol. *12*, 325–338.

Mercado-Pimentel, M.E., and Runyan, R.B. (2007). Multiple transforming growth factor-β isoforms and receptors function during epithelial-mesenchymal cell

transformation in the embryonic heart. In Cells Tissues Organs, (Karger Publishers), pp. 146–156.

Mi, L.Z., Brown, C.T., Gao, Y., Tian, Y., Le, V.Q., Walz, T., and Springer, T.A. (2015). Structure of bone morphogenetic protein 9 procomplex. Proc. Natl. Acad. Sci. U. S. A. *112*, 3710–3715.

Miettinen, P.J., Ebner, R., Lopez, A.R., and Derynck, R. (1994). TGF-beta induced transdifferentiation of mammary epithelial cells to mesenchymal cells: involvement of type I receptors. J Cell Biol *127*.

Miller, D.S.J., Bloxham, R.D., Jiang, M., Gori, I., Saunders, R.E., Das, D., Chakravarty, P., Howell, M., and Hill, C.S. (2018). The Dynamics of TGF-β Signaling Are Dictated by Receptor Trafficking via the ESCRT Machinery. Cell Rep. *25*, 1841-1855.e5.

Miller, D.S.J., Schmierer, B., and Hill, C.S. (2019). TGF-β family ligands exhibit distinct signalling dynamics that are driven by receptor localisation. J. Cell Sci. *132*, 1–14.

Miller, S.A., Dykes, D.D., and Polesky, H.F. (1988). A simple salting out procedure for extracting DNA from human nucleated cells. Nucleic Acids Res. *16*, 1215.

Mitchell, H., Choudhury, A., Pagano, R.E., and Leof, E.B. (2004). Ligand-dependent and -independent transforming growth factor-β receptor recycling regulated by clathrin-mediated endocytosis and rab11. Mol. Biol. Cell *15*, 4166–4178.

Mitra, M.S., Lancaster, K., Adedeji, A.O., Palanisamy, G.S., Dave, R.A., Zhong, F., Holdren, M.S., Turley, S.J., Liang, W.C., Wu, Y., et al. (2020). A Potent Pan-TGFβ Neutralizing Monoclonal Antibody Elicits Cardiovascular Toxicity in Mice and Cynomolgus Monkeys. Toxicol. Sci. *175*, 24–34.

Mohammadi, H., and Sahai, E. (2018). Mechanisms and impact of altered tumour mechanics. Nat. Cell Biol. *20*, 766–774.

De Monte, L., Reni, M., Tassi, E., Clavenna, D., Papa, I., Recalde, H., Braga, M., Di Carlo, V., Doglioni, C., and Protti, M.P. (2011). Intratumor T helper type 2 cell infiltrate correlates with cancer-associated fibroblast thymic stromal lymphopoietin production and reduced survival in pancreatic cancer. J. Exp. Med.

208, 469–478.

Monteran, L., and Erez, N. (2019). The dark side of fibroblasts: Cancer-associated fibroblasts as mediators of immunosuppression in the tumor microenvironment. Front. Immunol. *10*, 1835.

Morianos, I., Papadopoulou, G., Semitekolou, M., and Xanthou, G. (2019). Activin-A in the regulation of immunity in health and disease. J. Autoimmun. *104*, 1–15.

Morikawa, M., Derynck, R., and Miyazono, K. (2016). TGF- β and the TGF-β family: Context-dependent roles in cell and tissue physiology. Cold Spring Harb. Perspect. Biol. *8*, 1–25.

Morrison, G.M., Oikonomopoulou, I., Migueles, R.P., Soneji, S., Livigni, A., Enver, T., and Brickman, J.M. (2008). Anterior Definitive Endoderm from ESCs Reveals a Role for FGF Signaling. Cell Stem Cell *3*, 402–415.

Moskowitz, I.P., Wang, J., Peterson, M.A., Pu, W.T., Mackinnon, A.C., Oxburgh, L., Chu, G.C., Sarkar, M., Berul, C., Smoot, L., et al. (2011). Cardiac-specific transcription factor genes Smad4 and Gata4 cooperatively regulate cardiac valve development. PNAS *108*, 4006–4011.

Mullen, A.C., Orlando, D.A., Newman, J.J., Lovén, J., Kumar, R.M., Bilodeau, S., Reddy, J., Guenther, M.G., Dekoter, R.P., and Young, R.A. (2011). Master transcription factors determine cell-type-specific responses to TGF-β signaling. Cell *147*, 565–576.

Munger, J.S., Harpel, J.G., Gleizes, P.E., Mazzieri, R., Nunes, I., and Rifkin, D.B. (1997). Latent transforming growth factor-β: Structural features and mechanisms of activation. Kidney Int. *51*, 1376–1382.

Munz, B., Smola, H., Engelhardt, F., Bleuel, K., Brauchle, M., Lein, I., Evans, L.W., Huylebroeck, D., Balling, R., and Werner, S. (1999). Overexpression of activin A in the skin of transgenic mice reveals new activities of activin in epidermal morphogenesis, dermal fibrosis and wound repair. EMBO J. *18*, 5205–5215.

Murakami, M., Kamimura, D., and Hirano, T. (2019). Pleiotropy and Specificity: Insights from the Interleukin 6 Family of Cytokines. Immunity *50*, 812–831.

Naba, A., Clauser, K.R., Hoersch, S., Liu, H., Carr, S.A., and Hynes, R.O. (2012).

The matrisome: In silico definition and in vivo characterization by proteomics of normal and tumor extracellular matrices. Mol. Cell. Proteomics *11*, 1–18.

Nagasaki, T., Hara, M., Nakanishi, H., Takahashi, H., Sato, M., and Takeyama, H. (2014). Interleukin-6 released by colon cancer-associated fibroblasts is critical for tumour angiogenesis: Anti-interleukin-6 receptor antibody suppressed angiogenesis and inhibited tumour-stroma interaction. Br. J. Cancer *110*, 469–478.

Nall, A. V., Brownlee, R.E., Colvin, C.P., Schultz, G., Fein, D., Cassisi, N.J., Nguyen, T., and Kalra, A. (1996). Transforming growth factor β1 improves wound healing and random flap survival in normal and irradiated rats. Arch. Otolaryngol. - Head Neck Surg. *122*, 171–177.

Nastos, A., Pogge Von Strandmann, E., Weber, H., and Ryffel, G.U. (1998). The embryonic expression of the tissue-specific transcription factor HNF1α in Xenopus: Rapid activation by HNF4 and delayed induction by mesoderm inducers. Nucleic Acids Res. *26*, 5602–5608.

Ngo, P., Ramalingam, P., Phillips, J.A., and Furuta, G.T. (2006). Collagen gel contraction assay. Methods Mol. Biol. *341*, 103–109.

Nguyen, E. V., Pereira, B.A., Lawrence, M.G., Ma, X., Rebello, R.J., Chan, H., Niranjan, B., Wu, Y., Ellem, S., Guan, X., et al. (2019). Proteomic profiling of human prostate cancer-associated fibroblasts (CAF) reveals LOXL2-dependent regulation of the tumor microenvironment. Mol. Cell. Proteomics *18*, 1410–1427.

Ni, X., Tao, J., Barbi, J., Chen, Q., Park, B. V., Li, Z., Zhang, N., Lebid, A., Ramaswamy, A., Wei, P., et al. (2018). YAP is essential for treg-mediated suppression of antitumor immunity. Cancer Discov. *8*, 1026–1043.

Nickel, W., and Seedorf, M. (2008). Unconventional Mechanisms of Protein Transport to the Cell Surface of Eukaryotic Cells. Annu. Rev. Cell Dev. Biol. *24*, 287–308.

Nieto, M.A., Huang, R.Y.Y.J., Jackson, R.A.A., and Thiery, J.P.P. (2016). EMT: 2016. Cell *166*, 21–45.

Öhlund, D., Elyada, E., and Tuveson, D. (2014). Fibroblast heterogeneity in the cancer wound. J. Exp. Med. *211*, 1503–1523.

Öhlund, D., Handly-Santana, A., Biffi, G., Elyada, E., Almeida, A.S., Ponz-Sarvise,

M., Corbo, V., Oni, T.E., Hearn, S.A., Lee, E.J., et al. (2017). Distinct populations of inflammatory fibroblasts and myofibroblasts in pancreatic cancer. J. Exp. Med. *214*, 579–596.

Ohno, M., Karagiannis, P., and Taniguchi, Y. (2014). Protein expression analyses at the single cell level. Molecules *19*, 13932–13947.

Ongusaha, P.P., Kwak, J.C., Zwible, A.J., Macip, S., Higashiyama, S., Taniguchi, N., Fang, L., and Lee, S.W. (2004). HB-EGF is a potent inducer of tumor growth and angiogenesis. Cancer Res. *64*, 5283–5290.

Oskarsson, T., Acharyya, S., Zhang, X.H.F., Vanharanta, S., Tavazoie, S.F., Morris, P.G., Downey, R.J., Manova-Todorova, K., Brogi, E., and Massagué, J. (2011). Breast cancer cells produce tenascin C as a metastatic niche component to colonize the lungs. Nat. Med. *17*, 867–874.

Östman, A., and Augsten, M. (2009). Cancer-associated fibroblasts and tumor growth - bystanders turning into key players. Curr. Opin. Genet. Dev. *19*, 67–73.

Özdemir, B.C., Pentcheva-Hoang, T., Carstens, J.L., Zheng, X., Wu, C.C., Simpson, T.R., Laklai, H., Sugimoto, H., Kahlert, C., Novitskiy, S. V., et al. (2014). Depletion of carcinoma-associated fibroblasts and fibrosis induces immunosuppression and accelerates pancreas cancer with reduced survival. Cancer Cell *25*, 719–734.

Panopoulou, E., Murphy, C., Rasmussen, H., Bagli, E., Rofstad, E.K., and Fotsis, T. (2005). Activin A suppresses neuroblastoma xenograft tumor growth via antimitotic and antiangiogenic mechanisms. Cancer Res. *65*, 1877–1886.

Park, D., Sahai, E., and Rullan, A. (2020a). SnapShot: Cancer-Associated Fibroblasts. Cell *181*, 486–486.

Park, D., Wershof, E., Boeing, S., Labernadie, A., Jenkins, R.P., George, S., Trepat, X., Bates, P.A., and Sahai, E. (2020b). Extracellular matrix anisotropy is determined by TFAP2C-dependent regulation of cell collisions. Nat. Mater. *19*, 227–238.

Partecke, L.I., Sendler, M., Kaeding, A., Weiss, F.U., Mayerle, J., Dummer, A., Nguyen, T.D., Albers, N., Speerforck, S., Lerch, M.M., et al. (2011). A syngeneic orthotopic murine model of pancreatic adenocarcinoma in the C57/BL6 mouse using the panc02 and 6606PDA cell lines. Eur. Surg. Res. *47*, 98–107.

Partridge, E.A., Le Roy, C., Di Guglielmo, G.M., Pawling, J., Cheung, P., Granovsky, M., Nabi, I.R., Wrana, J.L., and Dennis, J.W. (2004). Regulation of cytokine receptors by golgi N-glycan processing and endocytosis. Science (80-.). *306*, 120–124.

Pastar, I., Stojadinovic, O., Krzyzanowska, A., Barrientos, S., Stuelten, C., Zimmerman, K., Blumenberg, M., Brem, H., and Tomic-Canic, M. (2010). Attenuation of the transforming growth factor β-signaling pathway in chronic venous ulcers. Mol. Med. *16*, 92–101.

Paulsson, J., and Micke, P. (2014). Prognostic relevance of cancer-associated fibroblasts in human cancer. Semin. Cancer Biol. *25*, 61–68.

Pereira, B.A., Vennin, C., Papanicolaou, M., Chambers, C.R., Herrmann, D., Morton, J.P., Cox, T.R., and Timpson, P. (2019). CAF Subpopulations: A New Reservoir of Stromal Targets in Pancreatic Cancer. Trends in Cancer *5*, 724–741.

Petersen, C.P., and Reddien, P.W. (2009). Wnt Signaling and the Polarity of the Primary Body Axis. Cell *139*, 1056–1068.

Pickup, M.W., Laklai, H., Acerbi, I., Owens, P., Gorska, A.E., Chytil, A., Aakre, M., Weaver, V.M., and Moses, H.L. (2013). Stromally derived lysyl oxidase promotes metastasis of transforming growth factor-β-deficient mouse mammary carcinomas. Cancer Res. *73*, 5336–5346.

Pickup, M.W., Hover, L.D., Polikowsky, E.R., Chytil, A., Gorska, A.E., Novitskiy, S. V., Moses, H.L., and Owens, P. (2015). BMPR2 loss in fibroblasts promotes mammary carcinoma metastasis via increased inflammation. Mol. Oncol. *9*, 179–191.

Pinto, M.L., Rios, E., Durães, C., Ribeiro, R., Machado, J.C., Mantovani, A., Barbosa, M.A., Carneiro, F., and Oliveira, M.J. (2019). The two faces of tumor-associated macrophages and their clinical significance in colorectal cancer. Front. Immunol. *10*, 18–75.

del Pozo Martin, Y., Park, D., Ramachandran, A., Ombrato, L., Calvo, F., Chakravarty, P., Spencer-Dene, B., Derzsi, S., Hill, C.S., Sahai, E., et al. (2015). Mesenchymal Cancer Cell-Stroma Crosstalk Promotes Niche Activation, Epithelial Reversion, and Metastatic Colonization. Cell Rep. *13*, 2456–2469.

Puram, S. V., Tirosh, I., Parikh, A.S., Patel, A.P., Yizhak, K., Gillespie, S.,

Rodman, C., Luo, C.L., Mroz, E.A., Emerick, K.S., et al. (2017). Single-Cell Transcriptomic Analysis of Primary and Metastatic Tumor Ecosystems in Head and Neck Cancer. Cell *171*, 1611–1624.

Purvis, J.E., and Lahav, G. (2013). Encoding and decoding cellular information through signaling dynamics. Cell *152*, 945–956.

Qiu, S.Q., Waaijer, S.J.H., Zwager, M.C., de Vries, E.G.E., van der Vegt, B., and Schröder, C.P. (2018). Tumor-associated macrophages in breast cancer: Innocent bystander or important player? Cancer Treat. Rev. *70*, 178–189.

Radcliffe, P.A., and Mitrophanous, K.A. (2004). Multiple gene products from a single vector: “Self-cleaving” 2A peptides. Gene Ther. *11*, 1673–1674.

Ramachandran, A., Vizán, P., Das, D., Chakravarty, P., Vogt, J., Rogers, K.W., Müller, P., Hinck, A.P., Sapkota, G.P., and Hill, C.S. (2018). TGF-β uses a novel mode of receptor activation to phosphorylate SMAD1 / 5 and induce epithelial-to-mesenchymal transition. Elife *7*, e31756.

Ran, F.A., Hsu, P.D., Wright, J., Agarwala, V., Scott, D.A., and Zhang, F. (2013). Genome engineering using the CRISPR-Cas9 system. Nat Protoc *8*, 2281–2308.

Rhim, A.D., Oberstein, P.E., Thomas, D.H., Mirek, E.T., Palermo, C.F., Sastra, S.A., Dekleva, E.N., Saunders, T., Becerra, C.P., Tattersall, I.W., et al. (2014). Stromal elements act to restrain, rather than support, pancreatic ductal adenocarcinoma. Cancer Cell *25*, 735–747.

Roberts, A.B., Sporn, M.B., Assoian, R.K., Smith, J.M., Roche, N.S., Wakefield, L.M., Heine, U.I., Liotta, L.A., Falanga, V., and Kehrl, J.H. (1986). Transforming growth factor type β: Rapid induction of fibrosis and angiogenesis in vivo and stimulation of collagen formation in vitro. Proc. Natl. Acad. Sci. U. S. A. *83*, 4167–4171.

Roberts, A.B., Tian, F., Byfield, S.D.C., Stuelten, C., Ooshima, A., Saika, S., and Flanders, K.C. (2006). Smad3 is key to TGF-β-mediated epithelial-to-mesenchymal transition, fibrosis, tumor suppression and metastasis. Cytokine Growth Factor Rev. *17*, 19–27.

Robinson, T.O., and Schluns, K.S. (2017). The potential and promise of IL-15 in immuno-oncogenic therapies. Immunol. Lett. *190*, 159–168.

Rodrigues, M., Kosaric, N., Bonham, C.A., and Gurtner, G.C. (2019). Wound

healing: A cellular perspective. Physiol. Rev. *99*, 665–706.

Rodríguez-Ruiz, M.E., Rodríguez, I., Mayorga, L., Labiano, T., Barbes, B., Etxeberria, I., Ponz-Sarvise, M., Azpilikueta, A., Bolaños, E., Sanmamed, M.F., et al. (2019). TGFb blockade enhances radiotherapy abscopal efficacy effects in combination with anti-PD1 and anti-CD137 immunostimulatory monoclonal antibodies. Mol. Cancer Ther. *18*, 621–631.

Rørth, P. (2009). Collective cell migration. Annu. Rev. Cell Dev. Biol. *25*, 407–429.

Rothová, M., Hölzenspies, J.J., Livigni, A., Villegas, S.N., and Brickman, J.M. (2016). Differentiation of Mouse Embryonic Stem Cells into Ventral Foregut Precursors. Curr. Protoc. Stem Cell Biol. 1G.3.1-1G.3.12.

Roy, R., Wewer, U.M., Zurakowski, D., Pories, S.E., and Moses, M.A. (2004). ADAM 12 cleaves extracellular matrix proteins and correlates with cancer status and stage. J. Biol. Chem. *279*, 51323–51330.

Saadoun, S., Papadopoulos, M.C., Hara-Chikuma, M., and Verkman, A.S. (2005). Impairment of angiogenesis and cell migration by targeted aquaporin-1 gene disruption. Nature *434*, 786–792.

Sagner, A., and Briscoe, J. (2017). Morphogen interpretation: concentration, time, competence, and signaling dynamics. Wiley Interdiscip. Rev. Dev. Biol. *6*, e271.

Sahai, E., Astsaturov, I., Cukierman, E., DeNardo, D.G., Egeblad, M., Evans, R.M., Fearon, D., Greten, F.R., Hingorani, S.R., Hunter, T., et al. (2020). A framework for advancing our understanding of cancer-associated fibroblasts. Nat. Rev. Cancer *20*, 174–186.

Sanders, L.N., Schoenhard, J.A., Saleh, M.A., Mukherjee, A., Ryzhov, S., McMaster, W.G., Nolan, K., Gumina, R.J., Thompson, T.B., Magnuson, M.A., et al. (2016). BMP antagonist gremlin 2 limits inflammation after myocardial infarction. Circ. Res. *119*, 434–449.

Sangwan, V., and Park, M. (2006). Receptor tyrosine kinases: Role in cancer progression. Curr. Oncol. *13*, 191–193.

Sanz-Moreno, V., and Marshall, C.J. (2010). The plasticity of cytoskeletal dynamics underlying neoplastic cell migration. Curr. Opin. Cell Biol. *22*, 690–696.

Sanz-Moreno, V., Gaggioli, C., Yeo, M., Albrengues, J., Wallberg, F., Viros, A.,

Hooper, S., Mitter, R., Féral, C.C., Cook, M., et al. (2011). ROCK and JAK1 Signaling Cooperate to Control Actomyosin Contractility in Tumor Cells and Stroma. Cancer Cell *20*, 229–245.

Sato, C., Zhao, G., and Xenia G. Ilagan, M. (2012). An Overview of Notch Signaling in Adult Tissue Renewal and Maintenance. Curr. Alzheimer Res. *9*, 227–240.

Sato, S., Vasaikar, S., Eskaros, A., Kim, Y., Lewis, J.S., Zhang, B., Zijlstra, A., and Weaver, A.M. (2019). EPHB2 carried on small extracellular vesicles induces tumor angiogenesis via activation of ephrin reverse signaling. JCI Insight *4*, 1–18.

Schlunegger, M.P., and Grütter, M.G. (1992). An unusual feature revealed by the crystal structure at 2.2 Å resolution of human transforming growth fact or-β2. Nature *358*, 430–434.

Schmierer, B., and Hill, C.S. (2007). TGF β -SMAD signal transduction : Molecular specificity and functional flexibility. Nat. Rev. *8*, 970–982.

Schmierer, B., Tournier, A.L., Bates, P.A., and Hill, C.S. (2008). Mathematical modeling identifies Smad nucleocytoplasmic shuttling as a dynamic signal-interpreting system. PNAS *105*, 6608–6613.

Schmitz, J.M., McCracken, V.J., Dimmitt, R.A., and Lorenz, R.G. (2007). Expression of CXCL15 (Lungkine) in murine gastrointestinal, urogenital, and endocrine organs. J. Histochem. Cytochem. *55*, 515–524.

Schneyer, A., Sidis, Y., Xia, Y., Saito, S., Re, E. Del, Lin, H.Y., and Keutmann, H. (2004). Differential actions of follistatin and follistatin-like 3. In Molecular and Cellular Endocrinology, (Elsevier), pp. 25–28.

Schwertschlag, U.S., Trepicchio, W.L., Dykstra, K.H., Keith, J.C., Turner, K.J., and Dorner, A.J. (1999). Hematopoietic, immunomodulatory and epithelial effects of interleukin-11. Leukemia *13*, 1307–1315.

Seachrist, D.D., and Keri, R.A. (2019). The Activin Social Network: Activin, Inhibin, and Follistatin in Breast Development and Cancer. Endocrinology *160*, 1097–1110.

Seachrist, D.D., Sizemore, S.T., Johnson, E., Abdul-Karim, F.W., Weber Bonk, K.L., and Keri, R.A. (2017). Follistatin is a metastasis suppressor in a mouse model of HER2-positive breast cancer. Breast Cancer Res. *19*, 1–10.

Seder, C.W., Hnrtojo, W., Lin, L., Silvers, A.L., Wang, Z., Thomas, D.G., Giordano, T.J., Chen, G., Chang, A.C., Orringer, M.B., et al. (2009). Upregulated INHBA expression may promote cell proliferation and is associated with poor survival IN lung adenocarcinoma1 www.neoplasia.com. Neoplasia *11*, 388–396.

Shangguan, L., Ti, X., Krause, U., Hai, B., Zhao, Y., Yang, Z., and Liu, F. (2012). Inhibition of TGF-β/Smad signaling by BAMBI blocks differentiation of human mesenchymal stem cells to carcinoma-associated fibroblasts and abolishes their protumor effects. Stem Cells *30*, 2810–2819.

Shen, L., Smith, J.M., Shen, Z., Eriksson, M., Sentman, C., and Wira, C.R. (2007). Inhibition of human neutrophil degranulation by transforming growth factor-β1. Clin. Exp. Immunol. *149*, 155–161.

Sherman, M.H., Yu, R.T., Engle, D.D., Ding, N., Atkins, A.R., Tiriac, H., Collisson, E.A., Connor, F., Van Dyke, T., Kozlov, S., et al. (2014). Vitamin D receptor-mediated stromal reprogramming suppresses pancreatitis and enhances pancreatic cancer therapy. Cell *159*, 80–93.

Shi, Y., and Massagué, J. (2003). Mechanisms of TGF-beta signaling from cell membrane to the nucleus. Cell *113*, 685–700.

Shi, M., Zhu, J., Wang, R., Chen, X., Mi, L., Walz, T., and Springer, T.A. (2011). Latent TGF-β structure and activation. Nature *474*, 343–351.

Shibuya, M., and Claesson-Welsh, L. (2006). Signal transduction by VEGF receptors in regulation of angiogenesis and lymphangiogenesis. Exp. Cell Res. *312*, 549–560.

Sica, A., Larghi, P., Mancino, A., Rubino, L., Porta, C., Totaro, M.G., Rimoldi, M., Biswas, S.K., Allavena, P., and Mantovani, A. (2008). Macrophage polarization in tumour progression. Semin. Cancer Biol. *18*, 349–355.

Siegel, P.M., and Massagué, J. (2003). Cytostatic and apoptotic actions of TGF-β in homeostasis and cancer. Nat. Rev. Cancer *3*, 807–820.

Sierra-Filardi, E., Puig-Kröger, A., Blanco, F.J., Nieto, C., Bragado, R., Palomero, M.I., Bernabéu, C., Vega, M.A., and Corbí, A.L. (2011). Activin A skews macrophage polarization by promoting a proinflammatory phenotype and inhibiting the acquisition of anti-inflammatory macrophage markers. Blood *117*, 5092–5101.

Singel, K.L., and Segal, B.H. (2016). Neutrophils in the tumor microenvironment: trying to heal the wound that cannot heal. Immunol. Rev. *273*, 329–343.

Sjöblom, T., Jones, S., Wood, L.D., Parsons, D.W., Lin, J., Barber, T.D., Mandelker, D., Leary, R.J., Ptak, J., Silliman, N., et al. (2006). The consensus coding sequences of human breast and colorectal cancers. Science (80-.). *314*, 268–274.

Skowyra, M.L., Schlesinger, P.H., Naismith, T. V., and Hanson, P.I. (2018). Triggered recruitment of ESCRT machinery promotes endolysosomal repair. Science (80-.). *360*, 1.

Song, J., Oh, S.P., Schrewe, H., Nomura, M., Lei, H., Okano, M., Gridley, T., and Li, E. (1999). The type II activin receptors are essential for egg cylinder growth, gastrulation, and rostral head development in mice. Dev. Biol. *213*, 157–169.

Sorkin, A., and Von Zastrow, M. (2009). Endocytosis and signalling: Intertwining molecular networks. Nat. Rev. Mol. Cell Biol. *10*, 609–622.

Speetjens, F.M., Kuppen, P.J.K., Sandel, M.H., Menon, A.G., Burg, D., Van DeVelde, C.J.H., Tollenaar, R.A.E.M., De Bont, H.J.G.M., and Nagelkerke, J.F. (2008). Disrupted expression of CXCL5 in colorectal cancer is associated with rapid tumor formation in rats and poor prognosis in patients. Clin. Cancer Res. *14*, 2276–2284.

Staudacher, J.J., Bauer, J., Jana, A., Tian, J., Carroll, T., Mancinelli, G., Özden, Ö., Krett, N., Guzman, G., Kerr, D., et al. (2017a). Activin signaling is an essential component of the TGF-β induced pro-metastatic phenotype in colorectal cancer. Sci. Rep. *7*, 1–9.

Staudacher, J.J., Yazici, C., Carroll, T., Bauer, J., Pang, J., Krett, N., Xia, Y., Wilson, A., Papachristou, G., Dirmeier, A., et al. (2017b). Activin in acute pancreatitis: Potential risk-stratifying marker and novel therapeutic target. Sci. Rep. *7*, 1–10.

Steinbauer, M., Guba, M., Cernaianu, G., Köhl, G., Cetto, M., Kunz-Schughart, L.A., Geissler, E.K., Falk, W., and Jauch, K.W. (2003). GFP-transfected tumor cells are useful in examining early metastasis in vivo, but immune reaction precludes long-term tumor development studies in immunocompetent mice. Clin. Exp. Metastasis *20*, 135–141.

Steller, M.D., Shaw, T.J., Vanderhyden, B.C., and Ethier, J.F. (2005). Inhibin resistance is associated with aggressive tumorigenicity of ovarian cancer cells. Mol. Cancer Res. *3*, 50–61.

Stenvers, K.L., and Findlay, J.K. (2010). Inhibins: From reproductive hormones to tumor suppressors. Trends Endocrinol. Metab. *21*, 174–180.

Stockholm, D., Benchaouir, R., Picot, J., Rameau, P., Neildez, T.M.A., Landini, G., Laplace-Builhé, C., and Paldi, A. (2007). The Origin of Phenotypic Heterogeneity in a Clonal Cell Population In Vitro. PLoS One *2*, 1–13.

Stoitzner, P., Stössel, H., Wankell, M., Hofer, S., Heufler, C., Werner, S., and Romani, N. (2005). Langerhans cells are strongly reduced in the skin of transgenic mice overexpressing follistatin in the epidermis. Eur. J. Cell Biol. *84*, 733–741.

Strell, C., Paulsson, J., Jin, S.B., Tobin, N.P., Mezheyeuski, A., Roswall, P., Mutgan, C., Mitsios, N., Johansson, H., Wickberg, S.M., et al. (2019). Impact of Epithelial-Stromal Interactions on Peritumoral Fibroblasts in Ductal Carcinoma in Situ. J. Natl. Cancer Inst. *111*, 983–995.

Stuelten, C.H., DaCosta Byfield, S., Arany, P.R., Karpova, T.S., Stetler-Stevenson, W.G., and Roberts, A.B. (2005). Breast cancer cells induce stromal fibroblasts to express MMP-9 via secretion of TNF-alpha and TGF-beta. J Cell Sci. *118*, 2143–2153.

Tachibana, I., Imoto, M., Adjei, P.N., Gores, G.J., Subramaniam, M., Spelsberg, T.C., and Urrutia, R. (1997). Overexpression of the TGFβ-regulated zinc finger encoding gene, TIEG, induces apoptosis in pancreatic epithelial cells. J. Clin. Invest. *99*, 2365–2374.

Tao, J.J., Cangemi, N.A., Makker, V., Cadoo, K.A., Liu, J.F., Rasco, D.W., Navarro, W.H., Haqq, C.M., and Hyman, D.M. (2019). First-in-human phase i study of the activin a inhibitor, STM 434, in patients with granulosa cell ovarian cancer and other advanced solid tumors. Clin. Cancer Res. *25*, 5458–5465.

Tauriello, D.V.F., Palomo-Ponce, S., Stork, D., Berenguer-Llergo, A., Badia-Ramentol, J., Iglesias, M., Sevillano, M., Ibiza, S., Cañellas, A., Hernando-Momblona, X., et al. (2018). TGFβ drives immune evasion in genetically reconstituted colon cancer metastasis. Nature *554*, 538–543.

The Well Biosceince (2019). VitroGel Hydrogel Matrix.

Thomas, D.A., and Massagué, J. (2005). TGF-β directly targets cytotoxic T cell functions during tumor evasion of immune surveillance. Cancer Cell *8*, 369–380.

Thompson, T.B., Lerch, T.F., Cook, R.W., Woodruff, T.K., and Jardetzky, T.S. (2005). The structure of the follistatin: Activin complex reveals antagonism of both type I and type II receptor binding. Dev. Cell *9*, 535–543.

Thuault, S., Valcourt, U., Petersen, M., Manfioletti, G., Heldin, C.H., and Moustakas, A. (2006). Transforming growth factor-β employs HMGA2 to elicit epithelial-mesenchymal transition. J. Cell Biol. *174*, 175–183.

Tisdale, M.J. (2009). Mechanisms of cancer cachexia. Physiol. Rev. *89*, 381–410.

Toivonen, S., Lundin, K., Balboa, D., Ustinov, J., Tamminen, K., Palgi, J., Trokovic, R., Tuuri, T., and Otonkoski, T. (2013). Activin A and Wnt-dependent specification of human definitive endoderm cells. Exp. Cell Res. *319*, 2535–2544.

Toledo, M., Busquets, S., Penna, F., Zhou, X., Marmonti, E., Betancourt, A., Massa, D., López-Soriano, F.J., Han, H.Q., and Argilés, J.M. (2016). Complete reversal of muscle wasting in experimental cancer cachexia: Additive effects of activin type II receptor inhibition and β-2 agonist. Int. J. Cancer *138*, 2021–2029.

Tsai, J.H., and Yang, J. (2013). Epithelial-mesenchymal plasticity in carcinoma metastasis. Genes Dev. *27*, 2192–2206.

Ueno, N., Ling, N., Ying, S.Y., Esch, F., Shimasaki, S., and Guillemin, R. (1987). Isolation and partial characterization of follistatin: a single-chain Mr 35,000 monomeric protein that inhibits the release of follicle-stimulating hormone. Proc. Natl. Acad. Sci. U. S. A. *84*, 8282–8286.

Ungefroren, H., Witte, D., and Lehnert, H. (2018). The role of small GTPases of the Rho/Rac family in TGF-β-induced EMT and cell motility in cancer. Dev. Dyn. *247*, 451–461.

Valcourt, U., Kowanetz, M., Niimi, H., Heldin, C.-H., and Moustakas, A. (2004). TGF-β and the Smad Signaling Pathway Support Transcriptomic Reprogramming during Epithelial-Mesenchymal Cell Transition. Mol. Biol. Cell *16*, 1987–2002.

Vattulainen-Collanus, S., Akinrinade, O., Li, M., Koskenvuo, M., Li, C.G., Rao, S.P., Perez, V. de J., Yuan, K., Sawada, H., Koskenvuo, J.W., et al. (2016). Loss

of PPARγ in endothelial cells leads to impaired angiogenesis. J. Cell Sci. *129*, 693–705.

Vejda, S., Erlach, N., Peter, B., Drucker, C., Rossmanith, W., Pohl, J., Schulte-Hermann, R., and Grusch, M. (2003). Expression of activins C and E induces apoptosis in human and rat hepatoma cells. Carcinogenesis *24*, 1801–1809.

Verrecchia, F., and Mauviel, A. (2007). Transforming growth factor-β and fibrosis. World J. Gastroenterol. *13*, 3056–3062.

Verrecchia, F., Vindevoghel, L., Lechleider, R.J., Uitto, J., Roberts, A.B., and Mauviel, A. (2001). Smad3/AP-1 interactions control transcriptional responses to TGF-β in a promoter-specific manner. Oncogene *20*, 3332–3340.

Villarino, A. V., Kanno, Y., and O'Shea, J.J. (2017). Mechanisms and consequences of Jak-STAT signaling in the immune system. Nat. Immunol. *18*, 374–384.

Viloria, C.G., Obaya, A.J., Moncada-Pazos, A., Llamazares, M., Astudillo, A., Capellá, G., Cal, S., and López-Otín, C. (2009). Genetic inactivation of ADAMTS15 metalloprotease in human colorectal cancer. Cancer Res. *69*, 4926–4934.

Vizán, P., Miller, D.S.J., Gori, I., Das, D., Schmierer, B., and Hill, C.S. (2013). Controlling long-term signaling: receptor dynamics determine attenuation and refractory behavior of the TGF-β pathway. Sci. Signal. *6*, 1–12.

Wai, P.Y., and Kuo, P.C. (2004). The role of osteopontin in tumor metastasis. J. Surg. Res. *121*, 228–241.

Wakefield, L.M., and Hill, C.S. (2013). Beyond TGFβ: roles of other TGFβ superfamily members in cancer. Nat. Rev. Cancer *13*, 328–341.

Walton, K.L., Makanji, Y., and Harrison, C.A. (2012). New insights into the mechanisms of activin action and inhibition. Mol. Cell. Endocrinol. *359*, 2–12.

Walton, K.L., Johnson, K.E., and Harrison, C.A. (2017). Targeting TGF-β mediated SMAD signaling for the prevention of fibrosis. Front. Pharmacol. *8*, 1–11.

Wang, S.Y., Tai, G.X., Zhang, P.Y., Mu, D.P., Zhang, X.J., and Liu, Z.H. (2008). Inhibitory effect of activin A on activation of lipopolysaccharide-stimulated mouse macrophage RAW264.7 cells. Cytokine *42*, 85–91.

Wang, X., Inoue, S., Gu, J., Miyoshi, E., Noda, K., Li, W., Mizuno-Horikawa, Y., Nakano, M., Asahi, M., Takahashi, M., et al. (2005). Dysregulation of TGF-β1 receptor activation leads to abnormal lung development and emphysema-like phenotype in core fucose-deficient mice. Proc. Natl. Acad. Sci. U. S. A. *102*, 15791–15796.

Wang, X., Fischer, G., and Hyvönen, M. (2016). Structure and activation of pro-activin A. Nat. Commun. *7*, 12052.

Welt, C., Sidis, Y., Keutmann, H., and Schneyer, A. (2002). Activins, Inhibins, and Follistatins: From Endocrinology to Signaling. A Paradigm for the New Millennium. Exp. Biol. Med. *227*, 724–752.

De Wever, O., Nguyen, Q., Van Hoorde, L., Bracke, M., Bruyneel, E., Gespach, C., and Mareel, M. (2004). Tenascin-C and SF/HGF produced by myofibroblasts in vitro provide convergent proinvasive signals to human colon cancer cells through RhoA and Rac. FASEB J. *18*, 1016–1018.

De Wever, O., Hendrix, A., De Boeck, A., Westbroek, W., Braems, G., Emami, S., Sabbah, M., Gespach, C., and Bracke, M. (2010). Modeling and quantification of cancer cell invasion through collagen type I matrices. Int. J. Dev. Biol. *54*, 887–896.

Wiater, E., Harrison, C.A., Lewis, K.A., Gray, P.C., and Vale, W.W. (2006). Identification of distinct inhibin and transforming growth factor beta-binding sites on betaglycan: functional separation of betaglycan co-receptor actions. J. Biol. Chem. *281*, 17011–17022.

Wietecha, M.S., Pensalfini, M., Cangkrama, M., Müller, B., Jin, J., Brinckmann, J., Mazza, E., and Werner, S. (2020). Activin-mediated alterations of the fibroblast transcriptome and matrisome control the biomechanical properties of skin wounds. Nat. Commun. *11*, 1–20.

Wildeboer, D., Naus, S., Sang, Q.X.A., Bartsch, J.W., and Pagenstecher, A. (2006). Metalloproteinase disintegrins ADAM8 and ADAM19 are highly regulated in human primary brain tumors and their expression levels and activities are associated with invasiveness. J. Neuropathol. Exp. Neurol. *65*, 516–527.

Wilkinson, S., and Frame, M.C. (2016). The ROCKS on which tumour cells thrive. Elife *5*, e14511.

Wollert, T., and Hurley, J.H. (2010). Molecular mechanism of multivesicular body biogenesis by ESCRT complexes. Nature *464*, 864–869.

Wollert, T., Yang, D., Ren, X., Lee, H.H., Im, Y.J., and Hurley, J.H. (2009). The ESCRT machinery at a glance. J. Cell Sci. *122*, 2163–2166.

Wrighton, K.H., Lin, X., and Feng, X.-H. (2009). Phospho-control of TGF-β superfamily signaling. Cell Res. *19*, 8–20.

Wu, M.Y., and Hill, C.S. (2009). TGF-β Superfamily Signaling in Embryonic Development and Homeostasis. Dev. Cell *16*, 329–343.

Xu, R.H., Sampsell-Barron, T.L., Gu, F., Root, S., Peck, R.M., Pan, G., Yu, J., Antosiewicz-Bourget, J., Tian, S., Stewart, R., et al. (2008). NANOG Is a Direct Target of TGFβ/Activin-Mediated SMAD Signaling in Human ESCs. Cell Stem Cell *3*, 196–206.

Yagami, A., Orihara, K., Morita, H., Futamura, K., Hashimoto, N., Matsumoto, K., Saito, H., and Matsuda, A. (2010). IL-33 Mediates Inflammatory Responses in Human Lung Tissue Cells. J. Immunol. *185*, 5743–5750.

Yakymovych, I., Yakymovych, M., and Heldin, C.H. (2018). Intracellular trafficking of transforming growth factor β receptors. Acta Biochim. Biophys. Sin. (Shanghai). *50*, 3–11.

Yamaguchi, Y., Mann, D.M., and Ruoslahti, E. (1990). Negative regulation of transforming growth factor-β by the proteoglycan decorin. Nature *346*, 281–284.

Yan, H.H., Jiang, J., Pang, Y., Achyut, B.R., Lizardo, M., Liang, X., Hunter, K., Khanna, C., Hollander, C., and Yang, L. (2015). CCL9 Induced by TGFβ Signaling in Myeloid Cells Enhances Tumor Cell Survival in the Premetastatic Organ. Cancer Res. *75*, 5283–5298.

Yang, J., Antin, P., Berx, G., Blanpain, C., Brabletz, T., Bronner, M., Campbell, K., Cano, A., Casanova, J., Christofori, G., et al. (2020). Guidelines and definitions for research on epithelial–mesenchymal transition. Nat. Rev. Mol. Cell Biol. *21*, 341–352.

Ye, X., and Weinberg, R.A. (2015). Epithelial-Mesenchymal Plasticity: A Central Regulator of Cancer Progression. Trends Cell Biol. *25*, 675–686.

Yi, Y., Cheng, J.C., Klausen, C., and Leung, P.C.K. (2019). Activin A promotes ovarian cancer cell migration by suppressing E-cadherin expression. Exp. Cell

Res. *382*, 1–11.

Yu, G., and He, Q.Y. (2016). ReactomePA: An R/Bioconductor package for reactome pathway analysis and visualization. Mol. Biosyst. *12*, 477–479.

Yu, G., Wang, L.G., Han, Y., and He, Q.Y. (2012). ClusterProfiler: An R package for comparing biological themes among gene clusters. Omi. A J. Integr. Biol. *16*, 284–287.

Yu, Y., Xiao, C.H., Tan, L.D., Wang, Q.S., Li, X.Q., and Feng, Y.M. (2014). Cancer-associated fibroblasts induce epithelial-mesenchymal transition of breast cancer cells through paracrine TGF-β signalling. Br. J. Cancer *110*, 724–732.

Yuan, W., and Varga, J. (2001). Transforming Growth Factor-β Repression of Matrix Metalloproteinase-1 in Dermal Fibroblasts Involves Smad3. J. Biol. Chem. *276*, 38502–38510.

Zawel, L., Le Dai, J., Buckhaults, P., Zhou, S., Kinzler, K.W., Vogelstein, B., and Kern, S.E. (1998). Human Smad3 and Smad4 are sequence-specific transcription activators. Mol. Cell *1*, 611–617.

Zeisberg, E.M., Potenta, S., Xie, L., Zeisberg, M., and Kalluri, R. (2007). Discovery of endothelial to mesenchymal transition as a source for carcinoma-associated fibroblasts. Cancer Res. *67*, 10123–10128.

Zhang, A., Qian, Y., Ye, Z., Chen, H., Xie, H., Zhou, L., Shen, Y., and Zheng, S. (2017). Cancer-associated fibroblasts promote M2 polarization of macrophages in pancreatic ductal adenocarcinoma. Cancer Med. *6*, 463–470.

Zhang, H., Wang, X., Shen, Z., Xu, J., Qin, J., and Sun, Y. (2015). Infiltration of diametrically polarized macrophages predicts overall survival of patients with gastric cancer after surgical resection. Gastric Cancer *18*, 740–750.

Zhang, J., ten Dijke, P., Wuhrer, M., and Zhang, T. (2020a). Role of glycosylation in TGF-β signaling and epithelial-to-mesenchymal transition in cancer. Protein Cell 1–18.

Zhang, W., Jiang, Y., Wang, Q., Ma, X., Xiao, Z., Zuo, W., Fang, X., and Chen, Y.G. (2009). Single-molecule imaging reveals transforming growth factor-β-induced type II receptor dimerization. Proc. Natl. Acad. Sci. U. S. A. *106*, 15679–15683.

Zhang, W., Yuan, J., Yang, Y., Xu, L., Wang, Q., Zuo, W., Fang, X., and Chen,

Y.G. (2010). Monomeric type I and type III transforming growth factor-B receptors and their dimerization revealed by single-molecule imaging. Cell Res. *20*, 1216–1223.

Zhang, W., Wang, H., Sun, M., Deng, X., Wu, X., Ma, Y., Li, M., Shuoa, S.M., You, Q., and Miao, L. (2020b). CXCL5/CXCR2 axis in tumor microenvironment as potential diagnostic biomarker and therapeutic target. Cancer Commun. *40*, 69–80.

Zheng, B., Sage, M., Sheppeard, E.A., Jurecic, V., and Bradley, A. (2000). Engineering Mouse Chromosomes with Cre-loxP: Range, Efficiency, and Somatic Applications. Mol. Cell. Biol. *20*, 648–655.

Zhou, X., Wang, J.L., Lu, J., Song, Y., Kwak, K.S., Jiao, Q., Rosenfeld, R., Chen, Q., Boone, T., Simonet, W.S., et al. (2010). Reversal of Cancer Cachexia and Muscle Wasting by ActRIIB Antagonism Leads to Prolonged Survival. Cell *142*, 531–543.

Zi, Z., and Klipp, E. (2007). Constraint-Based Modeling and Kinetic Analysis of the Smad Dependent TGF-β Signaling Pathway. PLoS One *2*, 1–11.

Zimmerman, L.B., De Jesús-Escobar, J.M., and Harland, R.M. (1996). The Spemann organizer signal noggin binds and inactivates bone morphogenetic protein 4. Cell *86*, 599–606.